School of Engineering

Influence of Polymer Modification on Cracking and Fatigue of Asphalt Mixtures

Thesis submitted in accordance with the requirements of the University of Liverpool for the degree of Doctor in Philosophy by

Ian Michael Lancaster

June 2016

ABSTRACT

Efficient road networks are an integral aspect of the transport infrastructure of any modern economy and sound pavement design, along with effective maintenance programmes, are crucial to the continued quality and value of these assets. Polymer modification of the asphalt is frequently used to enhance the pavement durability performance. However, the benefits of polymer modification are not always clear to the designing engineer. Laboratory tests to assess asphalt performance often require large quantities of material, highly specialised test equipment and considerable amounts of time. Whilst the advantages of polymer modification on deformation resistance are well accepted, its impact on cracking and fatigue is less well defined. This research was therefore undertaken to quantify the effect of polymer modification on the cracking and fatigue performance of asphalt, and to develop methods to minimise the time and materials required to perform the laboratory assessments.

A novel technique to analyse the performance of full asphalt mixtures utilising a standard laboratory dynamic shear rheometer (DSR) was developed using very small sample sizes. The technique was validated by comparing the results to existing testing geometries, with the new method shown to depict the viscoelastic behaviour of the asphalt.

The asphalt's fundamental fracture mechanics properties were investigated via the semi circular bending geometry, with the improved performance of the polymer modified asphalts in terms of fracture toughness and strain energy release rate demonstrated. A crack growth law based on the generalised J-integral was developed and used to determine characteristic material parameters which were used to predict pavement service life. Crack propagation of the semi-circular bending geometry under monotonic loading was modelled using the Extended Finite Element Method with the time dependent viscoelastic properties within the model determined using the small sample size technique, and modelled using a fractional viscoelastic element.

The calibrated model was used to predict the load-displacement behaviour of specimens, and the improved crack resistance of the polymer modified asphalts verified.

Binder fatigue behaviour was analysed using the DSR and the improved damage resistance of increasingly polymer modified binders verified. Asphalt fatigue was assessed using traditional large scale trapezoidal two point bending, cyclic semi-circular bending and small specimen sized tests on the DSR with the effect of polymer modification evaluated. Viscoelastic Continuum Damage (VECD) theory was successfully applied to the results with the potential for significant reductions in test durations using this approach demonstrated.

ACKNOWLEDGMENTS

This research has been supervised and guided throughout by Dr Hussain Al-Khalid whose wisdom and experience has helped me avoid many pitfalls and reach my goals. The academic support of Dr Steve Millard, Dr Zhenjun Yang, Dr Ioannis Kougioumtzoglou and Dr Siu-Kui Au is also greatly appreciated. I'd like to thank the Liverpool pavement group members and staff, in particular Marc Bratley and Dave Hunter, for their invaluable practical knowledge.

I would also like to thank all the other people and organisations that contributed and supported this research. In particular, LafargeTarmac for the supply of aggregates, Kraton Polymers for the supply of polymer, Prof Eyad Masad at Texas A&M University and Dr James Grenfell at Nottingham University for their assistance with surface energy measurements, and all the staff at PTS International for their assistance with fatigue testing with special thanks to Darren Foster and Anthony Collier.

I would like to thank all my Nynas colleagues for their technical support and patience during my studies. In particular, the assistance of Dr Ian Lancaster, Dr Hilde Soenen, Dr Per Redelius, Dr Timo Blomberg, Steve Armstrong and Jukka Laitinen is greatly appreciated.

Most importantly I would like to thank my family for their patience throughout this research. Without the support and understanding of my wife Heather, and the grateful reality check and distraction of our children James and Erin, none of this work would have been possible. Finally, of course, thank you to my parents whose support in my school and undergraduate years laid the foundation for this research.

Contents

1 INTRODUCTION

Naturally occurring bitumen has been used as an adhesive and waterproofing construction material since ancient times (Rullkotter and Nissenbaum 1988). The first recorded use of bitumen as part of an asphalt pavement was in ancient Babylon around 625 B.C. with the word asphalt deriving from the Greek word "asphaltos" meaning "secure". However, it was not until the 19th century that its use in paving applications really began to grow. By 1907 the use of refined bitumen from crude oil overtook that of natural bitumens, and as the number of motor vehicles rose in the early 20th century so did the number of roads to accommodate them and with that the current pavement engineering knowledge and innovation developed.

The technology of paved roads as we know them today began in the early 19th century. Early pavements had been produced using rounded gravel and stones, but John Macadam showed that compacted crushed angular aggregate would provide improvements in loading capacity and, by limiting the maximum aggregate size to 25mm, an improved ride quality. Coal tar was later used to bind the aggregate together to produce a "Tar Macadam" with the first pavement laid near Nottingham in 1848. In the early 20th century a wide range of proprietary tar and bitumen bound materials were in use, but as refined bitumen became widely available this became the binding material of choice.

As traffic volumes continued to grow it was recognised that improved mixtures and binders were needed to maintain the pavement's performance. The design of asphaltic pavement can be a complex process with a wide range of potential aggregates, binders and mixtures available, all with the ultimate objective of producing a pavement that has sufficient load bearing capacity for the traffic, is resistant to deformation, and has a long service life. With budgets for road maintenance under constant review the pavement lifetime is under increasing

scrutiny and in particular its ability to resist the modes of permanent damage such cracking and fatigue failure as seen in Figure 1-1.

Figure 1-1: Typical cracking observed in an asphaltic surface

The typical asphalt failure mechanisms of rutting, cracking, and long term fatigue durability have been practically addressed by improvements in mixture design and the addition of polymers to the bitumen to produce polymer modified bitumens (PmBs). In the USA the Strategic Highway Research Program (SHRP) led to the implementation of the Superpave (SUperior PERforming Asphalt PAVEments) system (Kennedy et al. 1994) for binder specification and asphalt design which further increased the use of polymer additives to increase the Performance Grade (PG) range of their binders. The use of PmBs in asphalt to resist deformation, i.e. rutting, is relatively well established (Valkering et al. 1990) but their use to improve fatigue life is less well defined even though in practice they have often been used with this purpose in mind (Delorme, de la Roche and Wendling 2007). However, there remains

a need to develop laboratory tests which can determine the fundamental properties of the modified asphalt, and hence provide a sound engineering basis for the specification of PmBs.

At a national United Kingdom level the 2015 “ALARM” survey (Asphalt Industry Alliance 2015) estimates that there exists a 13-year backlog of carriageway maintenance works in England and a shortfall of £12 billion in funding to achieve this. Under these financial pressures it is clearly not straightforward for a highways engineer to justify the additional up-front costs incurred by specifying polymer modified bitumen over penetration grade bitumen in their asphalts. However, if clear and practical testing methodologies can be developed, and the results quantified, then a longer life pavement construction can be achieved. Furthermore, as new road construction in the major emerging economies such as Brazil, Russia, India and China continues apace it is crucial that the pavement is constructed to the highest possible standards in the first instance to ensure long lasting highway networks.

1.1 Research Scope

This research is focussed on the study of PmBs and asphalt using the latest theoretical and modelling approaches, with particular emphasis on the cracking and fatigue behaviour of the materials. The programme of work is organised to validate existing models, and also to extend them to more completely incorporate the effects of polymer modification. The research aims to develop testing protocols which reduces both the time and material required to determine the fundamental properties of asphaltic materials.

The non-linear viscoelastic behaviour of bitumen and asphalt creates a highly challenging material to analyse. With the inclusion of PmBs in asphalt this analysis is further complicated due to the potential for recovery and healing of the material. The Superpave research programme provided the first widely recognised bitumen test indicator for fatigue cracking based on bitumen rheology (Anderson and Kennedy 1993). However, experience since then has shown that, especially for PmB, this is a

relatively poor indicator of on-site behaviour (Deacon et al. 1997, Tsai and Monismith 2001). Over the past two decades further studies have taken place to find alternative bitumen rheological parameters relating to asphalt fatigue performance with mixed degrees of success (Bahia et al. 2001, Cho et al. 2009). However, as bitumen is the adhesive material in the asphalt mix it appears clear that some relationship should exist between the properties of the bitumen and that of the asphalt.

The majority of state of the art research on asphalt fatigue has been undertaken using unmodified binders as the focus has been on developing the initial theory and models (Kutay, Gibson and Youtcheff 2008, Huang et al. 2007, Masad et al. 2008a, Underwood, Kim and Guddati 2006). By further analysing polymer modified mixtures not only will the existing models be tested, but extensions to them may be developed which can account for their enhanced performance characteristics.

A Paris-law approach is often taken as a first step in the modelling of fatigue cracking behaviour of asphalt, but this elastic model is unable to describe the true properties of the material due to asphalt's non-linear viscoelastic characteristics. Schapery's theoretical work (Schapery 1984) provided the basis for much of the fundamental research of the last 25 years by showing how the continuum damage mechanics problem could be simplified through the use of pseudo variables and the J-integral. Using this approach the energy dissipated in creating damage within the material may be separated into the linear and nonlinear viscoelastic responses (Daniel, Bisirri and Kim 2004, Masad et al. 2008b) allowing the fundamental material characteristics to be more clearly evaluated. Additionally, significant reductions in testing time may be achieved using this method by relating tests at high stresses and strains to performance at lower levels.

Many different testing geometries and procedures are used in the asphalt industry including 2, 3 and 4-point bending, indirect tensile fatigue, and uniaxial push-pull testing. This results in a significant degree of confusion for both specifiers and industrial practitioners as the results cannot easily be translated between the

different methods. Therefore, improved asphalt fatigue testing and analysis techniques would be of considerable benefit to industry. Furthermore, utilising standard bitumen testing equipment to determine asphalt properties would lead to significant savings in testing and analysis time and materials. Laboratory equipment for the rheological measurement of bitumen is now routinely available, and in recent years the torque capabilities of the modern devices has increased to such an extent that not only are they capable of measuring the viscoelastic properties of bitumen, damaging levels of strain are possible even in relatively stiff materials such as asphalt. A novel technique using such a device will be explored for small volume samples of full asphalt mixes.

1.2 Thesis Organisation

1.2.1 Chapter 2 : POLYMER MODIFIED BINDER MANUFACTURE AND CHARATERISATION

This chapter details the selection and manufacturing steps of the binders tested in this study. The binders produced were then analysed using a wide range of techniques from traditional empirical tests, to analytical and rheological analysis.

1.2.2 Chapter 3 : SMALL ASPHALT SPECIMEN SIZE METHODOLOGY

In this chapter a novel use of a dynamic shear rheometer and small sized specimens was developed to allow testing of dynamic properties of asphalt. The technique was validated by comparing the data produced to that from other testing geometries with the asphalt rheology modelled with a springpot model as well as traditional spring and dashpot models.

1.2.3 Chapter 4 : ASPHALT FRACTURE AND CRACK PROPAGATION

The measurement of asphalt fracture properties and crack propagation was explored within this chapter. The semi-circular bending (SCB) geometry was used to determine the fundamental material properties of fracture toughness and strain

energy release rates. Linear and non-linear models of crack propagation were explored, and the impact of polymer modification determined.

1.2.4 Chapter 5 : EXTENDED FINITE ELEMENT MODELLING

This chapter utilised the laboratory data generated in previous chapters to develop a finite element model capable of depicting the crack propagation in a monotonically loaded SCB specimen. The extended finite element technique was then used to allow realistic crack propagation to be modelled.

1.2.5 Chapter 6 : BITUMEN-AGGREGATE BOND STRENGTH MEASUREMENTS

The surface energy characteristics of the bitumen and aggregates used to manufacture the asphalt in previous chapters were explored in this chapter. The theoretical work of adhesion between the bitumen and aggregate was determined and techniques developed to determine the practical work of adhesion at high strain rates.

1.2.6 Chapter 7 : CONTINUUM DAMAGE MECHANICS ANALYSIS OF BITUMEN AND ASPHALT FATIGUE

In this chapter Viscoelastic Continuum Damage theory was applied to fatigue testing of bitumen using a rheometer and to asphalt using a number of different test geometries. The performance differences between unmodified and polymer modified materials were validated and the significant reductions in overall test time achieved using this theory demonstrated.

1.2.7 Chapter 8 : CONCLUSIONS AND RECOMMENDATIONS

This chapter summarises the findings of the research project and suggests further areas to be investigated.

2 POLYMER MODIFIED BINDER MANUFACTURE AND CHARATERISATION[†]

2.1 Introduction

In this chapter unmodified and PmBs were both assessed to quantify their properties and the improvements in performance of PmBs relative to the unmodified binders. Two options were available for the choice of PmBs to be used in this research. The first option was to obtain commercially available PmBs from the UK and/or Europe. This would have the advantage of the PmBs being ready-made and their suitability in asphalt already practically demonstrated in full scale pavement constructions. However, the significant disadvantage with this approach would be that the binders become 'black boxes' with limited or no information available regarding their base bitumen origin or polymer composition.

The second option, therefore, was to obtain penetration grade bitumen and produce the PmBs to known formulations. This would then allow comparisons to be made between known crude origins, polymer type, and polymer content. The disadvantage, of course, would be the extra work required to prepare the PmBs. However, it was felt that the advantages outweighed the disadvantages and also that

---

[†] This chapter includes results originally published in Lancaster I.M., and H. Al-Khalid, (2012) "Attenuated total reflection Fourier transform infrared spectroscopy of polymer modified bitumen" Journal of the Institute of Asphalt Technology, Issue 53,pp. 10-15, and Lancaster I.M. and H. Al-Khalid, (2012) "A rapid quantitative determination of polymer modified bitumen storage stability by FTIR" In: Tyrer M., Blacker A. and Bensted J. eds. Young Researchers' Forum in Construction Materials Society of Chemical Industry pp. 101 – 104, reproduced by permission.

by having the complete knowledge of the PmB composition there may also be increased opportunities for binder analysis and modelling.

This chapter, therefore, presents the detailed composition and analysis of the binders produced and utilised throughout this research.

2.2 Materials

Bitumen may be obtained from a wide variety of crude oil sources, although not all are suitable for use in paving applications. Within the European Union the prevailing standard for the specification of penetration grade bitumen is EN12591 (BSI 2009), and compliance with this standard is mandatory under the Construction Products Regulations for the application of CE-marking.

In this research bitumen was obtained from three different crude origins which are typically used within the EU, namely Venezuelan, Russian, and Middle Eastern. A 50/70 grade was chosen as the base binder for this research as this is a typical penetration grade that would be used throughout large parts of Europe. A 30/45 Venezuelan bitumen was also obtained as a comparative harder grade. The empirical testing mandated by EN12591:2009 of Needle Penetration (Pen), Softening Point (SP), and resistance to short term ageing via the Rolling Thin Film Oven Test (RTFOT), as shown in Figure 2-1, were performed on the binders and reported in Table 2-1, with estimated errors in the results included based on the repeatability values stated in the EN methods.

The temperature susceptibility bitumen may be determined by measuring viscosity over a range of temperatures, but this is practically inconvenient. Pfeiffer and Van Doormaal (1936) showed that temperature and the log of Pen were directly proportional to each other, and also that the SP corresponded to a Pen of 800 dmm. From this they developed a general equation to describe temperature susceptibility known as the Penetration Index (PI)

$$PI = \frac{1952 - 500\log(penentration) - 20SP}{50\log(penetration) - SP - 120}$$ **Equation 2-1**

Typical paving grade bitumen have a PI in the range -1.5 to +0.7. More highly temperature susceptible bitumens have a more negative PI, and less temperature susceptible bitumen such as oxidised and blown bitumens have more positive PI values.

Figure 2-1 : Short term ageing in the Rolling Thin Film Oven Test

	30/45 Venezuelan	50/70 Venezuelan	50/70 Russian	50/70 Middle Eastern
Penetration at 25°C (100g, 5s)	35 dmm (± 2 dmm)	61 dmm (± 2 dmm)	56 dmm (± 2 dmm)	61 dmm (± 2 dmm)
Softening Point	55.0 °C (± 1.0 °C)	50.4 °C (± 1.0 °C)	50.8 °C (± 1.0 °C)	52.2 °C (± 1.0 °C)
Penetration Index	-0.82 (± 0.3)	-0.63 (± 0.3)	-0.74 (± 0.3)	-0.18 (± 0.3)
After resistance to hardening at 163°C				
Retained Penetration	74% (± 7%)	64% (± 7%)	54% (± 7%)	59% (± 7%)
Increase in Softening Point	5.8 °C (± 1.5 °C)	4.2 °C (± 1.5 °C)	7.8 °C (± 1.5 °C)	6.5°C (± 1.5 °C)
Change in mass	- 0.21% (± 0.15%)	-0.38% (± 0.15%)	-0.23% (± 0.15%)	-0.16% (± 0.15%)

Table 2-1: Empirical properties of the base penetration grade bitumens

2.3 Polymer Modified Bitumen Production

PmBs are typically used in practical situations to enhance the performance of asphalt. Typical classes of polymer employed in the manufacture of PmBs include EVA (Ethylene Vinyl Acetate), SEBS (Styrene Ethylene Butadiene Styrene), EBA (Ethylene Butyl Acetate), SBR (Styrene Butadiene Rubber), and SBS (Styrene-Butadiene-Styrene). Whilst it is difficult, for commercial confidentiality reasons, to obtain accurate figures it is generally accepted that the most common type of modifier currently used in the production of PmBs is SBS.

SBS is a block copolymer comprising of two end blocks of polystyrene and a central block of polybutadiene as shown in Figure 2-2, with “a” repeating units of styrene in the initial polystyrene block, “b” repeating units of butadiene in the middle

polybutadiene block, and “c” repeating units of styrene in the final polystyrene block. Polystyrene is a tough durable polymer with a glass transition temperature (Tg) of approximately +100°C whereas polybutadiene is a rubbery polymer with Tg typically less than -90°C. It is the combination of these two polymer’s properties of low temperature polybutadiene flexibility and high service temperature polystyrene rigidity that makes the use of SBS in bitumen modification so prevalent. The styrene groups have a tendency to self-associate which are then attached to one another by the polybutadiene chains. During bitumen modification the SBS absorbs the oily components from the bitumen and swells in size, but the SBS network is retained leading to the modified binder having an increased elastic behaviour at elevated temperatures and reduced brittle behaviour at lower temperatures.

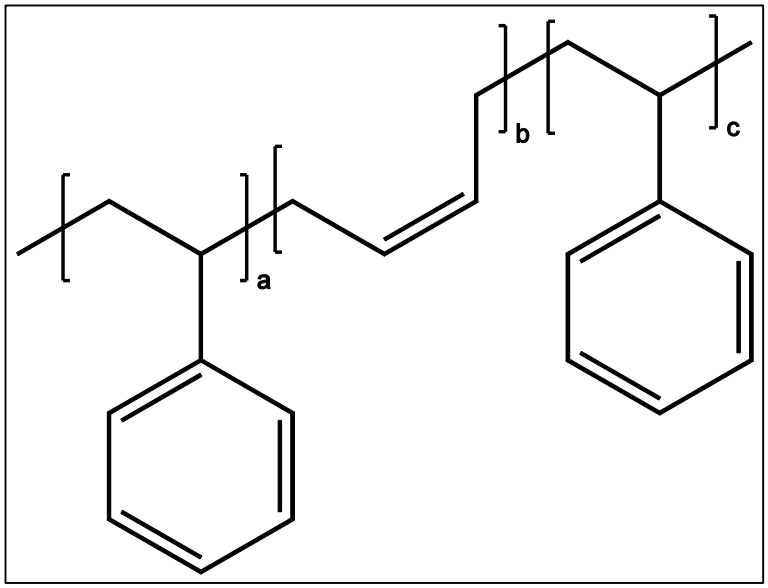

Figure 2-2: Schematic of Styrene-Butadiene-Styrene Block Copolymer

To have the most relevance to current practice this research was conducted using a widely used commodity grade of SBS, namely Kraton 1101. Kraton 1101 is a linear SBS with physical properties supplied by Kraton Polymers as shown in Table 2-2.

Property	Test method	Units	Typical Value
Bound styrene	Kraton Method 03	% mass	31
Volatile matter	Kraton Method 04	% mass	0.3
Total extractables	Kraton Method 05	% mass	1.0
Solution viscosity (measured 25% mass solution in toluene at 25°C)	Kraton Method 06	Pa.s	4.0
Antioxidant content	Kraton Method 08	% mass	>= 0.14
Melt flow rate 200°C/5kg	ISO 1133	g/10 min	<1
Specific gravity	ISO 2781	Mg/m^3	0.94
Hardness Shore A, 30s	ISO 868		69
Tensile strength	ISO 37	MPa	33
300% Modulus	ISO 37	MPa	2.9
Elongation at break	ISO 37	%	880

Table 2-2 : Kraton 1101 typical properties

To produce the PmB the bitumen was heated to 180°C before incorporating the SBS using a high shear mixer, as shown in Figure 2-3, with high shear processing continuing for 2 hours at 6000 rpm. Whilst thermal oxidation of the bitumen and degradation of the SBS will occur after extended periods Linde and Johansson (1992) demonstrated that even at 200°C after 3 hours the degree of polymer degradation was small.

The polymer addition levels were chosen to reflect those understood to be currently used in practical pavement constructions. The completed binder was then removed from the reaction vessel, partitioned into 500g containers and allowed to cool to room temperature to avoid repeatedly reheating one large bulk sample during subsequent testing.

Figure 2-3: Laboratory high shear mixer for the preparation of polymer modified binders

2.4 Empirical Binder Analysis

The same industry standard empirical tests were carried out on the PmBs as for the base bitumens with the results presented in Table 2-3, with the estimated errors in the results included based on the repeatability values stated in the EN methods.

	50/70 Venezuelan	50/70 Venezuelan	50/70 Venezuelan	50/70 Russian	50/70 Middle Eastern
Polymer Content (By weight)	2.5%	5.0%	7.5%	5.0%	5.0%
Penetration at 25°C (100g, 5s)	46 dmm (± 2 dmm)	42 dmm (± 2 dmm)	31 dmm (± 2 dmm)	31 dmm (± 2 dmm)	40 dmm (± 2 dmm)
Softening Point	56.4°C (± 1.5°C)	84.0°C (± 1.5°C)	87.8°C (± 1.5°C)	84.5°C (± 1.5°C)	77.6°C (± 1.5°C)
Penetration Index	0.08 (± 0.3)	4.39 (± 0.3)	4.13 (± 0.3)	3.72 (± 0.3)	3.41 (± 0.3)
After resistance to hardening at 163°C					
Retained Penetration	65% (± 7%)	76% (± 7%)	84% (± 7%)	84% (± 7%)	74% (± 7%)
Increase in Softening Point	9.8°C (± 3.0°C)	-8.9°C (± 3.0°C)	-6.8°C (± 3.0°C)	-9.6°C (± 3.0°C)	8.8°C (± 3.0°C)
Change in mass	-0.36% (± 0.15%)	-0.30% (± 0.15%)	-0.28% (± 0.15%)	-0.18% (± 0.15%)	-0.02% (± 0.15%)

Table 2-3 : Empirical binder test results

The SP increased with polymer content leading to a large rise in SP at higher polymer contents. In addition to the binders that were to be used in later chapters for the production of asphalt, further SBS content PmBs were produced to generate a more complete 'S-curve' for the 50/70 Venezuelan bitumen as shown in Figure 2-4. The large rise in SP can be seen to occur at approximately 4% polymer content, as after this point the polymer network becomes a continuous phase within the PmB.

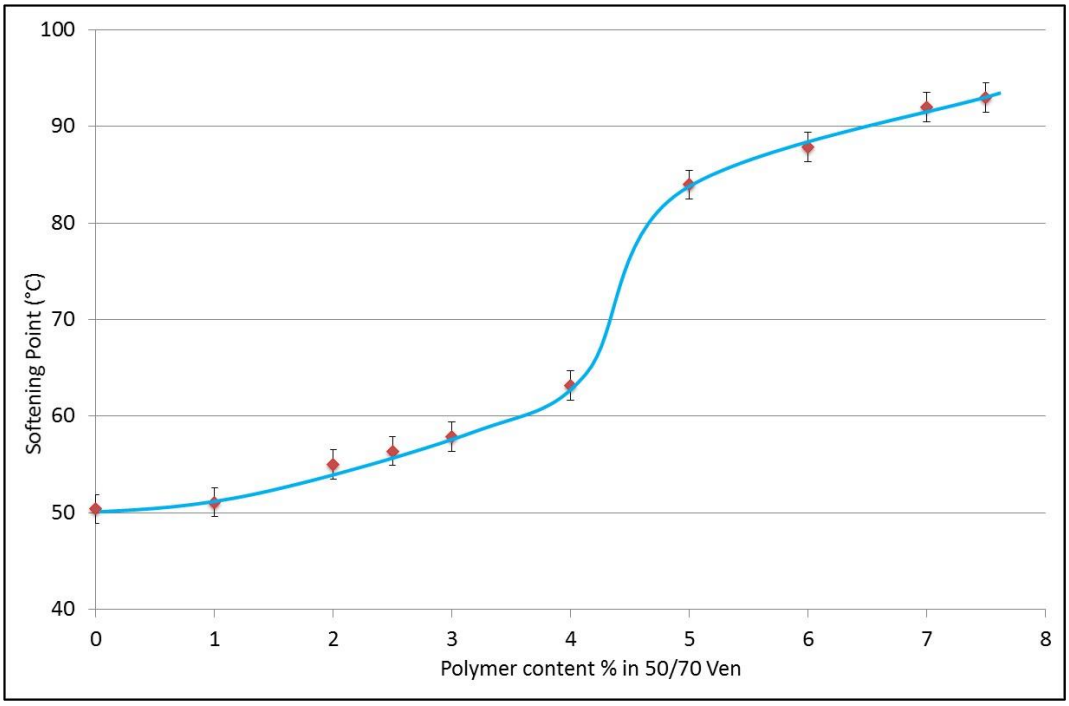

Figure 2-4 : Softening Point versus polymer content in 50/70 Venezuelan bitumen

The modified binders can also be seen to have a higher PI than the unmodified binders. Whilst the PI equation is based on a number of assumptions it does provide a general overview of performance and suggests that the PmBs have improved temperature susceptibility.

2.4.1 Dynamic viscosity profiles

The dynamic viscosity according to EN13302 (BSI 2010) of the binders was determined at 150°C and 180°C using a Brookfield rotational viscometer as reported in Table 2-4. At intermediate temperature bitumen exhibits non-Newtonian behaviour whilst at increasing temperatures it tends towards Newtonian flow although studies have shown that non-Newtonian behaviour is still present for PmB's (Yildirim, Solaimanian and Kennedy 2000). Therefore, as the purpose of these tests was to determine in service behaviour, a shear rate of 28 s^{-1} was used as an appropriate shear rate for pumping and mixing of the binders.

	Dynamic Viscosity at 150°C / Pa.s	Dynamic Viscosity at 180°C / Pa.s
50/70 Venezuelan	0.255 (± 5%)	0.088 (± 5%)
50/70 Venezuelan + 2.5% SBS	0.540 (± 5%)	0.175 (± 5%)
50/70 Venezuelan + 5.0% SBS	1.210 (± 5%)	0.385 (± 5%)
50/70 Venezuelan + 7.5% SBS	2.570 (± 5%)	0.780 (± 5%)
30/45 Venezuelan	0.385 (± 5%)	0.130 (± 5%)
50/70 Russian	0.200 (± 5%)	0.068 (± 5%)
50/70 Russian + 5.0% SBS	1.230 (± 5%)	0.380 (± 5%)
50/70 Middle Eastern	0.306 (± 5%)	0.103 (± 5%)
50/70 Middle Eastern + 5.0% SBS	1.320 (± 5%)	0.460 (± 5%)

Table 2-4 : Binder Brookfield viscosities

The penetration grade bitumens all display broadly similar viscosities, but as expected the increasing polymer content led to a large increase in the viscosity of the PmB. It is widely accepted that the optimum viscosity of a binder to achieve satisfactory coating in asphalt production is 0.2 Pa.s (Heukelom 1973), with this information used during asphalt production in later chapters.

The testing carried out thus far provides only an empirical assessment of the binder properties. For instance, the polymer grade used and the composition of the base binder both have an effect on the detailed shape of the curve in Figure 2-4, hence SP alone may only be used as a qualitative measure of the binder's polymer content. To obtain further fundamental properties of the binders, particularly the PmBs, additional analytical testing was carried out.

2.5 Fourier Transform Infra Red (FTIR) Spectroscopy analysis

Infra-red radiation in the region of 4000 – 400cm^{-1} is absorbed by chemical bonds producing vibrations which are characteristic of the molecule's structure. Beer's Law (or sometimes Beer-Lambert's Law) states that there is linear relationship between absorbance and concentration as given in Equation 2-2.

Absorbance (A) = Molar absorbtivity (ε) x Path length (l) x Concentration (c)

Equation 2-2

SBS and bitumen are both complex hydrocarbons and possess many of the same molecular bonds. However, in the fingerprint region (1500 - 400cm^{-1}) there are two absorbing bands which are found in SBS but not in bitumen which, whilst rather weak chromophores, are sufficiently strong enough to be used for identification and quantitative analysis purposes. These chromophores are shown in Figure 2-5 and are the C-H out-of-plane bending of trans-alkene (butadiene) at 966cm^{-1} and the C-H out-of-plane bending in monoalkylated aromatics (styrene) at 699cm^{-1}.

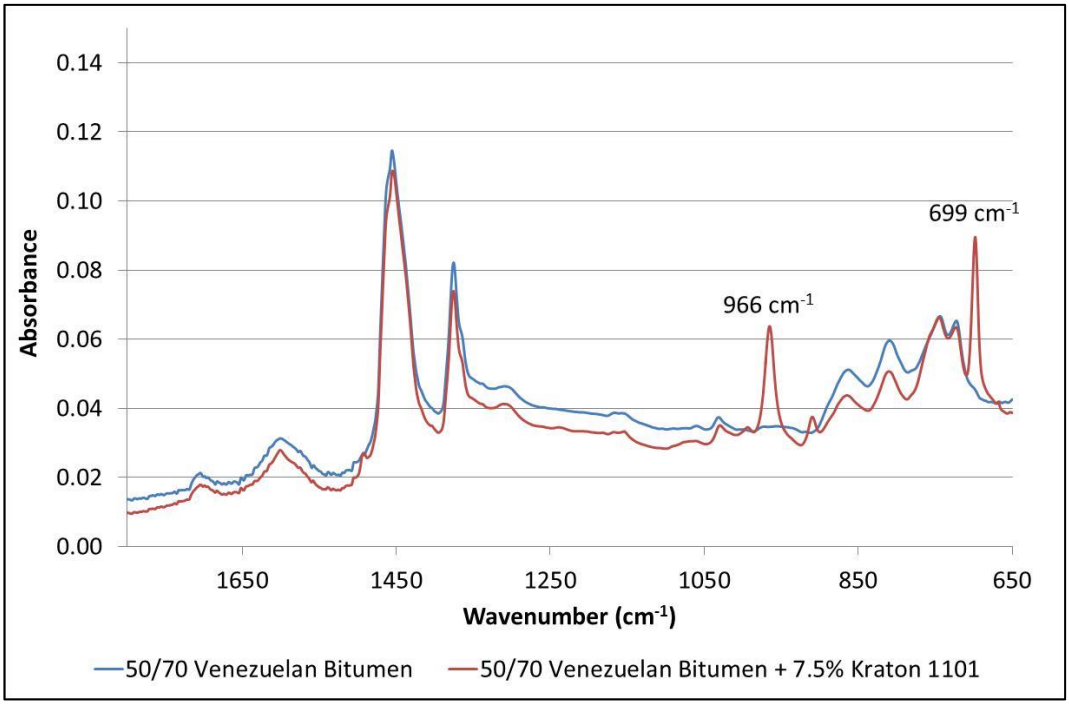

Figure 2-5 : FTIR Spectra of the fingerprint region of an unmodified, and SBS modified Venezuelan Bitumen, with the styrene and butadiene peaks highlighted

In a traditional transmission Infra-Red spectrometer the IR beam passes through the analysed sample to a detector. As bitumen is opaque in all but very thin films transmission IR analysis is very difficult to practically achieve. Bitumen may be analysed in transmission if it is first dissolved in an appropriate solvent, and previous studies (Lu, Isacsson and Ekblad 1999, Masson, Pelletier and Collins 2001, Zhang, Yu and Han 2011, Sun, Zhang and Zhang 2011) have successfully used this approach to determine the polymer content of PmBs in transmission. However, producing

samples in this way is not straightforward requiring considerable time and care to achieve reliable samples. Furthermore, cleaning is messy and time consuming, and, due to the presence of solvent, health, safety and environmental considerations must be made regarding its use and eventual disposal.

To analyse opaque materials the attenuated total reflection (ATR) method is more suitable (Yut and Zofka 2011) as shown schematically in Figure 2-6. In this method the sample to be analysed is placed in contact with the surface of the ATR crystal. The incident IR beam passes into the ATR crystal at an angle exceeding the critical angle, and when it reaches the surface of the crystal it penetrates 1 to 2 microns into the sample where the chemical bonds in the sample are excited. Depending on the size of the crystal the beam may then reflect within the crystal and back to the sample multiple times before finally being reflected back to a detector.

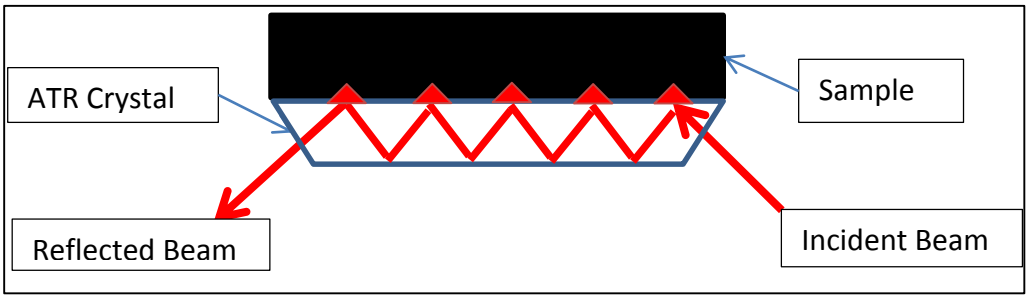

Figure 2-6: Schematic of a 5 bounce ATR

ATR crystals can be manufactured from a range of materials, and the choice depends on the type of sample to be analysed and the expected sample throughput. The most frequently encountered material is Zinc Selenide due to its comparatively low cost and good IR transmission properties. Large multiple reflection crystals are readily available but Zinc Selenide is rather soft and therefore can easily be scratched and permanently damaged during cleaning. Alternative ATR crystal materials include Germanium and Silicon, but the most robust choice is diamond. The potential to cause damage to the diamond during cleaning and use is low, and the sample size is very small as the single bounce diamond is only 2mm in diameter. Diamond does,

however, have poor IR transmission in the range 2300 to 1800 cm^{-1} which can limit its potential study targets. For the analysis of bitumen this does not present a problem as there are no bonds of interest in this range. The cost of a diamond cell is obviously higher than the alternatives, but prices have fallen and for single reflection systems are now within the budgets of most laboratories.

In order to establish the polymer content of an unknown sample, a value for the molar absorbtivity, ε, must be found from Beer's Law. Within the spectrometer, the path length, l, is fixed as the beam travels the same distance for each sample under test and is known by the spectrometer software from the geometry in use. Therefore, by measuring the absorbance at 699cm^{-1} and 966cm^{-1} of known polymer content PmBs the molar absorbtivity may be determined and subsequently used in the analysis of unknown polymer content binders.

Spectra for all the binders produced in section 2.3 were collected using 16 scans at a resolution of 4cm^{-1} over the full range 400 – 4000cm^{-1}. These were then analysed by software included with the spectrometer to determine ε.

2.5.1 Classical polymer storage stability testing

Whilst a wide range of polymers are used to produce modified binders, the majority only have limited compatibility with the base bitumen which can lead to separation of the phases (Kraus 1982). Numerous tests have been developed to determine the compatibility and storage stability of polymer modified binders, and in the UK the 'beer can test' was historically popular which, as the name suggests, filled a beer can sized container with modified binder. Since the introduction of the European framework specification for PmBs EN14023 (BSI 2010) methods have been standardised across Europe and the method in current use is EN13399 (BSI 2010) often referred to as the 'toothpaste tube test'.

In this method, modified binder is poured into an aluminium tube which is approximately 160mm high by 25mm diameter until it is about three quarters full.

The end of the tube is folded over to seal the tube to minimise binder oxidation. The tube is then placed vertically in an oven at 180°C for three days, although other temperatures may also be used. Whilst ensuring the tube remains vertical the tube is then removed from the oven and allowed to cool to ambient temperature. A heated knife is then used to divide the tube into three portions. The middle portion is discarded, with the top and bottom portions retained for analysis as shown in Figure 2-7. As the quantity of binder in each section is relatively small it is usually only possible to obtain a SP, although multiple tubes may be combined if additional tests such as Pen are required. The difference between the test results of the top and bottom portions is used as an indicator of storage stability with a difference in SP of less than 5°C taken as the limit for a storage stable binder. For SBS modified binders there is a tendency for the polymer to migrate to the top of the tube, which leads to an increase in SP relative to the bottom.

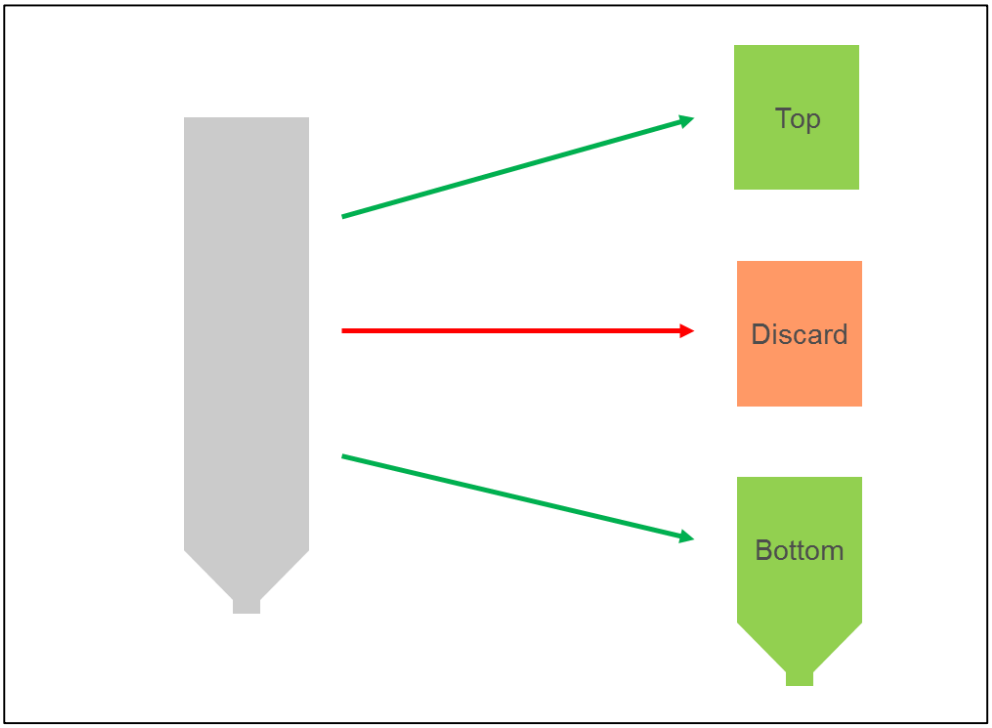

Figure 2-7 : Schematic of storage stability test

In this research no attempt was made to stabilise the modified binders during their production and as a result all the binders were found to be unstable as reported

in Figure 2-8. However, by not stabilising the binders the inherent differences in the polymer compatibility of each of the crude sources could be assessed. The Russian bitumen displayed the best polymer compatibility with the lowest difference in SP, and the Middle Eastern bitumen displaying the poorest compatibility with the highest difference in SP.

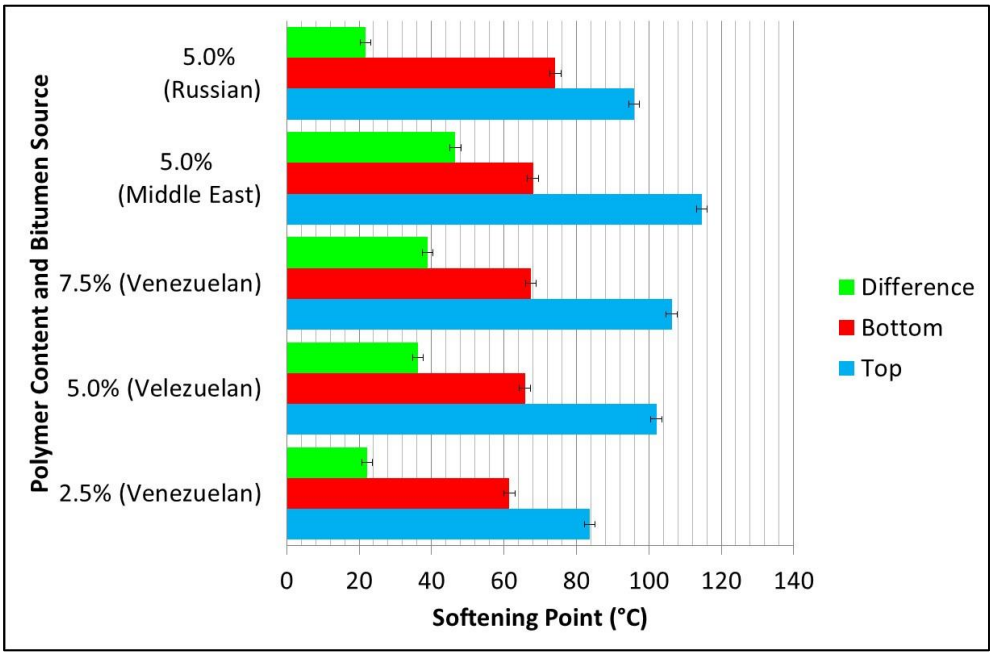

Figure 2-8 : Softening Point storage stability results

2.5.2 Methodology for FTIR analysis of polymer modified bitumen storage stability

Once the sections had been heated for SP testing a heated glass rod was used to transfer a small quantity of binder, typically less than 0.1g, to the diamond ATR cell, and the binder's spectrum recorded. To record the spectrum and clean the ATR cell in preparation for subsequent tests was very simple due to the small sample size and robust nature of the diamond cell, with the entire operation complete in under five minutes. A SP test, by comparison, uses far more binder and, if preparation, testing, and cleaning are considered, may take up to an hour to complete.

Once the top and bottom sections from all the binders had been tested, the polymer concentration was determined using Beer's Law and the results presented in Figure 2-9. As observed in the empirical SP testing earlier, the different bitumen origins show clear differences in storage stability results with the Russian bitumen again having the best compatibility.

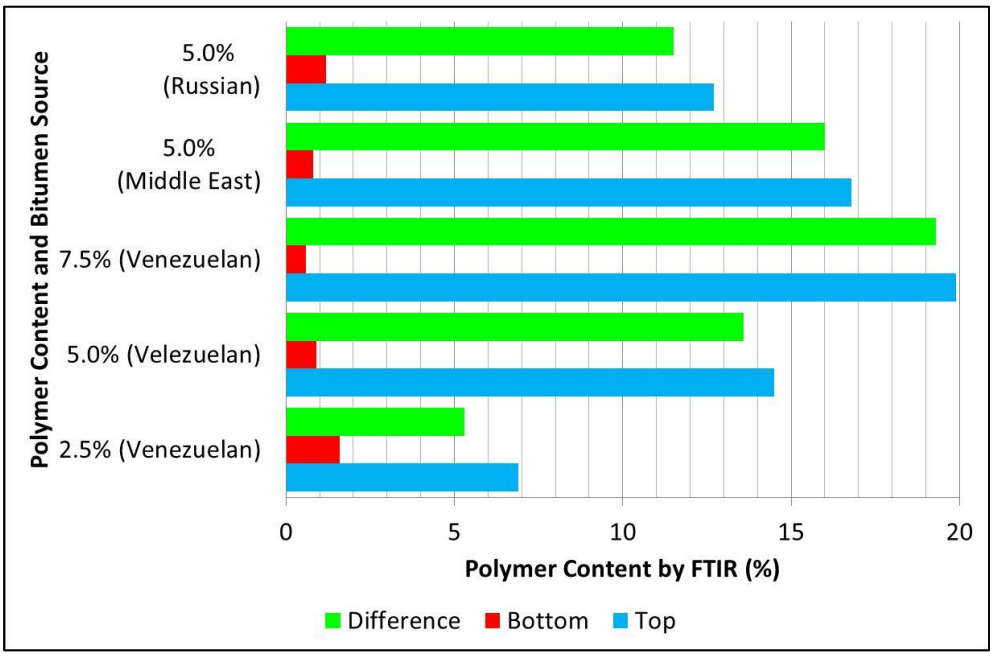

Figure 2-9 : Quantitative polymer storage stability results by FTIR

2.6 Fluorescence microscopy

Ultraviolet (UV) fluorescence microscopy has been utilised by researchers to study the dispersion of polymers in bitumen (Soenen, Lu and Redelius 2008, Isacsson and Lu 1999). As bitumen has little or no UV fluorescence and polymers fluoresce strongly it is easy to visualise the dispersion of the polymer within the binder. In this research an Olympus BX41 microscope using a high pressure mercury arc lamp as the UV light source was used with the images digitally recorded on a PC using an attached Firewire camera at a magnification level of 50 times as shown in Figure 2-10. The image scale was calibrated using the graticule shown in Figure 2-11.

Figure 2-10 : Microscope with UV light source and digital camera attachment.

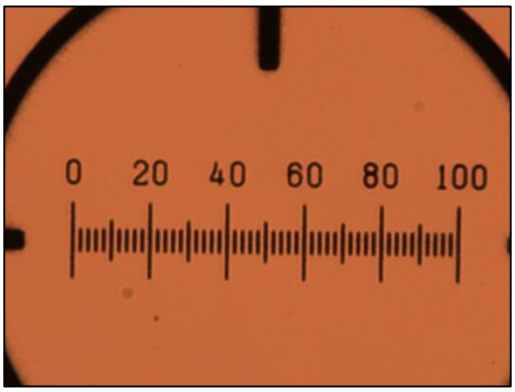

Figure 2-11 : 100 micron length calibration graticule at 50x

2.6.1 Polymer dispersion of Polymer Modified Binders

EN 13632 (BSI 2010) describes a method for producing specimens for visual analysis of polymer dispersion by creating fracture surfaces in the binder for subsequent microscopy. Whilst this method is valid it was found to be time consuming and the quality of the specimen variable, so in this research a simpler method was used. Each binder was heated to 180°C, stirred, and a heated glass rod

used to transfer a drop of the binder to a cold glass slide. Whilst the drop was still molten a cover slip was placed onto the hot binder and the binder allowed to cool to ambient producing a finished slide as shown in Figure 2-12. Due to the very small sample size this cooling occurs in a matter of a few seconds locking the polymer structure in place.

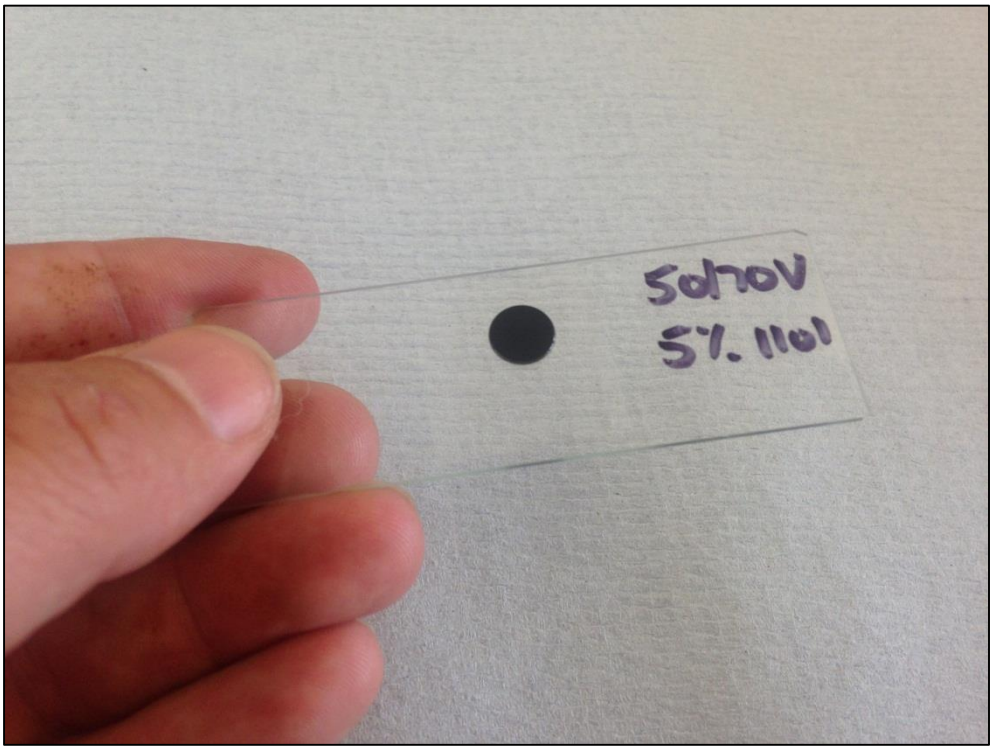

Figure 2-12 : Microscopy slide produced using the binder drop method

Micrographs were recorded of each of the PmBs before and after short term ageing (RTFOT) and are shown in Table 2-5.

	As Produced	After RTFOT
50/70 Venenzuelan + 2.5% Kraton 1101	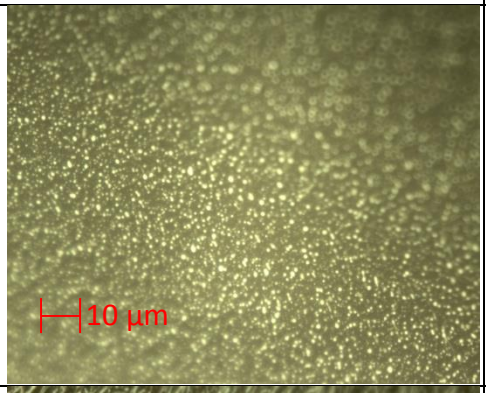	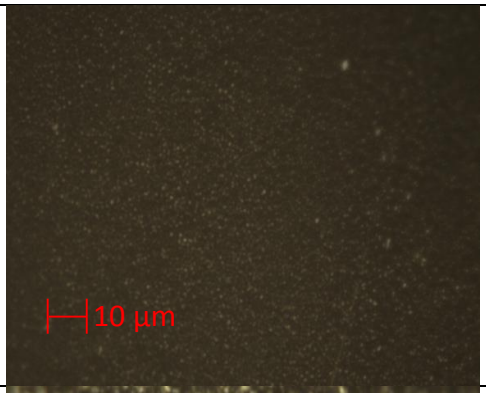
50/70 Venenzuelan + 5.0 % Kraton 1101	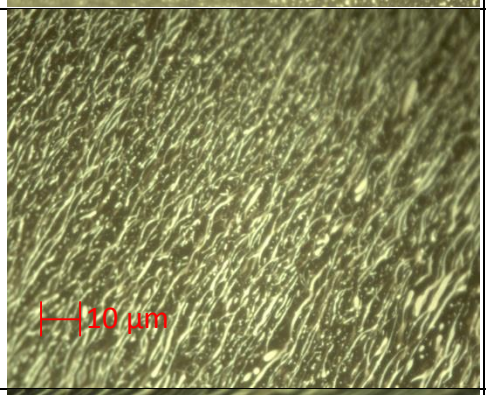	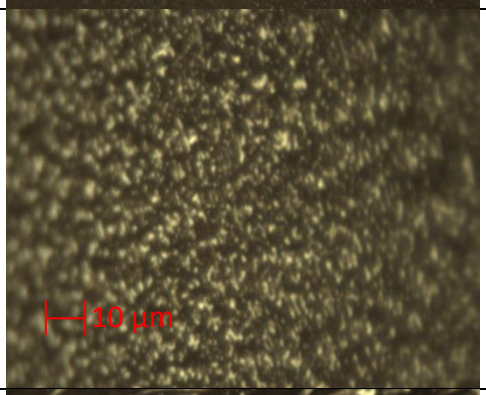
50/70 Venenzuelan + 7.5% Kraton 1101	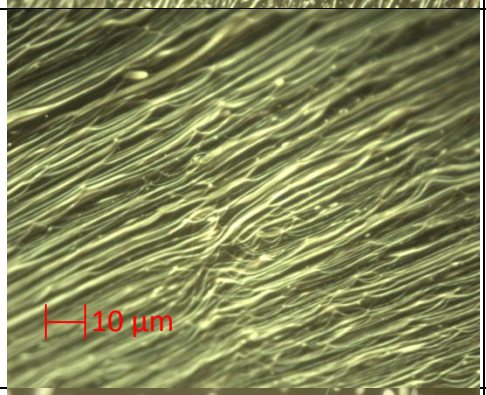	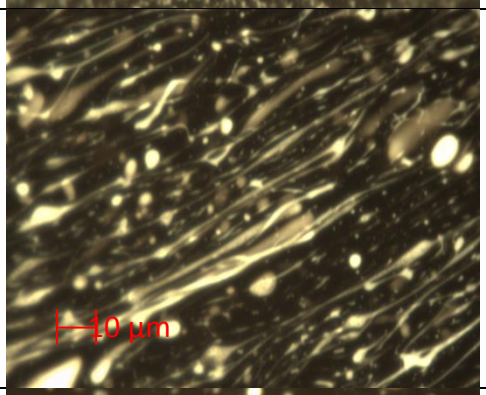
50/70 Middle Eastern + 5.0 % Kraton 1101	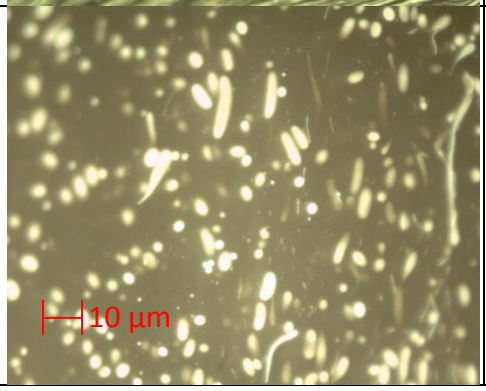	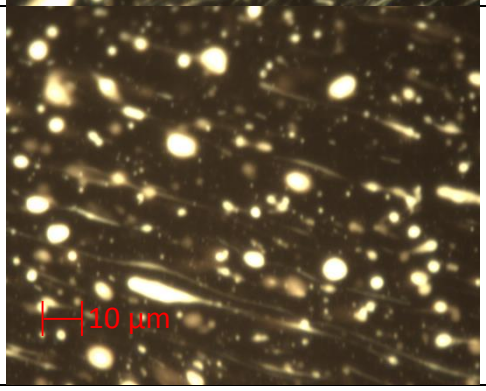

50/70 Russian + 5.0 % Kraton 1101	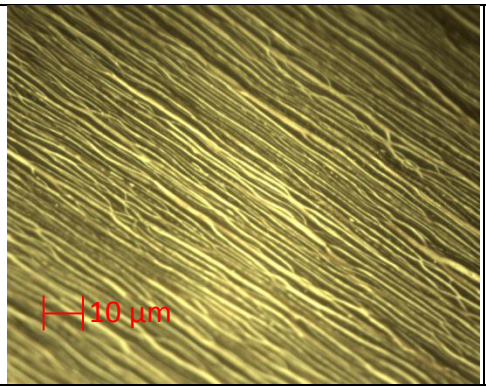	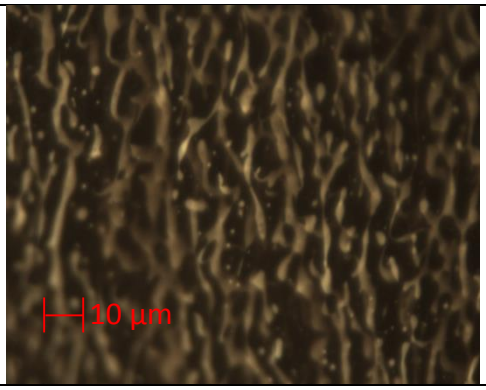

Table 2-5 : Micrographs of PmBs before and after RTFOT ageing

At 2.5% SBS in the Venezuelan bitumen the polymer forms discrete dispersed domains with a continuous bitumen phase. As the polymer content is increased to 5.0% SBS the polymer domains becomes almost continuous, with a limited number of isolated polymer rich areas. This correlates well with Figure 2-4 which suggested from SP measurements that above 4% the polymer would become the dominant within the PmB structure. At the highest polymer concentration of 7.5% SBS a continuous polymer network has now formed. Similar patterns are observed after short term ageing, although the structure is less well defined suggesting an element of separation of the polymer from the bitumen. After RTFOT the 5.0% SBS has far less structure than before RTFOT, whereas at 7.5% the continuous structure remains after RTFOT. This suggests that to maintain a continuous polymer network in an asphalt once it has been mixed and paved a higher polymer concentration is required than would be predicted by analysing only binders prior to RTFOT.

In the 5.0% SBS modified Middle Eastern bitumen large discrete polymer domains are observed, with high contrast between these and the background bitumen. This suggests relatively poor compatibility between the Middle Eastern bitumen and SBS. The Russian bitumen displays a different behaviour with a continuous polymer phase both before and after RTFOT, indicating improved polymer / bitumen compatibility. These observations are in agreement with the compatibility ranking found by classical and FTIR techniques in sections 2.5.1 and 2.5.2 respectively.

2.6.2 UV fluorescence assessment of storage stability

During the assessment of storage stability in 2.5.1 slides were also produced for UV microscopy, and these are shown in Table 2-6.

	Top Section	Bottom Section
50/70 Venenzuelan + 2.5% Kraton 1101	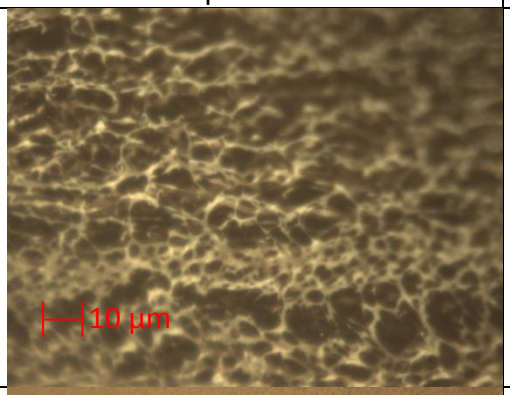	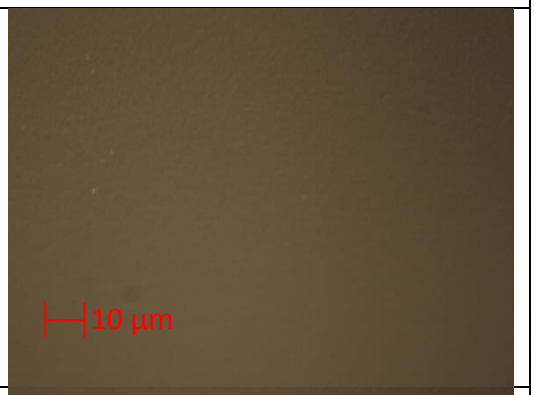
50/70 Venenzuelan + 5.0 % Kraton 1101		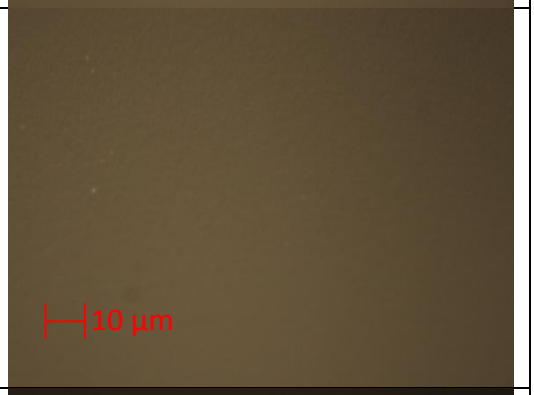
50/70 Venenzuelan + 7.5% Kraton 1101		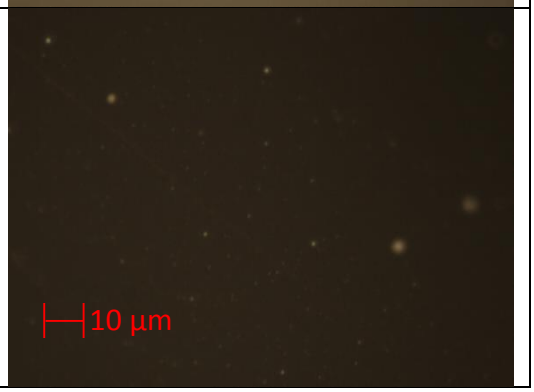

50/70 Middle Eastern + 5.0 % Kraton 1101	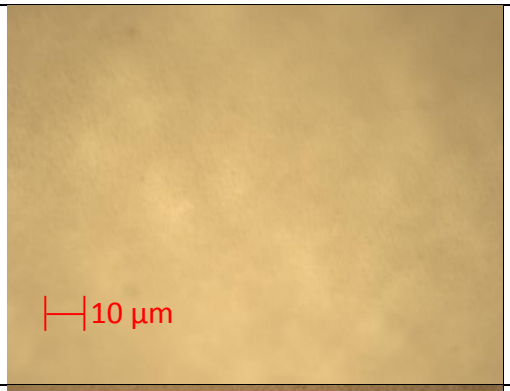	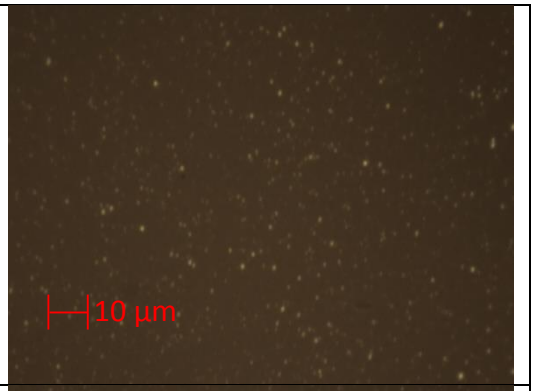
50/70 Russian + 5.0 % Kraton 1101	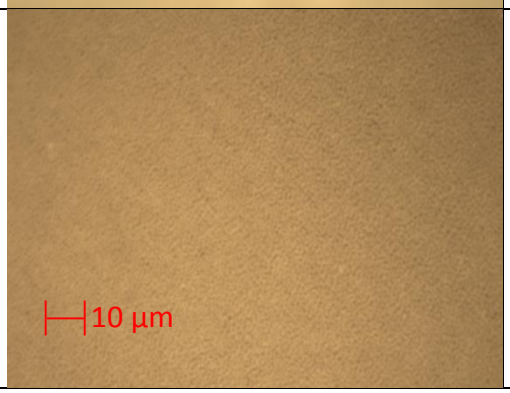	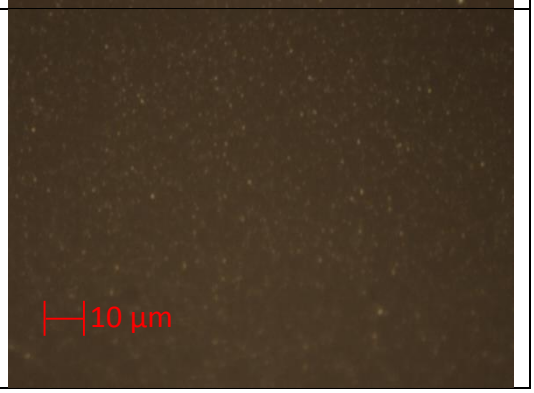

Table 2-6 : Micrographs of top and bottom sections of storage stability tubes

Due to the instability in the PmBs the majority of the samples show no structure at all in the top section which was shown by FTIR to be far in excess of 10% SBS. As a result of its overall lower polymer content the 50/70 Venezuelan with 2.5% SBS does show the structure of a continuous polymer network which is similar to that of the original sample of 50/70 Venezuelan with 7.5% SBS. This is also in agreement with the findings of the FTIR analysis.

However, as a result of the high level of instability in all these binders there is no more useful information that can be gained from UV analysis of the storage stability samples, and therefore this technique is better suited to the study of polymer dispersion in the original and short term aged binders.

2.7 Rheological characterisation

Rheology is the defined as the study of the flow behaviour of all types of matter, although in practice is it usually restricted to materials with properties intermediate to those of liquids and solids. Whilst material flow behaviour studies have been

undertaken for many centuries it was Bingham and Reiner who first coined the term rheology as part the formation of The Society of Rheology in 1929 with Heraclitus' quote "τα παντα ρει" or "everything flows" taken as the subject's motto.

Figure 2-13 considers the deformation behaviour of a cuboid of ideal material with a fixed base and a force applied to its top plane. If the material is purely elastic then it will deform according to Hooke's law of elastic deformation to a new position by a fixed displacement. Conversely for a viscous liquid then when the force is applied it will continue to deform at a constant velocity.

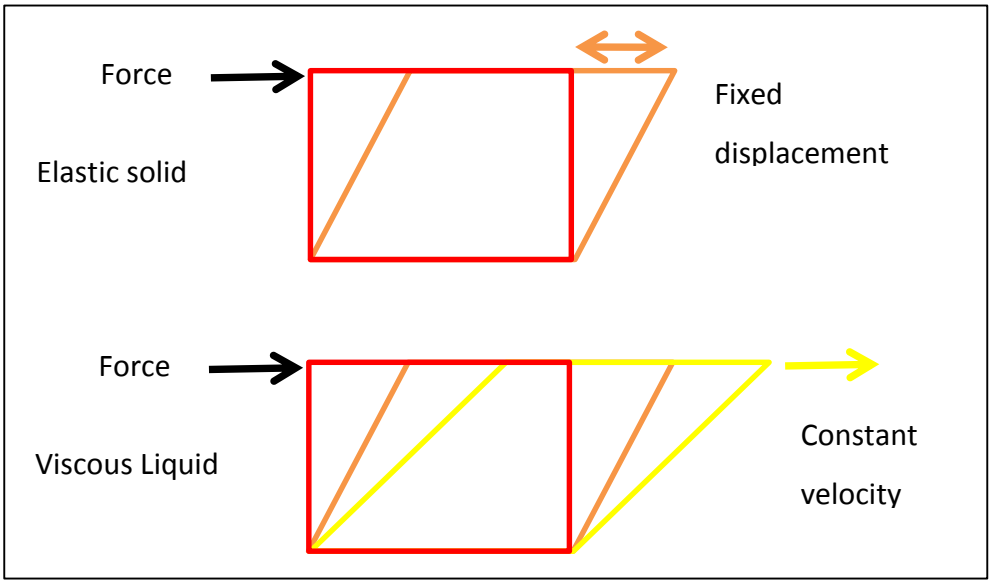

Figure 2-13 : Schematic of deformation behaviour of elastic and solid materials

In a dynamic mechanical test material behaviour may be determined by applying a sinusoidal varying stress, σ, to the specimen at a fixed amplitude and frequency. The resultant deformation, or shear strain γ, will also vary sinusoidally but lags behind the applied stress by the phase angle δ as shown in Figure 2-14.

.

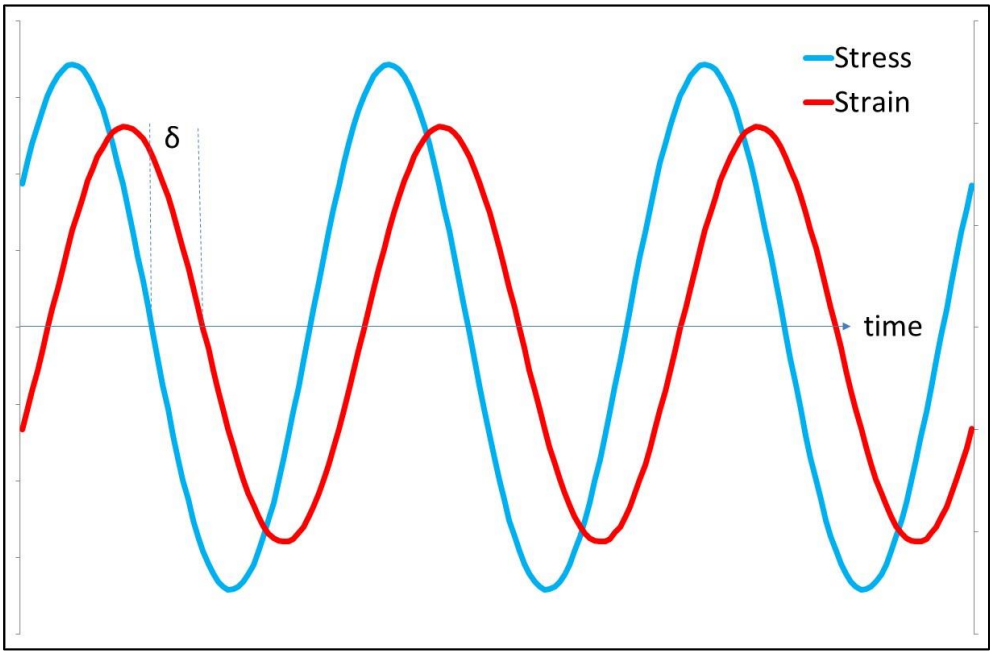

Figure 2-14 : Typical shear and stress waveforms in dynamic oscillatory test

For a perfectly elastic solid the phase angle would be equal to zero, whereas for a purely viscous liquid the phase angle would be 90°. Viscoelastic materials, such as bitumen and asphalt, exhibit phase angles between 0° and 90° with the value depending on the frequency, applied stress and temperature of the test.

For a test with strain amplitude γ_0 and stress amplitude σ_0 the sinusoidally varying strains and stresses are

$$\gamma = \gamma_0 \sin(\omega t) \qquad \textbf{Equation 2-3}$$

$$\sigma = \sigma_0 \sin(\omega t + \delta) \qquad \textbf{Equation 2-4}$$

where ω is the angular frequency in radians/second, and t is the time.

2.7.1 The Dynamic Shear Rheometer

Any device which measures flow is known as a rheometer. A Dynamic Shear Rheometer (DSR) applies a dynamic shear stress to the specimen to be analysed and records the resultant displacement. A modern DSR is a general purpose piece of

laboratory equipment which is routinely used to analyse a wide range of materials including foodstuffs, cosmetics, coatings, adhesives, and construction materials. It is a very versatile piece of equipment which may operate over a broad temperature range, typically -40°C to 150°C, and execute a wide range of test modes including simple viscometry, oscillation, creep, recovery, and stress relaxation. The Strategic Highways Research Program (SHRP) in the 1990's introduced the widespread use of DSRs to the analysis of bituminous binders. Whilst a DSR can accommodate many different test geometries the common practice for bitumen analysis is to use a parallel plate arrangement. As shown schematically in Figure 2-15, the specimen under test of radius r and height h is held between the two parallel plates. The bottom plate is fixed whilst the top plate is oscillated by applying a torque M. Within the rheometer the angular displacement, θ, is then recorded by an optical encoder system.

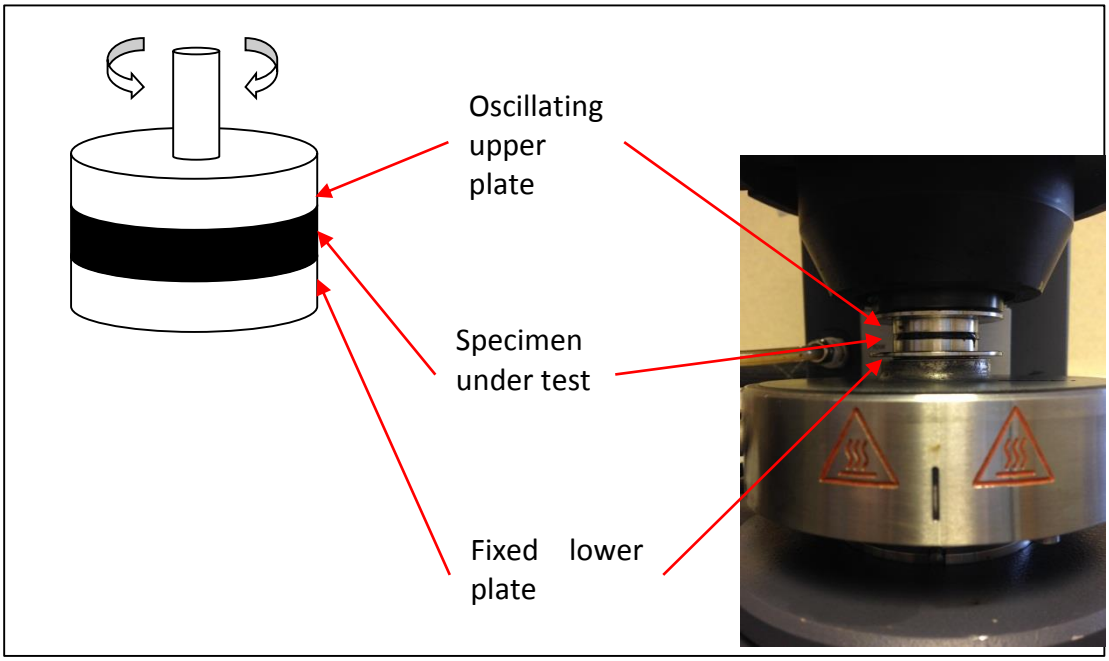

Figure 2-15 : Schematic representation of DSR specimens (left) and actual sample (right) under test

In an oscillatory test the complex shear modulus G*, storage modulus G' and loss modulus G'' may then be determined as

$$|G^*| = \sigma_0 / \gamma_0 \qquad \textbf{Equation 2-5}$$

$$G' = |G^*| \cos \delta \qquad \textbf{Equation 2-6}$$

$$G'' = |G^*| \sin \delta \qquad \textbf{Equation 2-7}$$

The two other commonly performed tests are creep and relaxation. In a creep test a fixed stress is applied to the specimen and the strain recorded over time to determine the creep compliance J(t) as

$$J(t) = \gamma(t) / \sigma_0 \qquad \textbf{Equation 2-8}$$

In a relaxation test an instantaneous strain is applied to the specimen and the stress recorded over time to determine the stress relaxation D(t) as

$$D(t) = \sigma(t) / \gamma_0 \qquad \textbf{Equation 2-9}$$

In the two decades since the initial implementation of the SHRP recommendations and widespread introduction of DSRs there has been a significant enhancement in rheometer performance. The specification of the TA 2000-ex used in this research is compared to a typical bitumen rheometer in use in the 1990s in Table 2-7 where the improvements in torque range and displacement resolution are particularly notable. Further improvements in frequency ranges and angular displacement resolution continue to be made by the rheometer manufacturers, but for increases in maximum torque a Dynamic Mechanical Analysis (DMA) instrument is required which is considerably costlier than a DSR and more readily suited to the analysis of solid samples.

	Typical post SHRP rheometer	TA 2000-ex
Torque Range	10 µNm – 10 mNm	0.1 µNm – 200 mNm
Frequency Range	1 x 10^{-5} to 100Hz	1.2 x 10^{-7} to 100 Hz
Angular Displacement Resolution	1 µ rad	40 n rad
Normal Force Range	n/a	0.005 to 50N

Table 2-7 : Typical post SHRP and AR 2000ex Rheometer Specifications

2.7.2 *Oscillatory frequency sweeps*

To characterise the binders oscillatory frequency sweep tests were performed from 0.1Hz to 10Hz at a strain level of 1% to ensure the bitumen remained within the linear viscoelastic range. The temperature was varied from 5°C to 80°C to capture the full behaviour of the binder in service. Over this temperature range the complex modulus varies from 10 Pa to over 10^8 Pa. Even for a modern DSR this wide range cannot be accurately captured using only one test geometry. To overcome this data is typically produced using a 25mm plate at high temperatures, and an 8mm plate at intermediate to low temperatures with a cross-over occurring at complex modulus of approximately 100,000 Pa. In practice, rather than relying on a fixed modulus to change plate geometries extra data with each plate diameter is generated and the datasets compared to find cross-over point. A plot of this data as complex modulus versus phase angle is commonly known as a 'black diagram' as shown in Figure 2-16 for the 50/70 Venezuelan binder with increasing SBS content.

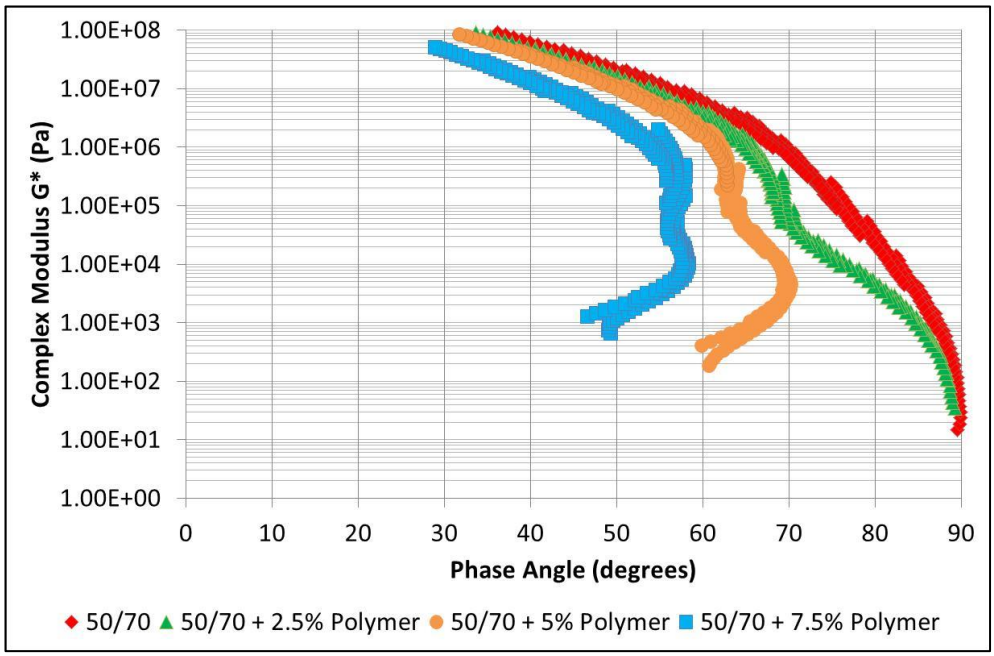

Figure 2-16: Rheological black diagrams of the unmodified and modified Venezuelan 50/70 binders

As can be seen the increasing SBS content leads primarily to a shift in the phase angle of the binder towards more elastic behaviour over a wider range of test temperatures.

2.7.3 Mastercurve generation

Whilst black diagrams offer a quick overview of a binders performance it is more meaningful to plot G* against frequency at a fixed temperature. However, as discussed earlier, there is an upper mechanical limit of 100Hz that the DSR can achieve whereas at very low frequencies, whilst testing is physically possible, each complete data point would take hours or even days to generate rendering this approach impractical.

As bitumen is a thermorheologically simple material its response to time and temperature are directly related. For instance, bitumen's response to loading at high temperature and short duration is equivalent to the response at a low temperature and long duration. It is therefore possible to employ the Time Temperature Superposition (TTS) principle to produce a so-called mastercurve of all the data at a specified temperature.

To create a mastercurve the complex modulus from the frequency sweep testing at each temperature is plotted as a function of frequency on a log-log chart. A reference temperature for the mastercurve is chosen and the data for this frequency sweep fixed. The frequency sweep data for the other temperatures is then shifted horizontally until a single smooth curve is created for all the data points. The amount of horizontal shift necessary for each curve is known as the time-temperature shift factor a(T). This shifting process may be performed manually by eye, by spreadsheet optimisation calculations, or more conveniently automatically using the software suppled with the rheometer.

Once the a(T) have been determined and the mastercurve created it is also possible to generate mastercurves at other temperatures. Typically the Williams-

Landel-Ferry (WLF) Equation 2-10 is used to determine the shift factors (Williams, Landel and Ferry 1955) for temperature ranges away from the glass transition temperature of the material.

$$\boldsymbol{Log\ a(T)} = \frac{-\boldsymbol{C_a(T-T_0)}}{\boldsymbol{C_b+(T-T_0)}} \qquad \textbf{Equation 2-10}$$

Where C_a is a dimensionless constant, C_b is a constant with units of Kelvin, T is the measurement temperature in Kelvin, and T_0 is the reference temperature in Kelvin.

As the glass transition of bitumen is typically of the order of minus 30°C, and bitumen only becomes a Newtonian fluid at very high temperatures, this WLF approach is appropriate for the generation of bitumen mastercurves.

Mastercurves of all the binders produced were generated at a reference temperature of 20°C as this was the temperature where the majority of the future asphalt testing was to take place. Figure 2-17 and Figure 2-18 show the effect of crude source of the bitumen behaviour. The 30/45V is stiffer across the full frequency range than any of the 50/70 bitumens tested which is as expected for the harder grade. The 50/70 Venezuelan, Middle Eastern, and Russian demonstrate broadly similar complex moduli. However, the phase angle of the 50/70 Venezuelan bitumen is noticeably higher than the other bitumens indicating a more viscous character.

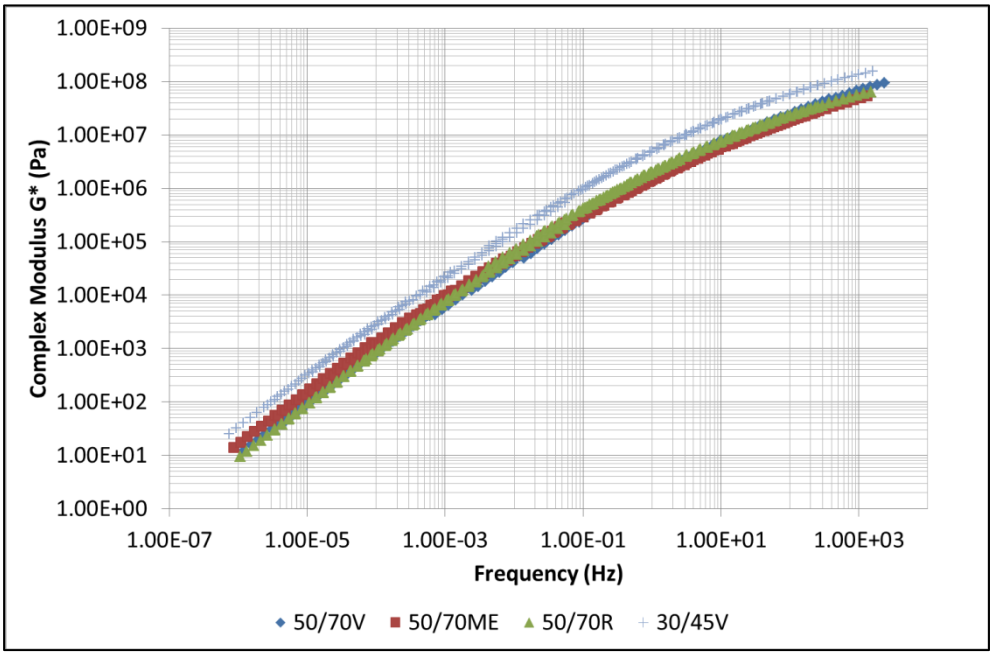

Figure 2-17 : Complex Modulus mastercurve at 20°C comparing unmodified binders

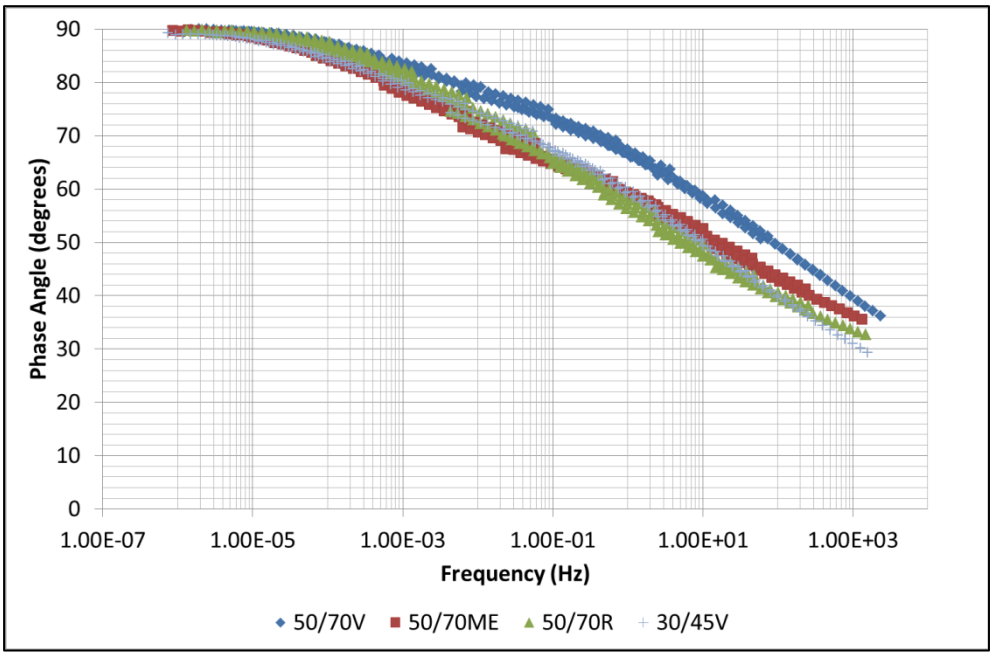

Figure 2-18 : Phase Angle mastercurve at 20°C comparing unmodified binders

Figure 2-19 and Figure 2-20 show the effect of increasing polymer modification levels. At low frequencies, corresponding to high temperatures, the complex modulus is increased by over an order of magnitude. Also, the phase angle is

significantly reduced, indicating a binder with more elastic characteristics. It is for these reasons that polymer modification is often used to mitigate rutting in pavements. At high frequencies the effects are less pronounced, but the PmBs can be seen to have a lower modulus and reduced phase angle than the base bitumen.

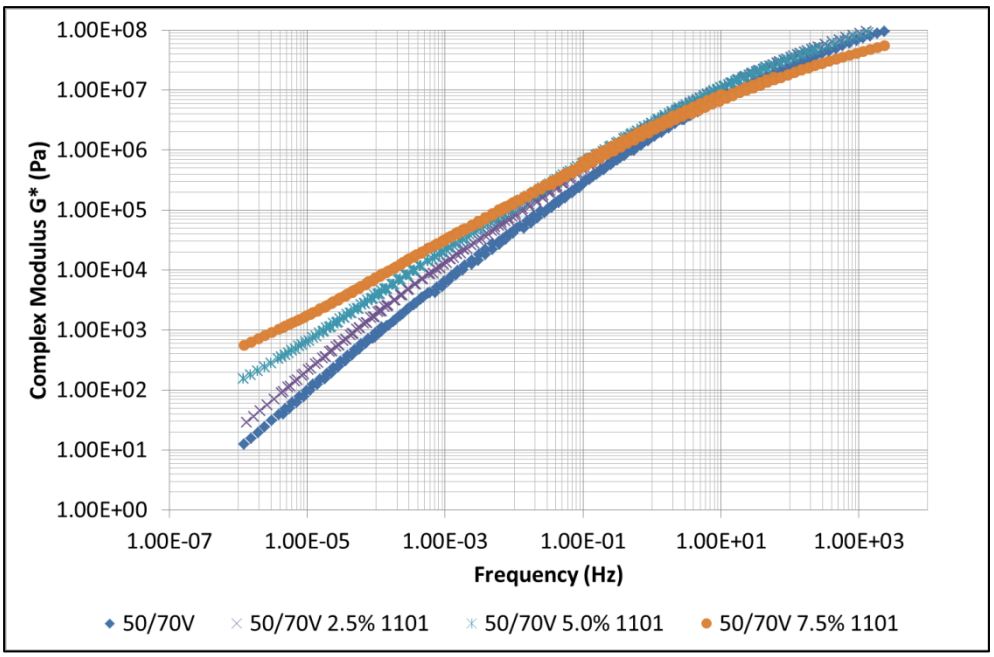

Figure 2-19 : Complex Modulus mastercurve at 20°C comparing polymer concentration levels

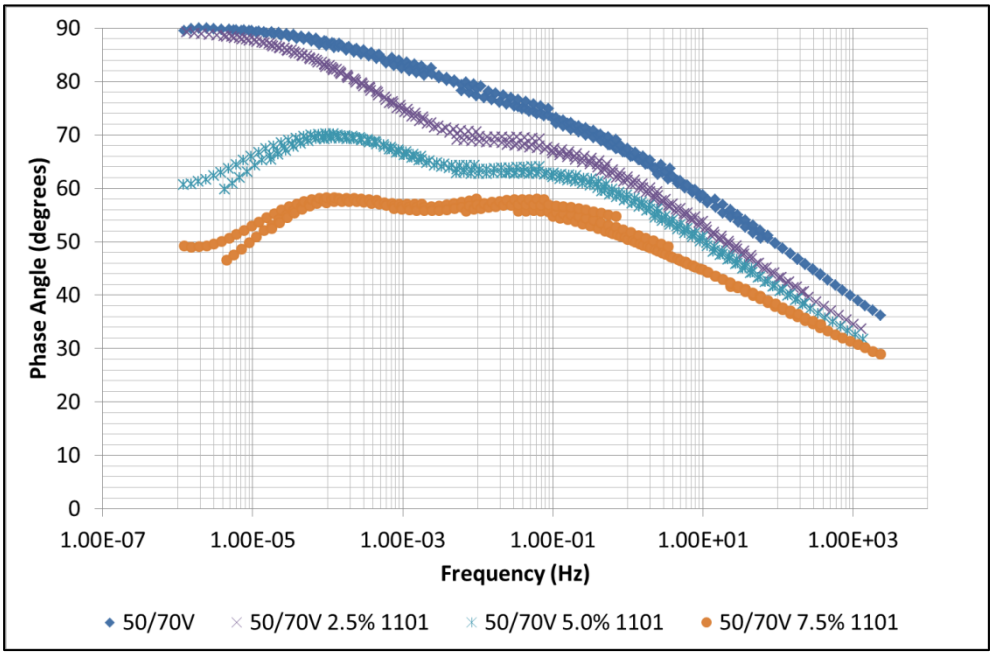

Figure 2-20 : Phase Angle mastercurve at 20°C comparing polymer concentration levels

Figure 2-21 and Figure 2-22 compare the effect of PmB base bitumen origin. The modified Russian bitumen has the highest modulus at low frequencies, so should have the best high temperature performance in service. The phase angles for all three PmBs are all similar with a good compromise between elastic and viscous performance across the full range of frequencies. This indicates that at high temperatures / low frequencies the binders will be able to resist rutting, and at low temperatures / high frequencies they will not become brittle and susceptible to cracking.

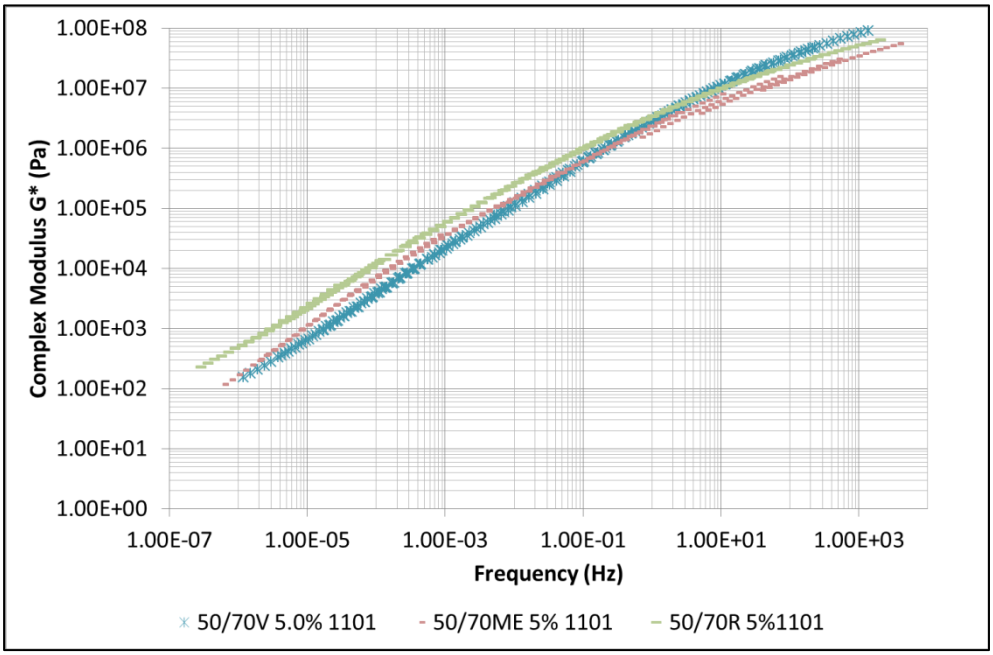

Figure 2-21 : Complex Modulus mastercurve at 20°C comparing bitumen origin effect on polymer modified binders

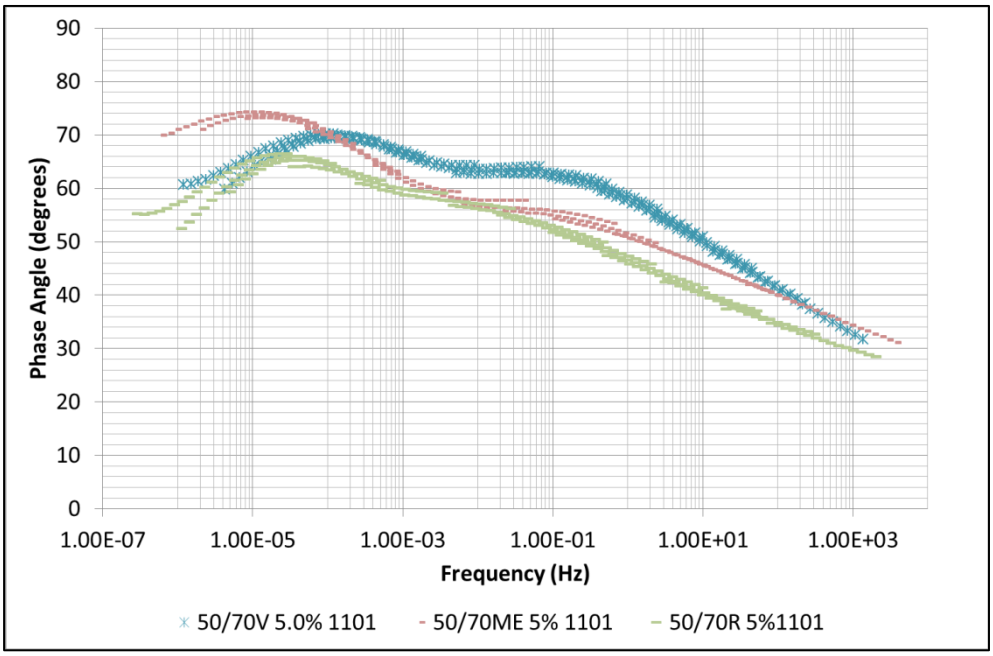

Figure 2-22 : Phase angle mastercurve at 20°C comparing bitumen origin effect on polymer modified binders

2.7.4 Effect of short term ageing (RTFOT)

The same frequency sweep tests were performed on the binders after short term ageing. Figure 2-23 and Figure 2-24 demonstrate that for a typical penetration grade bitumen the ageing leads to an increase in modulus across all frequencies. Similarly there is a drop in phase angle at low to intermediate temperatures, with purely viscous behaviour only occurring at very low frequencies corresponding to temperatures well above the binder's SP.

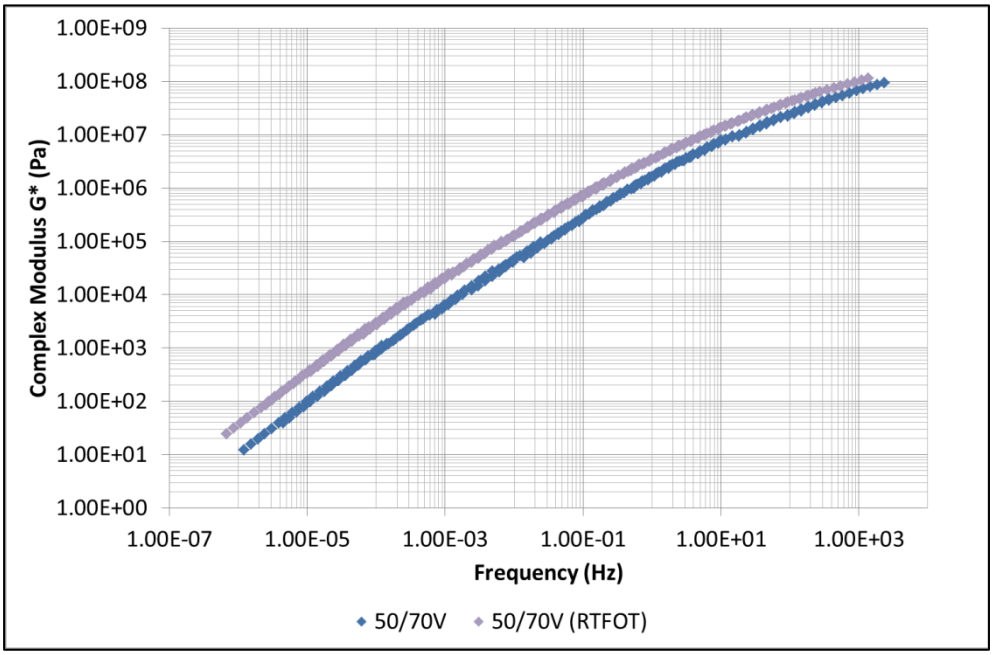

Figure 2-23 : Complex Modulus mastercurve at 20°C comparing 50/70V before and after RTFOT

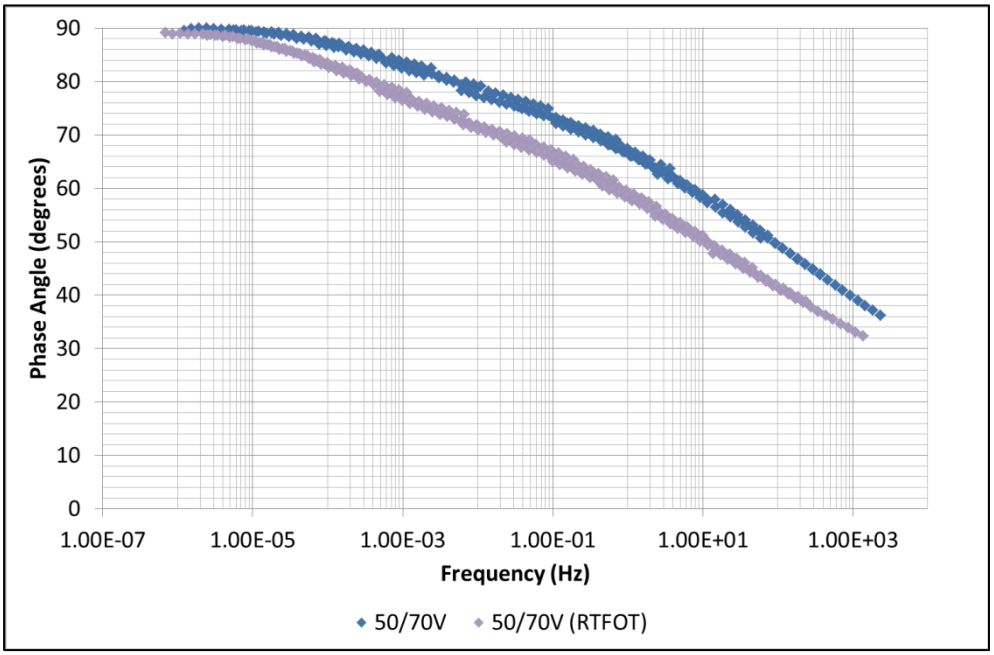

Figure 2-24 : Phase angle mastercurve at 20°C comparing 50/70V before and after RTFOT

In Figure 2-25 and Figure 2-26 the same effects are demonstrated in a PmB. Compared to the previous unmodified binder there is less change in either modulus or phase angle indicating an improved performance of the binder in its resistance to short term ageing. However, at low frequencies after RTFOT the binder has a higher phase angle than before RTFOT. This is in line with the empirical testing in Table 2-1 which showed a drop in softening point for this binder, and in Table 2-5 which showed a breakdown in the polymer matrix after RTFOT.

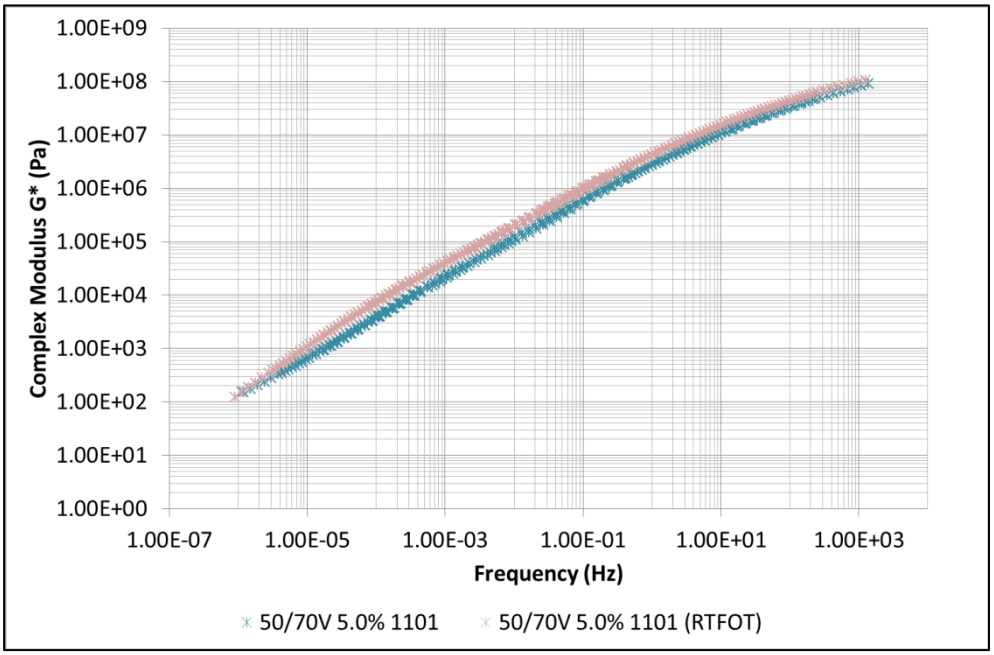

Figure 2-25 : Complex Modulus mastercurve at 20°C comparing 50/70V + 5% 1101 before and after RTFOT

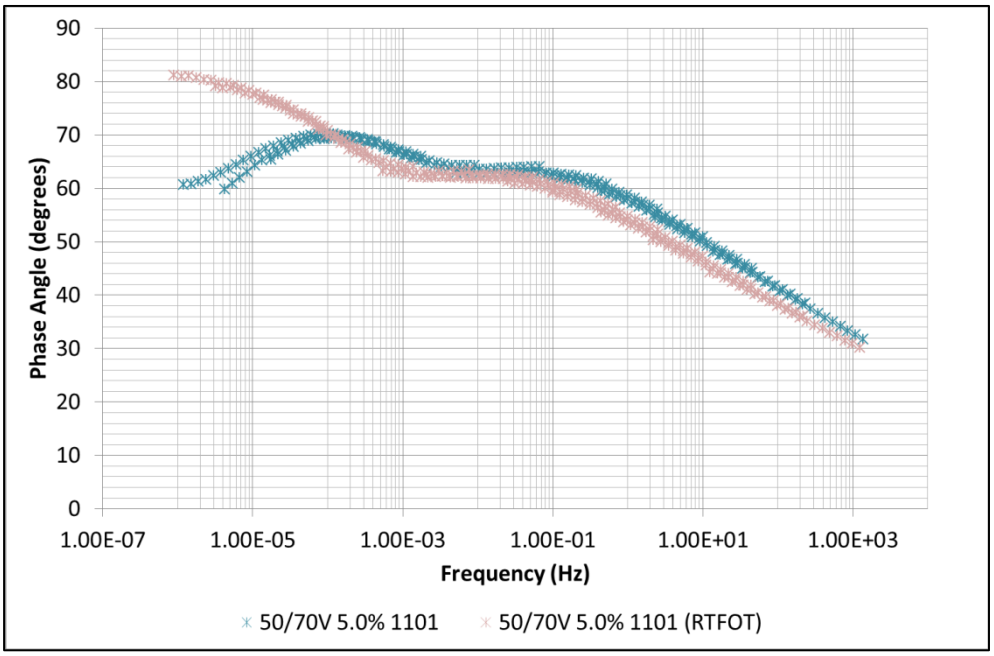

Figure 2-26 : Phase angle mastercurve at 20°C comparing 50/70V + 5% 1101 before and after RTFOT

The standard empirical measurement of the effect of short term ageing is the change in penetration, SP, and mass after RTFOT as reported previously in Table 2-3. A qualitative graphical interpretation of rheological data as carried out above offers many insights to the binder's behaviour. However, a more analytical assessment can be made by measuring the change in rheological properties after RTFOT to define a binder ageing index at any desired test temperature or frequency as in Equation 2-11.

$$\boldsymbol{Ageing\ Index} = \frac{\boldsymbol{Complex\ Modulus\ before\ ageing}}{\boldsymbol{Complex\ Modulus\ after\ RTFOT\ ageing}}$$

Equation 2-11

In this study the conditions chosen were 5°C and 10Hz, as the condition with the highest modulus and most elastic response, 25°C and 0.4Hz, as a typical in service condition, and 60°C and 0.1Hz as a high temperature condition, and the calculated results shown in Figure 2-27.

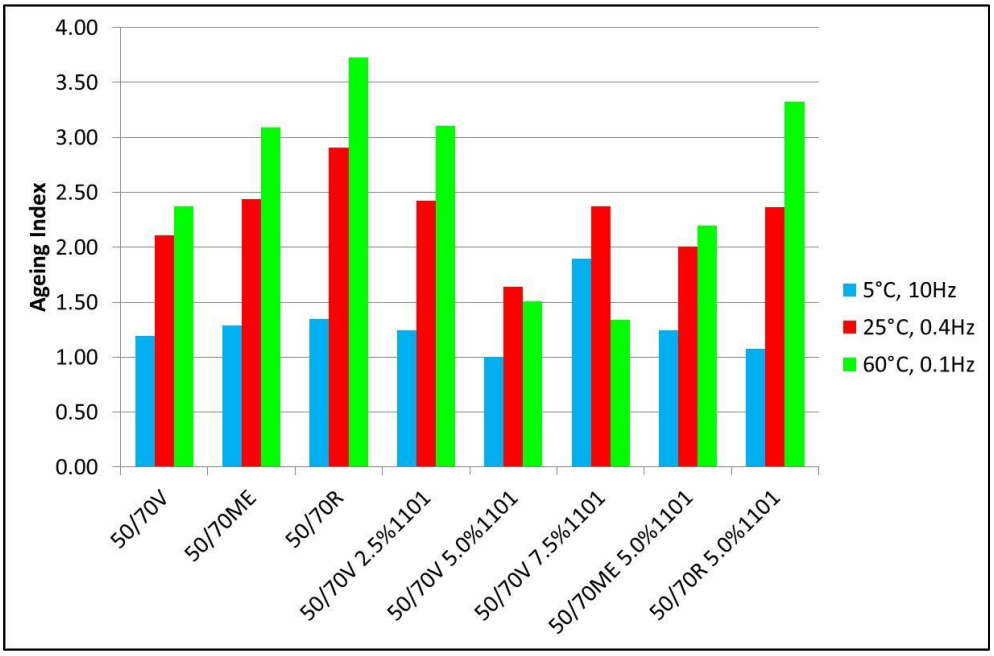

Figure 2-27 : Ageing Indices of the binders

The ageing index at 5°C is broadly similar for most of the binders. The exception is the 50/70V with 7.5% polymer which shows a comparatively high degree of ageing, which could be due to the highly unstable nature of this binder. For the unmodified binders the ageing index ranking is in the same order as the increase in SP in Table 2-1, with the 50/70 Venezuelan showing the least ageing, and the 50/70 Russian the most. For all three crude origins polymer modification leads to a lower ageing index, indicating an improved resistance to ageing.

2.7.5 Correlation of DSR results to empirical properties

Gershkoff (1995) produced a relationship as shown in Equation 2-12 between the DSR complex modulus at 25°C and 0.4Hz and the penetration of unmodified binders.

Log G*(25°C, 0.4Hz) = 8.8 – 1.95 log (Penetration 25°C, 5s, 100g)

Equation 2-12

The empirical and rheological results produced in this study were fitted to this equation as shown in Figure 2-28.

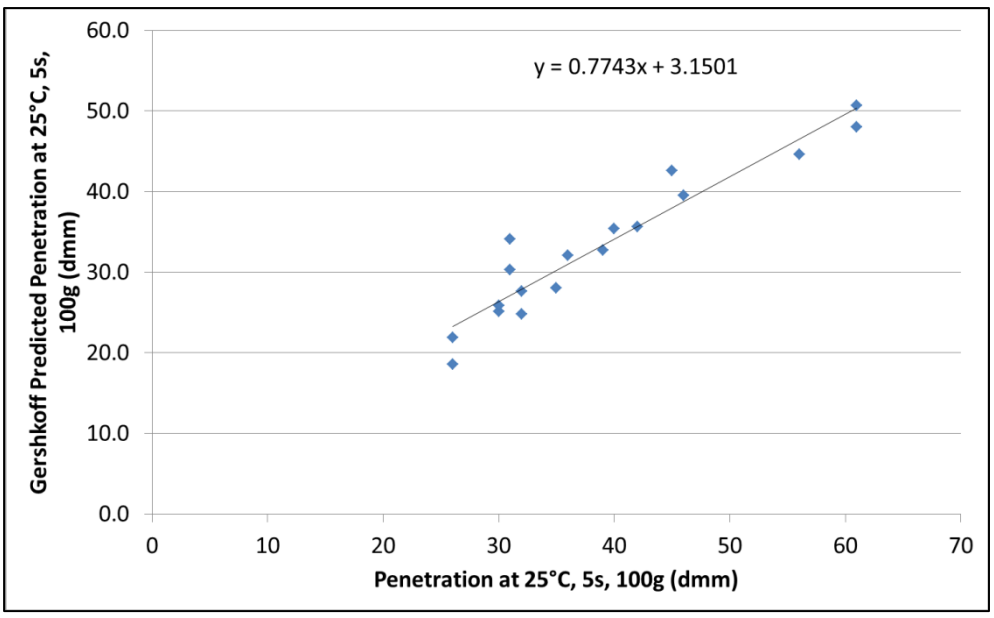

Figure 2-28 : Predicted Penetration using the Gershkoff relationship

As can be seen the Gershkoff relationship consistently underestimates the Pen of the binders in this study. Therefore, the results from this research were used to generate a new relationship between G* and the penetration of all the binders studied both before and after RTFOT, shown graphically in Figure 2-29.

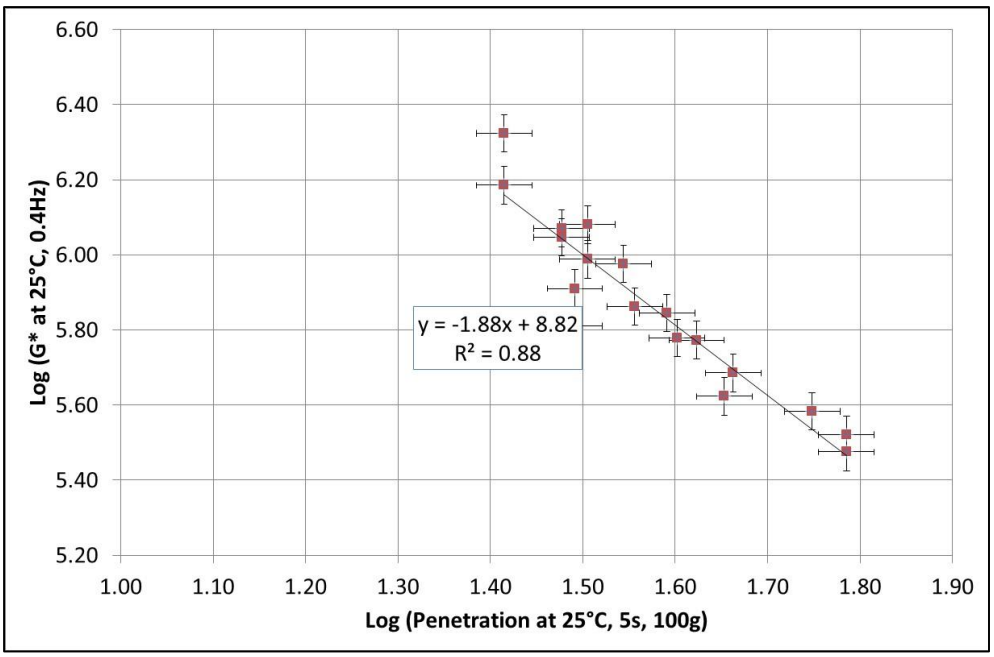

Figure 2-29 : Relationship between G* and Penetration for all binders

A new model is therefore proposed in Equation 2-13 which is similar to Gershkoff's but has an improved fit to the data in this study. It must however be noted that this was produced using a relatively small number of data points and over a relatively limited range of Pen, so further refinement will be required as more data is gathered.

Log G*(25°C, 0.4Hz) = 8.82 – 1.88log(Penetration 25°C, 5s, 100g)

Equation 2-13

2.8 Concluding Remarks

This chapter summarised the production and analysis of polymer modified bitumens for use in later chapter's asphalt studies. Their empirical and fundamental

properties were explored with the rheological properties of the binders studied and the effect of polymer modification demonstrated. The impact of bitumen crude source on the microscopic polymer morphology was explored with clear differences in bitumen/polymer compatibility observed.

Attenuated Total Reflection Fourier Transform Infrared spectroscopy with a diamond cell was used to quantitatively measure the polymer content of SBS modified bitumen. Furthermore, a more rapid quantitative spectroscopic method for the determination of storage stability as an alternative to the traditional empirical softening point measurement was developed.

3 ANALYSIS OF SMALL ASPHALT SPECIMENS[‡]

3.1 INTRODUCTION

Bitumen and asphalt are viscoelastic materials, in contrast to other elastic construction materials such as steel or concrete, and require relatively complex testing protocols to accurately determine their fundamental properties.

For asphalt, the majority of routinely performed tests have been standardised as either ISO, ASTM or EN methods and require highly specialised test equipment with considerable quantities of material necessary to produce specimens for analysis. Furthermore, for methods requiring shaped specimens which cannot be produced directly the specimens must be sawn to the correct dimension which is both wasteful of material and demands significant experience to achieve consistently.

In this chapter a method was developed using a standard DSR and small asphalt specimens to evaluate their viscoelastic properties, hence significantly reducing additional equipment costs and material consumption. The complex modulus and phase angle results of the small specimens tested in torsion were compared to a more traditionally sized specimen tested in compression.

[‡] This chapter includes results originally published in Lancaster I.M., and H. Al-Khalid, (2013) "Viscoelastic characterisation of asphalt using small specimen sizes" Proceedings of the 5th European Asphalt Technology Association Conference, Braunschweig, Germany, Paper no. 36, and Lancaster I.M., and H. Al-Khalid, (2013) "Inter-conversion between oscillatory and quasi-static loading to evaluate asphalt behavior in the Dynamic Shear Rheometer" Proceedings of the 2nd Meeting and Technical Conference of the Middle East Society of Asphalt Technologists, American University of Sharjah, United Arab Emirates, Paper no. 30, reproduced by permission.

3.2 Materials and Mix Design

To produce the asphalt for this research two sources of aggregate were obtained, both from LafargeTarmac UK. These were greywacke gritstone from Bayston Hill, Shrewsbury, and limestone from Pant, North Wales, shown in Figure 3-1. The specific gravities were determined as 2690 kg/m3 and 2640 kg/m3 for the Bayston Hill and Pant aggregates respectively.

Figure 3-1 : Bayston Hill (left) and Pant (right) aggregates during determination of their specific gravity.

The Bayston Hill aggregate is an acidic high Polished Stone Value (PSV) material used in surface courses demanding high skid resistance such as Hot Rolled Asphalt (HRA) and Stone Mastic Asphalt (SMA). The aggregate from Pant quarry is more usually used in binder and base course materials and is basic in nature.

Each of the two aggregate sources were used to design an AC10 close surface course recipe based mixture by following the guidance in PD6691 (BSI 2007). The grading curves of the two aggregate skeletons are shown in Figure 3-2, with a binder

content of 5.2% w/w for both mixtures. Each of the nine binders described in chapter 2 were then used to produce a total of eighteen asphalt mixtures for testing. Each mixture was coded using a three-letter code where the first letter indicated the aggregate source A = limestone, B = gritstone, the second letter the crude origin, V = Venezuelan bitumen, M = Middle Eastern, R = Russian, and the final letter indicating the level of SBS polymer with 0, L, M, H equated to 0, 2.5, 5.0, and 7.5% w/w of polymer. For the 30/45 bitumen a final letter of 3 was used.

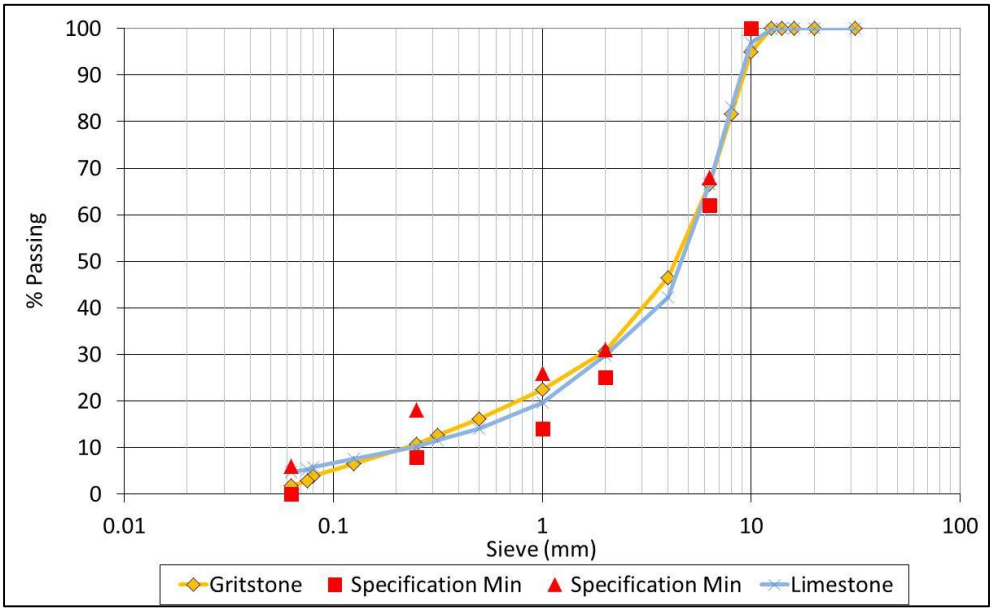

Figure 3-2 : "AC10 Close surface course" grading curves

3.3 Fine Aggregate Matrix Mixtures

Within asphalt the mastic portion is usually defined as a mixture of bitumen and filler passing the 63micron sieve and may be analysed on the DSR using the same standard geometries as bitumen. An intermediary scale material between mastics and asphalt are materials referred to as Fine Aggregate Matrix (FAM) composed of binder, filler, and small aggregates taken from the full scale asphalt. Researchers demonstrated (Kim, Little and Lytton 2002, Kim, Lee and Little 2006) how the DSR could also be used to apply cyclic torsional shear loads to specially designed

specimens 12mm diameter by 50mm high under both controlled stress and strain modes as shown schematically in Figure 3-3.

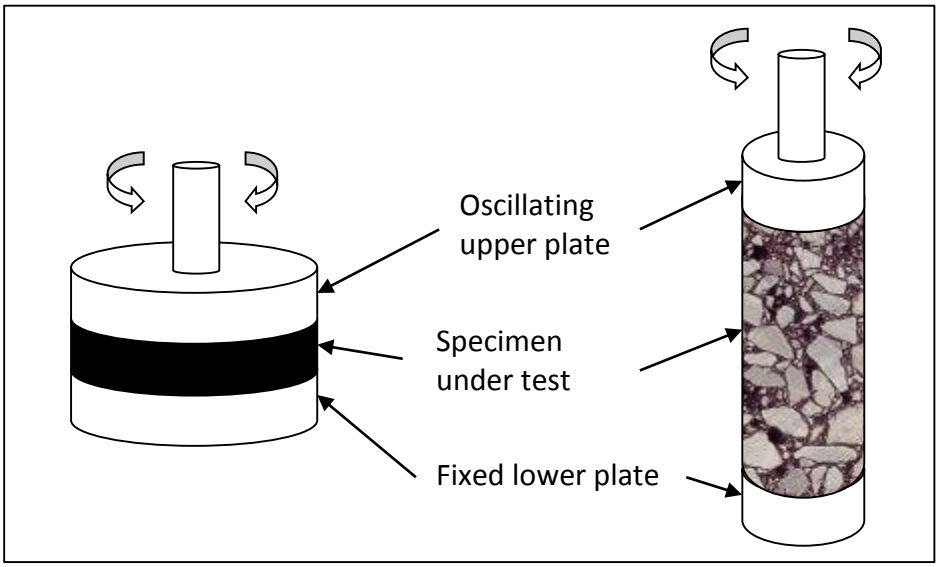

Figure 3-3 : Schematic comparison of bitumen and FAM/asphalt samples mounted on a DSR

However, for the study of FAM specimens to be of most value in pavement design it is crucial that the FAM mixture is designed to be representative of the equivalent full asphalt mixture. Kim used sand passing the 2.36mm sieve and a fixed binder content of 8% by mass to produce his specimens. Zollinger (2005) developed an alternative procedure for manufacturing FAMs utilising a fixed binder to filler ratio mixture that was mixed with aggregate passing the 1.18mm sieve (#16 in US terminology) from the full mixture aggregate grading. This was compacted to a void content of 11%, and cores drilled for further testing. Although these materials were successfully tested in torsional fatigue mode (Branco et al. 2008, Masad et al. 2008b), it was recognised that there were deficiencies in the design of the FAM. In particular, by using a fixed binder content for all mixtures, the effects of aggregate density, shape and overall grading were not taken into account. A new methodology was developed where a batch of the full asphalt mixture was produced at target binder content, and the loose asphalt mixture passed through a 1.18mm sieve. The material

passing the 1.18mm sieve was collected and the binder content determined using an ignition oven. FAM specimens were then produced using the binder content as determined by ignition.

Both these studies used the 1.18mm sieve as the cut-off point for fine aggregate as this is the convention followed in the US. However, the standards in Europe for aggregates, EN 13043 (BSI 2002), are different where fine aggregate is defined as aggregate with sizes D less than or equal to 2 mm and containing particles which mostly are retained on a 0.063 mm sieve.

To more closely align with European practises in this research a FAM was designed from bitumen and aggregate passing the 2mm sieve. The initial concept for determining the binder content of the FAM was to calculate the binder to filler ratio in the full asphalt mixture, and then produce a FAM with the same binder to filler ratio as shown in Table 3-1.

		% Mass	% Volume
Full mixture	> 63 µm	90.2	83.2
	Filler	4.6	4.2
	Bitumen	5.2	12.6
FAM	2 mm - 63 µm	71.0	56.7
	Filler	13.5	10.8
	Bitumen	15.5	32.5

Table 3-1 : Mixture composition with a binder to filler ratio by volume of 3.0

A trial laboratory FAM mix was produced and it was visually apparent that there was a large excess of binder in the mixture. An attempt was made to compact the mixture using the gyratory compactor, but with no success.

An alternative method for calculating the required binder content was therefore sought. A number of approaches are available for surface area calculation, each with the target of determining mixture's binder film thickness. One approach is based on surface area factors determined by Hveem (ASTM D1560-92). An alternative calculation is the "binder richness modulus" found in BS 594987 (BSI 2007) which was developed in France, and is now gaining wider usage as part of the design process for Enrobé à Module Élevé (EME). Equation 3-1 was used to calculate the binder richness modulus.

$$\boldsymbol{B_{PPC} = K\alpha(\Sigma)^{1/5}} \qquad \textbf{Equation 3-1}$$

Where B_{PPC} = Binder content in parts per hundred, K = Binder richness modulus, α = Specific gravity correction factor, and Σ = Aggregate specific surface area factor

A spreadsheet solver function was then used to calculate the required binder content for the FAM with the same binder richness factor, K = 3.45, as the full mixture, as reported in Table 3-2.

Mixture	Σ (m^2/kg)	K	B_{PPC} %
Limestone full mixture	9.95	3.45	5.49
Limestone FAM	30.21	3.45	6.84

Table 3-2 : Binder contents of the full asphalt mixtures and their corresponding FAM

This method produced specimens which could be compacted by gyratory compactor and cored as shown in Figure 3-4.

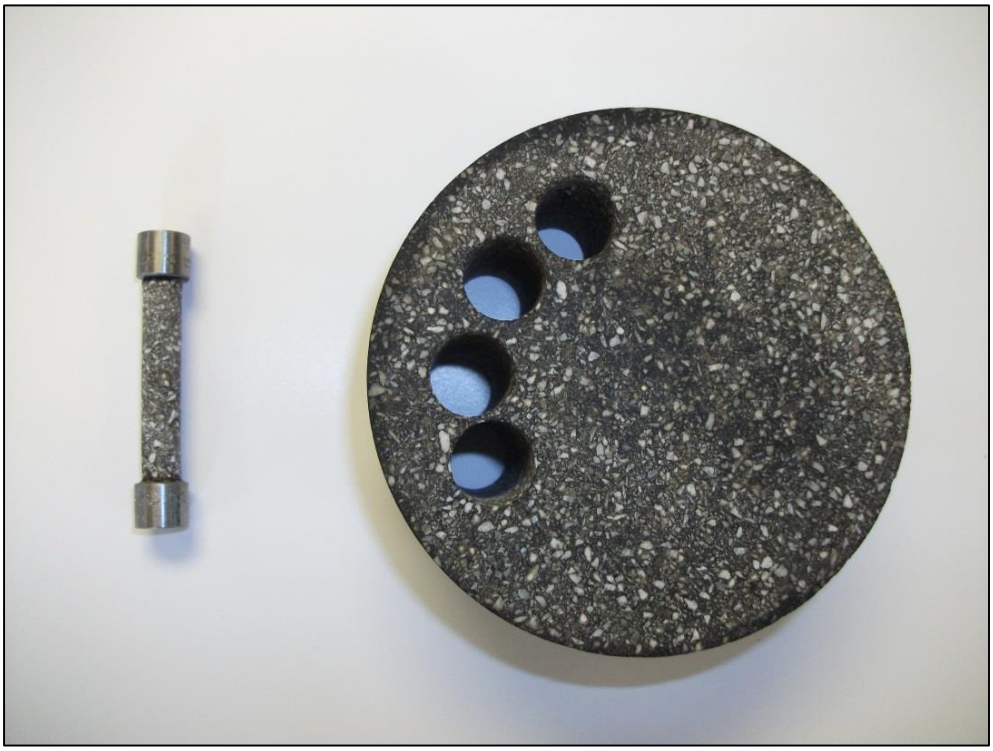

Figure 3-4 : Cut surface of limestone FAM 100mm diameter gyratory core produced using equivalent binder richness modulus, and specimen core for DSR analysis

However, the concern remained that the FAM did not accurately represent that found in the full asphalt mix. As a consequence, directly correlating the results of FAM analysis with those of a complete asphalt mixture may not be possible which would limit its relevance in fundamental pavement design work. It was therefore decided to attempt to produce and analyse full asphalt mixtures using the DSR technique.

3.4 Uniaxial analysis of traditional asphalt specimens

Prior to attempting to utilise the DSR to analyse full asphalt mixtures a more traditional test method was necessary to obtain reference results. Many different test geometries have been used for determining asphalt stiffness modulus, but the closest traditional form to DSR specimens was considered to be tall cylindrical specimens. EN12697-26 (BSI 2004) includes guidance for the preparation of specimens for uniaxial testing which states that the specimen must have a diameter between 50 and 160mm, and greater than or equal to four times the nominal maximum aggregate size of the mixture. Furthermore, the height of the specimen should be between 1.8 and 3.0 times its diameter. To achieve this, 300mm square by 100mm deep asphalt slabs of asphalt types AV0, AVM, BV0 and BVM were manufactured by laboratory roller compactor to a target void content of 5% as shown in Figure 3-5.

Figure 3-5 : Asphalt slab compaction

After demoulding, the slab was cut in half by diamond sawing, and then cored to produce 63mm diameter cylindrical specimens. The ends of the specimens were then trimmed to remove edge effects to a height of 126mm, as shown in Figure 3-6.

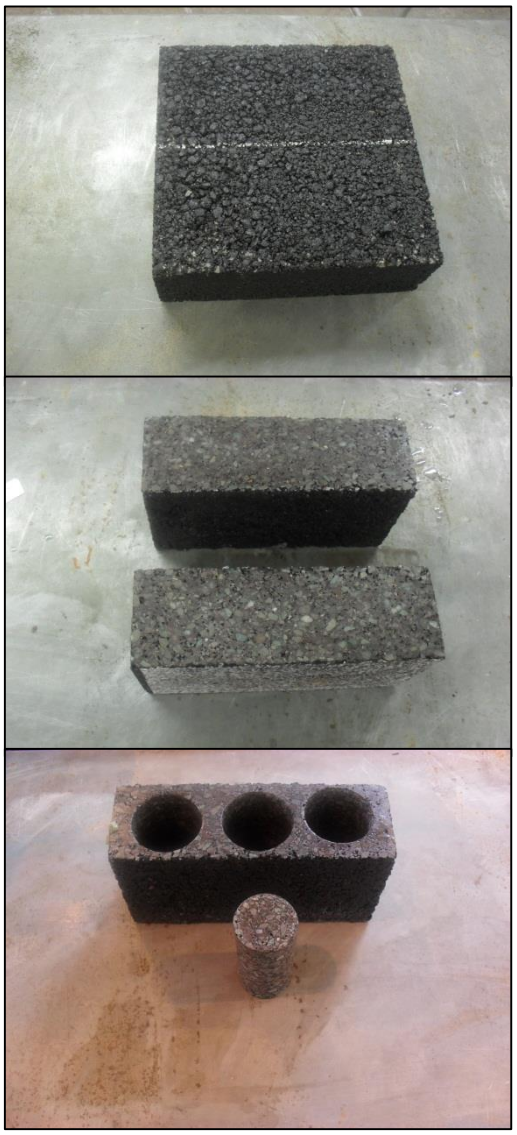

Figure 3-6 : Cylindrical specimen preparation cored from large slabs

To analyse the specimens a pneumatically driven universal testing machine was employed housed within a temperature controlled cabinet. To ensure homogenous temperature distribution within the specimens they were conditioned to 20°C for a minimum of four hours prior to testing. Vertical deformation was recorded by mounting reference points 100mm apart on diametrically opposite sides of the

specimen using epoxy resin which was allowed to cure for a minimum of 4 hours before progressing. Once the epoxy had hardened targets were attached to the bottom reference points and linear variable differential transformers held at the top reference points as shown in Figure 3-7.

Figure 3-7 : Uniaxial specimen testing arrangement

As recommended by previous researchers (Witzcak et al. 2000, Kim, Little and Lytton 2002) the applied load was chosen so that the specimen remained within the linear viscoelastic range, and hence ensuring no material damage occurred. An initial holding load of 0.02kN was used with sinusoidally varying loads of 500N applied to the specimen. In comparison to the frequencies available during DSR testing a more limited range of test frequencies could be achieved with this setup ranging from 0.1Hz to 10Hz with 60 loading cycles applied at frequencies below 1Hz, and 120 loading cycles applied at 1Hz and higher. The actuator position, applied load, and vertical specimen deformation were recorded during testing by a PC using the software attached to the equipment. Every 10^{th} cycle the complete waveform data was also captured with 100 data points per cycle.

The axial loading stress, σ_a, was calculated using

$$\boldsymbol{\sigma_a = \frac{P}{A}} \qquad \textbf{Equation 3-2}$$

where P is the applied loading force, and A is the specimen cross sectional area.

The recoverable axial strain, ε_a, was calculated using

$$\boldsymbol{\varepsilon_a = \frac{\Delta}{L}} \qquad \textbf{Equation 3-3}$$

where Δ is the deformation amplitude, and L is the gauge length between the reference points, which for these experiments was 100mm.

The complex modulus, E*(ω), at frequency ω was then determined as

$$\boldsymbol{E^*(\omega) = \frac{\sigma_a}{\varepsilon_a}} \qquad \textbf{Equation 3-4}$$

The phase angle, δ_{E^*}, was also determined as the phase lag between the peak applied loading and the measured peak strain. To ensure stable results were obtained the values of E* and δ_{E^*} were recorded as the mean result of last 30 cycles at each frequency.

3.5 Small asphalt specimen size testing

To produce specimens for DSR testing small cores 50mm high and 14mm in diameter were diamond core drilled from full asphalt mixtures. To enable the most direct comparison to the results of the uniaxial specimen testing the small cores were taken from between the locations in the large asphalt slabs where the uniaxial specimens had been drilled, as shown in Figure 3-8. Prior to coring the bulk asphalt was trimmed to 50mm thickness to avoid additional later cutting of the small specimens.

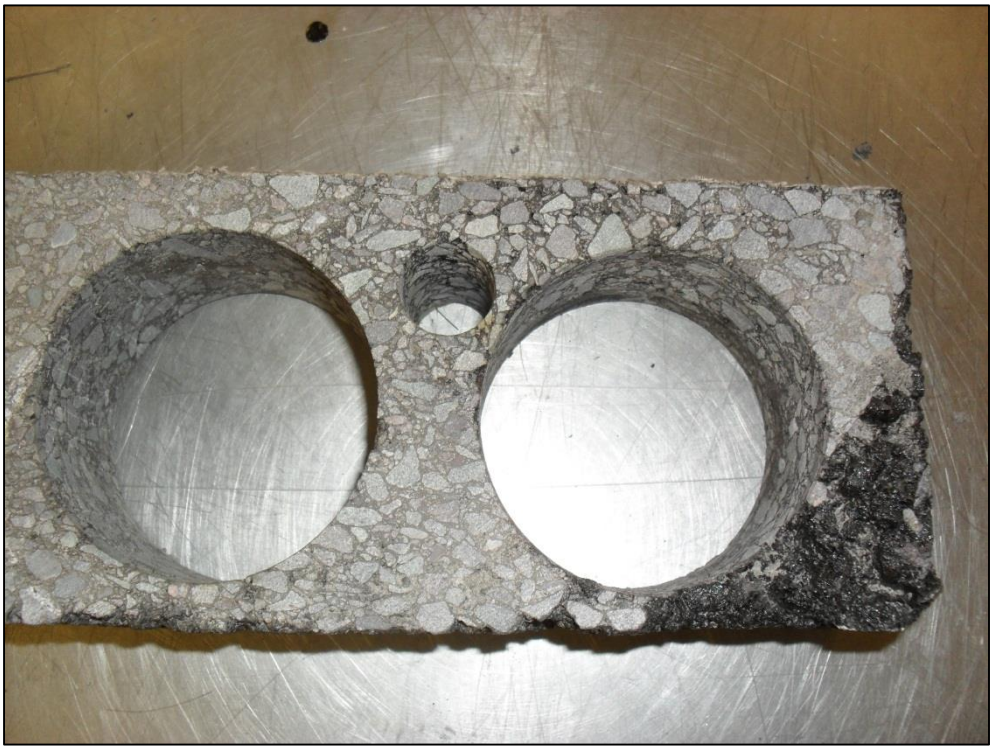

Figure 3-8 : ***Small specimen core taken from bulk material***

The small cores were bonded to mounting stubs using cyanoacrylate adhesive and bespoke specimen mounts manufactured to fit the DSR as shown in Figure 3-9 with the small diameter cores mounted on the DSR as shown in Figure 3-10. The DSR was located in a temperature controlled room at 20°C to ensure that the specimens and equipment were all at thermal equilibrium prior to and during testing, with the DSR's Peltier plate and upper heated plate also temperature controlled to 20°C to further ensure accurate temperature control.

Figure 3-9 : Bespoke DSR mounts

Figure 3-10 : Small diameter core mounted on the DSR

Frequency sweeps were performed from 0.001Hz to 100Hz with 3 points per decade at a strain of 0.001% to ensure the asphalt remained in the linear viscoelastic range. The complex shear modulus, G*(ω), and phase angle, δ_{G^*}, were then determined from Equations 2-3, 2-4, and 2-5 in the same manner as for bitumen in Chapter 2.

3.6 Small specimen frequency sweep results

For each asphalt mixture the average results of the oscillatory testing of three specimen tests are shown in Figure 3-11 and Figure 3-12 below.

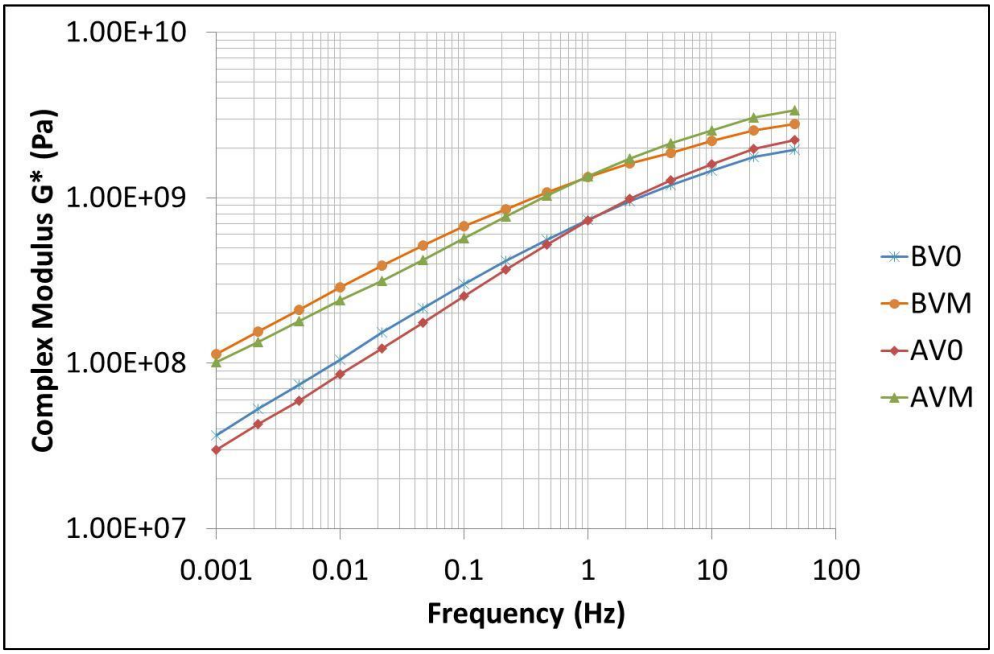

Figure 3-11 : Complex modulus versus frequency for small sample testing at 20°C

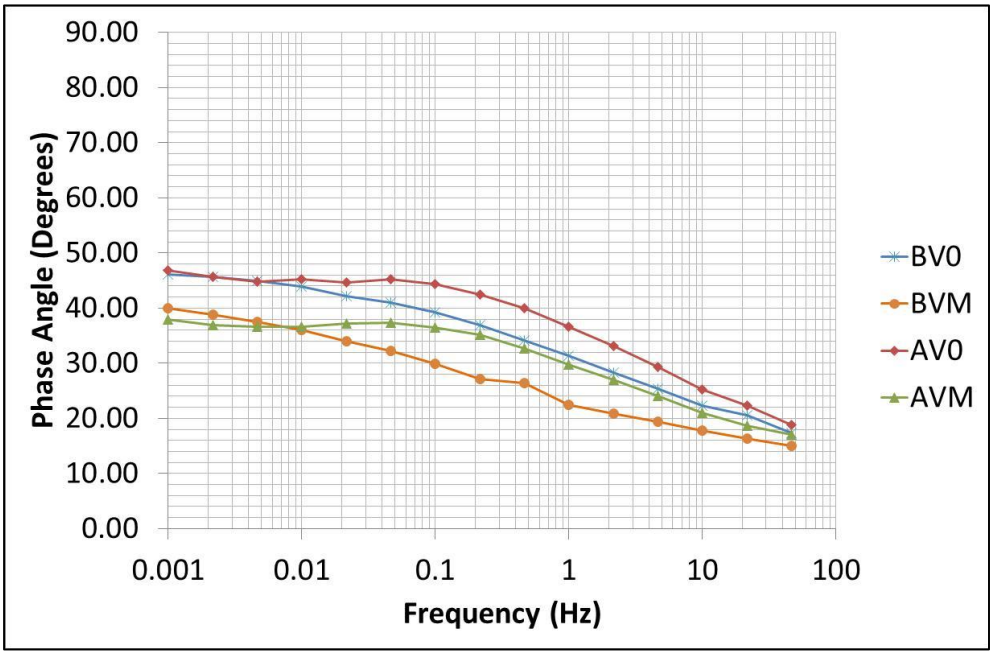

Figure 3-12 : Phase angle versus frequency for small sample testing at 20°C

As expected for asphalt there is an increase in complex modulus and decrease in phase angle at higher frequencies. Polymer modification of the asphalt produces an increase in the complex modulus at all frequencies, and a decrease in the phase angle. This indicates that the polymer modified asphalts will exhibit a higher load bearing capacity due to the increase complex modulus, and also reduced wheeltracking deformation through the combination of improved elastic response and increased complex modulus. These tests demonstrate that the small specimen testing on the DSR has the capability to determine the asphalt's fundamental performance behaviour, and is capable of differentiating between modified and unmodified binders.

3.7 Comparison of test methods

Whilst the general behaviour of the small specimen testing was as expected, to determine the absolute accuracy of the results a comparison to results from the uniaxial testing was made.

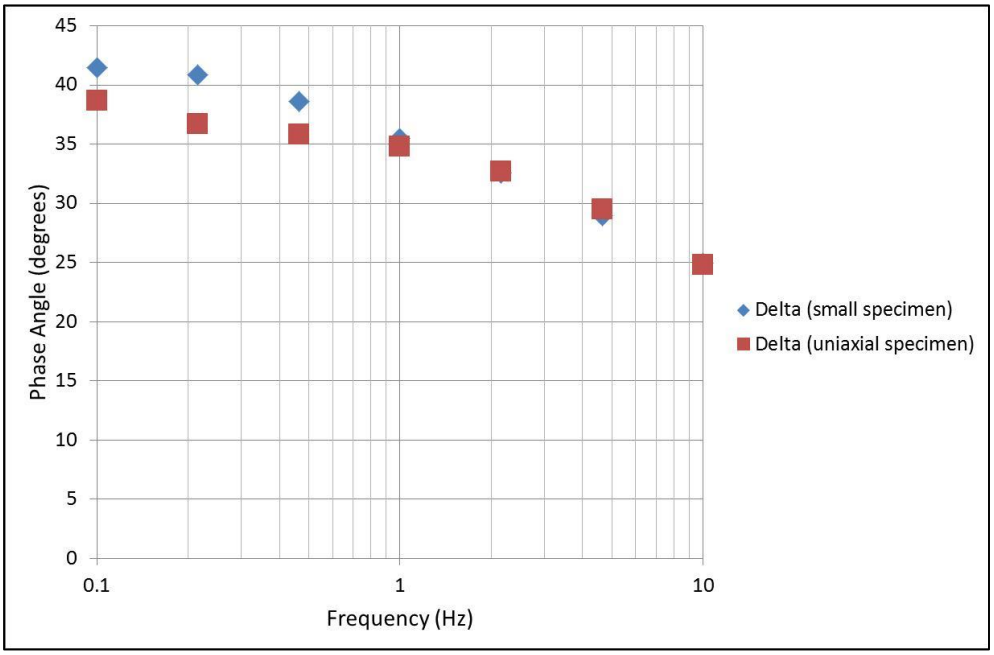

Figure 3-13 : Comparison of phase angle results for asphalt AV0 at 20°C

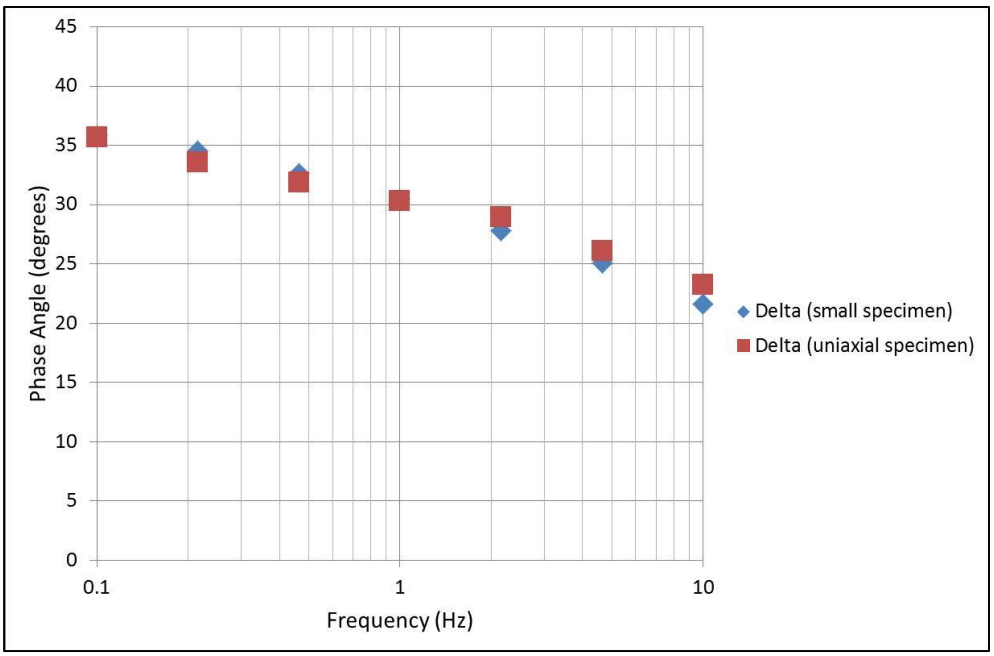

Figure 3-14 : Comparison of phase angle results for asphalt AVM at 20°C

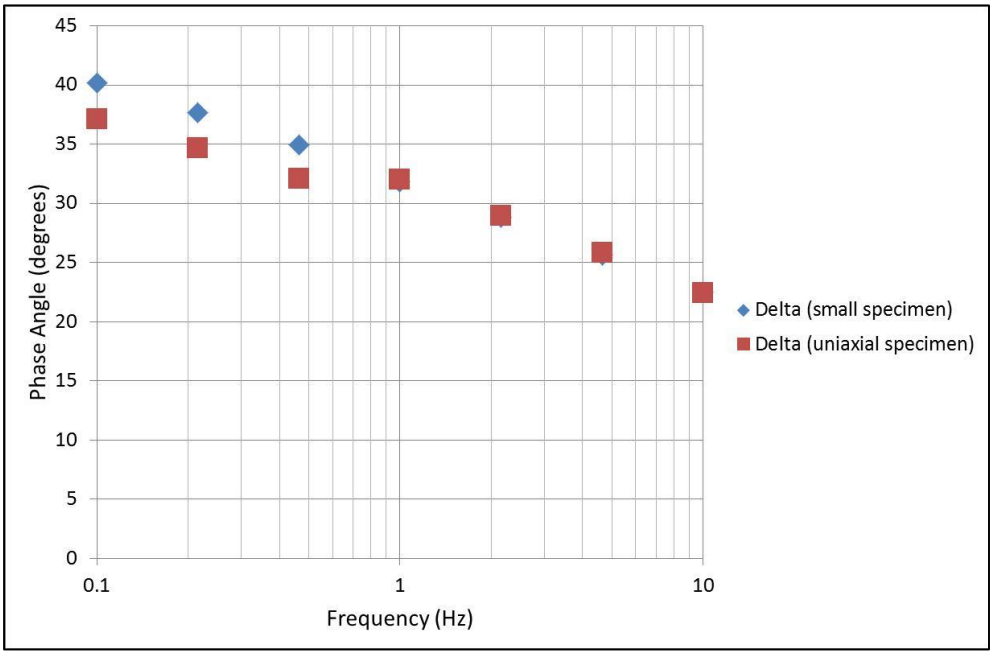

Figure 3-15 : Comparison of phase angle results for asphalt BV0 at 20°C

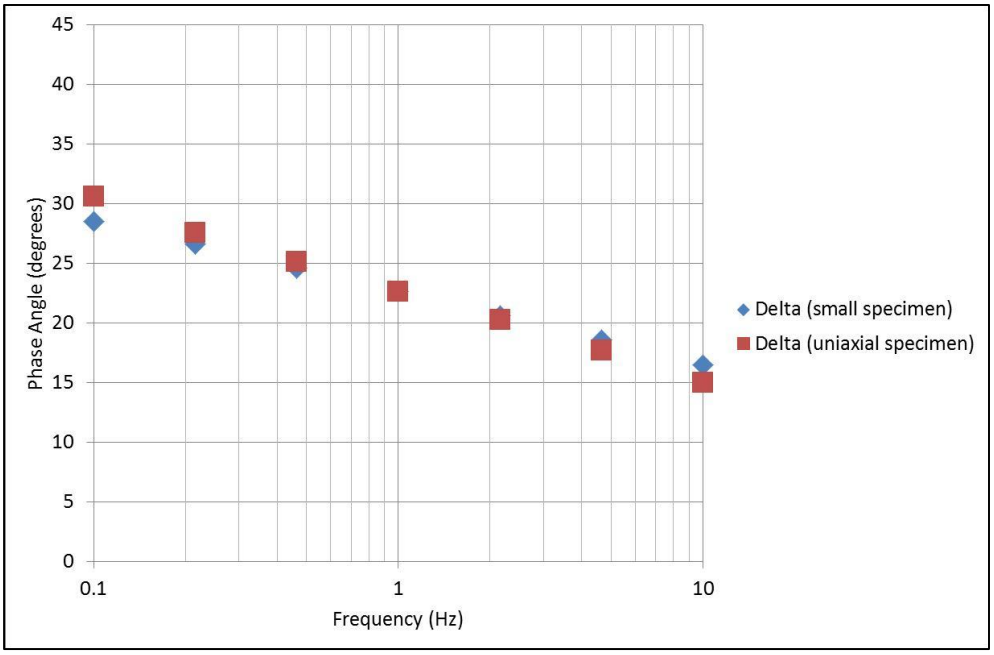

Figure 3-16 : Comparison of phase angle results for asphalt BVM at 20°C

The phase angle results, shown in Figure 3-13, Figure 3-14, Figure 3-15 and Figure 3-16 demonstrate a reasonably good agreement between δ_{G^*} and δ_{E^*}. However, as found by Di Benedetto et al. (2011) there is some small variation between δ_{G^*} and

δ_{E^*}. When the relatively large nominal maximum aggregate size of the small specimens is considered the degree of agreement is remarkable. This suggests that the majority of the asphalt's viscoelastic properties are a direct consequence of the mastic and fine aggregate behaviour as, even though the overall specimen diameter is small, these fine components are still functioning in the same manner as usual in a full sized asphalt. This further highlights the importance of FAM design as discussed earlier if FAM studies are to be representative of full asphalt mixture performance.

The complex modulus results are shown in Figure 3-17, Figure 3-18, Figure 3-19 and Figure 3-20. Again, for both G* and E*, the expected increase in complex modulus with increasing frequency was obtained, with analogous increases in G* and E* for both testing protocols.

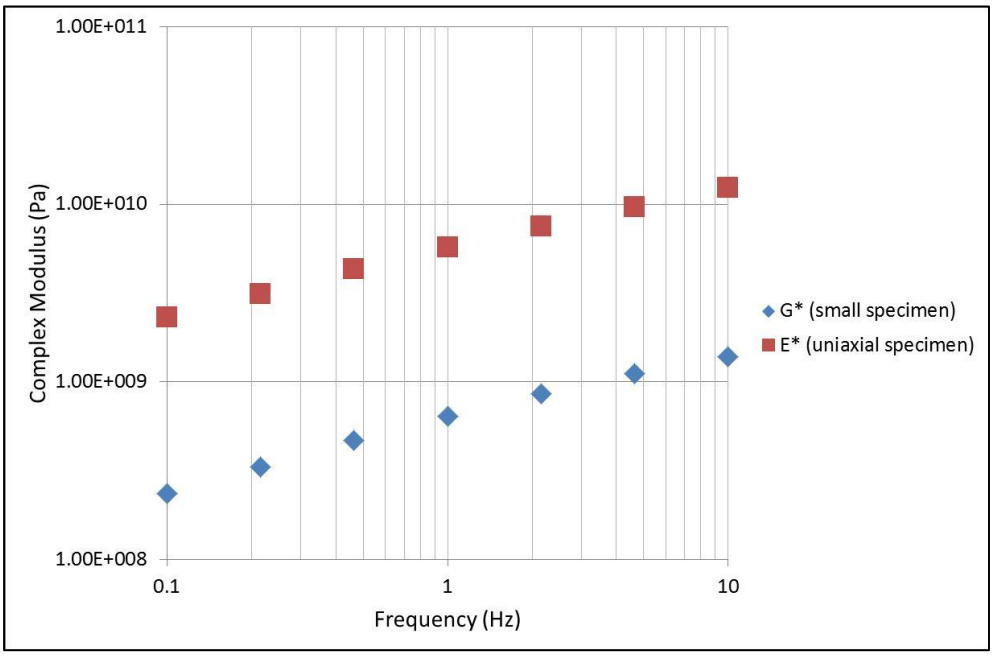

Figure 3-17 : Comparison of complex modulus results for asphalt AV0 at 20°C

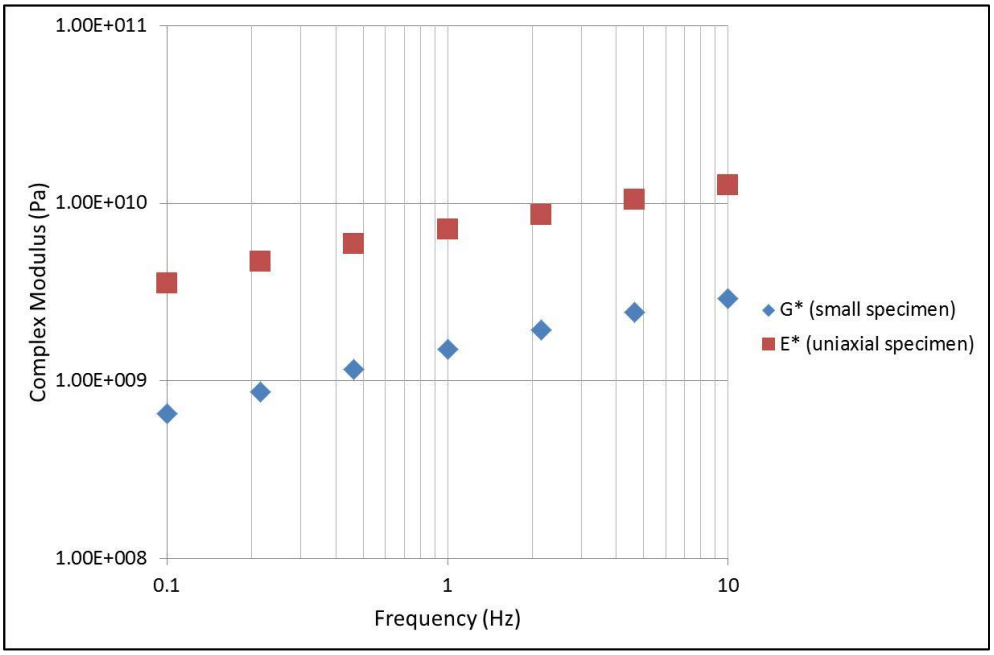

Figure 3-18 : Comparison of complex modulus results for asphalt AVM at 20°C

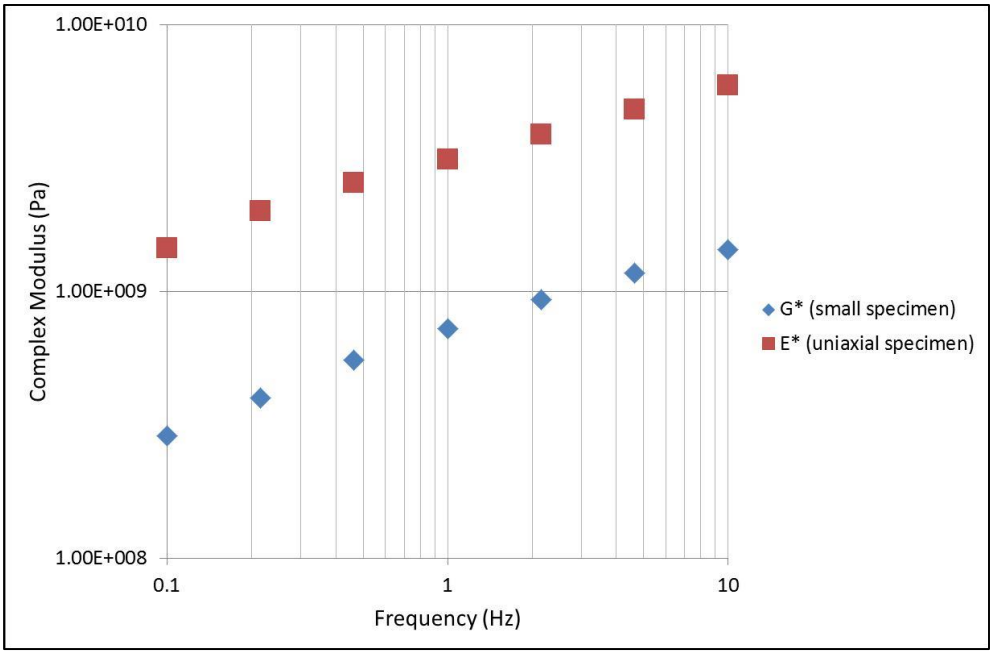

Figure 3-19 : Comparison of complex modulus results for asphalt BV0 at 20°C

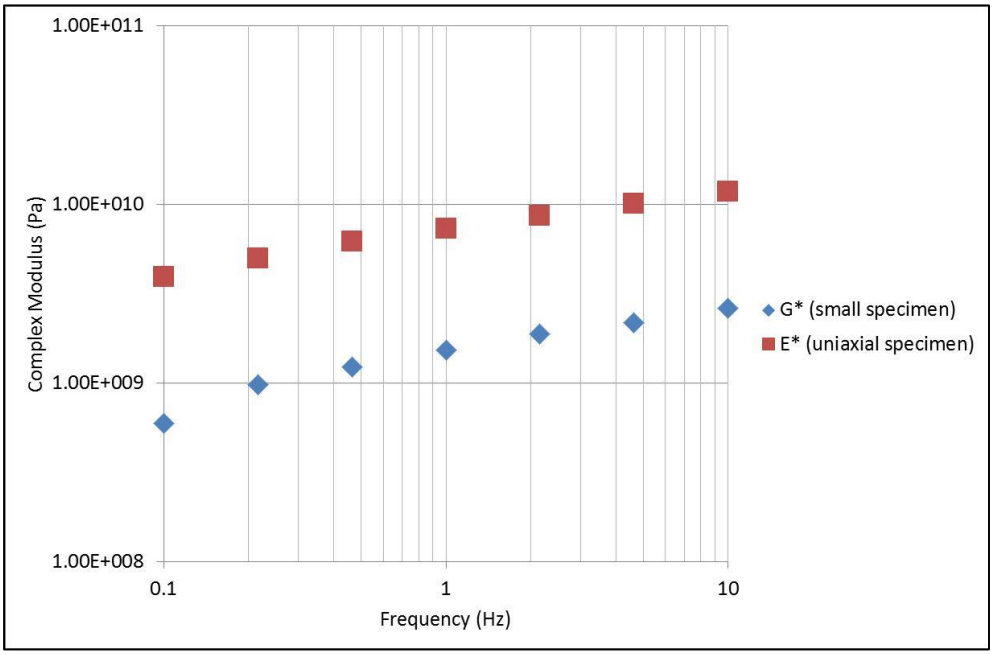

Figure 3-20 : Comparison of complex modulus results for asphalt BVM at 20°C

The complex Poisson's ratio, v*, relates the complex modulus from small specimen testing, G*(ω), to the complex shear modulus from uniaxial testing, E*(ω), as

$$\boldsymbol{\nu^* = \frac{E^*(\omega)}{2G^*(\omega)} - 1} \qquad \textbf{Equation 3-5.}$$

For asphalt at 20°C Poisson's ratio is usually assumed to be 0.3 or 0.35. However, Sousa and Monismith (1987) showed that asphalt's Poisson's ratio is both temperature and frequency dependent.

Figure 3-21 shows the calculated Poisson's ratio for asphalt BV0 calculated using Equation 3-5. The linear elastic limiting value for Possion's ratio is 0.5, and as can be seen the calculated values are far higher than this, although Equation 3-5 is only valid for isotropic materials. Previous researchers (Underwood et al. 2005, Zhang, Luo and Lytton 2012) have demonstrated that asphalt is anisotropic and that it may have values of v* greater than 0.5 (Clec'h, Sauzeat and Di Benedetto 2010).

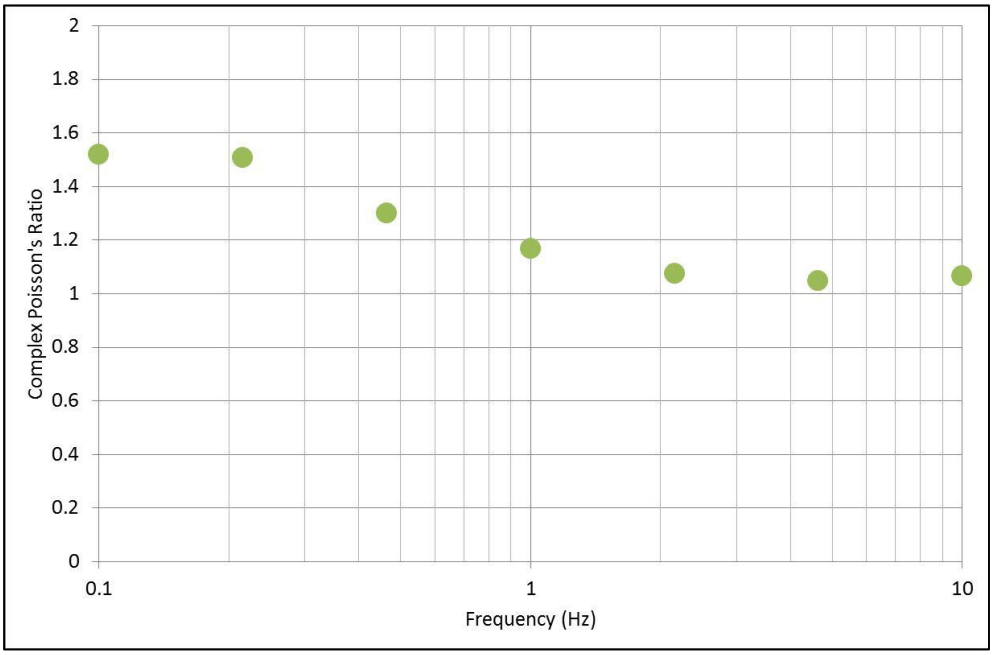

Figure 3-21 : Calculated Poisson's ratio for asphalt BV0 at 20°C

3.8 PVC beam comparison

As a verification of the DSR and uniaxial equipment a test was performed on a sample of PolyVinyl Chloride (PVC) which, due to its similar modulus to asphalt, is regularly used as a surrogate calibration material. The results obtained are shown in Figure 3-22 and Figure 3-23 below.

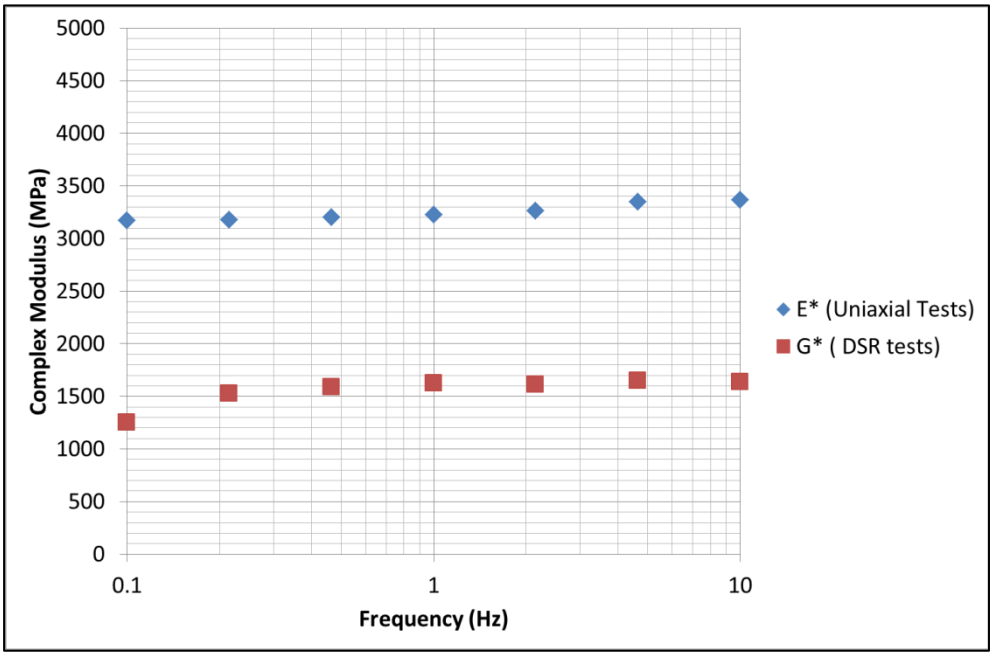

Figure 3-22 : Reference PVC material complex modulus results

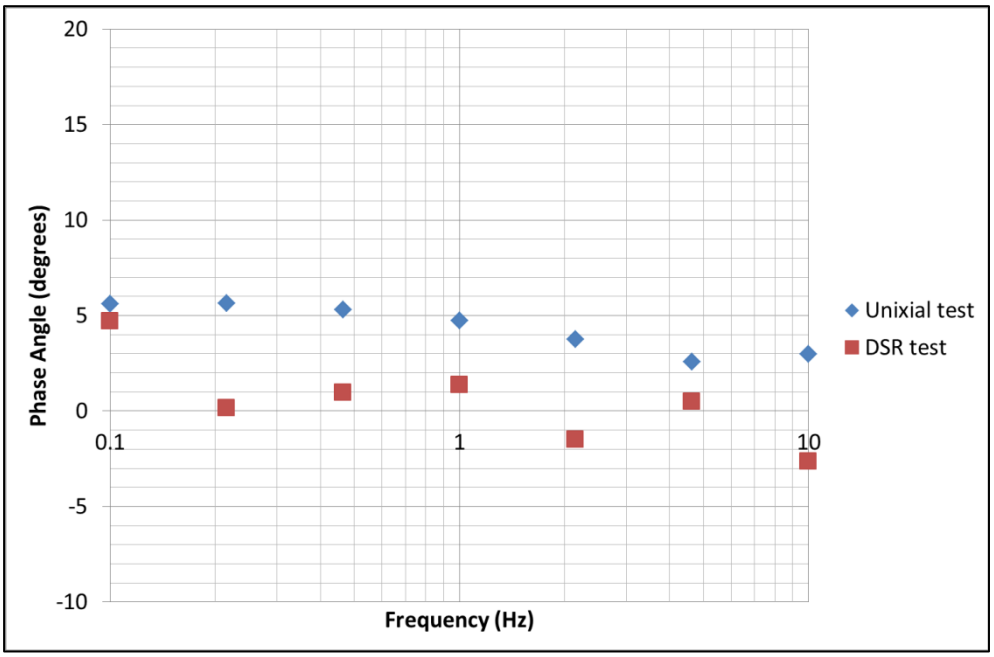

Figure 3-23 : Reference PVC material phase angle results

Unlike asphalt PVC exhibits a consistent modulus with frequency, and this is observed with both small and large specimen tests. Also, as expected for a purely elastic material, the phase angle was measured as close to zero at all frequencies. It

should be noted that to simplify the phase angle figure negative phase angles are reported, whereas in fact a phase angle of -1° corresponds to a measured phase angle of 359°.

3.9 Rheological Models

3.9.1 Standard spring and dashpot models

Viscoelastic materials have traditionally been modelled using springs and dashpots combined in series and/or parallel (Malkin and Isayev 2012). The simplest viscoelastic element, referred as a Maxwell element, is a single spring and dashpot in series. This element has a characteristic relaxation time, λ, which is the ratio of the dashpot viscosity and the spring stiffness. Simple materials may be characterised with a single Maxwell element, but to accurately model the viscoelastic behaviour of bitumen and asphalt a large number of elements are necessary to produce a generalised Maxwell model (Wiechert 1893) as shown in Figure 3-24.

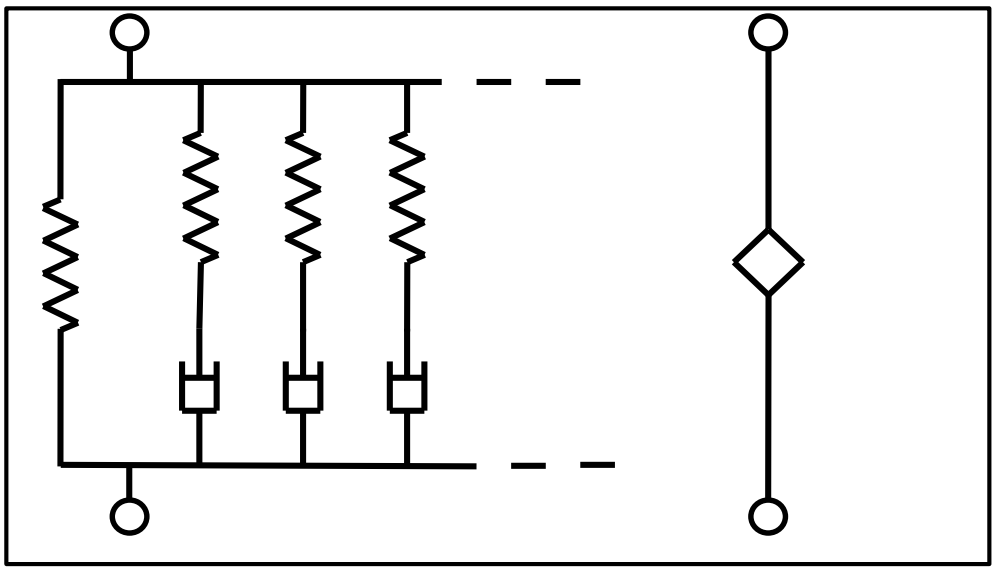

Figure 3-24 : Schematic representations of generalised Maxwell and springpot models.

Generalised Maxwell models of creep compliance and stress relaxation of bitumen and asphalt typically require at least 5 Maxwell elements to achieve a good model fit, with as many as 10 Maxwell elements sometimes necessary.

Mathematically a generalised Maxwell model for creep compliance can be formed as shown in Equation 3-6, with the equivalent stress relaxation model shown in Equation 3-7.

$$\boldsymbol{J(t) = J_0 + \sum_{n=1}^{N} J_n(1 - exp(-t/\lambda_n)) + t/\eta_0}$$ **Equation 3-6**

where J_0 is the instantaneous compliance, J_n and λ_n are characteristic compliance and timescale elements, η_0 is the zero shear viscosity, and the N elements are known as the discrete retardation spectrum $L_d(\lambda)$.

$$\boldsymbol{D(t) = D_0 - \sum_{m=1}^{M} D_m(1 - exp(-t/\tau_n))}$$ **Equation 3-7**

where D_0 is the glassy modulus, D_m and τ_m are characteristic relaxation modulus and timescale elements, and the M elements are known as the discrete relaxation spectrum $H_d(\tau)$.

3.9.2 Interconversion of rheological parameters

To completely characterise the linear viscoelastic behaviour of a material using oscillatory, creep and relaxation testing is not always possible or practical. At low frequencies oscillatory testing may be very time consuming. Creep tests may also require long test periods to achieve steady state flow and there is a risk of exceeding the linear viscoelastic limits and permanently damaging the material. Equally, when targeting low strains within the linear viscoelastic limits, stress relaxation tests may encounter measurement difficulties due to the rheometer's torque and displacement limits.

It is, however, possible to mathematically convert between the oscillatory, creep and stress relaxation tests. Therefore, by choosing the most appropriate test mode for the material and equipment, only one test is required, with oscillatory testing most usually employed.

Equation 3-6 and Equation 3-7 can be more fully generalised using continuous functions for the retardation and relaxation spectra $L(\lambda)$ and $H(\tau)$ as

$$J(t) = J_0 + \int_{-\infty}^{\infty} L(\lambda)(1 - exp(-t/\lambda))dln\lambda + t/\eta_0$$ **Equation 3-8**

$$G(t) = G_0 - \int_{-\infty}^{\infty} H(\tau)(1 - exp(-t/\tau))dln\tau$$ **Equation 3-9**

The storage and loss compliance and moduli can then be related to the spectra and vice-versa (Tschoegl 1989) by

$$J'(\omega) = J_0 + \int_{-\infty}^{\infty} L(\lambda)\frac{1}{1+\omega^2\lambda^2}dln\lambda$$ **Equation 3-10**

$$J''(\omega) = \int_{-\infty}^{\infty} L(\lambda)\frac{\omega\lambda}{1+\omega^2\lambda^2}dln\lambda + t/\eta_0$$ **Equation 3-11**

$$G'(\omega) = D_0 - \int_{-\infty}^{\infty} H(\tau)\frac{1}{1+\omega^2\tau^2}dln\tau$$ **Equation 3-12**

$$G''(\omega) = D_0 - \int_{-\infty}^{\infty} H(\tau)\frac{\omega\tau}{1+\omega^2\tau^2}dln\tau$$ **Equation 3-13**

Once J'(ω), J''(ω), G'(ω) and G''(ω) have been determined from the oscillatory test it is therefore possible to calculate L(λ) and H(τ) and hence J(t) and D(t). With current desktop computing power these interconversions can be performed in a matter of seconds, and the necessary functions have been included as part of most current rheological software (Elster, Honerkamp and Weese 1991).

3.9.3 Fractional models

For a classical Hookean spring, the applied stress is directly proportional to the resultant strain. Similarly, the stress for a dashpot is proportional to the first order derivative of strain with time. The term "spring-pot" was introduced by Koeller (1984) for a single linear viscoelastic element with intermediate properties between those of an elastic spring and a viscous dashpot where the "spring-pot" stress is proportional to the fractional derivative of strain with time, i.e.

$$\sigma(t) = K\frac{d^\alpha}{dt^\alpha}\gamma(t)$$ **Equation 3-14**

Where K and alpha are material constants

3.9.4 Power Law Creep and Relaxation Model

Whilst Generalised Maxwell models produce a satisfactory degree of fit the large number of coefficients can be practically inconvenient to handle. Also, the physical relevance of the coefficients may be difficult to deduce.

An alternative model for the linear viscoelastic creep and relaxation behaviour is a simpler power law function. Since the early years of modern rheological study the good degree of fit of power laws to many linear viscoelastic materials has been accepted (Nutting 1929, Scott-Blair and Gaffyn 1949). The power law function, Equation 3-15, has the powerful practical advantage of only requiring two model fitting parameters.

$$\boldsymbol{J(t) = At^{\beta}} \qquad \textbf{Equation 3-15}$$

where A and β are model parameters.

3.9.5 Application of Fractional Calculus

The use of calculus and derivatives of functions to determine rates of change is commonly encountered in engineering problems. However, whilst these solutions are usually first or second derivatives of functions it is also possible mathematically to consider fractional powers of the differentiation operator. The origins of this branch of mathematics, known as fractional calculus, began in the late 17th century but the first generalised equations formed in the 19th century with the most commonly encountered being the Riemann-Liouville fractional integral. This states that the fractional integral I of order α of a function f(x) is

$$\boldsymbol{I_a^{\alpha} f(x) = \frac{1}{\Gamma(\alpha)} \int_a^x (x-\tau)^{\alpha-1} f(\tau) d\tau} \qquad \textbf{Equation 3-16}$$

Where Γ is the gamma function

Fractional calculus has applications across a wide range of engineering problems, but in this study was used to transform between creep and relaxation. From rheology

theory if we assume that the material is initially at rest then the stress-strain history is given by the Boltzmann superposition integral shown below in the Duhamel form is

$$\boldsymbol{\sigma(t) = \int_0^t D(t-\tau)\frac{d\gamma(\tau)}{d\tau}d\tau}$$ **Equation 3-17**

If we assume a relaxation model of the form

$$\boldsymbol{D(t) = \frac{B_\beta}{\Gamma(1-\beta)}t^{-\beta}}$$ **Equation 3-18**

where B_β and β are model fitting parameters

Then by substituting Equation 3-18 into Equation 3-17 we find

$$\boldsymbol{\sigma(t) = \frac{B_\beta}{\Gamma(1-\beta)}\int_0^t (t-\tau)^{-\beta}\frac{d\gamma(\tau)}{d\tau}d\tau}$$ **Equation 3-19**

which is a form of the Riemann-Liouville fractional integral.

The Laplace transform of Equation 3-18 is

$$\boldsymbol{D(s) = B_\beta s^{\beta-1}}$$ **Equation 3-20**

As shown by Scott-Blair and Gaffyn (1949) the Laplace transforms of creep and relaxation are simply related by

$$\boldsymbol{D(s)J(s) = s^{-2}}$$ **Equation 3-21**

And therefore by combining Equation 3-20 and Equation 3-21

$$\boldsymbol{J(s) = \frac{1}{B_\beta s^{1+\beta}}}$$ **Equation 3-22**

By taking the inverse Laplace transform of Equation3-22 the creep function is derived as

$$\boldsymbol{J(t) = \frac{1}{B_\beta \Gamma(1+\beta)}t^{\beta}}$$ **Equation 3-23**

By substituting$A = \frac{1}{B_\beta \Gamma(1+\beta)}$ in Equation 3-18 Celauro et al. (2009) showed that the stress relaxation becomes

$$\boldsymbol{D(t) = \frac{t^{-\beta}}{A\beta\Gamma(\beta)\Gamma(1-\beta)}} \qquad \textbf{Equation 3-24}$$

This approach therefore allows the complete linear viscoelastic creep behaviour to be modelled using only two parameters A and β, which is simple to achieve using readily available curve fitting procedures, and the relaxation modulus also to be determined using the same two parameters. This was applied to the creep and relaxation of elastomers by Di Paola, Pirrotta and Velenza (2011) where A and β of relaxation experiments was used to successfully predict creep behaviour. Celauro et al. (2009) used the same approach to model the creep and recovery behaviour of paving grade bitumens.

3.10 Small specimen creep and relaxation results

The fine displacement and strain resolution of currently available DSRs allow direct measurements of D(t) and J(t) to be made on the small asphalt specimens. Using traditional full sized specimens this is not straightforward as it is limited by LVDT resolution when combined with the requirement to work within the undamaged linear viscoelastic range.

To determine D(t) for the small asphalt specimens the applied strain was 0.001% with a test duration of 600 seconds. A practical limitation of stress relaxation testing is that the strain cannot be applied instantaneously; therefore the smallest realistically achievable strain rise-time of 0.1 seconds was used. To determine J(t) the applied torque was 1000 µN with a test time of 600 seconds.

The use of fractional rheological functions to model asphalt's creep and relaxation behaviour was demonstrated by Oeser et al. (2006, 2008) by employing a power law function to create the fractional elements. In this study a power law function was used to model the creep and relaxation characteristics of small asphalt specimens. A

least squares optimisation algorithm (Nocedal and Wright 2006) was used to determine A and β in Equation 3-15 as shown in Figure 3-25 and Figure 3-26.

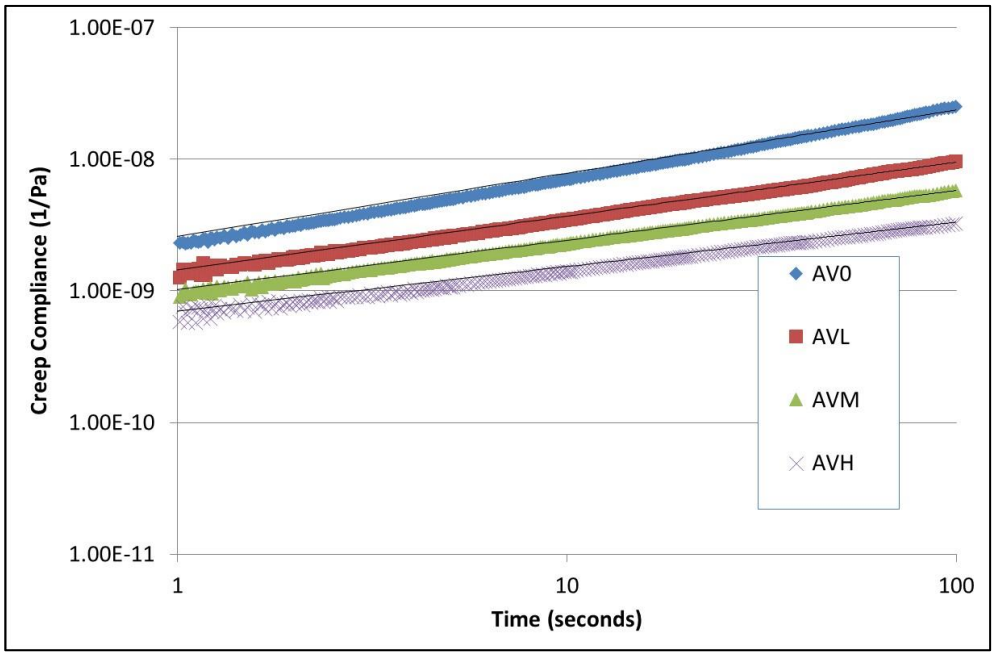

Figure 3-25 : Asphalt creep compliance at 20°C and power law curve fitting for asphalts AV0, AVL, AVM and AVH

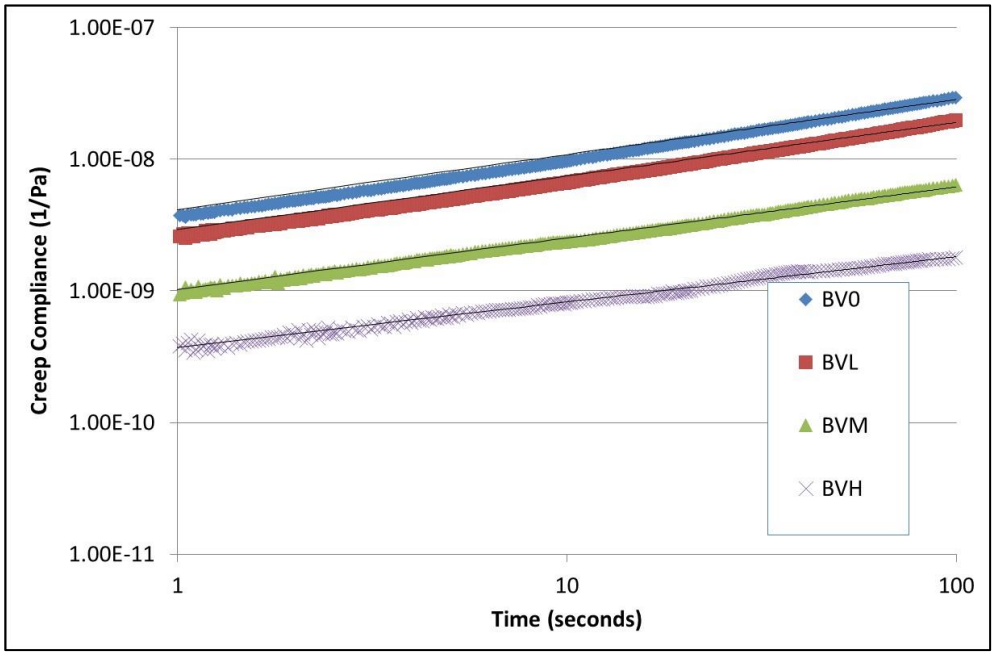

Figure 3-26 : Asphalt creep compliance at 20°C and power law curve fitting for asphalts BV0, BVL, BVM and BVH

The model fitting parameters A and β are reported in Table 3-3. With increasing polymer content, the β value decreases with increasing polymer content as the asphalt becomes more elastic. Similarly, with increasing polymer content, the asphalt stiffness increases, which is mirrored by decreases in the model parameter A.

	A	β	R^2
AV0	2.59 x 10^{-9} 1/Pa	0.481	98.7%
AVL	1.44 x 10^{-9} 1/Pa	0.409	97.4%
AVM	1.02 x 10^{-9} 1/Pa	0.376	98.7%
AVH	9.06 x 10^{-10} 1/Pa	0.337	95.8%
BV0	4.15 x 10^{-9} 1/Pa	0.418	98.1%
BVL	2.91 x 10^{-9} 1/Pa	0.408	98.7%
BVM	1.03 x 10^{-9} 1/Pa	0.388	93.9%
BVH	3.74 x 10^{-10} 1/Pa	0.343	97.6%

Table 3-3 : Creep model coefficients

The relaxation modulus was modelled using Equation 3-24 with values for A and β taken from the results in Table 3-3. As can be seen in Figure 3-27 and Figure 3-28, a reasonably good agreement with the experimental data is observed, validating the use of the fractional calculus model concept.

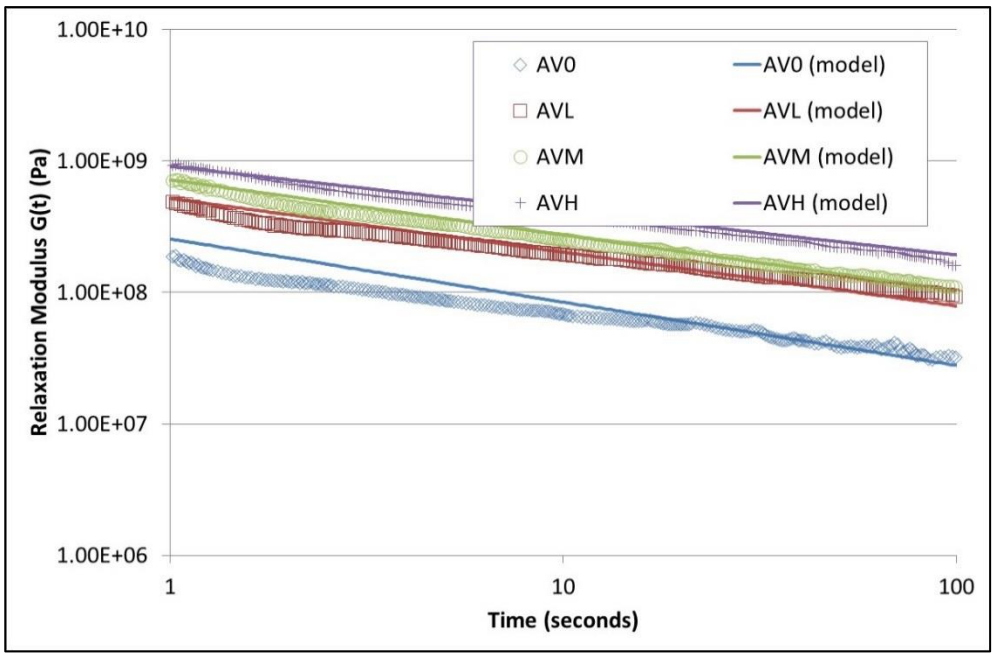

Figure 3-27 : Measured and modelled asphalt relaxation at 20°C for asphalts AV0, AVL, AVM and AVH

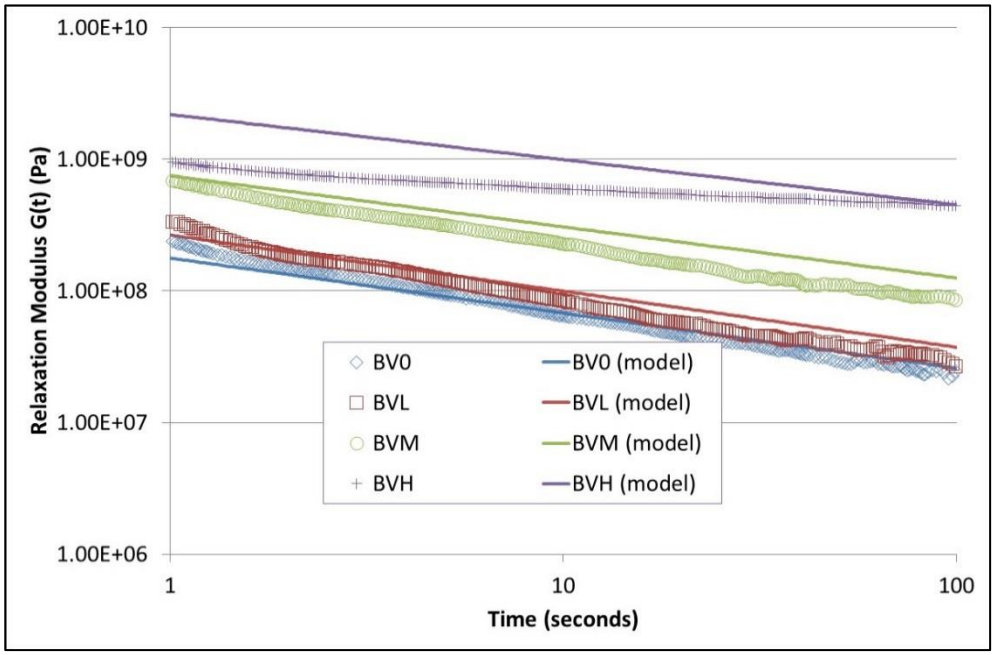

Figure 3-28 : Measured and modelled asphalt relaxation at 20°C for asphalts BV0, BVL, BVM and BVH

3.11 Concluding Remarks

This chapter has demonstrated that the viscoelastic characteristics of full asphalt mixtures may be determined using a Dynamic Shear Rheometer and small specimens, with a good correlation of phase angle to large specimens tested in uniaxial cyclic compression, even with a nominal maximum aggregate size near to that of the small specimen's diameter. This confirms that the asphalt's viscoelastic properties are dominated by the mastic and fine aggregate behaviour rather than the larger aggregate packing orientation. The linear viscoelastic complex modulus was also found to follow the expected patterns in both large and small specimen testing.

The use of the small specimen test method to differentiate between the creep compliance of unmodified and polymer modified asphalt was also demonstrated. The effective use of a power law to model the creep compliance of asphalt using only two parameters was demonstrated, with fractional calculus utilised to interconvert between creep and relaxation.

4 ASPHALT FRACTURE AND CRACK PROPAGATION§

4.1 Introduction

Traffic loading of the pavement produces tensile strains at the bottom of the pavement layer as depicted in Figure 4-1. Similarly, the daily temperature changes create temperature gradients within the structure causing thermal stresses to also develop.

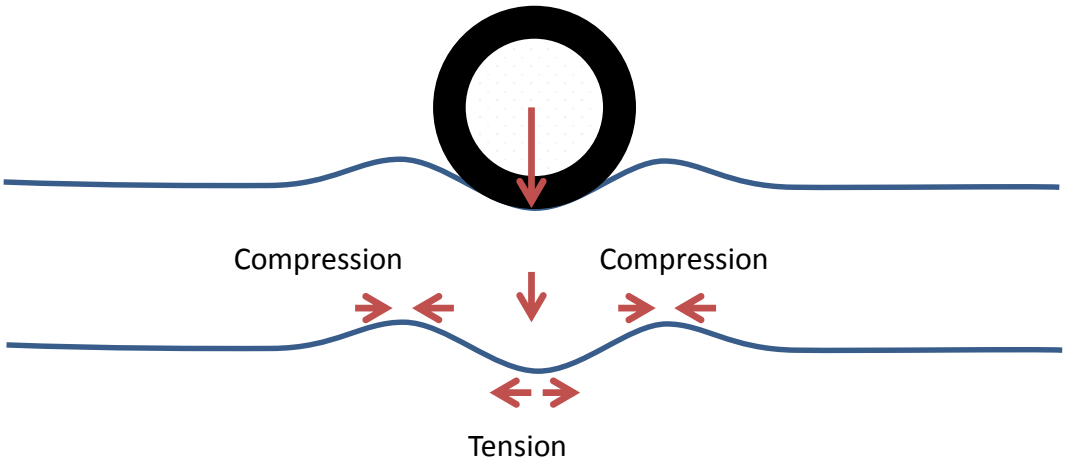

Figure 4-1 : Tension and compression in the pavement due to traffic loading

---

§ This chapter includes results originally published in Lancaster I.M., and H. Al-Khalid, (2014) "Crack propagation in the cyclic semi-circular bending test" Proceedings of the ICE - Construction Materials, Volume 167, Issue 4, pp. 191 –200 (doi:10.1680/coma.13.00025) and Lancaster I.M. and H. Al-Khalid, (2011) "Crack growth analysis of polymer modified asphalt using linear and non linear fracture mechanics" In: Nikolaides A.F. eds. Proceedings of the 5th Int. Conf. on Bituminous Mixtures & Pavements. International Conference on Bituminous Mixtures & Pavements, Hyatt Regency. Thessaloniki: Aristotle University of Thessaloniki, pp. 612-623, reproduced by permission.

After repeated traffic loadings and thermal cycles these stresses initiate cracking at the weakest points in the structure which then propagate up through the pavement leading eventually to its fracture.

This chapter investigates the effect of polymer modification of asphalt on its fracture properties. The fracture toughness, fracture energy and Paris Law crack propagation will be determined using Linear Elastic Fracture Mechanics (LEFM) and the Semi-Circular Bending (SCB) geometry. The J-integral will also be used to assess crack propagation and asphalt damage characterisation.

4.2 Fracture Mechanics Background

Material failures due to fracture are a serious problem to be considered by engineers as all realistic materials contain cracks and flaws which are initiation sites for fracture failure to occur. Structures must be designed so that they can withstand the expected loadings, and also predict how fast and where any crack will propagate within the structure so an acceptable safe service life may be determined.

When a load is applied to a crack the type of fracture which occurs in the material is usually described in terms of the fracture modes depicted in Figure 4-2. Mode I, crack opening, is the most commonly encountered mode as cracks have a tendency to grow on the plane of maximum tensile stress. Mode II is the in-plane shearing or sliding mode, and mode III is the tearing or anti-plane shear mode. In practical situations combinations of these modes often occur during crack extension, and in this case the failure is referred to as mixed-mode.

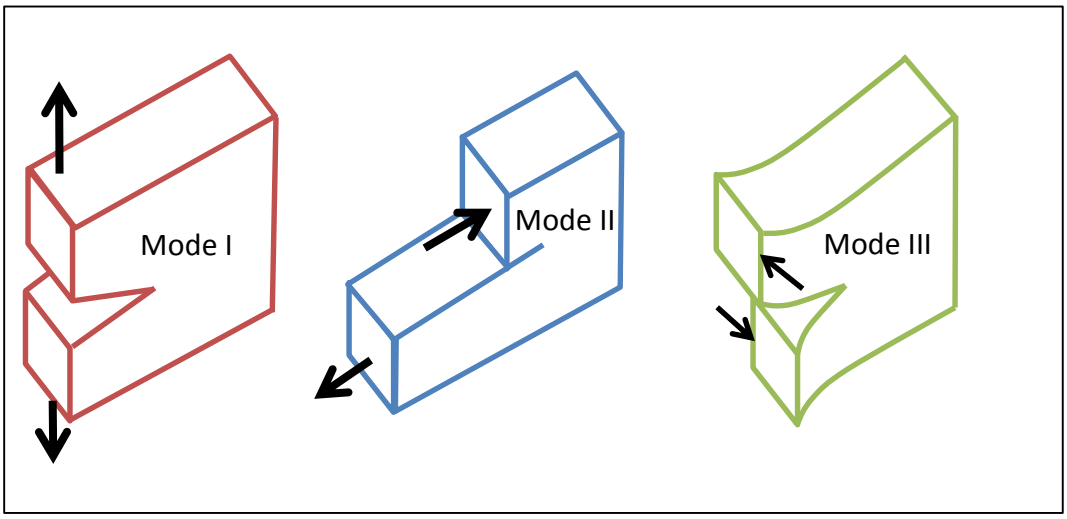

Figure 4-2 : Fracture modes I, II and III

The modern study of fracture mechanics began with the work of Griffith in the early part of the twentieth century. He investigated the fracture stress of glass fibres as a function of their diameter and found that as the diameter tended to zero the fracture stress tended to the theoretical strength, but at large diameters was around a hundred times lower. Inglis (1913) had calculated the stress concentrations at holes in plates and showed these were far greater than the nominal stress applied to the plate. Griffith (1921) assumed that defects within the fibres would lead to these high stress concentrations, and attributed the difference in measured fracture stresses to the presence of defects within the fibres and reasoned that as the diameter the fibre increased the volume increased and therefore the number of defects in the fibre also increased. Furthermore, by introducing artificial flaws to the fibres of known length, a, Griffith was able to show that for a fracture stress σ_f,

$$\sigma_f a^{-\frac{1}{2}} \approx \text{constant} \qquad \textbf{Equation 4-1}$$

Griffith went on to consider the energy required to fracture the sample in terms of the surface energy of the material and was able to show that

$$G_c = \frac{\sigma_f^2 \pi a}{E}$$ **Equation 4-2**

Where G_c is the critical energy release rate and E is Young's Modulus

4.3 Stress Intensity Factors and Fracture Energy

Whilst Griffith had worked with brittle glass, Irwin and co-researchers in the 1950's were studying ductile steel. They were able to show how the critical stress intensity factor, K_c, could be used quantify the driving force at the crack tip (Irwin 1957).

$$\mathbf{K_c = \sigma_f \sqrt{\pi a}}$$ **Equation 4-3**

Combining Equation 4-2 and Equation 4-3 we find for plane stress

$$G_c = \frac{K_c^2}{E}$$ **Equation 4-4**

And more generally for stresses $\sigma < \sigma_f$ the non-critical values for G and K are related as

$$G = \frac{K^2}{E}$$ **Equation 4-5**

Similarly, for plain strain

$$G = \frac{K^2}{E}(1 - \upsilon^2)$$ **Equation 4-6**

Where ν is Poisson's ratio.

To accommodate any specific geometry a dimensionless parameter, Y, may be introduced to give

$$K = \sigma Y \sqrt{\pi a}$$ **Equation 4-7**

The mode I critical stress intensity factor, K_{IC}, for a material is also referred to as fracture toughness and is a quantitative approach of expressing the resistance to brittle fracture in the presence of a crack. Once a material's fracture toughness is

known it is straightforward to determine when a material will fail for any specified crack length and loading.

Another method of quantifying a material's response to fracture is via its fracture energy, G_f, which is the rate of energy dissipation as the crack initiates until the material fails due to crack propagation. To determine G_f the work of fracture is divided by the ligament area. Practically in a monotonic test this is simply determined by dividing the area under the load-displacement curve by the product of the specimen thickness and ligament area.

4.4 J-integral

At very low temperatures asphalt is still a viscoelastic material albeit with primarily elastic characteristics, but at intermediate and high temperatures behaves in a nonlinear elasto-visco-plastic manner. Therefore, to accurately depict fracture in asphalt during service, a more general analysis is required. Cherepanov (1967) and Rice (1968) independently considered the case of plastic crack propagation and proposed the J-integral as a new fracture parameter which is defined by Equation 4-8 and depicted in Figure 4-3.

$$\boldsymbol{J = \oint_{\Gamma}\left(W dy - T_i \frac{\partial u_i}{\partial x} ds\right)} \qquad \textbf{Equation 4-8}$$

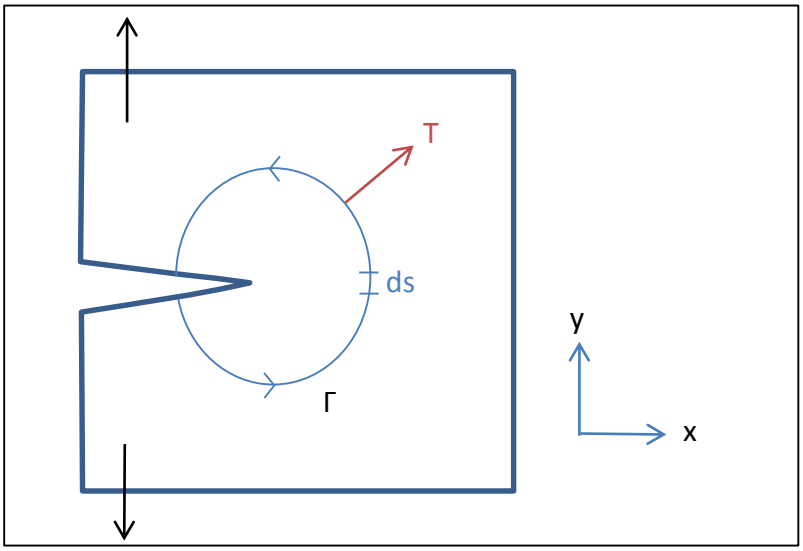

Figure 4-3 : Contour integral evaluation around a crack tip

where Γ is the contour integral around the crack tip, W is the strain energy per unit volume, T is a traction vector on the contour Γ normal to it, u_i is the displacement in the x direction, and dS is the arc length on contour Γ.

For a body under monotonic loading the J-integral is equal to the strain energy release rate for a crack. The critical strain energy release rate, J_{IC}, defines the point where large-scale plastic yielding during crack propagation occurs under mode I loading. Rice (1968) proposed that the critical J_{IC}, can be calculated using

$$J_{IC} = -\frac{1}{b}\left(\frac{dU}{da_0}\right) \qquad \textbf{Equation 4-9}$$

where b is the sample thickness, a_0 is the notch depth, and U is the sample strain energy to failure, which is the area under the load-displacement curve to failure. Hence J_{IC} may be practically determined from the slope of the best fit line of a plot of fracture energy per unit thickness against notch depth.

4.5 Semi Circular Bend Testing

To determine K and J the most common specimen geometries are the single edge notch bend (SENB) and the compact tension (CT) as shown in Figure 4-4.

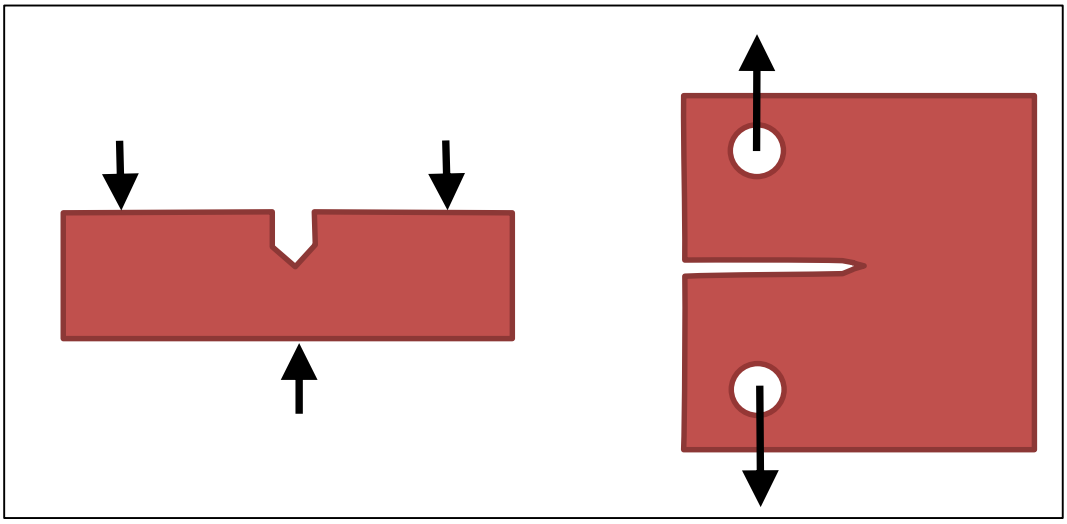

Figure 4-4 : Single Edge Notch Bend (left) and Compact Tension (right) geometries.

These geometries are well characterised and are well suited to testing of metals, or other easily machined materials. However, whilst they have been applied directly to asphalt (Anderson et al. 1992, Sewell et al. 2000) or with modified geometries such as the disk shaped compact tension test (Wagnoner, Buttlar and Paulino 2005) the specimen preparation is not straightforward requiring large quantities of material and significant time and difficulty in sawing and drilling the specimen to the required shape.

An alternative geometry that is particularly suitable for materials which are easily sampled by coring is the Semi-Circular Bend (SCB). As a consequence, disciplines including glaciology (Adamson, Shapiro and Dempsey 1997), geology (Chang, Lee and Jeon 2002), and pavement analysis (Molenaar et al. 2002) have all made use of this geometry to study material fracture properties. It is particularly suitable for asphalt as not only can site cores be taken but many of the standard laboratory asphalt compaction devices such as Duriez, Marshall, and Gyratory compaction all directly produce the necessary cylindrical specimens.

The notched SCB, as shown in Figure 4-5, has been utilised by a number of authors to analyse the fracture and fatigue properties of asphalt (Hofman et al. 2003,

Mohammad, Wu and Mull 2004, Artamendi and Khalid 2006, Hassan and Khalid 2010, Huang, Shu and Zuo 2013, Abdo, Jung and Baek 2013, Walubita et al. 2013).

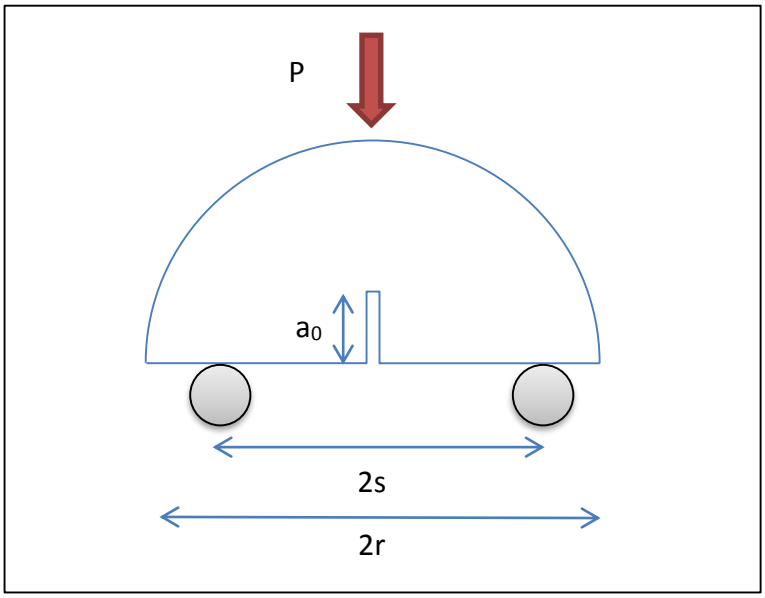

Figure 4-5 : Schematic of notched SCB geometry

Where P is the applied load, r is the sample radius, 2s is the support width, and a_0 is the initial notch depth.

One disadvantage of the SCB is the geometry factor Y cannot be analytically determined, but Lim, Johnson and Choi (1993) used Finite Element Analysis (FEM) to determine an approximate relationship for the normalised mode I stress intensity factor Y_1 for the SCB geometry with span to diameter ratio of 0.8 as

$$\boldsymbol{Y_1 = 4.782 - 1.219(a_0/r) + 0.063exp(7.045(a_0/r))} \quad \textbf{Equation 4-10}$$

Huang, Keming and Zeng (2009) also used FEM to show that the stiffness modulus, E, for the SCB is

$$\boldsymbol{E = 1.997(e^{1.175s/r} - 1)\frac{P}{d}} \quad \textbf{Equation 4-11}$$

where d is the vertical deflection at the middle point of the lower surface of the specimen.

It was also shown that for a specimen of thickness b, the horizontal stress σ_{hor} was,

$$\sigma_{hor} = \frac{6Ps}{bd^2} \qquad \textbf{Equation 4-12}$$

4.6 Specimen Preparation

To produce the test specimens the asphalt mixtures described in section 3.2 were used. Gyratory specimens 150mm in diameter by approximately 120mm high were manufactured to the design target air void content of 5.0%. Two test specimens 150mm diameter by 50mm thick were then cut by diamond sawing from the large gyratory specimen. The Indirect Tensile Stiffness Modulus (ITSM) of each core was determined at 20°C according to EN 12697-26 annex C (BSI 2004). The bulk density and air void content of each core were determined using methods EN 12697-6 (BSI 2012) procedure B and EN 12697-8 (BSI 2003) and summarised in Table 4-1.

With increasing polymer content, it was observed that the stiffness of the mixture increased significantly. Interestingly whilst the Venezuelan and Middle Eastern 50/70 produced similar stiffness asphalt, the Russian bitumen based asphalt was stiffer in both aggregate type mixtures. The asphalt manufactured using the harder 30/45 binder produced similarly high stiffness materials to those with the more highly polymer modified binders, which enabled the direct comparison of modified and unmodified asphalt at comparable stiffness.

Asphalt Reference	Void Content (%)	ITSM @ 20°C (MPa)
AV0	4.8	3997
AVL	5.2	4662
AVM	4.5	6003
AVH	5.2	7260
AV3	5.2	6789
AM0	4.9	4012
AMM	5.1	6214
AR0	4.5	5068
ARM	4.9	6812
BV0	5.8	3648
BVL	5.3	4915
BVM	6.2	5454
BVH	5.3	5692
BV3	5.2	5388
BM0	5.4	3517
BMM	5.2	5512
BR0	5.2	4998
BRM	5.4	7234

Table 4-1 : Summary of asphalt voids and stiffness properties

To produce the SCB test specimens each core was sawn in half to produce two semi-circular samples as shown in Figure 4-6.

Figure 4-6 : Limestone (left) and gritsone (right) semicircular samples prior to notching

4.7 Monotonic Test Results

To determine K_{IC} and J_{IC} notch depths of 9, 19, and 29mm were made in the specimens using a diamond tipped tile cutter to produce notches of a nominal 3.0mm width, ω. Testing was performed using a pneumatically driven universal testing machine at 20°C in a temperature controlled cabinet with each sample being conditioned for a minimum of four hours to ensure temperature equilibrium had been achieved within the sample.

The same span to diameter ratio of 0.8 was used in all tests. Two displacement control rates were used with load applied at 5mm/min for the majority of the tests with a sub-set of tests loaded at 0.5mm/min. The force measured using the load cell and non-contact transducers glued to the specimen were used to record the specimen vertical deformation and crack mouth opening displacement as shown in

Figure 4-7 and Figure 4-8. A high speed digital camera was used to record the crack propagation for specimens tested at 0.5mm/min vertical displacement.

Figure 4-7 : SCB specimen with non-contact transducers glued in position

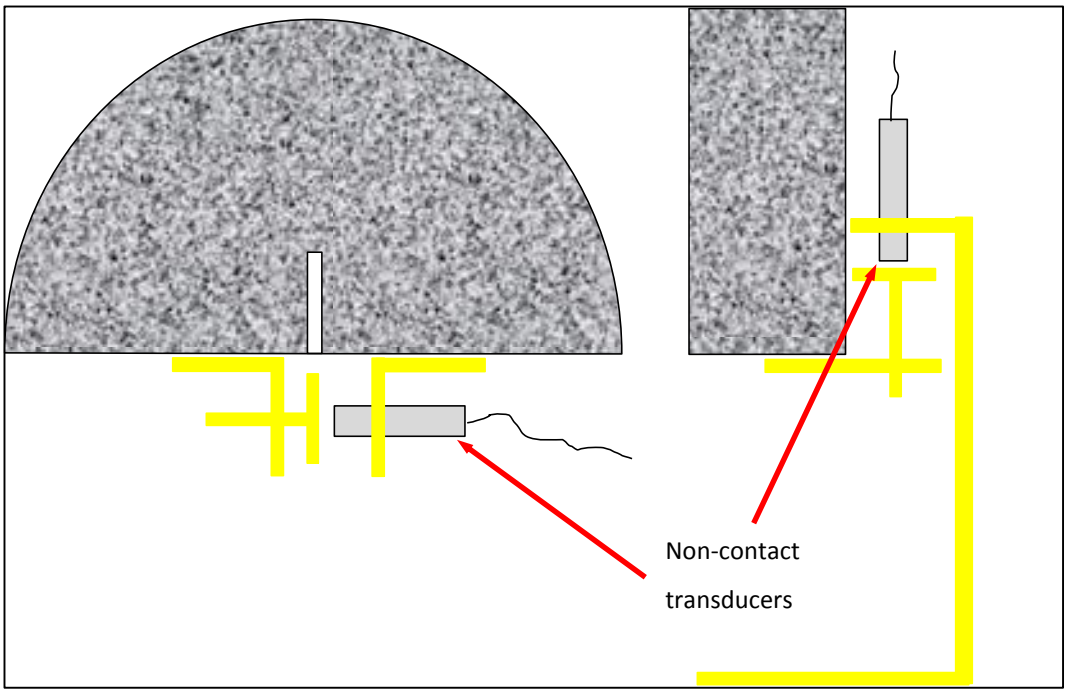

Figure 4-8 : Schematic of SCB specimen during test showing positioning of the non-contact transducers.

Equation 4-7 and Equation 4-9 were then used to calculate K_{IC} and J_{IC} and the results summarised in Table 4-2 and Table 4-3, with typical load displacement curves shown in Figure 4-9 and Figure 4-10.

Asphalt Reference	K_{IC} (N/mm$^{3/2}$)	J_{IC} (J/mm^2)
AV0	16.8	1.91
AVL	20.6	2.27
AVM	24.6	2.76
AVH	21	1.90
AV3	23.9	0.60
AM0	16.2	1.82
AMM	21.6	2.54
AR0	15.9	1.78
ARM	23.5	2.81
BV0	15.9	1.38
BVL	18.2	1.51
BVM	20.5	1.20
BVH	21.6	1.18
BV3	22.1	0.78
BM0	17.2	1.08
BMM	23.1	1.34
BR0	18.8	1.16
BRM	25.2	1.42

Table 4-2 : K_{IC} and J_{IC} determined by SCB measurements at 20°C at 5mm/min

Asphalt Reference	K_{IC} (N/mm$^{3/2}$)	J_{IC} (J/mm^2)
AV0	6.63	1.33
AVL	6.49	1.72
AVM	10.8	2.06
AVH	9.06	1.79
AV3	8.2	1.43

Table 4-3 : K_{IC} and J_{IC} determined by SCB measurements at 20°C at 0.5mm/min

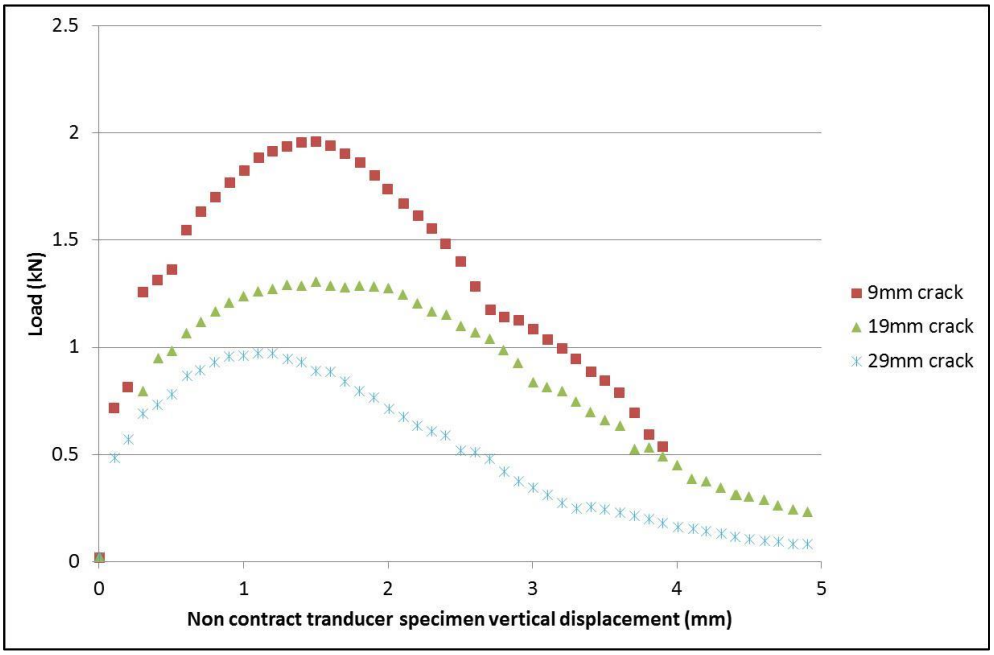

Figure 4-9 : Load-vertical displacement curves for asphalt AV0 (0.5mm/min) with crack depths of 9, 19, and 29mm

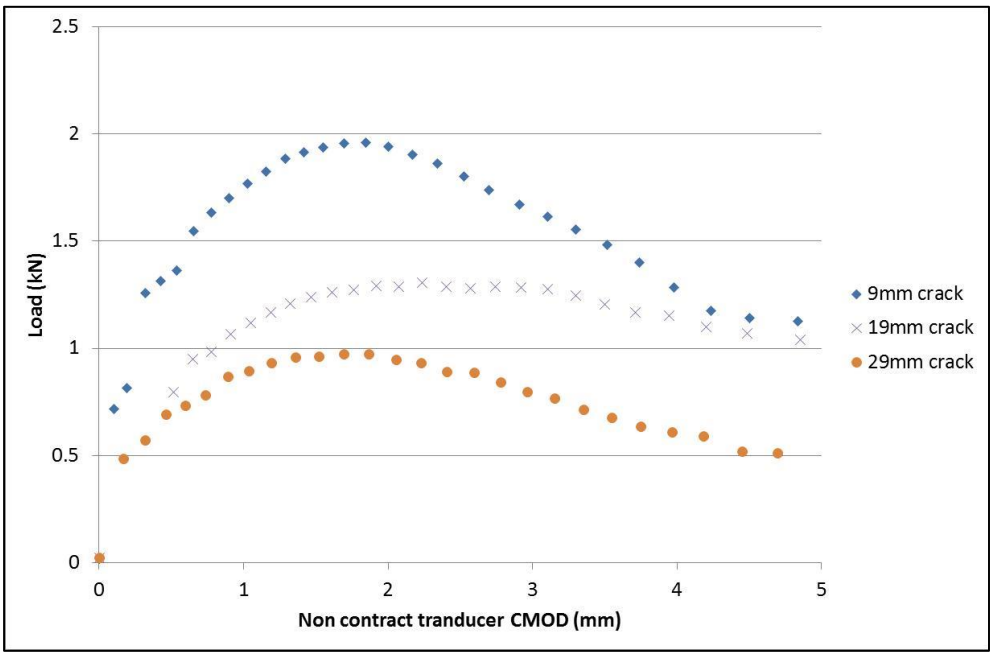

Figure 4-10 : Load-CMOD curves for asphalt AV0 (0.5mm/min) with crack depths of 9, 19, and 29mm

Similar results have been determined by other researchers for K_{IC} and J_{IC} (Hassan and Khalid 2010, Haryanto and Takahashi 2008, Mull, Othman and Mohammad 2002) indicating the test setup was performing as expected. The energy released during the test is a combination of elastic and plastic deformations, with K_{IC} related to the elastic component. These results confirm that, as expected, at lower loading rates the energy released due to purely elastic deformation is lower as more plastic flow occurs during the test.

Increasing polymer content for all crude sources leads to a higher K_{IC}. However, the harder AV3 and BV3 asphalts have similar K_{IC} to the more highly modified 50/70 asphalts indicating that polymer content and K_{IC} are not directly related. Figure 4-11 demonstrates that there is a moderate correlation between K_{IC} tested with a loading rate of 5mm/min and ITSM at 20°C, which is reasonable as both tests are measuring the elastic properties of the asphalt. Furthermore, if the two circled outliers are removed the R^2 increases to 0.84.

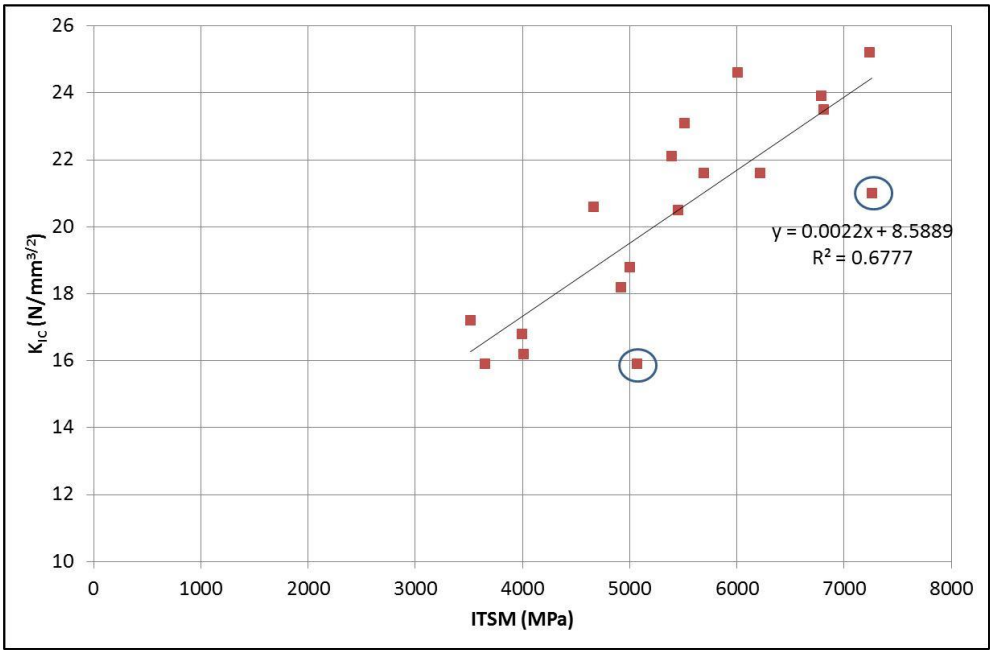

Figure 4-11 : Correlation between K_{IC} (5mm/min loading rate) and ITSM at 20°C

K_{IC} was found to be similar for the mixtures with the same binder containing either limestone or gritstone. However, J_{IC} was higher for 8 of the 9 binders in the limestone based asphalts indicating greater plastic flow prior to failure. This may be a consequence of differences in aggregate shape and interlock. Whilst the overall grading curves shown in Figure 3-2 were similar the filler content of 4.8% for the limestone mixture was significantly higher than the 1.8% for the gritstone mixture. The differences in J_{IC} could, therefore, also be a consequence of different deformation of the mastic although further mix design experiments would be necessary to confirm this.

J_{IC} was found to be larger for the polymer modified asphalts than the unmodified asphalts as a result of the polymer allowing significant plastic flow prior to catastrophic specimen fracture. Furthermore, J_{IC} for the AV3 and BV3 was very low as in this case the brittle failure occurred. This demonstrates that J_{IC} is a better indicator of polymer modification than K_{IC}.

4.8 Rotational Factor Determination by Image Analysis

In addition to K_{IC} and J_{IC} a further fundamental material fracture parameter is the crack tip opening displacement, δ, shown schematically in Figure 4-12 for the notched SCB geometry used in this research.

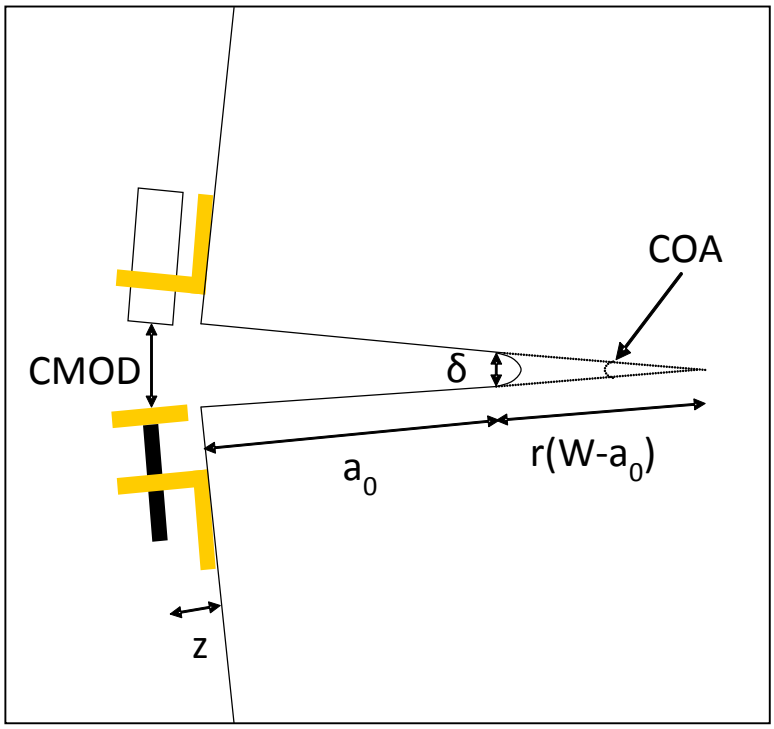

Figure 4-12 : Schematic of crack opening and measured properties

Where δ = Crack Tip Opening Displacement (CTOD), CMOD = Crack Mouth Opening Displacement = $CMOD_{elastic}$ + $CMOD_{plastic}$, z = sensor height above sample, r = rotational factor (dimensionless factor showing the relative position of the apparent hinge above the crack tip), and COA = crack opening angle

From fracture mechanics theory the J-integral and δ are related by

$$\boldsymbol{J = m\sigma_y\delta} \qquad \textbf{Equation 4-13}$$

where m = plastic constraint factor, and σ_y = yield stress

This relationship has been shown to be valid beyond the linear elastic limit into elastic plastic fracture (Shih 1981). In the case of elastic-plastic failure the total δ contains distinct elastic and plastic components as shown in Equation 4-14. The elastic component is the elastic strain energy release rate, which itself is a function of the mode I stress intensity factor K_I (Wells 1961) and the plastic component is calculated from the $CMOD_{plastic}$ using the plastic hinge model rotational factor r.

$$\delta = \delta_{elastic} + \delta_{plastic} = \frac{K_I^2}{m\sigma_y E} + \frac{CMOD_{plastic} \times r(W - a_o)}{a_o + r(W - a_o) + z}$$ **Equation 4-14**

Without prior knowledge of the rotational factor, r, it is not possible to determine δ from measurements of CMOD at peak load. However, visual measurements may be made using image analysis software from the digital photographs recorded during the monotonic SCB test. Firstly the crack is analysed prior to the application of any load, with the notch width, ω, measured at points where the notch sides are parallel away from the curved notch end as shown in Figure 4-13 and Figure 4-14.

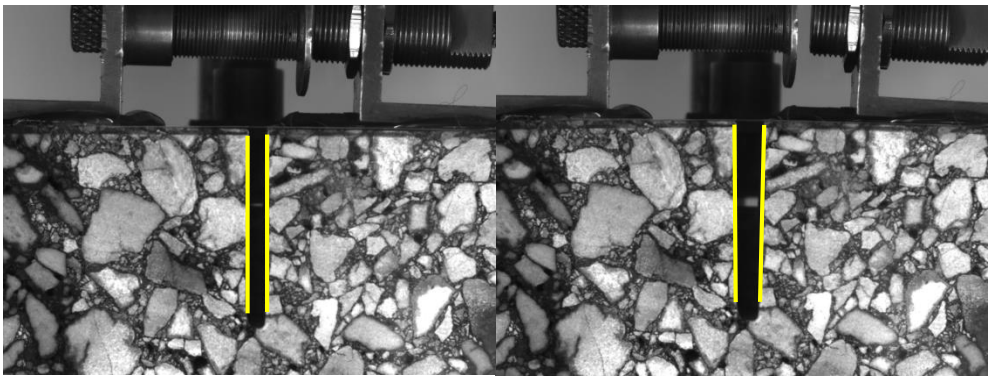

Figure 4-13 : Typical displacements observed during crack opening

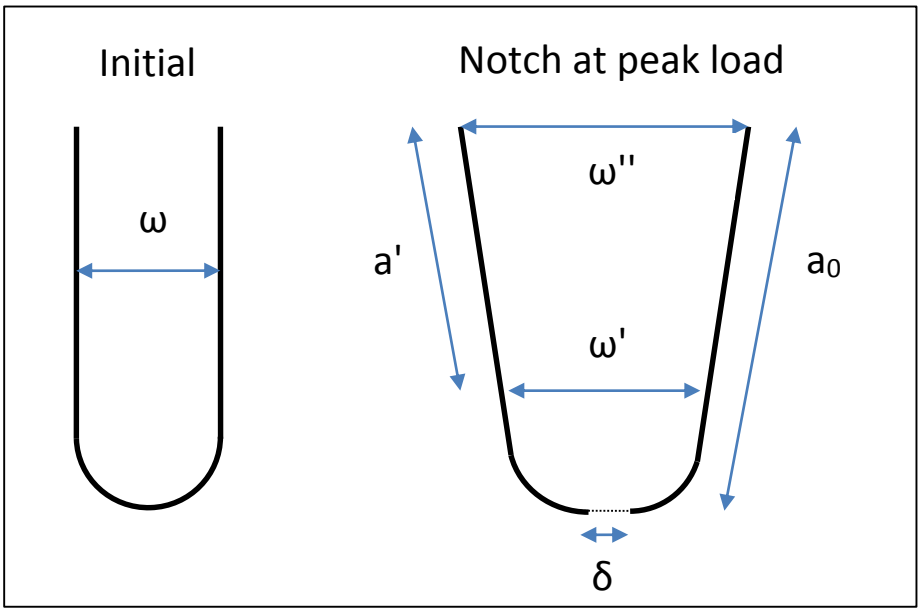

Figure 4-14 : Crack measurements taken by image analysis measurements

A second set of measurements are then performed on the photograph corresponding to the peak load. The measurements taken were the opened notch width at the mouth of the crack, ω'', and the opened notch width, ω', at a distance a', down the notch. Equation 4-15 may then be used to determine δ by a similar triangles construction, with the results shown in Table 4-4

$$\delta = (\omega'' - \omega) - \frac{a_0}{a'}\left[(\omega'' - \omega) - (\omega' - \omega)\right]$$

Equation 4-15.

Asphalt with Binder	AV0	AVL	AVM	AVH	AV3
δ (mm)	0.53	0.33	0.22	0.20	0.30

Table 4-4 : Summary of average δ for 0.5 mm/min vertical displacement monotonic SCB tests

Figure 4-15 shows a typical load displacement curve for a material undergoing elastic and plastic flow. As can be seen the initial part of the curve is linear, but then deviates as plastic deformation occurs. The CMOD can then be separated into its

elastic and plastic components by drawing a line parallel to the elastic loading line as shown in Figure 4-15.

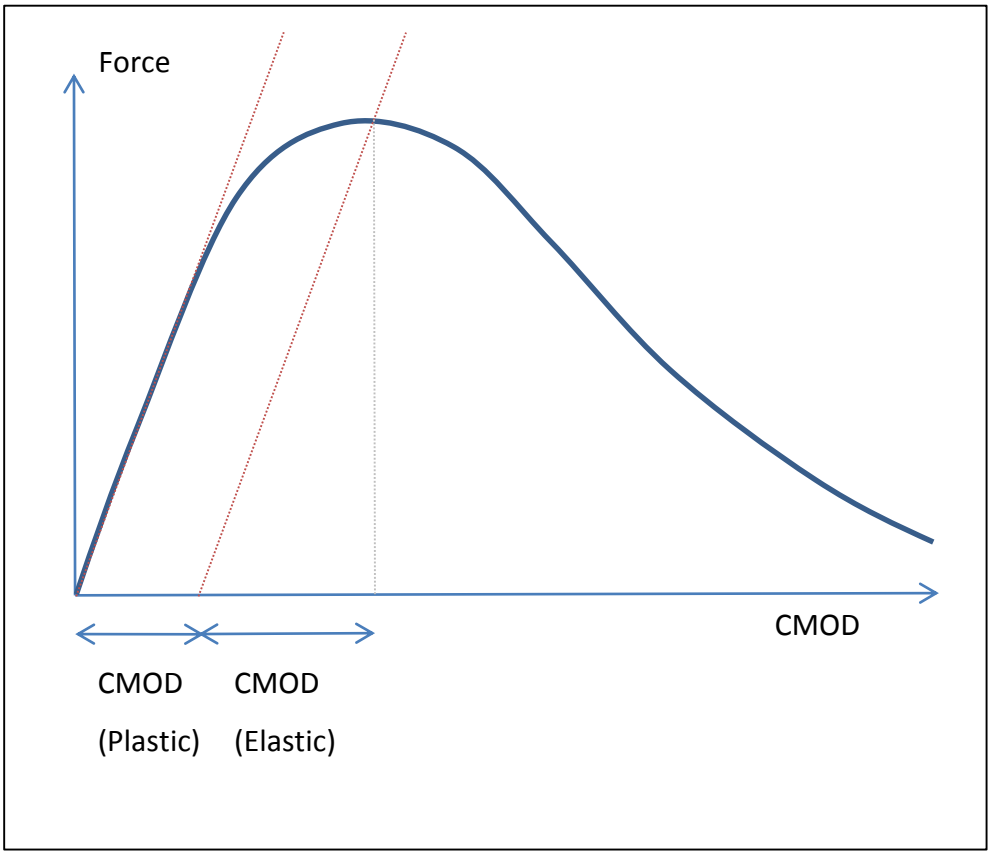

Figure 4-15 : Decomposition of CMOD into plastic and elastic components

For a typical monotonic SCB test performed at 20°C and 0.5mm/min only a very small linear elastic response is observed at the start of the test, as shown in Figure 4-16, with the majority of the curve until peak load being non-linear. Therefore, an assumption was made that $CMOD_{total}$ was approximately equal to $CMOD_{plastic}$.

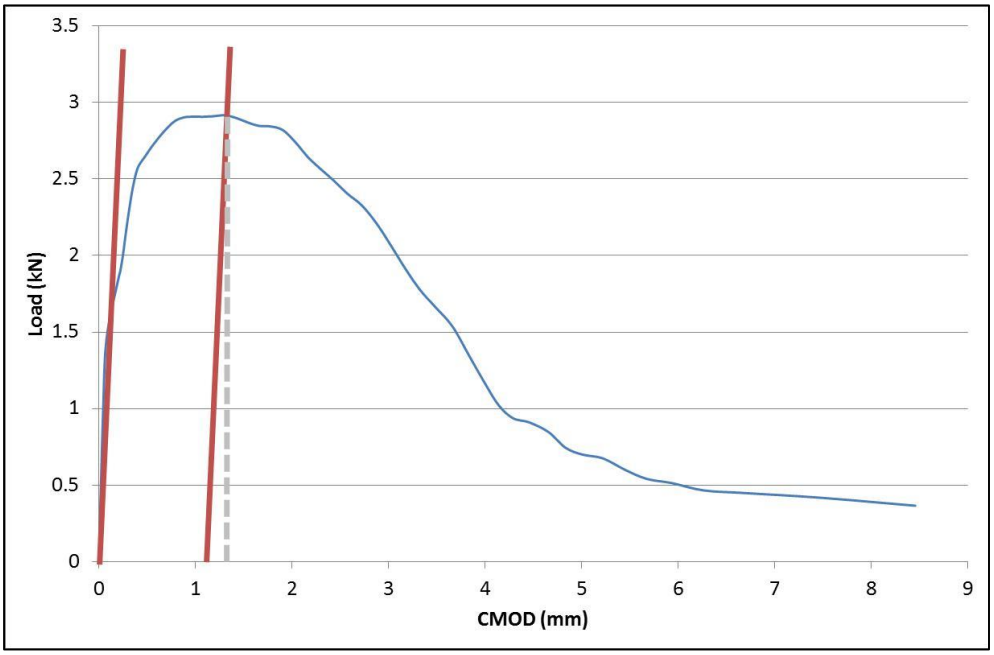

Figure 4-16 : Load versus CMOD for asphalt AVM (9mm crack)

By assuming that $CMOD_{plastic} = CMOD_{total}$ the plastic component of Equation 4-14 may be taken as equal to δ and rearranged as:

$$r = \frac{\delta(z + a_0)}{(CMOD - \delta) \times (W - a_0)}$$ **Equation 4-16**

Equation 4-16 was then used to determine the three a_o/W ratios used in these experiments as shown in Table 4-5. There is no commonly accepted value of r for the SCB although Haryanto and Takahashi (2008) used an alternative approach and found r in the range 0.07 to 1.375. Values for the other commonly used fracture geometries are provided in ASTM E1290 (ASTM 2008) with r=0.46 for the compact tension geometry and r=0.4 for the single edge notched beam. Therefore, the values determined in this study are reasonable and fall within the expected range.

a_o/W	0.123	0.260	0.397
Mean r	0.09	0.13	0.24

Table 4-5 : Calculated rotational factor r for a_o/W values used in the tests

4.9 Cyclic testing

4.9.1 Paris Law

Monotonic testing provides direct information of a material's ability to resist large tensile forces, and fracture will only occur when $K_I >= K_{IC}$. In reality most cracking is a result of multiple smaller load applications where $K_I < K_{IC}$, where fracture will not occur completely but instead the crack will propagate incrementally through the material.

Experimentally this crack propagation is usually measured in terms of crack growth per number of cycles, da/dN, as a function of the stress intensity range, ΔK, with a typical result shown in Figure 4-17.

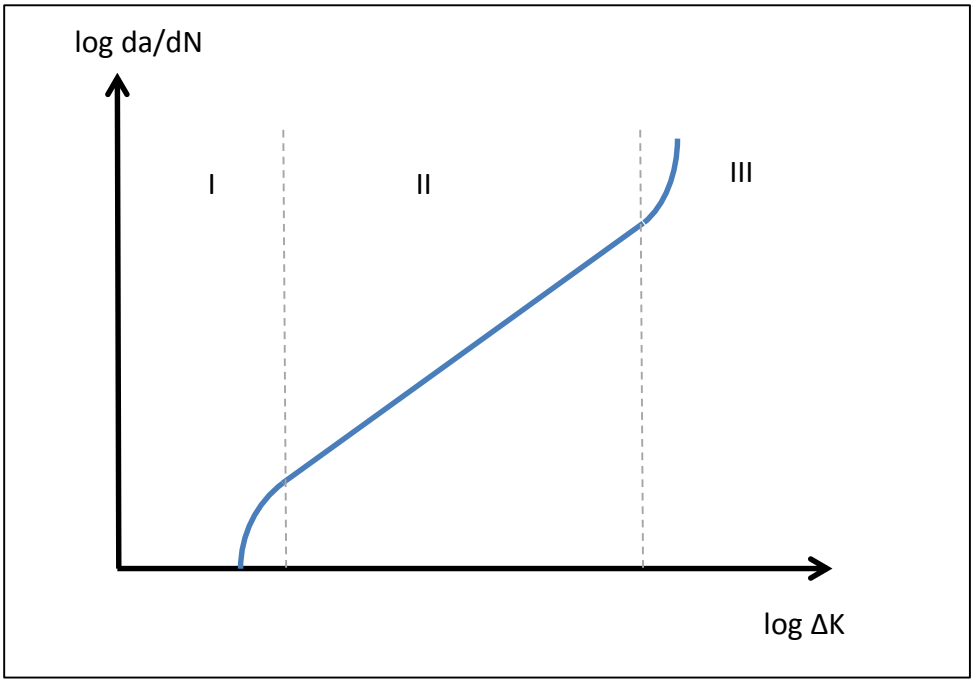

Figure 4-17 : Schematic of typical crack growth rate phases

The material behaviour is characterised by three phases. In region I, at very low ΔK there is a threshold value below where cracks will not propagate, and once ΔK exceeds the threshold value crack growth begin but is not straightforward to characterise and is controlled primarily by the material's microstructure and flow properties. In pavements the term endurance limit has been used to describe a

structure where the stress produced at the pavement base is at or below the threshold limit and, in theory, should permanently resist crack propagation although this does exclude other external factors such as environmental changes or subgrade failure.

In region III ΔK approaches K_{IC} and the crack growth rate accelerates as the material becomes unstable leading to eventual fracture. However, in region II the crack growth is stable and governed by the well-known Paris Law (Paris and Erdogan 1963) which is a power law linking da/dN and ΔK via material constants A and n.

$$\boldsymbol{da/dN = A(\Delta K_I)^n} \qquad \textbf{Equation 4-17}$$

Equation 4-7 may therefore be recast in terms of cyclic loading as

$$\boldsymbol{\Delta K_I = (\Delta P/2rb) Y_I \sqrt{\pi a}} \qquad \textbf{Equation 4-18}$$

where ΔP is the applied load range, r is the specimen radius, b is the sample thickness, and r is the sample radius.

However, this approach is only valid under LEFM conditions and should only be considered as a first approximation for complex materials such as asphalt.

4.9.2 J-integral analysis

To extend crack growth analysis to more accurately depict time dependent viscoelastic materials a more general model using the J-integral was developed. Schapery (1984) employed the J-integral and energy release rate as introduced by Rice (1968) to investigate non-linear crack growth in viscoelastic materials. In this model an extended elastic-viscoelastic correspondence principle was developed which stated that the constitutive equations for elastic and viscoelastic materials were equivalent if the stresses and strains were replaced with pseudostresses, σ^R, and pseudostrains, γ^R, as

$$\boldsymbol{\gamma^R = \frac{1}{E_R} \int_0^t D(t-\tau) \frac{\partial \gamma}{\partial \tau} d\tau} \qquad \textbf{Equation 4-19}$$

$$\sigma^R = E_R \int_0^t J(t-\tau)\frac{\partial \sigma}{\partial \tau} d\tau$$ **Equation 4-20**

Where E_R is a reference modulus, D(t) is the relaxation modulus, and J(t) the creep compliance.

Schapery also used the correspondence principle to relate the J-integral to the work of fracture, W_f, necessary to produce failure in an element at time t and position α within the failure zone as

$$W_f = E_R \int_0^{t_i} J(t-\tau)\frac{\partial J_V}{\partial \tau} d\tau$$ **Equation 4-21**

Where J_v is the viscoelastic J-integral, and t_i is the time taken to initiate the crack, as shown in Figure 4-18.

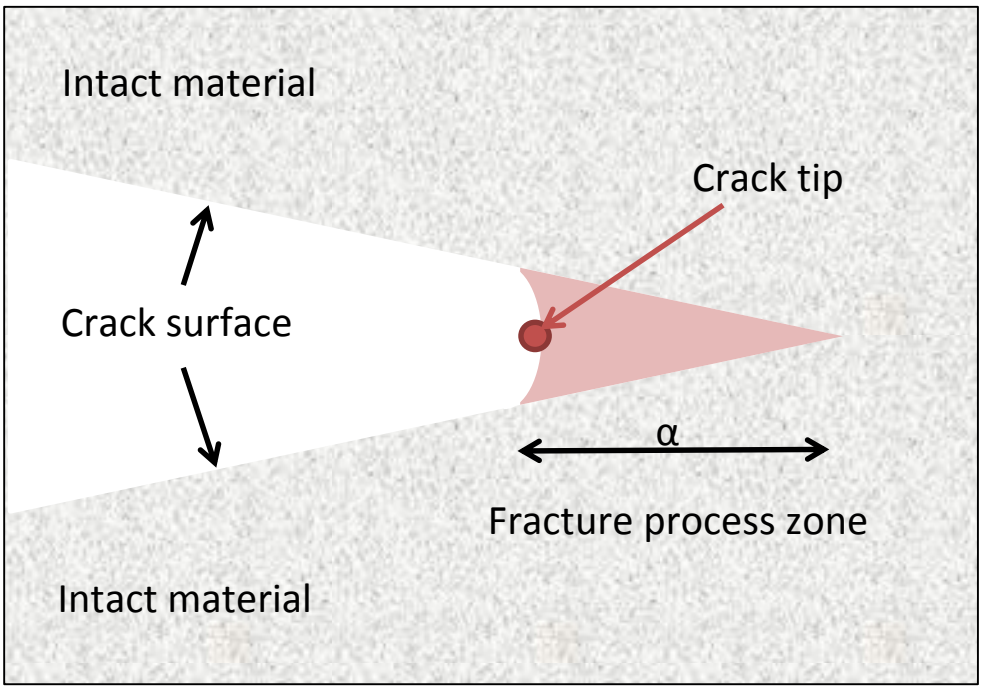

Figure 4-18 : Schematic view of the crack tip and fracture process zone

For a fully elastic material the creep compliance is a constant, J, and the reference modulus E_R may be chosen to be equal to J^{-1}. In this case it is clear that Equation 4-21 reduces to the well-known fracture mechanics result of $W_f=J_v$. Therefore, instead

of expressing the Paris Law in terms of K or J an alternative model for the crack growth rate is suggested in Equation 4-22 in terms W_f.

$$\frac{dc}{dN} = A_W[W_f]^{n_W} \quad \textbf{Equation 4-22}$$

In plain strain the viscoelastic J-integral is related to the mode one stress intensity factor by

$$J_V = (1 - \nu^2)\frac{K_I^2}{E_R} \quad \textbf{Equation 4-23}$$

Where ν is Poisson's ratio

Substituting Equation 4-23 into Equation 4-21

$$W_f = (1 - \nu^2)\int_0^{t_i} J(t_i - \tau)\frac{\partial K_I^2}{\partial \tau} d\tau \quad \textbf{Equation 4-24}$$

Allowing W_f to be calculated from experimental data

4.9.3 Cyclic Test Results

The same experimental setup was used as for the monotonic tests. All specimens were notched with an initial notch depth of 9mm and prior to testing these specimens were painted with white emulsion to provide a clearer determination of the crack location on the front face of the specimen. During the test an external floodlight was also used to provide a consistent illumination of the specimen face to further improve the consistency of the crack location recording as shown in Figure 4-19. As the testing period could potentially extend for many hours rather than record the crack at fixed time intervals a photograph was only taken every 0.1mm of permanent vertical deformation, leading to approximately 50 frames per test.

Figure 4-19 : SCB specimen under test with camera and light source

A sinusoidally varying load was applied to each specimen at 1Hz. For each asphalt mixture three specimens were analysed using a 1kN peak to peak loading, with additional specimens analysed at 0.5kN and 2kN. A typical crack propagation is shown in Figure 4-20, and typical measured values of vertical displacement and CMOD shown in Figure 4-21 and Figure 4-22

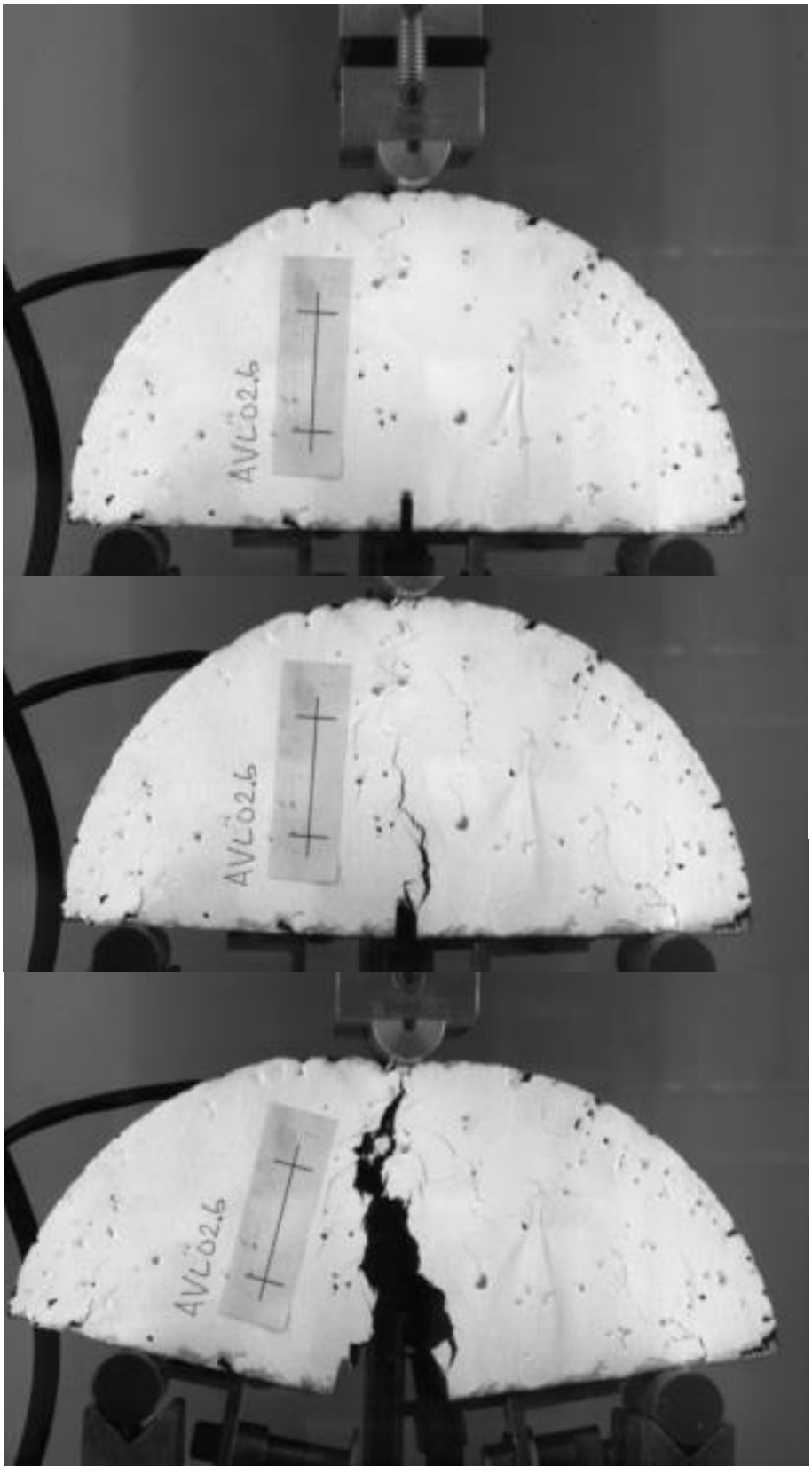

Figure 4-20 : Typical crack propagation during cyclic testing of asphalt AVL

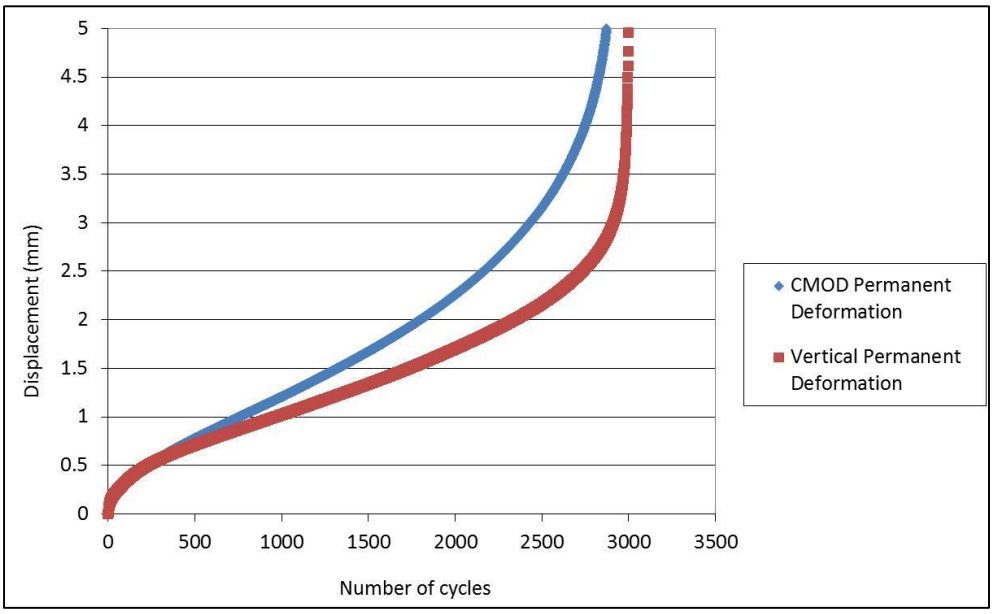

Figure 4-21 : Measured Permanent Deformation for AV0 1kN Peak-to-Peak Load

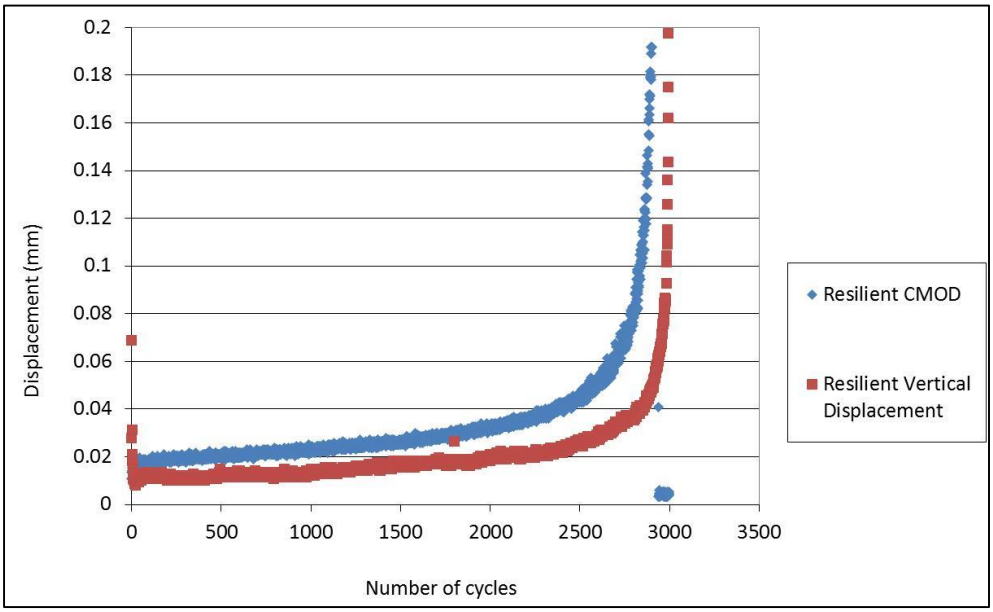

Figure 4-22 : Measured Resilient Displacement for AV0 1kN Peak-to-Peak Load

The average number of cycles to failure is shown in Figure 4-23 for specimens with 1kN peak to peak loading. As can be seen there is a general increase in the number of cycles to failure with increasing levels of polymer content, with the limestone mixture outperforming the gritstone mixture.

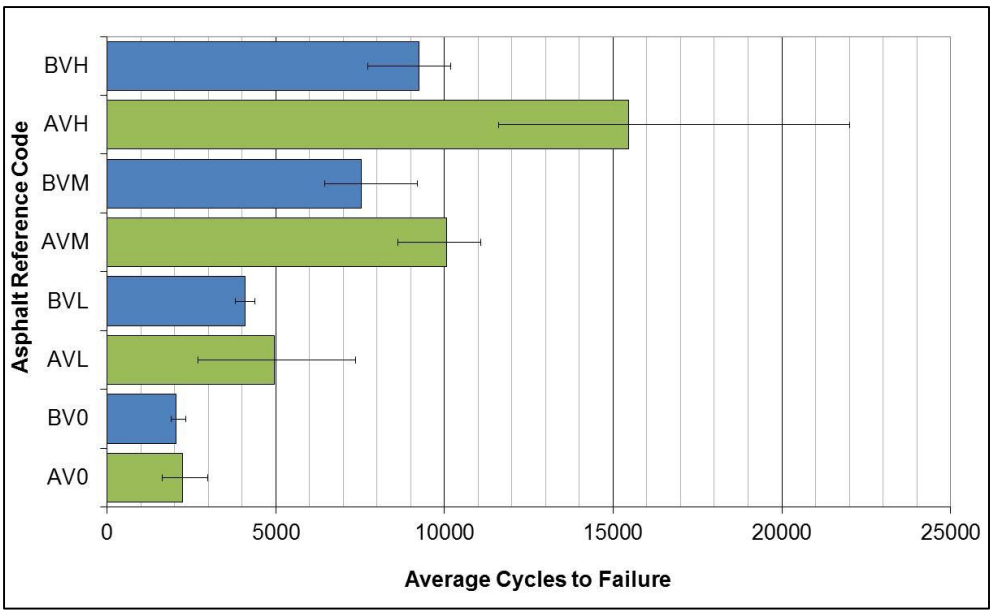

Figure 4-23 : Average cycles to failure of asphalt mixtures under test at 1kN peak to peak applied stress

4.9.4 Paris Law analysis

A traditional Paris Law LEFM approach was first employed to determine crack growth rates of the asphalts and material constants in Equation 4-17. The experimental results for specimens tested at 1kN peak to peak loading are shown graphically in Figure 4-24 for asphalt AVO, with the Paris Law constants summarised in Table 4-6. The graphical results for all the asphalts are included in Appendix A.

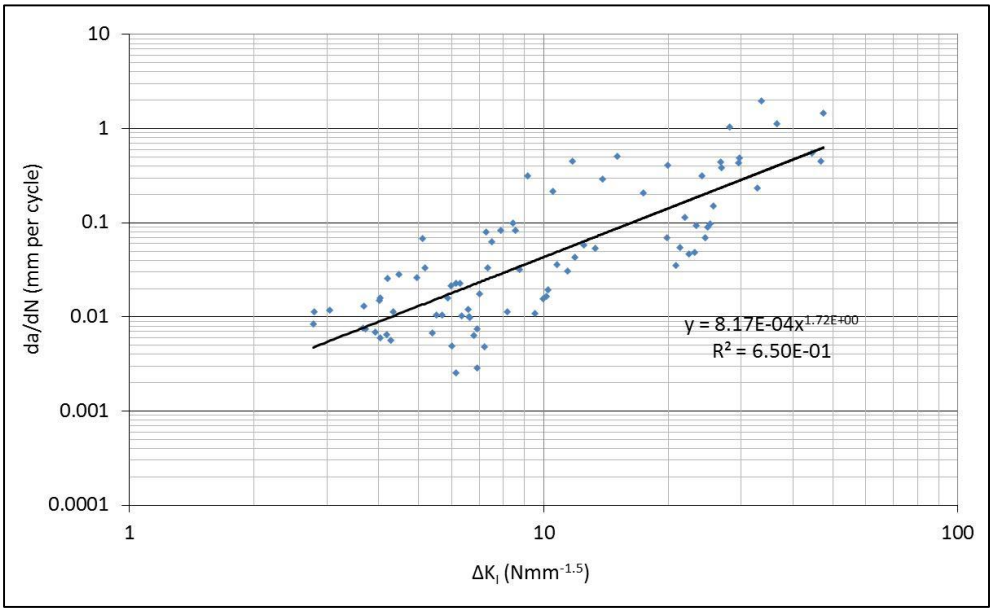

Figure 4-24 : Crack growth rate versus ΔK_1 for AV0

	A (mm/cycle(Nmm$^{-1.5}$)^n)	n	R^2
AV0	8.17E-04	1.72	0.65
AVL	3.99E-04	1.88	0.63
AVM	3.60E-05	2.69	0.71
AVH	1.03E-04	2.00	0.59
BV0	4.01E-04	2.08	0.63
BVL	2.74E-04	2.38	0.49
BVM	1.14E-04	2.17	0.82
BVH	1.24E-04	2.41	0.84

Table 4-6 : Paris Law constants determined at 1kN peak to peak loading

For both aggregate types it can be seen that as the polymer content increases and the number of cycles to failure increases there is a decreasing trend in the Paris Law constant 'A'. The exponent 'n' shows smaller variation with a lesser tendency to increase with increasing polymer modification levels.

However, the practical difficulties in accurately measuring the crack propagation are revealed by the wide range of R^2 correlations from 0.49 to 0.86. Whilst the crack measurements are made on the camera facing side of the specimen, the actual crack tip position could be anywhere within the bulk of the specimen. Furthermore, whilst the crack propagation and vertical deflection of the specimen are obviously related, by only triggering the camera at 0.1mm vertical displacement intervals an error is introduced in accurately capturing the number of cycles necessary required to propagate the crack.

4.9.5 Work of fracture analysis

To determine the work of fracture during crack growth Equation 4-24 was evaluated. To simplify the algebra K_I may be re-written as

$$\boldsymbol{K_I = P(t)G(a)} \qquad \textbf{Equation 4-25}$$

where $\boldsymbol{G(a) = Y\sqrt{\pi a}}$

The applied loading stress P(t) is

$$\boldsymbol{P(t) = \frac{A_0}{2rb}(1 - cos(2\pi ft))} \qquad \textbf{Equation 4-26}$$

where A_0 is the peak to peak applied loading, f is the frequency of loading, r is the sample radius, b is the sample thickness, and t is time.

Substituting Equation 4-25 into 4-24 therefore gives

$$\boldsymbol{W_f = (1 - \nu^2)G^2(a)\int_0^{t_i} J(t_i - \tau)\frac{\partial P^2(t)}{\partial \tau}d\tau} \qquad \textbf{Equation 4-27}$$

And expanding P(t) and differentiating with respect to τ we find that

$$W_f = \frac{A_0^2 \pi f (1-\nu^2) G^2(a)}{r^2 b^2} \int_0^{t_i} J(t_i - \tau) sin(2\pi f t)(1 - cos(2\pi f t)) d\tau$$

Equation 4-28

When the integral portion of Equation 4-28 is evaluated the function has the general shape shown in Figure 4-25.

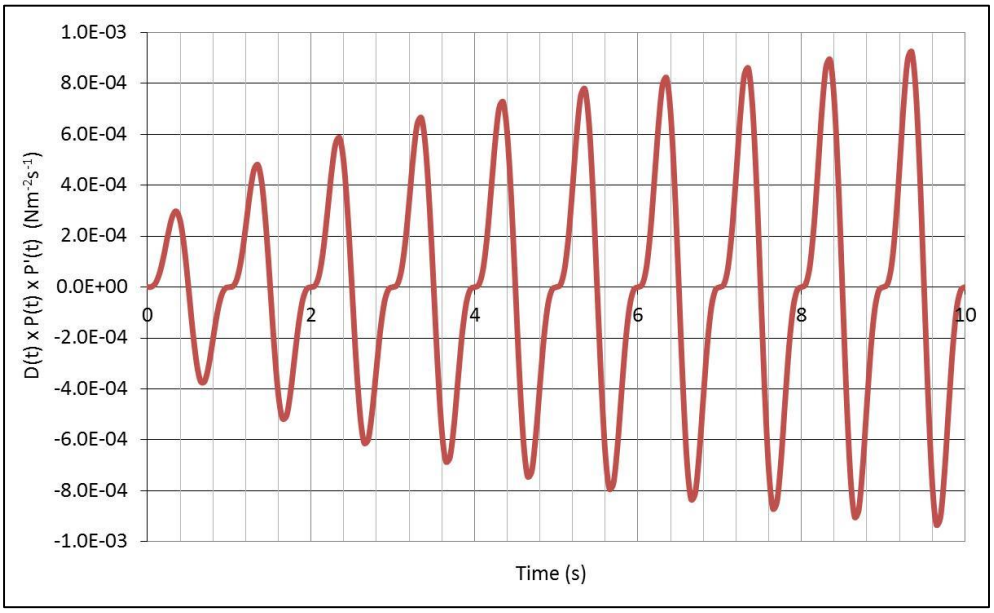

Figure 4-25 : Typical function of the contents of the integral to be evaluated

To correctly evaluate Equation 4-28 the selection of t_1 is vitally important. Kuai et al. (2009, 2010) analysed compact tension specimens using a similar approach but only evaluated the work of fracture once the change from cycle *i* to *i*+1 tends to zero. However, this only occurs when the creep compliance reduces to a constant, and therefore $W_f = J_v$ and the analysis reverts to a simple Paris Law. To correctly include the time dependent effects in this research the integral is evaluated from t=0 until the measured time t_1 where the crack is observed to have propagated.

The creep compliance data from the DSR, the mode I SCB stress intensity factor, and the applied haversine loading function were therefore used to calculate W_f

during crack growth using Equation 4-28 over the time taken for the crack to propagate. For all the asphalts tested Poisson's ratio was assumed to be 0.35.

These results are shown graphically in Figure 4-26 for asphalt AVO, with results for all the asphalts included in Appendix A. The crack growth rate parameters A_n and n_w for Equation 4-22 are summarised in Table 4-7.

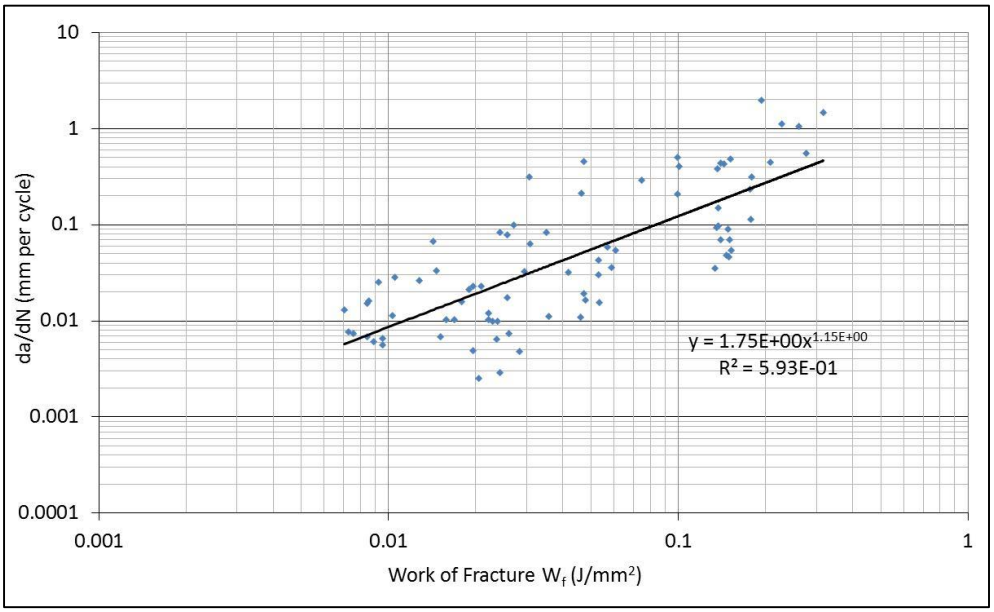

Figure 4-26 : Crack growth rate versus W_f for AV0

	A_W (mm/cycle$(Jmm^{-2})^{n_W}$)	n_W	R^2
AV0	1.75	1.15	0.59
AVL	1.99	1.08	0.61
AVM	19.7	1.66	0.67
AVH	0.92	0.99	0.48
BV0	4.75	1.39	0.53
BVL	4.11	1.18	0.31
BVM	3.42	1.27	0.75
BVH	18.12	1.42	0.86

Table 4-7 : Constants for equation 6 determined at 1kN peak to peak loading

Kuai et al. (2009 and 2010) found values of A_w and n_w at 20°C ranging from 0.62 to 19.6 and 1.32 to 1.63 respectively for the compact tension specimen, with similar results found in this research. Surprisingly no clear trends were found between the degree of polymer modification and the values of A_w and n_w as observed earlier in the traditional Paris Law analysis.

A wide range of R^2 correlations was again found. As can be seen in Figure 4-27 there are many smaller cracks throughout the specimen in addition to the main central growing crack. Localised cracking can also be seen in the loading point and at the supports. The energy required to form these cracks is not captured in the current model, and therefore further contributes to error.

Alternative methods to record crack propagation and specimen deformation have been investigated by other researchers (Aragão and Kim 2011; Nguyen et al., 2013) with encouraging results, and it is evident that an improved approach to determining

the precise location of the crack tip is necessary to more accurately model its behaviour.

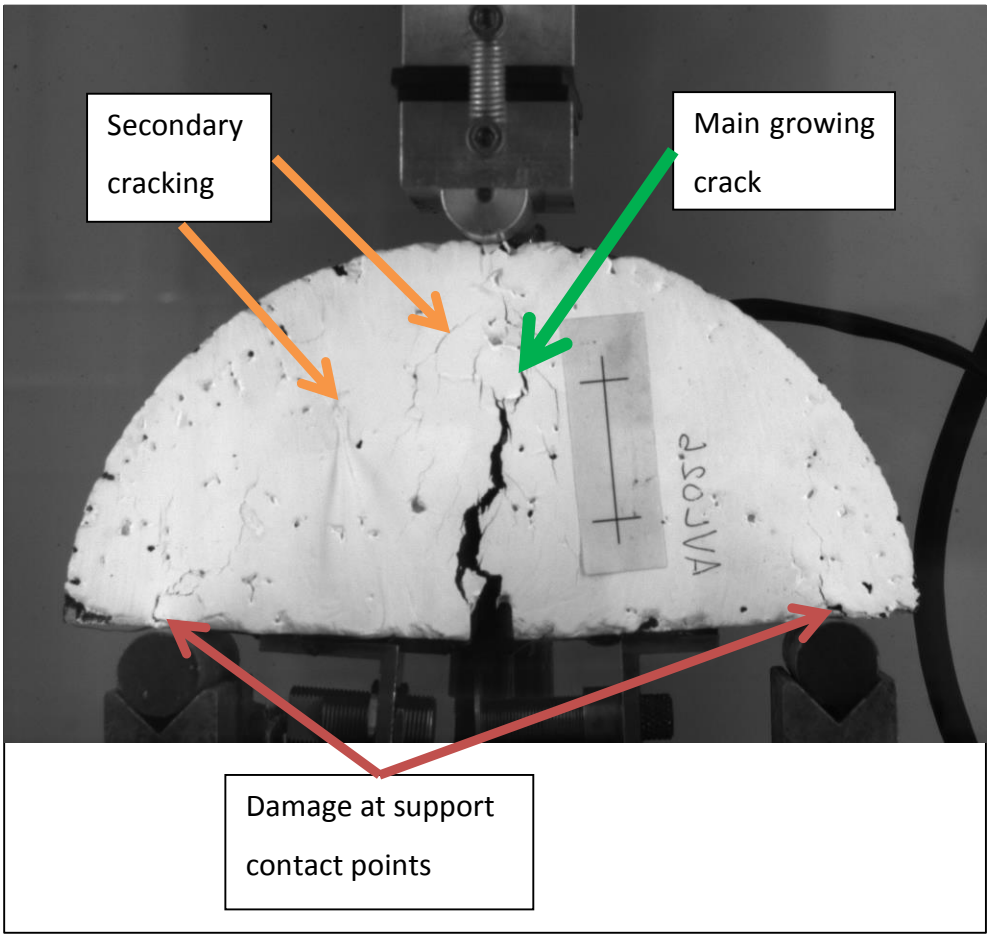

Figure 4-27 : Crack types generated during cyclic test

4.9.6 Prediction of Pavement Service Life

HD26 of the UK Design Manual for Roads and Bridges (Highways Agency 2006) provides detailed pavement design guidance for the UK trunk road network. This document was used to design a typical three-layer pavement structure. The subgrade was a semi-infinite layer with a modulus of 100MPa. The second layer was a 300mm thick subbase with a modulus of 200MPa, with both the subgrade and subbase assumed to have a Poisson's ratio of 0.4. A single 320mm thick asphalt layer, with Poisson's ratio of 0.35 and moduli as reported in Table 4-1 completed the pavement structure.

The loading times encountered during the ITSM test are relatively long and fixed, whereas in reality traffic speeds are variable and loading times shorter. Therefore, the actual modulus of the asphalt would be greater than the ITSM values, but as a first approximation, this factor has not been included here.

The Shell BISAR software (Shell International Oil Products 1998) was used to simulate the pavement structure. This was loaded with a standard axle which is defined as applying a total load of 80kN. Therefore, each super single tyre applied a load of 40kN and the assumed tyre contract area was taken as 0.1575m^2. The stress and strain at the base of the asphalt layer were then calculated for each asphalt type.

By integrating the Paris Law, Collop, Sewell and Thom (2004) showed how the number of cycles required to propagate a crack through a known thickness layer may be determined

$$\boldsymbol{N = \frac{1}{A}\int_{a_0}^{h} \frac{da}{[\Delta K_I]^n}} \qquad \textbf{Equation 4-29}$$

As the modulus of the asphalt layer is significantly higher than that of the subbase it is assumed to behave as a bending beam when loaded. Therefore, the asphalt layer behaves as an edge cracked plate subject to pure bending and the stress intensity factor shown to be (Anderson 2005)

$$\boldsymbol{K_I = \sigma\sqrt{\pi a}\left(\sqrt{\frac{2h}{\pi a}tan\left(\frac{\pi a}{2h}\right)}\right)\sec(\pi a/2h)(0.923 - 0.199[1 - \sin(\pi a/2h)]^4)}$$

Equation 4-30

In a similar manner Equation 4-22 may be rearranged to give N in terms of W_f and the pseudo Paris-Law constants A_w and n_w

$$\boldsymbol{N = \frac{1}{A_W}\int_{a_0}^{h} \frac{da}{[\Delta W_f]^{nW}}} \qquad \textbf{Equation 4-31}$$

By assuming that the time between crack growth steps is long relative to the relaxation of the material W_f is reduced to $W_f = J_v$, and, therefore,

$$N = \frac{1}{A_W}\left(\frac{E_R}{(1-\nu^2)}\right)^{n_W} \int_{a_0}^{h} \frac{da}{[\Delta K_I^2]^{n_W}} \qquad \textbf{Equation 4-32}$$

An initial crack length of 1mm was assumed and Equation 4-32 and Equation 4-34 integrated numerically to h=320mm at which point the crack had propagated completely through the asphalt layer and the pavement failed. The results using the Paris Law approach (A and n) and the pseudo Paris Law (A_w and n_w) are summarised in Table 4-8.

	N (msa) from Paris Law	N (msa) from J-integral Pseudo Paris Law
AV0	1.70E-02	8.06E-02
AVL	3.06E-02	6.10E-02
AVM	2.55E-01	1.09E+00
AVH	8.99E-02	6.08E-02
BV0	3.46E-02	1.66E-01
BVL	3.93E-02	5.67E-02
BVM	9.17E-02	1.59E-01
BVH	7.89E-02	9.98E-02

Table 4-8 Predicted number of standard wheel loads to pavement failure

The predicted time to pavement failure was longer in seven of the eight constructions when the J-integral approach was employed compared to the LEFM approach. The J-integral approach includes the additional plastic deformation energy which is the most probable cause of the increased lifetimes.

The number of load cycles to failure was found to be far lower that the values included in HD26. In part this is a consequence of assuming that the asphalt is already pre-cracked at the base of the asphalt layer which propagates to the asphalt surface.

Furthermore, no account of the commonly taken upscaling factor was included in this analysis to account for the differences between field and laboratory conditions (Molenaar 2007).

4.10 Concluding Remarks

In this chapter the SCB geometry was successfully used to evaluate the crack resistance of unmodified and polymer modified asphalts. Under monotonic loading at 20°C the response, particularly at lower loading rates, was found to be predominantly plastic rather than elastic. It was, therefore, demonstrated that a simple linearly elastic analysis of the results does not fully capture the behaviour of asphalt.

A new visual method of analysing the crack opening displacement of monotonically loaded SCB was successfully developed. This enabled new values for the rotational factor of the notched SCB geometry to be determined.

The effect of polymer modification was effectively investigated via the critical strain energy release rate, J_{IC}. As the polymer content of the asphalts was increased J_{IC} also increased indicating an improved resistance to debonding stresses and fracture.

The crack growth rate of cyclically loaded notched SCB asphalt was successfully investigated using image analysis technique with increasing polymer modification shown to produce an increase in the number of cycles to failure.

In order to more completely capture the visco-elastic plastic properties of the asphalt cracking a generalised J-integral work of fracture model was developed with a reasonable correlation between the work of fracture and the crack growth rate was found. Surprisingly there were no clear correlations found between the fracture model parameters and the level of polymer modification.

The results of the work of fracture model were used to predict the crack propagation within a typical UK flexible pavement construction assuming standard wheel loading conditions. This model was used to predict the number of wheel loadings to pavement failure and compared to a model based on a traditional linearly elastic response. In seven of the eight asphalt's studied a longer pavement lifetime was found using the J-integral approach. This demonstrated the importance of capturing the entire response of the asphalt to realistically predict pavement performance.

5 EXTENDED FINITE ELEMENT MODELLING**

5.1 Introduction

In applied science and engineering only relatively simple problems may be analytically resolved by the solution of their differential or integral equations. More typically the system being studied has complicated geometry, loading and material properties which do not allow analytical solutions to be calculated. In these cases, to find an approximate solution the complex system is divided into a large number of smaller bodies, known as Finite Elements, for which the physical properties of the smaller element can be described mathematically. These elements are then connected to one another at node points, leading to a very large number of simultaneous equations which may then be solved to find the unknown quantities at the nodes (i.e. displacements). It is then possible to calculate the stresses and strains within each of the elements and, by extension, of the whole system.

5.2 The eXtended Finite Element Method

The Finite Element Method (FEM) is very widely employed in engineering simulations, and as computing processing power continues to increase the complexity of models that can be analysed increases accordingly. However, when the model contains discontinuous elements such as cracks or inclusions the traditional FEM approach is not ideally suited. The classical approach to modelling cracks in FEM is to use a cohesive zone (CZ) model. A crack in the CZ model must

** This chapter includes results originally published in Lancaster I.M., H. Al-Khalid, and I. Kougioumtzoglou, (2013) "Extended FEM Modelling of Crack Propagation using the Semi-Circular Bending Test" Construction and Building Materials, Volume 48, pp. 270 – 277 (doi:10.1016/j.conbuildmat.2013.06.046), reproduced with permission.

have the edges of the elements aligned with the crack path as shown in Figure 5-1. Furthermore, a more highly refined mesh is necessary near to the crack tip to resolve singularities in the calculations. As the FEM simulation progresses the model must then be remeshed to ensure the crack path remains along element edges and the crack tip retains a sufficiently fine element density leading to this approach requiring a very high computational demand.

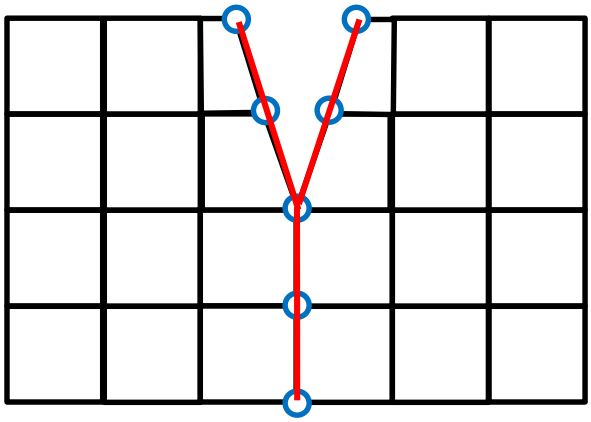

Figure 5-1 : Schematic of Cohesive Zone crack propagation modelling in FEM

Belytschko and Black (1999) and Moes, Dolbow and Belytschko (1999) employed the partition of unity theory (Melenk and Babuska 1996) to develop a model which allowed the crack location and propagation to be independent of the overall model's mesh, and this became known as the eXtended Finite Element Method (XFEM).

In this method the nodes of elements close to the discontinuity of interest, such as a crack, are enriched by including additional degrees of freedom and shape functions which allow the discontinuity to be independently modelled. As a consequence, as the crack propagates, there is no longer a requirement to re-mesh the model at each step as shown in Figure 5-2. A further advantage of XFEM is the crack is able to propagate in any direction within the bulk of the material which enables more realistic models to be developed. Due to the complex geometries and stress configurations encoutered in asphalt models XFEM is, therefore, particularly suitable approach for modelling crack propagation.

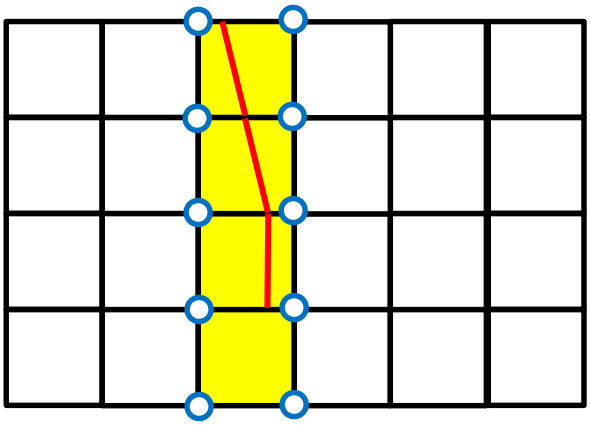

Figure 5-2 : Schematic of crack propagation modelling in XFEM

In a traditional FEM the displacement vector field ū is

$$\vec{u} = \sum_{i=1}^{N} N_i(x)\vec{u}_i \qquad \textbf{Equation 5-1}$$

where i is the set of all nodes in the domain, N_i is the standard finite element shape function of node i, and $\bar{u}_i$ are the nodal displacement vectors.

To model the discontinuity in XFEM additional nodes are included

$$\vec{u} = \sum_{i=1}^{N} N_i(x)\left[\vec{u}_i + H(x)\vec{a}_i + \sum_{\zeta=1}^{4} F_\zeta(x)\vec{b}_i^{\zeta}\right] \qquad \textbf{Equation 5-2}$$

where H(x) is the is the Heaviside function with value +1 on one side of the crack and -1 on the other, $\bar{a}_i$ and $\bar{b}_i^{\zeta}$ are vectors of additional nodal degrees of freedom, and $F_\zeta(x)$ is the elastic asymptotic crack-tip function.

5.3 Semi-Circular Bend Geometry Modelling

Modelling the notched SCB geometry, described in detail in chapter 4, is possible but challenging using CZ in a traditional FEM (Elseifi et al. 2012). However, the use of XFEM greatly simplifies the crack modelling procedure.

5.3.1 Stress Intensity Factors

Many commercially available packages exist to conveniently enable FEM models to be developed, and in this study Abaqus was used as it included native support for XFEM cracks. To verify the XFEM implementation the mode I Stress Intensity Factors (SIF) were calculated over a range of span to radius, and crack depth to radius ratios.

A 3D model of the notched SCB geometry was created comprised of 39476 elements. Most of the model was composed of 4 node linear tetrahedrons, with 8 node linear bricks with reduced integration and hourglass control close to the crack tip as shown in Figure 5-3.

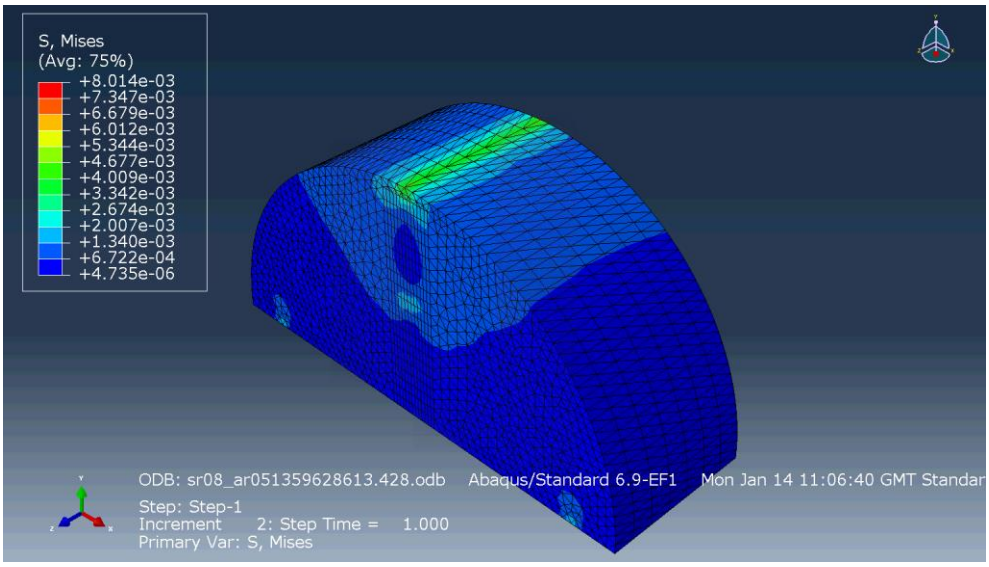

Figure 5-3 Abaqus Model for Stress Intensity Factor Calculation.

The SIF for models with span to radius ratios of 0.8, 0.61, and 0.5 with crack to radius ratios from 0.1 to 0.8 for each span was calculated. In Figure 5-4 the SIF results are plotted along with the values calculated by Lim, Johnson and Choi (1993). Good agreement between the two data sets was found confirming that the XFEM implementation in Abaqus was performing satisfactorily.

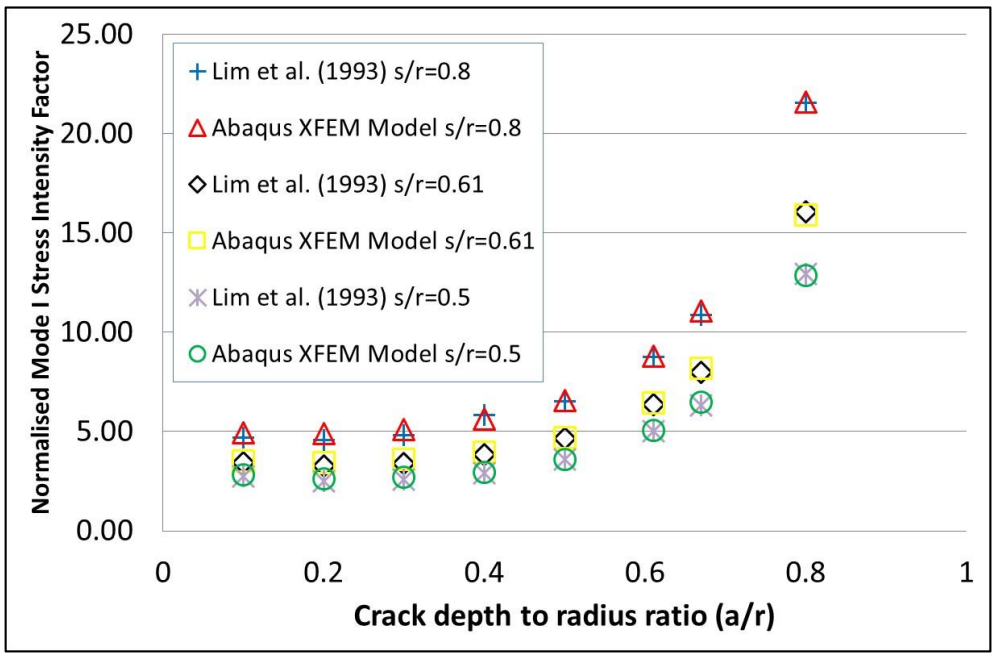

Figure 5-4 Stress Intensity Factors for SCB with Span to Radius ratios 0.5, 0.61 and 0.8.

5.3.2 Monotonic SCB Crack Propagation Model

A model including crack propagation was then developed for the monotonic SCB test in Abaqus version 6.11-2, and to reduce the computational time a 2D model was created. Rather than creating a full 3D model this was justified as, due to symmetry, there are no changes in the z-plane.

The model was created using 600 4-node bilinear plane stress quadrilateral elements with reduced integration and hourglass control. A span to radius ratio of 0.8 was used to match that of the experiments performed in Chapter 4, with XFEM cracks 9, 19, and 29mm long. A typical crack propagation generated by the model is shown in Figure 5-5 with the crack progressing in a mode I direction as envisaged.

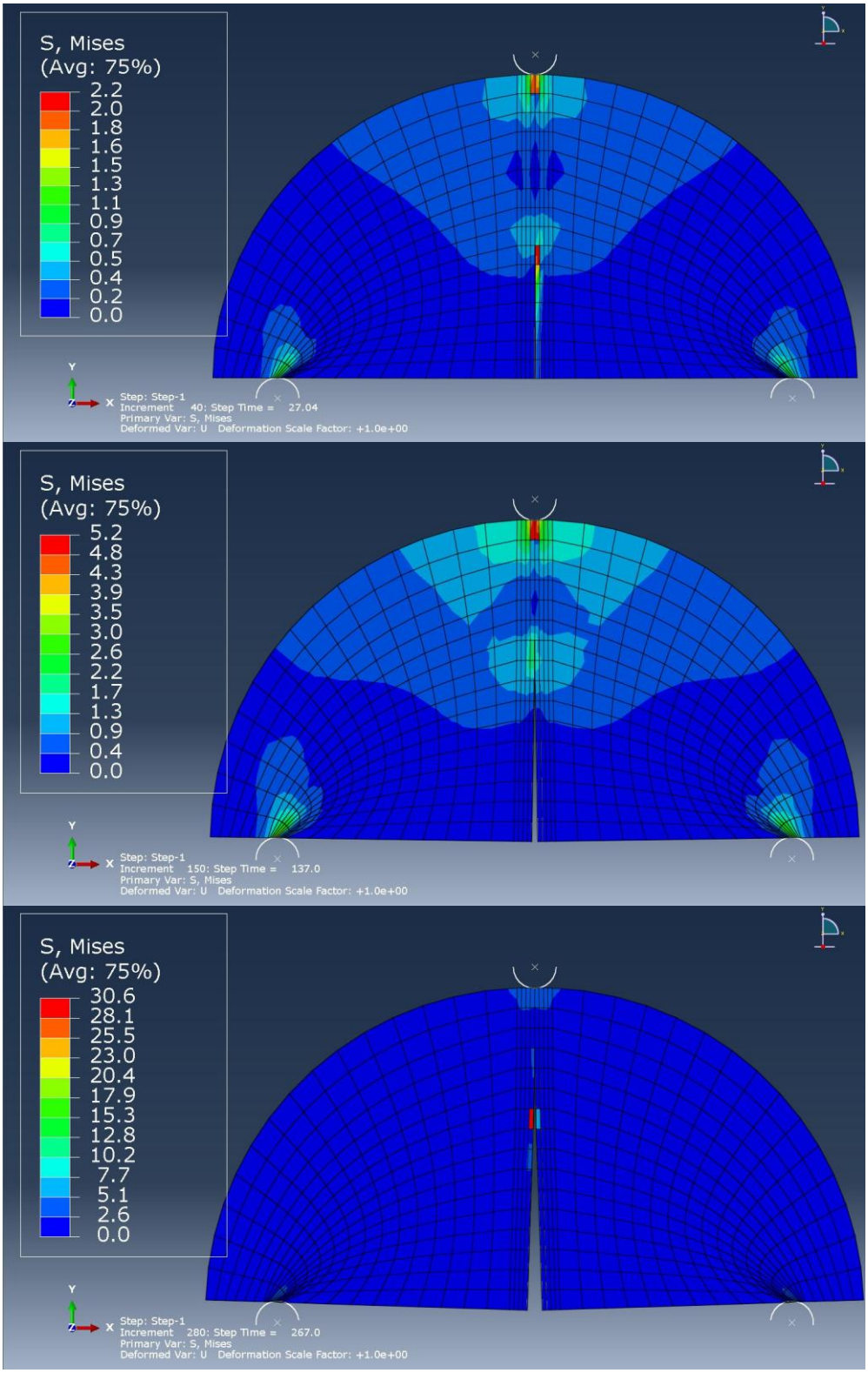

Figure 5-5 : Typical Crack propagation in the Abaqus XFEM model

The time dependent viscoelastic material characteristics were included in the model for each asphalt type by entering the creep results determined in Chapter 3 using the fractional derivative springpot model.

The other material properties necessary for the model were Young's modulus, fracture energy and maximum cohesive stress. The maximum principle stress determines the point where damage is initiated in the XFEM model. When the ratio of the maximum principle stress of the material, $\sigma^0_{max,}$ and the calculated maximum principle stress in the XFEM model, σ_{max}, is equal to 1 damage initiation occurs. To avoid damage initiation from compressive stresses $\sigma_{max} = 0$ if $\sigma_{max}<0$, and $\sigma_{max} = \sigma_{max}$ if $\sigma_{max}\geq 0$. This is usually denoted using the Macaulay bracket <> as in Equation 5-3,

$$f = \left(\frac{\langle \sigma_{max} \rangle}{\sigma^0_{max}} \right) \qquad \textbf{Equation 5-3}$$

Damage evolution may then be described by either the displacement at failure or, as used in this research, the failure fracture energy.

To determine the appropriate values for CZ FEM models Aragao and Kim (2011) and Elseifi et al. (2012) followed a trial and error procedure until a correspondence was found to laboratory experiments. A similar method was followed in this research as detailed in Figure 5-6.

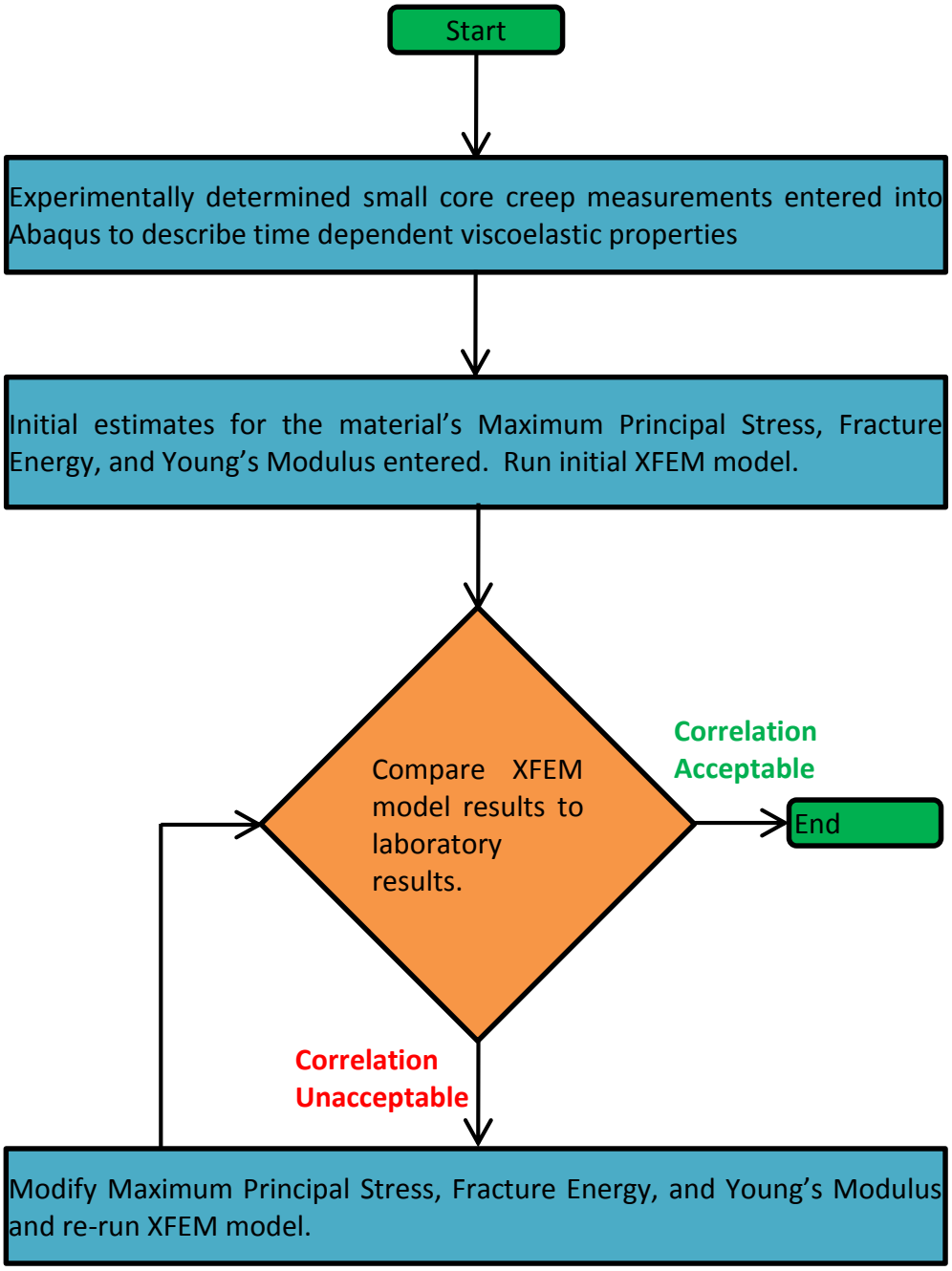

Figure 5-6 : Procedure to optimise XFEM model input parameters

The results from the optimised XFEM models for asphalts AV0, AVL, AVM and AVH are shown in Figure 5-7, Figure 5-8, Figure 5-9 and Figure 5-10

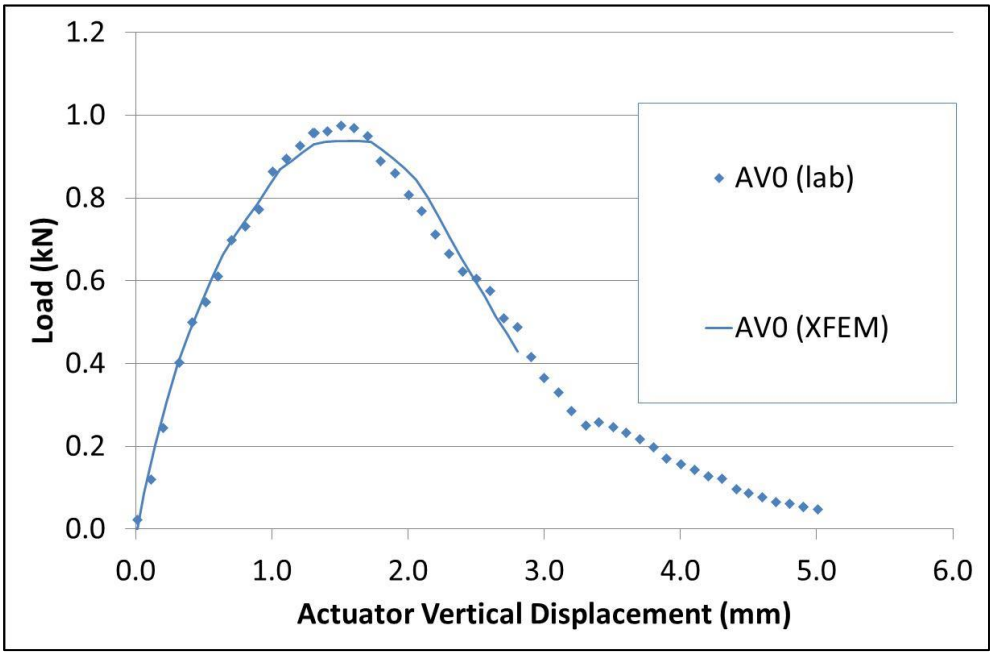

Figure 5-7 : XFEM model compared to laboratory SCB testing for asphalt AV0

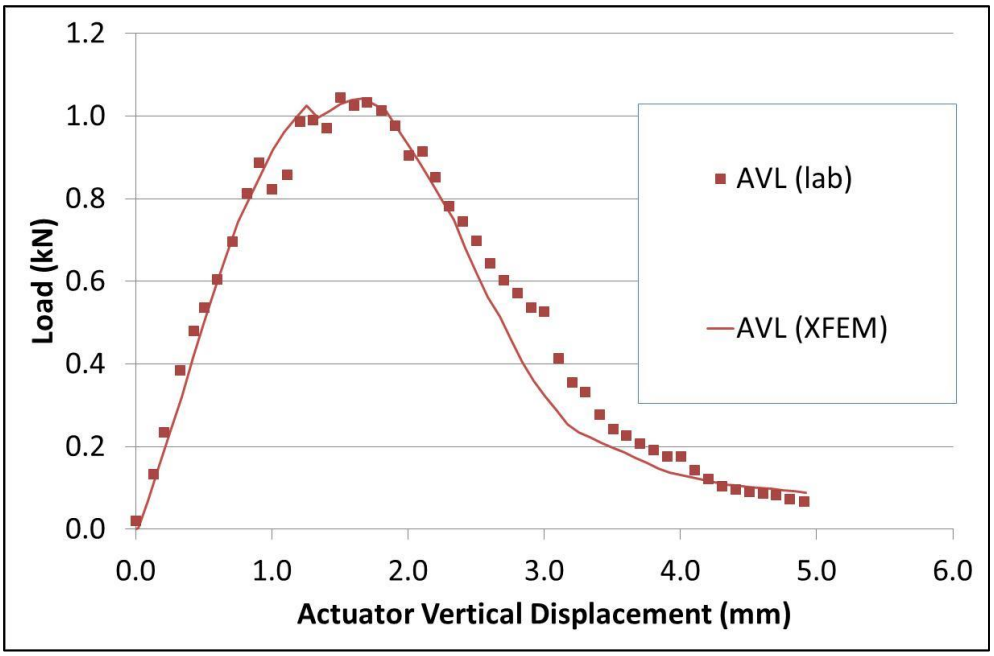

Figure 5-8 : XFEM model compared to laboratory SCB testing for asphalt AVL

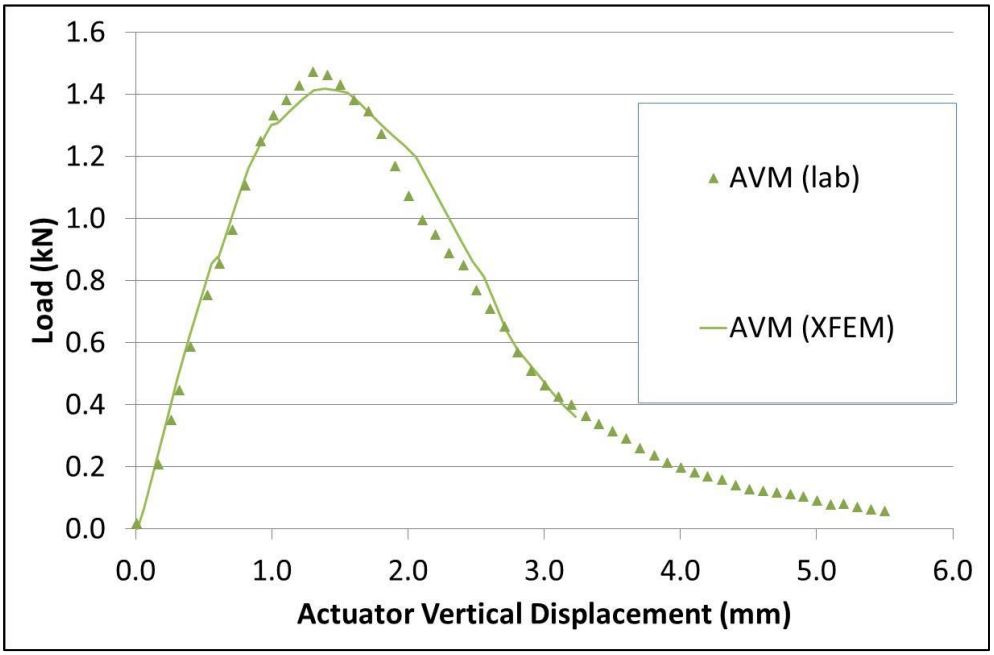

Figure 5-9 : XFEM model compared to laboratory SCB testing for asphalt AVM

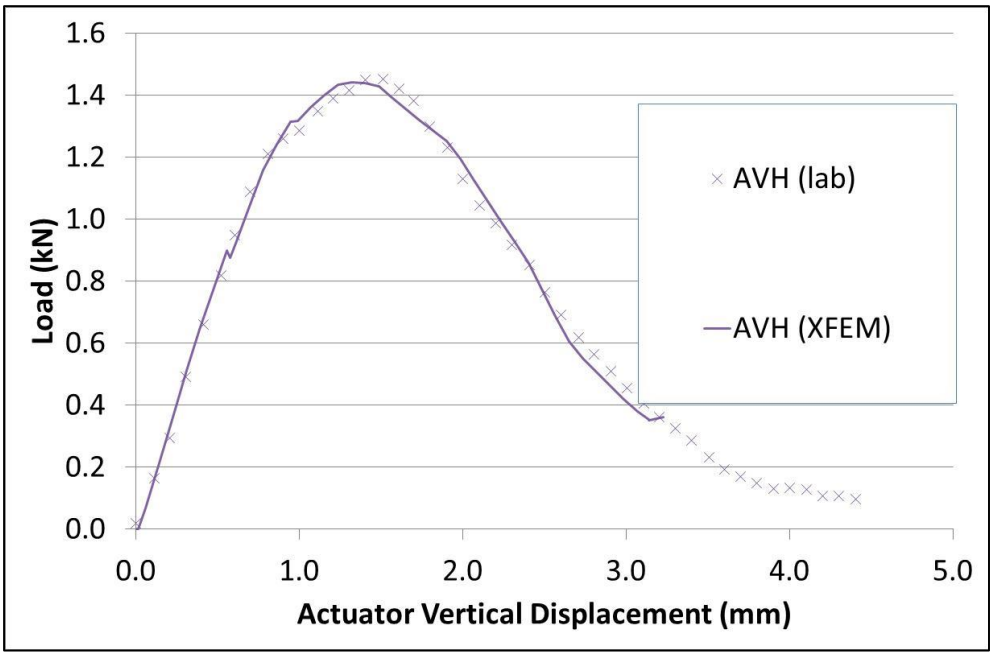

Figure 5-10 : XFEM model compared to laboratory SCB testing for asphalt AVH

The XFEM models predict the load-displacement behaviour of the laboratory experiments with a reasonable accuracy. The increase in peak loads and, therefore, fracture energies is captured with increasing polymer modification of the asphalt.

To assess the model sensitivity to input material properties the fracture energy, Young's modulus, and maximum principle stress were each varied by +/- 10%. These results are shown for asphalt AV0 in Figure 5-11, Figure 5-12, and Figure 5-13. The changes observed are intuitively correct with increasing fracture energy producing an increase in peak load and displacement, increasing Young's modulus producing a steeper initial load-displacement curve, and increasing maximum principle stress producing a higher peak load.

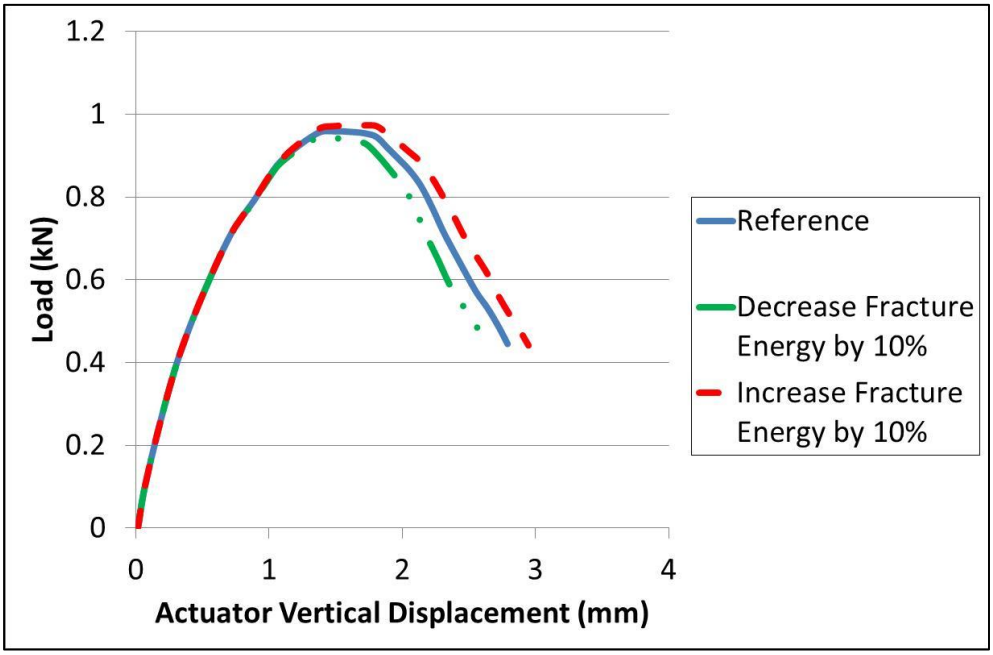

Figure 5-11 : Effect on XFEM model of changes in Fracture Energy of asphalt AV0

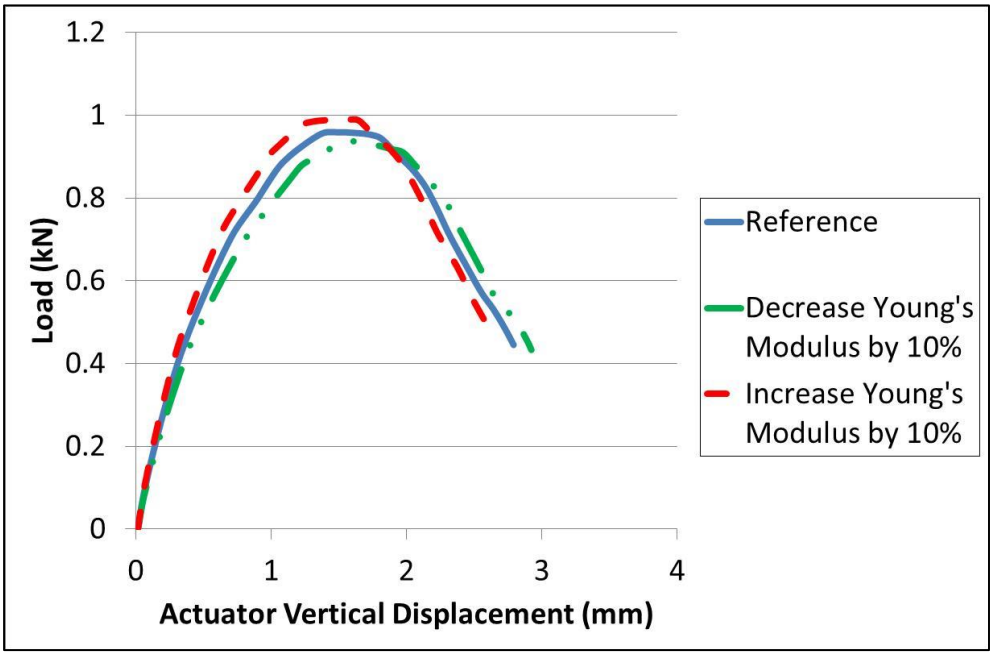

Figure 5-12 : Effect on XFEM model of changes in Young's Modulus of asphalt AV0

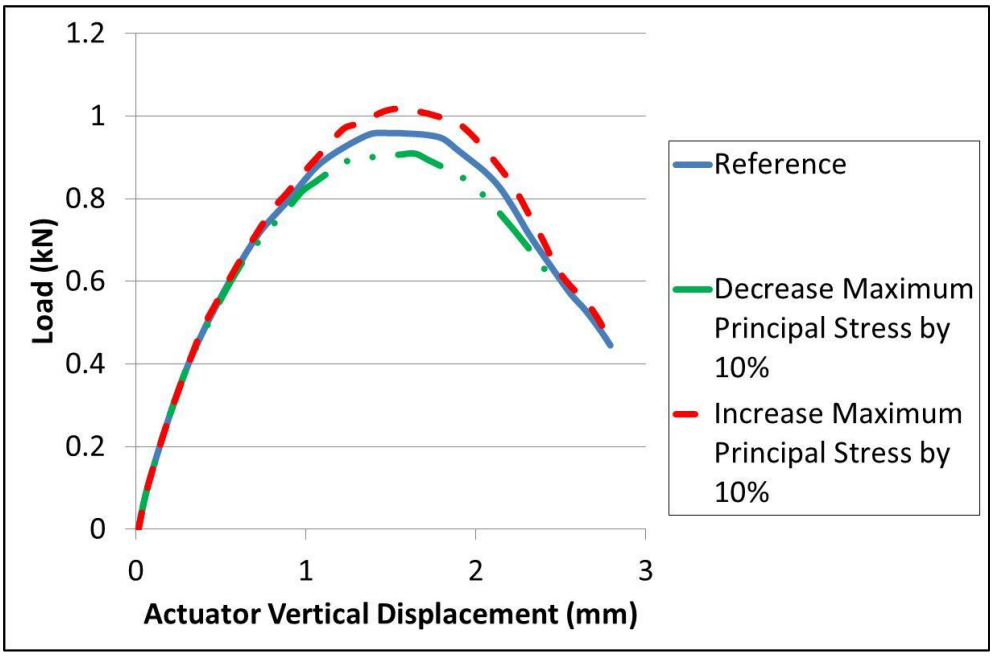

Figure 5-13 : Effect on XFEM model of changes in Maximum Principal Stress of asphalt AV0

The 29mm initial crack length calibrated models were then used to validate the model against experimental data from 9 and 19mm initial crack length tests for asphalts AV0, AVL, AVM, and AVH as shown in Figure 5-14, Figure 5-15, Figure 5-16 and Figure 5-17 respectively.

The peak loads and displacements are in reasonably good agreement with laboratory data, but as with all fracture data a consideration must be made for material variability. For the 9mm crack depths the simulation failed shortly after the peak load and displacement occurred due to the minimum time increment achievable in the software being reached.

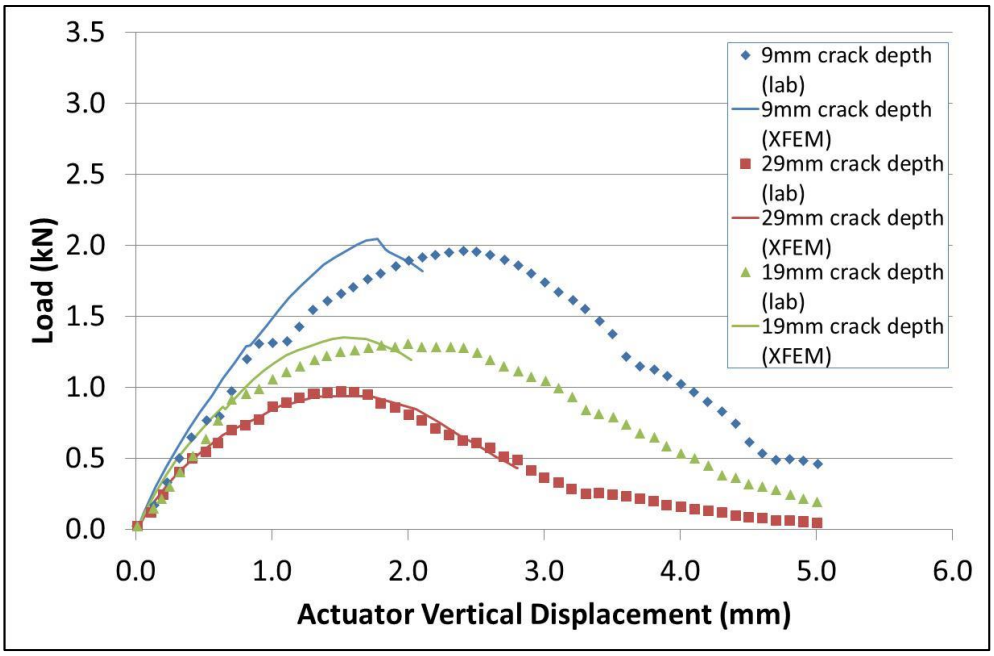

Figure 5-14 : XFEM predictions for asphalt AV0 with 9 and 19mm initial cracks

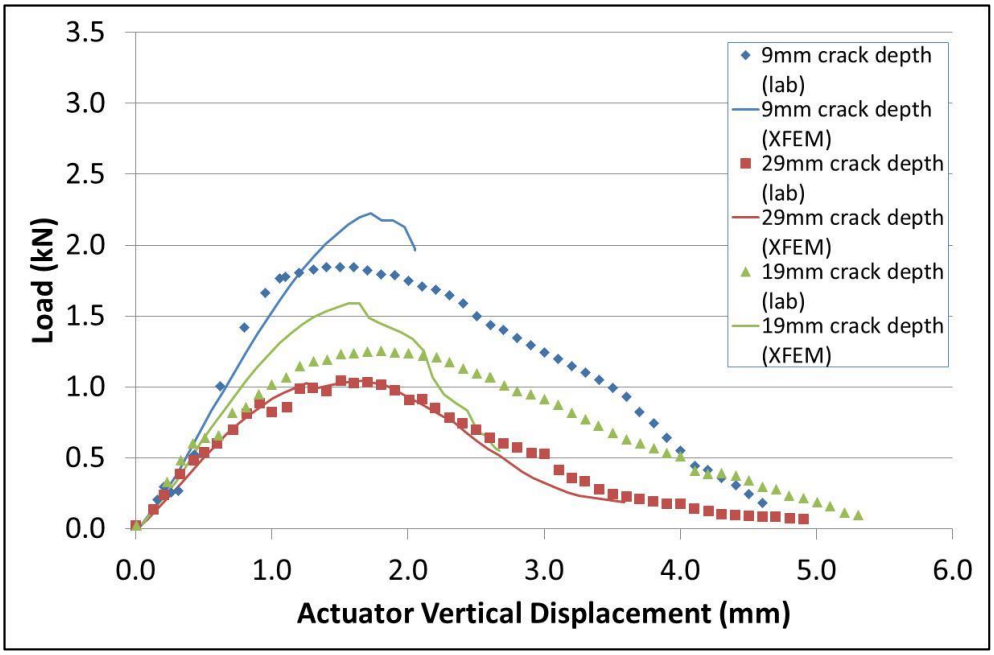

Figure 5-15 : XFEM predictions for asphalt AVL with 9 and 19mm initial cracks

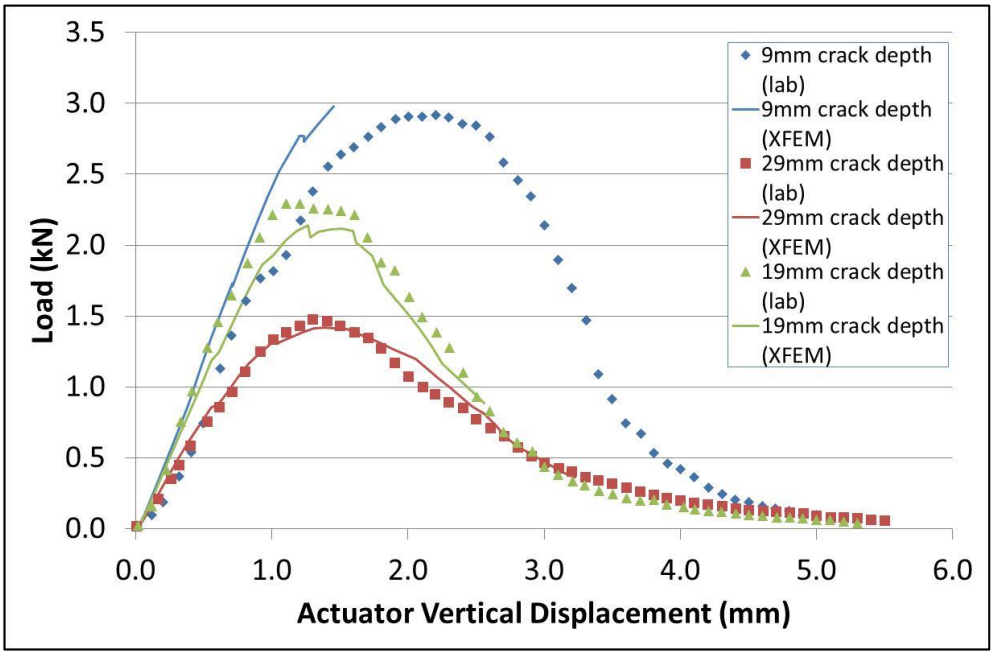

Figure 5-16 : XFEM predictions for asphalt AVM with 9 and 19mm initial cracks

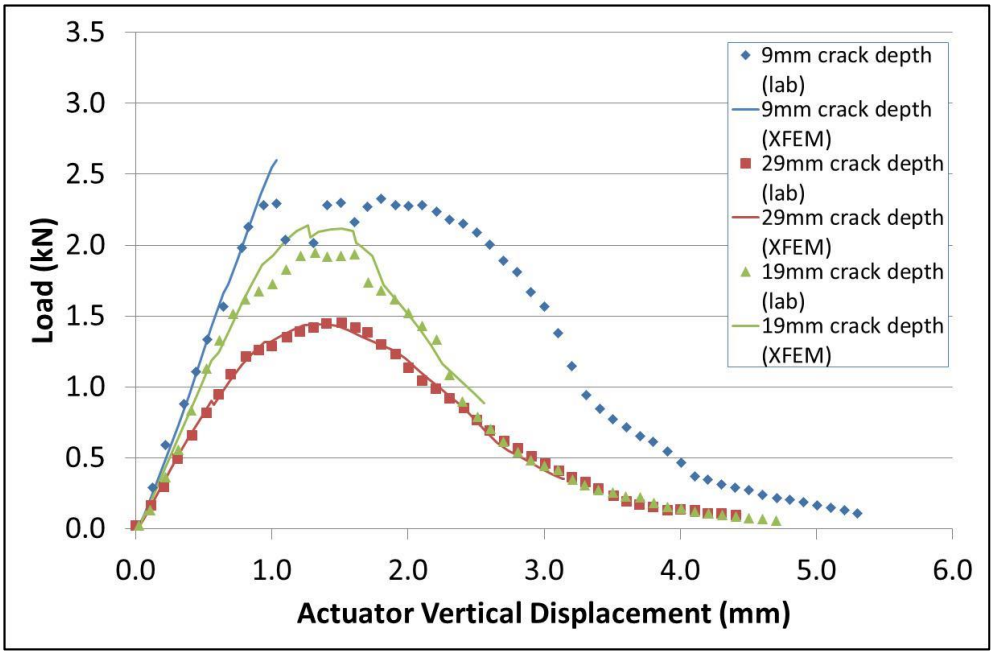

Figure 5-17 : XFEM predictions for asphalt AVH with 9 and 19mm initial cracks

5.3.3 Potential for mixed mode modelling

The advantages of crack propagation modelling using XFEM suggest that it would be particularly suitable for studies of mixed mode crack propagation. To assess this, a crack was modelled at an angle of 45° and was allowed to propagate as shown in Figure 5-18. As can be seen, the crack is free to propagate along a path determined by the simulation and, unlike traditional FEM approaches, does not require any user input to determine the crack direction during its development although further practical work would be required to verify these predictions.

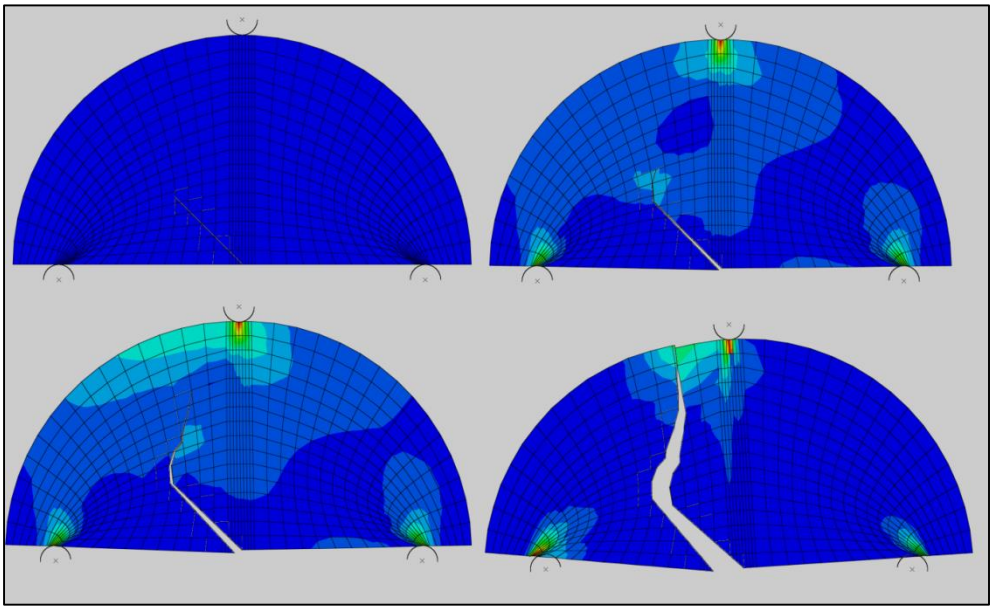

Figure 5-18 Mixed mode crack propagation in the Abaqus XFEM model.

5.4 Concluding Remarks

This chapter has successfully verified the application of the Extended Finite Element Method to mode I cracking of polymer modified asphalt in the Semi-Circular Bending geometry. It has been shown that XFEM in conjunction with experimentally determined linear viscoelastic creep properties can be a promising framework for efficient modelling of complex asphalt cracks.

6 BITUMEN-AGGREGATE BOND STRENGTH MEASUREMENTS

6.1 Introduction

The primary role of bitumen in asphalt is to bind the aggregate particles together to produce a structurally sound material. To produce fracture in asphalt energy must be applied to the system which exceeds a combination of the adhesive bond energy between the bitumen and aggregate, and the cohesive energy within the bitumen film and aggregate. In general, the aggregates in asphalt are the strongest element in the mixture so fracture occurs as a result of cohesive failure within the bitumen film, or adhesive failure between the bitumen and aggregate. Asphalt's bulk fracture properties, such as fracture toughness determined in Chapter 4, may be practically measured but the heterogeneous nature of asphalt means that factors such as aggregate interlock and void content also have a significant influence on the result.

To assess the fundamental nature of the bond the characteristics of the bitumen and aggregate must be determined in isolation from the bulk asphalt. In this chapter the Surface Free Energy (SFE) of the bitumen and aggregate was measured to calculate the theoretical adhesive and cohesive work of fracture. A testing procedure to determine the practical work of fracture between specially prepared aggregate specimens and bitumen was also developed and the relative values discussed.

6.2 Theories of Adhesion

All adhesives share the common goal of joining materials together, and in the specific case of asphalt, bitumen is the adhesive providing the bond between the aggregates. However, there is currently no single theory which fully describes adhesive bonding, but rather there are a range of theories covering individual aspects of adhesion with each type of adhesive bond relying to a greater or lesser extent on

aspects from these theories. These theories will be summarised below with their relevance to asphalt considered.

6.2.1 Mechanical Interlock Theory

At a microscopic level surface irregularities such as natural pores or cavities are present in most materials. During adhesive bonding the air trapped within these features is displaced by the adhesive allowing it to penetrate the substrate's surface. This produces a mechanical interlock contribution to the bond strength and was proposed by McBain and Hopkins (1925) as an intuitive explanation for the success of bonding to porous materials such as wood and unglazed porcelain. However, it did not explain bonding to smooth surfaces or the difficulties with poorly wetting surfaces and the theory was not widely accepted. Over time the development of the electron microscope allowed detailed analysis of surfaces to be made and new processes were developed as part of the aerospace field to bond synthetic polymers and metals. It therefore became apparent that microscopically rough surfaces produced stronger bonds than smooth surfaces (Venables 1984).

During asphalt mixing, the hot bitumen flows into the aggregate's pores which, assuming the binder is able to fully wet the aggregate, once cooled provides the mechanical interlock between them as shown schematically in Figure 6-1.

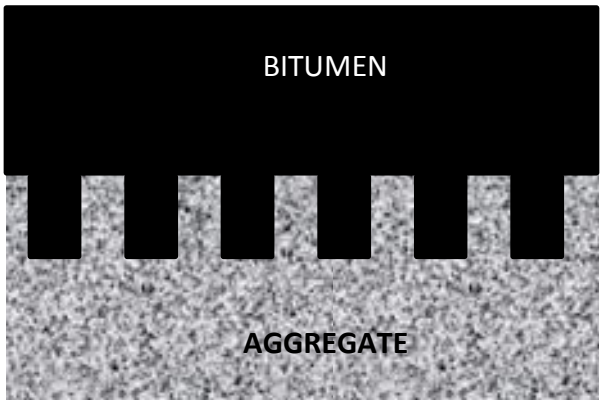

Figure 6-1 : Mechanical interlock between bitumen and asphalt

Terrar and Wagh (1992) investigated the effect of aggregate properties on bitumen stripping and, whilst primarily focussing on the impact of water, highlighted the importance of aggregate surface texture on the mechanical bond.

6.2.2 Diffusion Theory

The Diffusion Theory of adhesion attributes the bond to intermolecular entanglements at the bond interface. Typically this occurs when both the adhesive and substrate have the ability to flow or are heated above their melting point during bonding therefore allowing the two phases to diffuse into one another. Alternatively, in solvent based adhesives the substrate is solvated and molecules can diffuse into the adhesive. Both these situations replace the sharp boundary layer with a diffuse transition.

Whilst hot bitumen will flow into pores within the aggregate this is simply absorption of the bitumen into the aggregate producing a mechanical interlock bond as discussed earlier. Even during asphalt mixing at 180°C the aggregate is well below temperatures that would lead to any melting of its surface, and therefore there is no contribution to adhesion due to diffusion between aggregate and bitumen.

6.2.3 Molecular Interaction Theories

Molecular Interaction Theories cover a wide range of interatomic and intermolecular chemical forces which may contribute to the formation of an adhesive bond, with typical bond energies shown in Table 6-1.

Bond Type	Bond Energy (kJ/mol)
Covalent Bond (C - C)	350
Ionic Bond ($Na^+ \ldots Cl^-$)	450
Hydrogen Bonding ($H_2O \ldots H_2O$)	24
London Dispersion ($C_nH_{2n+2} \ldots C_nH_{2n+2}$)	2

Table 6-1 : Typical bond energies (Landrock and Ebnesajjad, 2008)

True adhesive chemical bonding involves either covalent or ionic bond formation between the adhesive and the substrate. A covalent bond is formed when pairs of electrons are shared between two atom's molecular orbitals. This is a thermodynamically stable configuration as the total energy of the combined atoms is lower than that of separate atoms, and as a consequence the energy required to break a covalent bond is high. An ionic bond is formed when the electrons are permanently transferred between the outer valance shells of two atoms producing charged ions of opposite charge, with the strong electrical attraction between the ions producing a strong bond.

The Van der Waals forces are the sum of all the remaining forces between molecules once covalent and ionic bonding forces have been excluded, and can be divided into dipole-dipole attractions (or repulsions) and dispersive forces.

Within heterogeneous molecules the electrons are not dispersed evenly throughout the molecule but instead electrons are drawn towards the more electronegative elements (Fluorine, Oxygen, Nitrogen, etc.) producing relatively electron rich areas and consequently electron poor areas. This leads to the formation of a molecular dipole which will tend align itself with other nearby dipoles. The most commonly encountered dipole-dipole attraction is hydrogen bonding in water as shown in Figure 6-2.

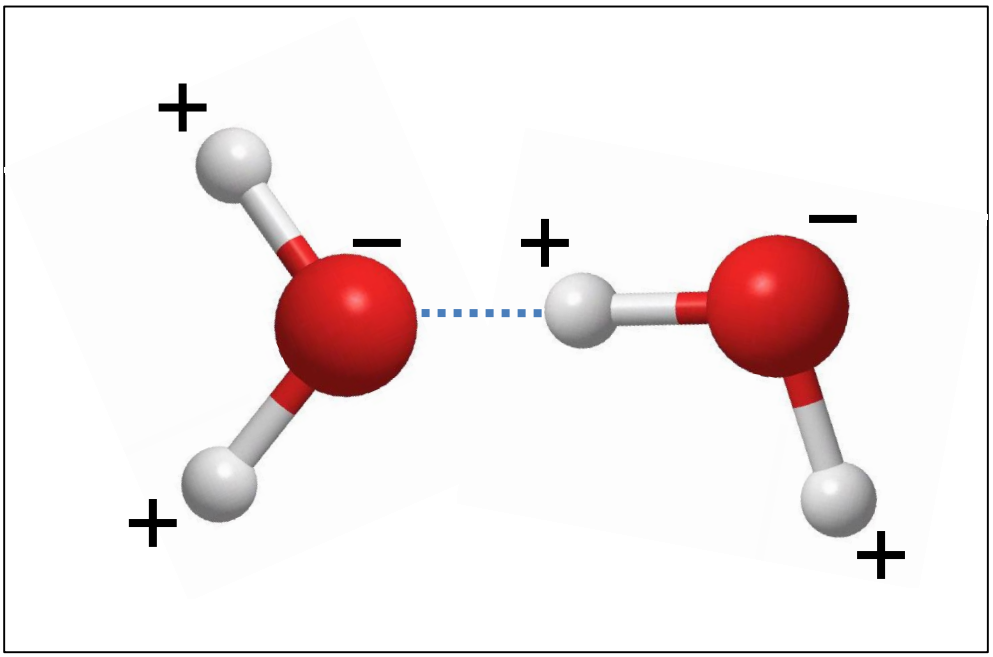

Figure 6-2 : Dipole-dipole hydrogen bonding in water

The weakest of the intermolecular forces is the London dispersive force. The electrons in atoms and molecules are in constant motion, and therefore at any time the electron distribution is not completely homogenous. As a consequence, instantaneous weak dipoles are constantly being formed within the electron field leading to a weak attraction developing between molecules.

6.2.4 Surface Free Energy Theory

An alternative to the chemical and electron transfer theories is to consider material surfaces from a thermodynamic perspective. Within the bulk of a condensed phase material, i.e. liquids and solids, each molecule is surrounded by neighbouring molecules and therefore experiences equal forces in all directions resulting in an overall net force of zero. However, molecules at the surface experience a stronger attraction to molecules within the bulk than those in the adjacent medium as shown schematically in Figure 6-3.

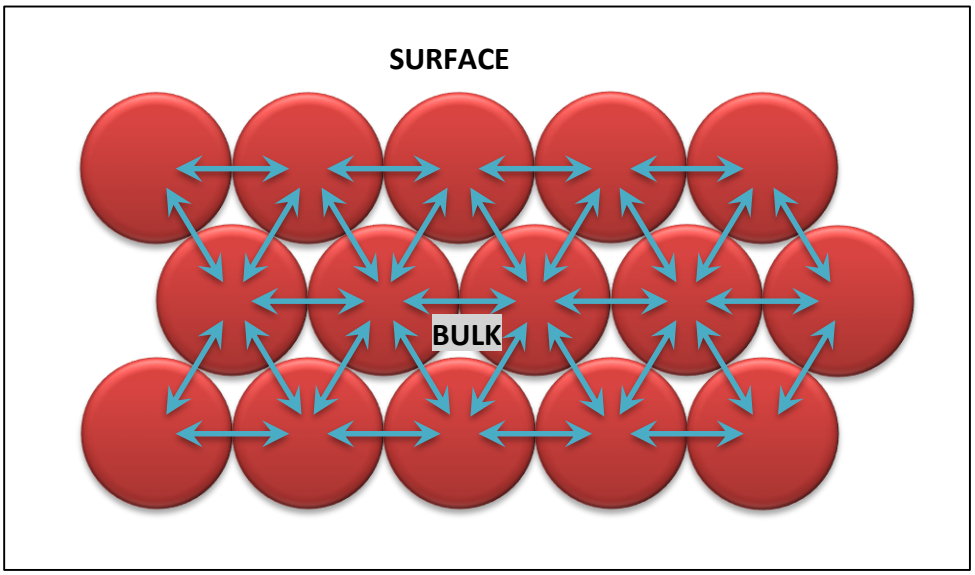

Figure 6-3 : Schematic of molecular forces in a condensed phase material

This results in a net excess of energy at the surface of the material which manifests itself as surface tension, or the surface free energy (SFE). Formally the SFE of any material, be it in a solid or liquid, is defined as the work needed to create new elemental area in a vacuum. The most common units for SFE are mJ/m^2, although some publications continue to use the equivalent non-SI unit ergs/cm^2.

Fowkes (1964) proposed that the total SFE, γ^{Total}, is a function of dispersive, or apolar, components and acid-base, or polar, components

$$\boldsymbol{\gamma^{Total} = \gamma^{LW} + \gamma^{AB}} \qquad \textbf{Equation 6-1}$$

Where γ^{LW} is the apolar Liftshitz-Van der Waals component, and γ^{AB} is the polar acid-base component.

Van Oss, Chaudhury and Good (1988) later proposed that the acid-base component may be described by individual acid and base elements

$$\boldsymbol{\gamma^{AB} = 2\sqrt{\gamma^{+}\gamma^{-}}} \qquad \textbf{Equation 6-2}$$

Where γ^{+} is the Lewis Acid component and γ^{-} is the Lewis Base component

Therefore, the total three-component SFE is

$$\boldsymbol{\gamma^{Total} = \gamma^{LW} + 2\sqrt{\gamma^{+}\gamma^{-}}} \qquad \textbf{Equation 6-3}$$

Using this theory it is possible to calculate the theoretical adhesive work of failure due to SFE, $\Delta W_{adhesive}$, between two materials 'A' and 'B' as

$$\boldsymbol{\Delta W_{adhesive} = 2\sqrt{\gamma_A^{LW}\gamma_B^{LW}} + 2\sqrt{\gamma_A^{+}\gamma_B^{-}} + 2\sqrt{\gamma_A^{-}\gamma_B^{+}}} \qquad \textbf{Equation 6-4}$$

For a material to fail in a cohesive manner requires the creation of two new surfaces of that material. Therefore, the cohesive work of fracture $\Delta W_{cohesive}$ is twice the SFE of the material.

$$\boldsymbol{\Delta W_{cohesive} = 2\gamma^{Total}} \qquad \textbf{Equation 6-5}$$

A three phase system may also be considered where the third material 'W' displaces the bond between 'A' and 'B'. This involves the creation of two new interfaces γ_{AW} and γ_{BW} and the removal of the original interface γ_{AB}, therefore the total work required to achieve this is

$$\boldsymbol{\Delta W_{ABW} = \gamma_{AW} + \gamma_{BW} - \gamma_{AB}} \qquad \textbf{Equation 6-6}$$

This has particular relevance to asphalt when the third material is water as it provides a thermodynamic assessment of the likelihood for water to break the bond between the bitumen and aggregate, and therefore lead to premature failure of the asphalt from water ingress. This approach has been shown to be useful in assessing the water sensitivity of aggregate-bitumen combinations (Cheng et al. 2002, Bhasin et al. 2006, Kringos, Scarpas and de Bondt 2008, Lyne et al. 2013, Canestrari et al. 2014, Grenfell et al. 2014).

However, the primary motivation of this research was to determine factors influencing fracture and fatigue in asphalt. In the laboratory, fracture and fatigue tests are almost exclusively carried out on dry specimens and, as has already been demonstrated, significant differences in performance between binders have been

measured. Therefore, whilst water sensitivity is recognised as an important practical factor for asphalt durability, the impact of water on asphalt fracture and fatigue was not considered of primary relevance to this research.

6.3 Surface chemistry of bitumen and aggregates

Bitumen is a highly heterogeneous mixture containing a very wide range of potentially thousands of different molecular species, with the composition varying between crude sources. Researchers have yet to confirm the internal structure of bitumen (Lesueur 2009, Redelius and Soenen 2015) but the majority of molecular species are known to be hydrocarbons with small quantities of heteroatoms of sulphur, oxygen and nitrogen also present. In an effort to simplify the chemistry the molecules within bitumen are frequently grouped as being asphaltenes, resins, aromatics and saturates. However, it should be noted that this is simply a convenient arbitrary grouping based on the relative solubility of chemical species in common organic solvents. The surface of bitumen is dominated by the weak Van der Waal forces and, due to the relatively small quantity of heteroatoms, dispersive forces dominate.

For an aggregate to be used in asphalt it must be sufficiently robust to withstand traffic and EN 13043 (BSI 2013) provides guidance on appropriate aggregate test methods. However, all common natural aggregates contain a proportion of silcates, ranging from medium to high levels in granites and basalts, to lower levels in limestones. At the aggregate surface silanol (Si-OH) groups are found which leads to an overall negative charge on the aggregate surface.

To improve adhesion between bitumen and aggregate, adhesion promoters are added to the bitumen phase with the most common class of adhesion promoter being cationic surface active molecules. These are composed of a long hydrophobic alkyl “tail” which is compatible with the bitumen phase, and a hydrophilic functional “head” group which is attracted to the negatively charged aggregate surface. Whilst many molecules could fulfil this role only a limited number possess sufficient thermal

stability to survive the high temperatures encountered during bitumen storage and asphalt manufacture. Polyamines, tallow amines, and amidoamines are widely used, with phosphate esters also encountered. The effectiveness of the cationic adhesion promoter is believed to be primarily due to Van der Waals attractions between the negatively charged silanol groups on the aggregate and the positively charged head group.

Silane chemistry provides an alternative approach to bitumen adhesion promoters (Mehta and Ranka 2015). As with the more traditional adhesion promoters they possess an alkyl tail, but the head is instead a alkoxysilane group. This reacts with the hydroxysilane groups on the aggregate surface through a condensation reaction to form a covalent siloxane bond and an alcohol. This reaction takes place at elevated temperatures during asphalt mixing whilst the alcohol generated during the reaction evaporates.

$$\text{=Si-OR'} + \text{OH-Si---} \rightarrow \text{=Si-O-Si---} + \text{HOR'}$$

The formation of a covalent bond provides far stronger adhesion than the electrostatic bonds of traditional cationic adhesion promotors. However, practically the application is more difficult as the alkoxysilane is readily hydrolysed at room temperatures and will self-condense rendering it ultimately inactive. The interactions between the aggregate surface and bitumen with and without bitumen adhesion promotor are shown in Figure 6-4 below.

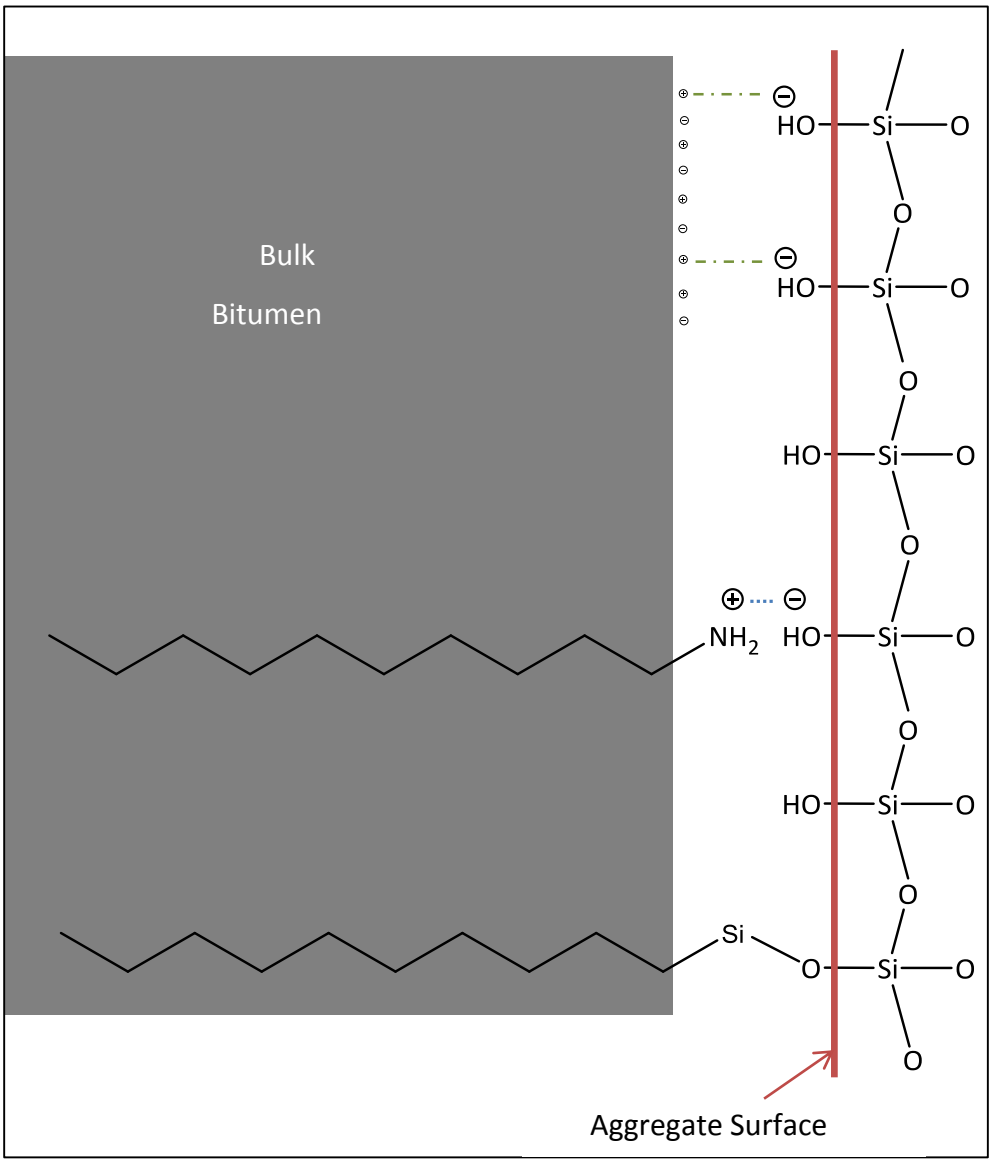

Figure 6-4 : Schematic of aggregate to bitumen adhesion with no additive (top), alkyl amines (middle) and silanes (bottom)

If the primary cause of asphalt fatigue failure is debonding at the aggregate-bitumen interface then the addition of adhesion promoter should lead to an improved bond and an improvement in fatigue lifetime. However, adhesion promoters are not routinely used to improve cracking and fatigue resistance in asphalt, and there is minimal evidence in the literature relating adhesion promoters to improvements in dry fatigue life. Hajj et al. (2012) assessed 5 different aggregates with adhesion promoters and found that for only 1 of the aggregates, a Californian

siliceous aggregate, showed improved dry fatigue performance with the other 4 aggregates including limestone, gravel and granites, showed no improvement.

6.4 Surface Free Energy Measurement Techniques

When a liquid droplet is placed on a solid surface it spreads across the surface of the solid in a process referred to as wetting. The adhesive forces between the liquid and solid allow the liquid to spread out, whereas the cohesive forces within the liquid restrict the spreading. The wetting is quantified by the contact angle, θ, at the liquid-solid boundary where a low contact angle indicates good wetting and a high contact angle poor wetting as shown in Figure 6-5.

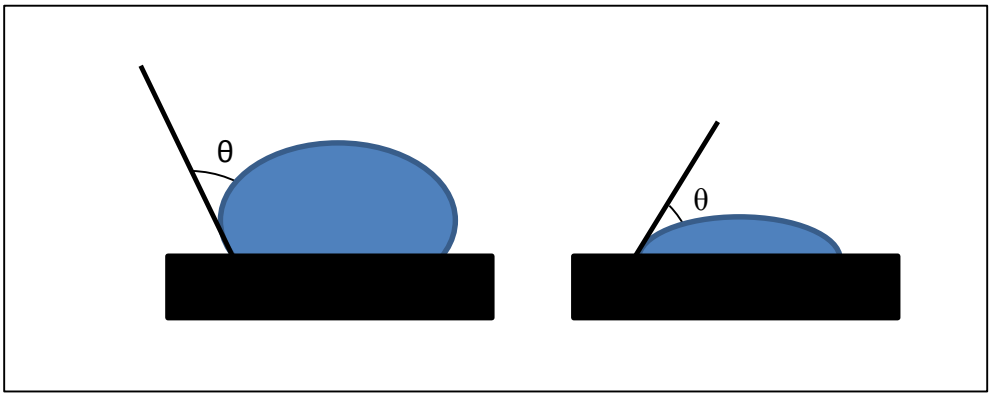

Figure 6-5 : Contact angle at liquid solid boundary demonstrating poor wetting (left) and good wetting (right)

The work of adhesion and contact angle are related through the Young-Dupré equation,

$$\gamma_L(cos\theta + 1) = \Delta W_{adhesion}$$ (for solid-liquid adhesion in a third medium V)

Equation 6-7

where γ_L is the SFE of the test liquid.

Combining Equation 6-4 and Equation 6-7 gives,

$$\gamma_L(cos\theta + 1) = 2\left\{\sqrt{\gamma_L^{LW}\gamma_S^{LW}} + \sqrt{\gamma_L^-\gamma_S^+} + \sqrt{\gamma_L^+\gamma_S^-}\right\} \quad \textbf{Equation 6-8}$$

Therefore, by measuring the contact angle between liquids with known surface energy components and a solid surface the solid's surface energy components may be determined by employing a minimum of three liquids and solving Equation 6-8 simultaneously. Additional test liquids can also be used to improve the accuracy of the result.

A wide range of methods have been developed to practically determine the surface energy components of both bitumen and aggregate. A detailed review of available methods was made by Little, Bhasin and Hefer (2006) with the most commonly encountered methods summarised below.

6.4.1 Sessile Drop Method

The simplest method to determine the surface energy components of bitumen is the static sessile drop (Wei and Zhang 2012) where a glass slide or aluminium sheet is coated with bitumen and the test probe liquid dropped onto it. The contact angle is measured optically using a goniometer allowing relatively low cost measurements to be made albeit with commensurately low accuracy. More advanced equipment uses image analysis algorithms to determine the shape of the drop, and hence the contact angle, but the difficulties in obtaining accurate results remain and this method is now rarely used for bitumen.

6.4.2 Wilhelmy Plate

To avoid the difficulties of directly measuring the contact angle the Wilhelmy Plate method may be employed and this is currently the most commonly used approach for determining the surface energy components of bitumen (Hefer, Bhasin and Little 2006, Bhasin et al. 2007, Howson et al. 2011, Grenfell et al. 2014). In this method the material to be analysed is inserted perpendicularly into the test liquid and the force exerted on the plate measured using a microbalance as shown in Figure

6-6 and Figure 6-7. As bitumen cannot be directly inserted on its own a glass slide which has been coated with hot bitumen and allowed to cool is typically used.

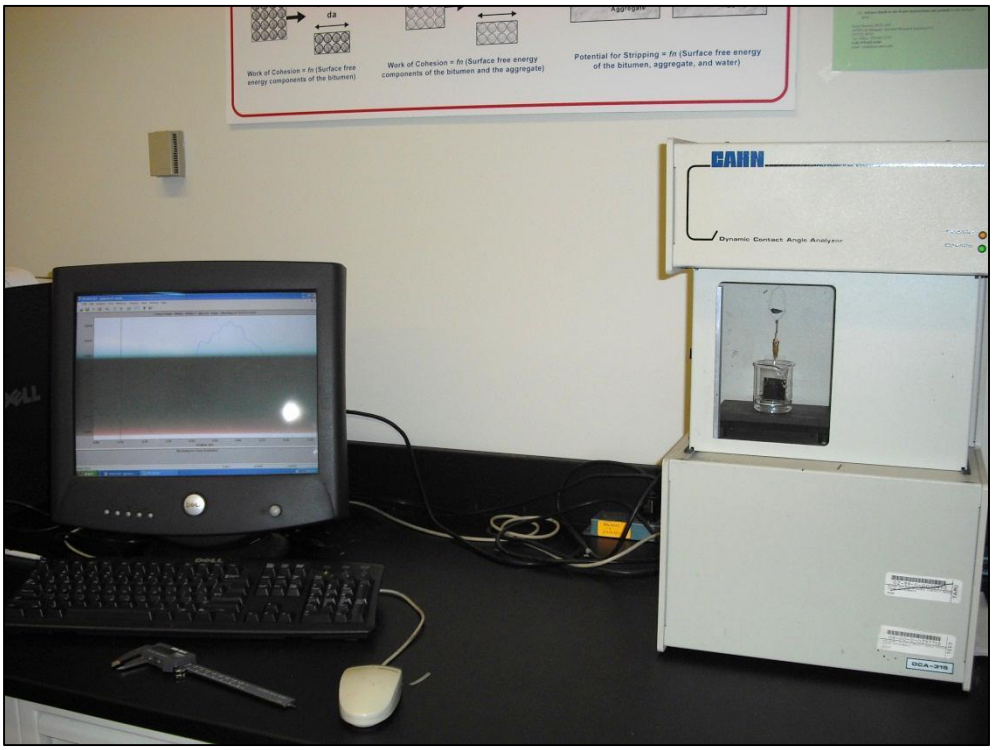

Figure 6-6 : Wilhelmy Plate apparatus

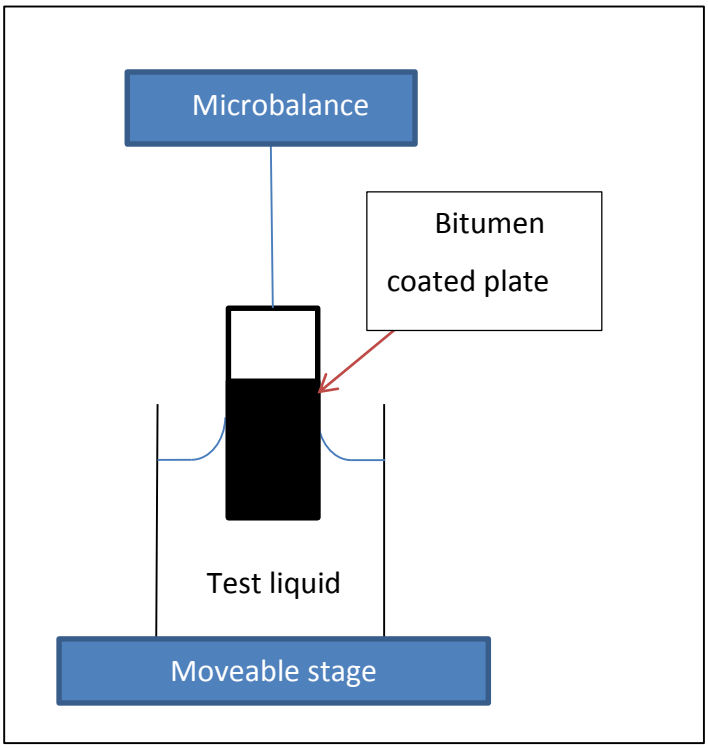

Figure 6-7 : Schematic of the Wilhelmy Plate apparatus

The contact angle, θ, between the liquid and the plate is calculated using

$$cos\theta = \frac{\Delta F + V_{immersed}(\rho_L - \rho_{air} g)}{P\gamma_L^{Total}} \qquad \textbf{Equation 6-9}$$

Where P is the perimeter of the coated plate, γ_L^{Total} is the liquid surface energy, θ is the contact angle between the bitumen and the liquid, V_m is the volume immersed in the liquid, ρ_L is the liquid density, ρ_{air} is the density of air, and g is acceleration due to gravity.

For bitumen measurements the five test liquids typically used are water, ethylene glycol, formamide, di-iodomethane and glycerol. Equation 6-8 may then be solved simultaneously to determine the SFE components of the bitumen.

As the plate advances and recedes into the liquid two different contact angles are measured, with the difference between the two known as the contact angle hysteresis. For a perfectly smooth and chemically homogeneous material the contact

angle hysteresis should be zero (Kwok et al. 1997) but in practice a difference is almost always observed. As the bitumen is applied hot to the glass plate and allowed to cool it is assumed that the internal forces within the binder will aim to minimise the surface area, and therefore produce a perfectly smooth surface. However, as bitumen contains many thousands of distinct molecular components the observed contact angle hysteresis is assumed to be due to this chemical heterogeneity. As the advancing contact angle occurs when the sample is first in contact with the probe liquid this is recommended as the result to be used for determining the surface energy components (Kwok et al. 1998).

6.4.3 Universal Sorption Device

Due to the high SFE of aggregates almost all probe liquids completely wet the surface making contact angle measurements impossible. Also, even when the aggregate surface is polished, there is still a significant micro-roughness which will affect the contact angle.

To resolve these issues the Universal Sorption Device, shown in Figure 6-8, has been developed (Bhasin and Little 2007) and is now considered to be the standard method for aggregate SFE determination.

Aggregate passing the 5 mm and retained on 2.36 mm sieve is typically used and is thoroughly washed and dried prior to analysis. The aggregate is placed in a basket connected to a microbalance inside a sealed chamber. The chamber is degassed and probe gasses introduced in steps of fixed partial pressures. The Specific Surface Area (SSA) is determined using the Brunauer–Emmett–Teller equation, and the equilibrium spreading pressure, π_e, of the gas with the aggregate surface is determined from the adsorption isotherm by

$$\boldsymbol{\pi_e = \frac{RT}{MA}\int_0^{p_0}\frac{n}{p}dp} \qquad \textbf{Equation 6-10}$$

where R is the universal gas constant, T is the test temperature, M is the probe vapour molecular weight, A is the Specific Surface Area of the aggregate, n is the mass of vapour absorbed per unit mass of aggregate, p is the vapour pressure, and p_0 is the maximum saturation vapour pressure.

The surface energy components of the vapour and solid phases and the spreading pressure are related to the total surface energy of the vapour by

$$\pi_e + 2\gamma_L = 2\left\{\sqrt{\gamma_L^{LW}\gamma_S^{LW}} + \sqrt{\gamma_L^-\gamma_S^+} + \sqrt{\gamma_L^+\gamma_S^-}\right\} \qquad \textbf{Equation 6-11}$$

As in the Wilhelmy Plate method a minimum of three probe liquids of known SFE are required so that Equation 6-11 can be solved simultaneously to determine the SFE components of the aggregate.

Figure 6-8 : Universal Sorption Device at Texas A&M

6.5 Binder Surface Free Energy Results

The SFE of the binders was determined using the Wilhelmy Plate technique, with the results in Table 6-2 below.

Binder	γ^{LW} (mJ/m^2)	γ^+ (mJ/m^2)	γ^- (mJ/m^2)	γ^{Total} (mJ/m^2)
Advancing				
50/70V	31.3	0	2.5	31.3
50/70V + 2.5% SBS	24.2	0	2.2	24.2
50/70V + 5.0% SBS	27.3	0	1.6	27.3
50/70V + 7.5% SBS	26.3	0	2.3	26.3
50/70R	17.8	0.1	2.9	18.8
50/70R + 5.0% SBS	20.2	0	6.1	21.2
50/70ME	20.2	0.1	1.3	20.9
50/70ME + 5.0% SBS	17.7	0	3.9	18.5
Receding				
50/70V	41.2	0.3	30.6	47.1
50/70V + 2.5% SBS	38.4	0.7	24.4	46.7
50/70V + 5.0% SBS	40.2	0.4	28.0	46.8
50/70V + 7.5% SBS	37.7	0.7	24.8	45.7
50/70R	40.7	0	17.6	41.3
50/70R + 5.0% SBS	43.1	0.6	12.9	48.4
50/70ME	41.3	0	17.1	42.6
50/70ME + 5.0% SBS	40.5	0.2	15.9	44.4

Table 6-2 : Bitumen SFE values determined using Wilhelmy Plate

As expected, due to the apolar nature of hydrocarbons, γ^{LW} was the dominant component of the all binder SFE results with only small or zero contributions from γ^+ and γ^- to the total SFE. The Venezuelan crude based binders had the highest SFE. As the presence of polymer at the surface of the binder had already been demonstrated by UV microscopy it was expected that, whilst SBS is also a hydrocarbon, there would

have been a noticeable difference in the SFE of the PmBs compared to the penetration grade binders. Surprisingly, however, this was not found to be the case.

6.6 Aggregate Surface Free Energy Results

The aggregate SFE was measured using the Universal Sorption Device, with the results in Table 6-3 below

	γ^{LW} (mJ/m^2)	γ^+ (mJ/m^2)	γ^- (mJ/m^2)	γ^{Total} (mJ/m^2)
Limestone	108.3	3.1	324.3	172.0
Gritstone	53.4	6.0	600.6	173.6

Table 6-3 : Aggregate SFE results determined using the Universal Sorption Device

Equation 6-11 was used to calculate $\Delta W_{adhesive}$ using both sets of results as shown in Figure 6-9.

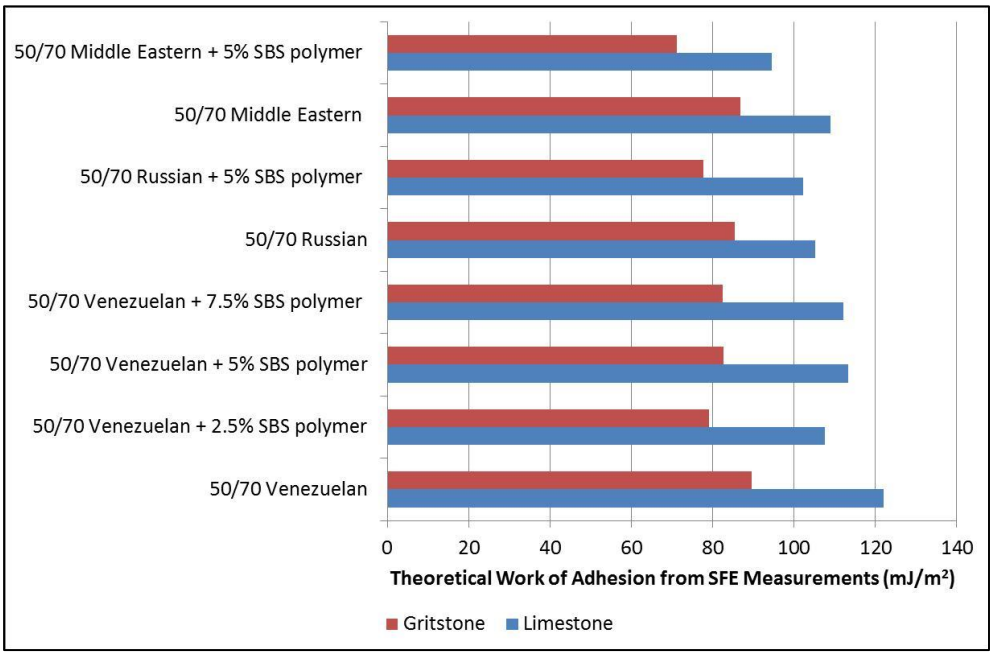

Figure 6-9 : Theoretical work of adhesion of binders to aggregates

The limestone-bitumen $\Delta W_{adhesive}$ was consistently higher than that for the gritstone-bitumen $\Delta W_{adhesive}$, with a mean increase of 32.3%. No clear trends were observed regarding binder crude source or polymer content.

Whilst, as discussed earlier, the effect of water on the bond was not measured in this study $\Delta W_{adhesive}$ in the presence of water may still be calculated using Equation 6-6 as shown in Table 6-4.

Binder	Limestone	Gritstone
50/70V	-97.5 mJ/m^2	-173.6 mJ/m^2
50/70V + 2.5% SBS	-104.6 mJ/m^2	-176.7 mJ/m^2
50/70V + 5.0% SBS	-99.7 mJ/m^2	-173.9 mJ/m^2
50/70V + 7.5% SBS	-102.4 mJ/m^2	-175.7 mJ/m^2
50/70R	-105.9 mJ/m^2	-169.2 mJ/m^2
50/70R + 5.0% SBS	-116.0 mJ/m^2	-184.0 mJ/m^2
50/70ME	-99.0 mJ/m^2	-164.8 mJ/m^2
50/70ME + 5.0% SBS	-116.0 mJ/m^2	-183.0 mJ/m^2

Table 6-4 : Adhesive Bond Energy in the presence of water

The energy ratio between the dry and wet adhesive bond energies, ER, was proposed by Bhasin et al. (2006) as a measure of moisture damage potential, with ER calculated for the binders and aggregates as shown in Table 6-5

$$\boldsymbol{ER} = \left|\frac{\boldsymbol{\Delta W_{adhesive}}}{\boldsymbol{\Delta W_{ABW}}}\right| \qquad \textbf{Equation 6-12}$$

Binder	Limestone	Gritstone
50/70V	1.25	0.52
50/70V + 2.5% SBS	1.03	0.45
50/70V + 5.0% SBS	1.14	0.47
50/70V + 7.5% SBS	1.09	0.47
50/70R	0.99	0.51
50/70R + 5.0% SBS	0.88	0.42
50/70ME	1.10	0.53
50/70ME + 5.0% SBS	0.82	0.39

Table 6-5 : Dry/wet bond energy ratios

A higher value of ER implies improved resistance to moisture, and a value of 0.8 has been proposed to distinguish good performing combinations from poor ones (Bhasin et al. 2006). The calculated values show that the limestone should have a far better resistance to moisture than the gritstone for all binders. This is intuitively correct as experience has shown that limestone has superior moisture resistance than more acidic aggregate sources. It is also interesting to note that there are only small differences in ER between the difference binders. Whilst the addition of polymers is not routinely employed to improve water sensitivity some studies have shown that polymer modification does have a positive effect (Kok and Yilmaz 2009, Moraes, Velasquez and Bahia 2011, Cui et al 2014). The results of this study suggest that any improvements are not a direct result of the surface energy of the binder, but rather it is the higher viscosity of polymer modified binders that reduces the mobility of the binder at ambient temperatures.

6.7 Practical Work of Adhesion

The viscoelastic properties of bitumen mean that whilst SFE measurements allow $\Delta W_{adhesive}$ to be calculated from a purely thermodynamic perspective, the physically measured practical work of adhesion, $\Delta W_{practical}$, includes other aspects such as

mechanical interlock at the aggregate-binder interface, ductile flow, and cohesive failure energy within the binder.

Marek and Herrin (1968) provided the first experimental evidence relating binder film thickness to its tensile strength and the mode of failure. At low film thickness the binder undergoes adhesive failure, with mixed mode failure as the film thickness increases, and eventually to a completely cohesive failure at thicker film thicknesses. The relationship between film thickness and failure mode was calculated by Lytton (2005) using micromechanics, as shown in Figure 6-10, and predicted that the transition from adhesive to cohesive failure occurs at a film thickness of less than 100 µm.

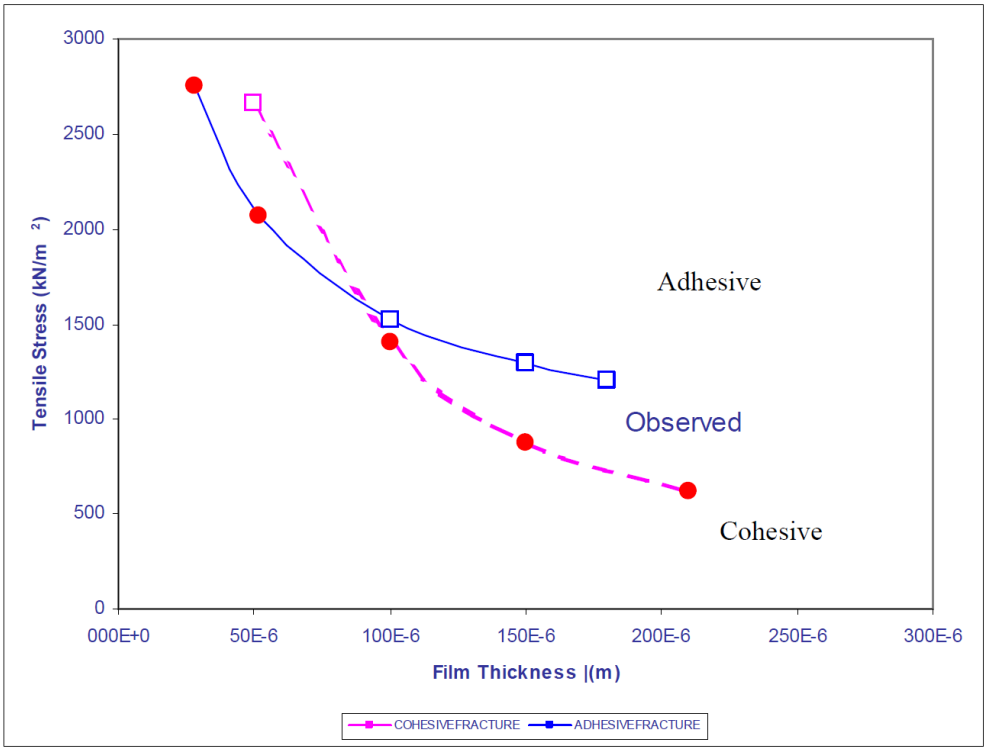

Figure 6-10 : Calculated Tensile Strength versus Asphalt Film Thickness (Constant Stress Conditions Assumed) (Lytton 2005)

A number of tests have been developed to measure the practical work of adhesion with the more common methods summarised below.

6.7.1 *Pneumatic Adhesion Tensile Test Instrument*

At typical service temperatures bitumen exhibits ductile flow when a load is applied prior to its failure. To reduce the impact of ductile flow on adhesion measurements very high strain rates are commonly used to produce a brittle failure mode as a consequence of the time-temperature equivalence properties of bitumen. Whilst time-temperature superposition is only valid in the linear regime researchers have shown that the principle may be extended into higher strain rate regimes (Vananroye et al. 2011)

The blister test (Dannenberg 1961, Williams 1969) was developed to assess the adhesion of organic coatings to metallic substrates, and has become one of the standard adhesion tests used in the coatings industry (EN ISO 4624, BSI 2003). This test was adapted to assess the adhesive bond strength between bitumen and aggregate by Kanitpong and Bahia (2003, 2005) as the Pneumatic Adhesion Tensile Test Instrument (PATTI) and has continued to be developed (Moraes, Velasquez and Bahia 2011) as shown in Figure 6-11 and Figure 6-12.

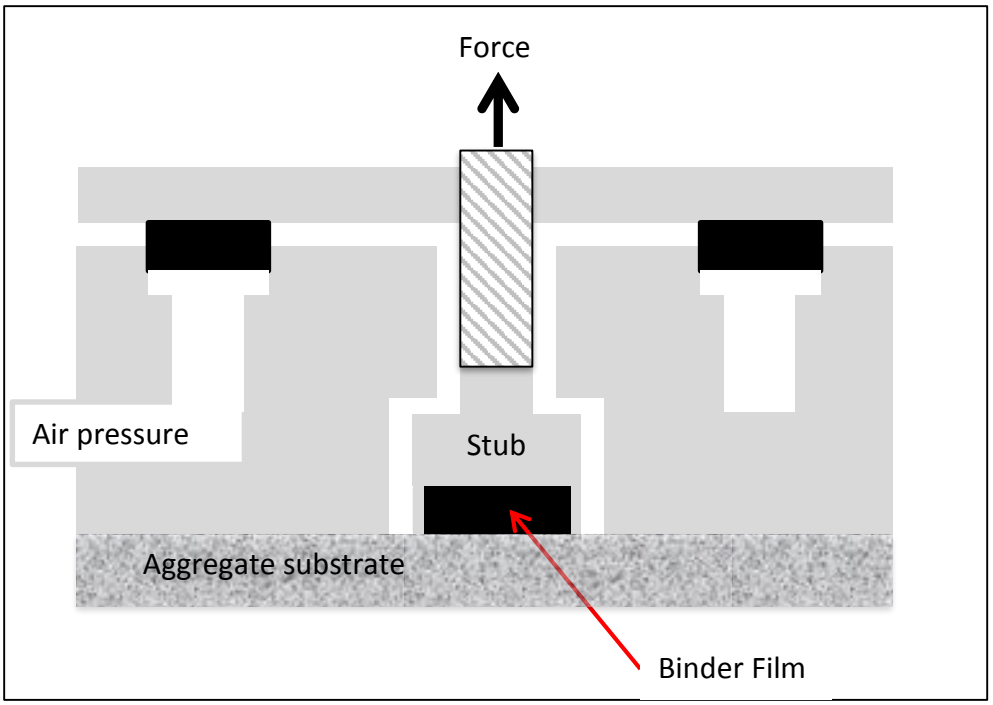

Figure 6-11 : Schematic of PATTI

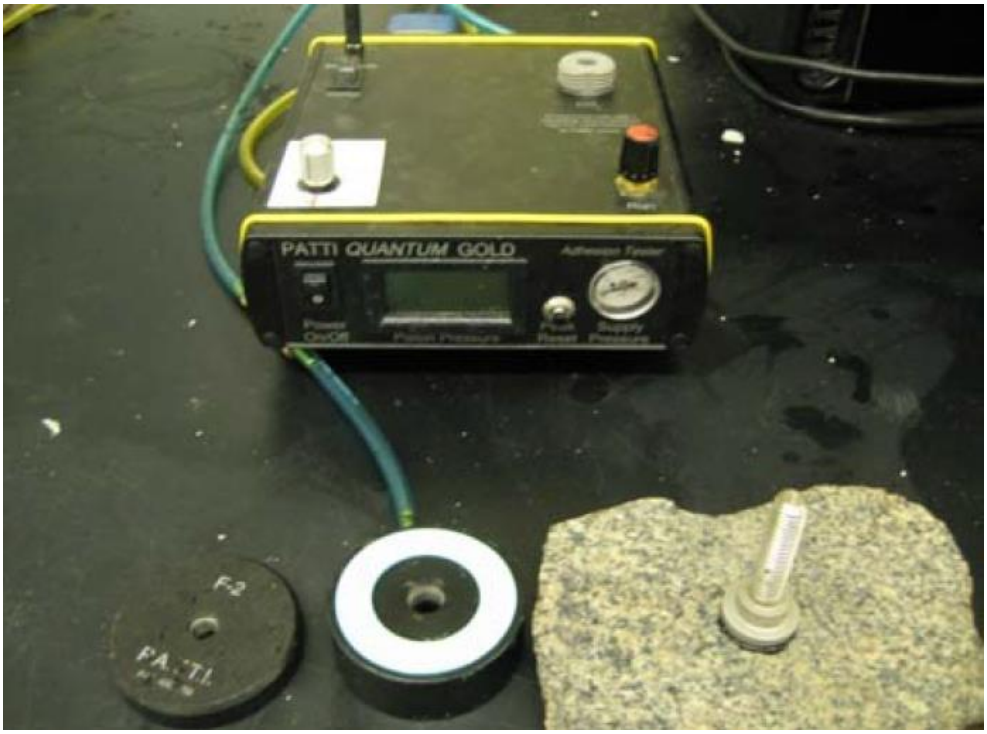

Figure 6-12 : PATTI device with pull off stub and aggregate substrate (Source: Moraes et al. 2011)

The pull-out stub is coated with bitumen, applied to the aggregate substrate, and conditioned for 24 hours prior before testing. The adhesion tester assembly is then placed over the stub and air pressure applied to the system which is increased until failure occurs due to either adhesive failure of the binder to the substrate, or cohesive failure within the binder. The failure pressure can then be used to calculate the pull-off tensile strength.

One advantage of the PATTI procedure is that the stub-bitumen-aggregate assemblies can be easily subjected to a range of environmental conditions, and has been used to assess the effect of moisture on the bond strength (Moraes, Velasquez and Bahia 2011). It does, however, use relatively thick bitumen films of typically between 200 and 800 µm depending on the design of the stub which is unrealistic compared to those found in asphalt mixtures. The original PATTI has been modified to include a measure of vertical displacement during the test (Merusi et al. 2013) to allow a calculation of the adhesion energy.

6.7.2 Peel tests

Within the coatings and adhesives industries a wide range of standard tests have been developed with the most common peel tests being the fixed arm and T-peel tests, as shown in Figure 6-13. In the fixed arm peel test a film is adhesively bonded to a substrate and the film pulled at a fixed angle, usually 90° or 180°, at a specified rate with the loading force recorded. The T-peel test is similar but employs two films adhesively bonded together with the end of one film held in a fixed position whilst the other is pulled 180° away.

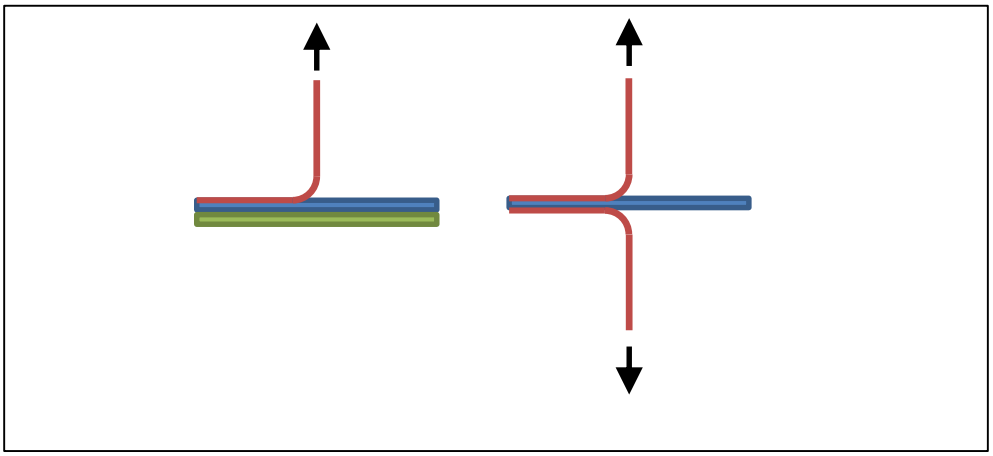

Figure 6-13 : Fixed arm (left) and T-peel (right) test methods

Horgnies et al. (2011) used the fixed arm test to assess bitumen's bond to dolomite and granite substrates and found cohesive failure with dolomite aggregate but adhesive failure with granite. Cui et al. (2014) adapted the fixed arm test to assess the bond strength of 40/60 penetration grade bitumen to four different classes of aggregate substrates. Bitumen was poured onto aggregate substrates to create a 250 µm film using stainless steel wire spacers to maintain the film thickness. A heated aluminium peel arm was then bonded to the bitumen surface and the assembly conditioned overnight at 20°C. Fixed arm peel tests were then carried out with a crosshead speed of 10mm/min and for all substrates the failure occurred cohesively. One SBS modified binder, of unspecified composition, was also assessed and whilst the failure was also cohesive presented over double the fracture energy of the 40/60.

Further tests were carried out on specimens immersed in water for 3 and 7 days where it was found that the fracture energy dropped significantly and the failure mechanism changed to adhesive failure with the 40/60 bitumen, whereas with the PmB the failure mode remained cohesive with only a small decrease in fracture energy.

6.7.3 Direct tension tests

The use of a servo-mechanical or hydraulic test frame to determine the bond strength in direct tension between two aggregate specimens bonded with bitumen is intuitively a simple method to measure the bond energy as both load and displacement are measured. However, due to the practical difficulties in producing specimens and performing the tests, it has only recently gained significant research interest.

Jakarni (2012) produced aggregate cores 25mm in diameter by 8mm high which where bonded with bitumen inside a mounting press, using a wide range of binder film thicknesses from 50 to 1000 μm assessed and loading rates of 20mm/min at 25°C used. As the binder thickness increased a transition from adhesive to cohesive failure was observed. However, as the aggregate discs were cut from a larger length of aggregate the surface roughness of each discs was not clearly specified, and precise knowledge of the binder film thickness across the width of the disc uncertain.

Grönniger and Wistuba (2013) drilled 13mm diameter cores from large quarry rocks to obtain long cylinders of aggregates between 60 and 100mm in length. These were fractured by applying a load at 50mm/min to the centre of the long core to produce a fracture surface. To produce bonded specimens the fractured ends were heated to 120°C with a heat gun, immersed by hand into hot bitumen, and then bonded together and held with a screw clamp for 6 hours. The bonded specimens were then tested at 1.5mm/min and their tensile strength determined. Whilst this method produced a matched aggregate fracture surface the binder film thickness was uncontrolled and the loading rate used was comparatively slow.

Howson et al. (2012) cored 19.1mm diameter specimens from limestone and andesite quarry rocks. These were cut to 10mm stubs and polished with 6µm aluminium oxide powder to produce a consistent aggregate surface. A DSR was used to produce bonded specimens with film thicknesses from 5 to 100µm using three different unmodified PG64-22 grade binders, which would be roughly equivalent to a European 50/70 penetration grade. The bonded specimens were then tested in direct tension with at 23°C with a loading rate of 0.01mm/sec, and additionally one binder was used to test at 10°C and 36°C and with loading rates of 0.005mm/sec and 0.02mm/sec. The authors found that the practical work of adhesion increased with loading rate and decreasing temperature, but that in all cases the energy was significantly higher than that predicted from surface energy measurements. Al-Haddad and Khalid (2015) followed a similar procedure and took nominally 12mm diameter cores from quarry rocks, and produced aggregate stubs with polished ends. A DSR was again used to prepare specimens with binder film thickness from 10 to 100 µm. Deformation rates of 30, 60 and 120mm/min were used at 10 and 20°C and the failure energy calculated. These studies demonstrated that production of a controlled binder film thickness specimen was practical, and a similar method was therefore developed to produce specimens for analysis.

6.8 Specimen Preparation

To produce specimens for adhesion testing large aggregate quarry rocks were obtained from Bayston Hill (gritstone) and Pant (limestone) quarries. From these rocks nominally 12mm diameter cores were drilled out as shown in Figure 6-14. The diameter of the cores was measured after drilling with a micrometer and in fact found to be 12.2mm.

Figure 6-14 : Coring from a large quarry rock

The long cores of rock were then roughly cut into small stubs approximately 20mm in length using a diamond tipped tile cutter. As the stubs would ultimately be bound to one another it was crucial that faces of the stubs were as perpendicular as possible to the sides of the stub. Furthermore, the influence of mechanical interlock on the adhesive bond strength would be minimised by using polished faces.

To achieve this, a parallel polishing tool was manufactured by drilling a hole in a solid aluminium disc with the same diameter as the stubs, and gluing small pieces of sapphire sheet to the disc's base to ensure the aluminium was not damaged during polishing. Each aggregate stub was then wet polished with successfully finer grit paper down to a 600 grit finish as shown in Figure 6-15 to produce a sub-micron surface roughness. Finally, each stub was washed in distilled water and dried overnight at 110°C with completed stubs shown in Figure 6-16. Approximately 60 stubs of each aggregate type were produced to enable the test programme to be completed.

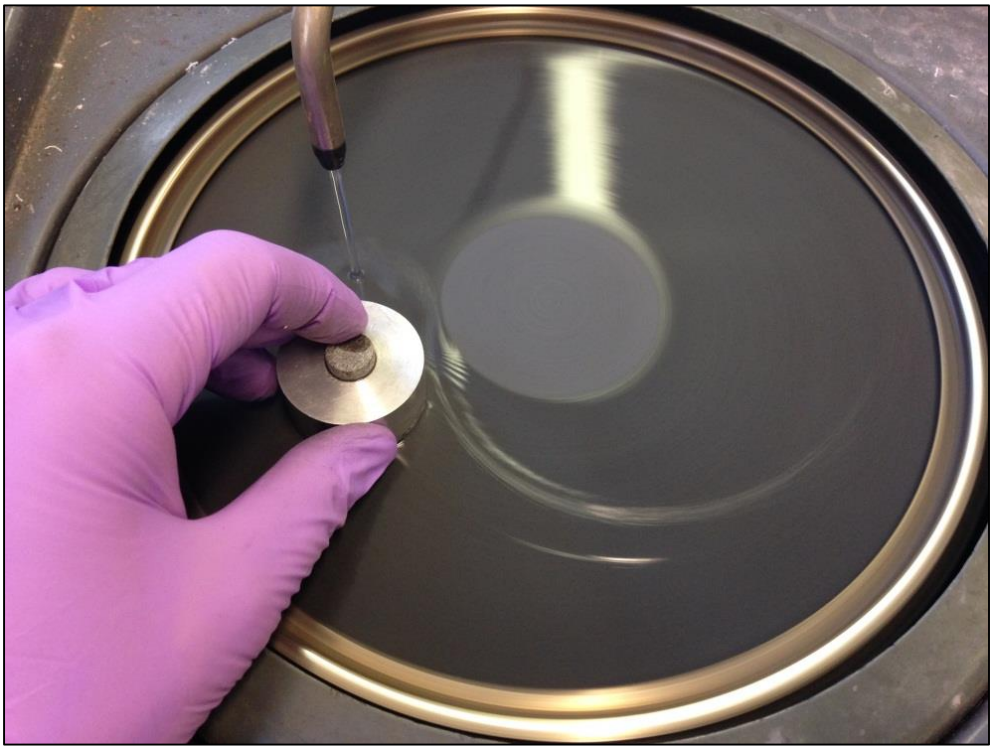

Figure 6-15 : Wet parallel polishing an aggregate stub

Figure 6-16 : Polished aggregate stubs of gritstone (left) and limestone (right)

The DSR crosshead can be vertically positioned with micron accuracy and has heating elements both top and bottom, so was ideally suited to the production of binder/aggregate bonded test specimens. Aggregate stubs were fixed in the holders previously used for small asphalt specimen testing and heated to 150°C. The gap between the stubs was zeroed and by repeatedly rotating the top stub and checking the zero position it was found that the side to side run-off was typically 5 to 10 µm. Previous authors (Howson et al. 2012, Al-Haddad and Khalid 2015) using similar preparation methods produced bonded specimens with film thicknesses as low as 10 µm, but with the observed run-off it was concluded that the minimum bitumen film thickness that could reliably be used was taken as 100 µm. Ideally a lower binder film thickness would have been used to more closely replicate those found in asphalt, so to compensate it was proposed that the highest practically achievable strain rate tests would be used during adhesion testing with the aim of generating an adhesive rather than cohesive failure.

To produce the bonded specimen a drop of hot bitumen at 150°C was transferred to the bottom heated aggregate stub using a heated glass rod and the top stub lowered onto the bitumen drop until the gap was fully filled. The assembly was then cooled in 20°C steps with the gap also being reduced at each stage to maintain a fully filled gap. Whilst it was expected that the bitumen would reduce in volume by around 7% due to the drop in temperature as the bitumen density increased, a far larger reduction in volume was observed. This was believed to be due to absorption into the aggregate surface, and further validates the importance of using heated aggregate stubs to more closely simulate full scale plant mixing.

Finally the temperature was reduced to 20°C and the gap reduced to 100 µm. Any excess bitumen was then trimmed away to leave the finished specimen as shown in Figure 6-17.

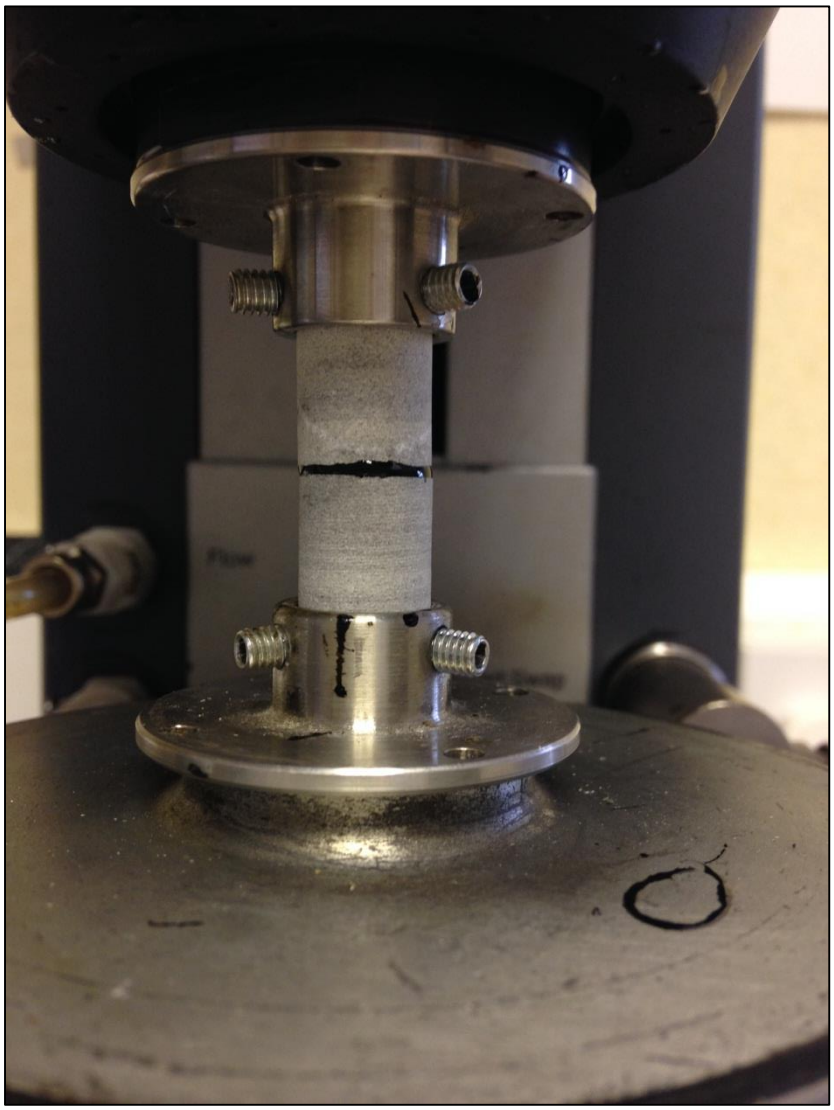

Figure 6-17 : Aggregate/bitumen assembly in preparation on the DSR

6.9 Split Hopkinson Pressure Bar Testing

To reduce the influence of ductile flow on the results the highest possible strain rates should be used to produce a brittle adhesive failure of the binder-aggregate bond. One experimental procedure where stress and strain may both be dynamically recorded at very high strain rates, of the order of 10^3 s^{-1}, is the split-Hopkinson pressure bar (SHPB) technique. The initial experiments in the development of the SHPB were carried out by Hopkinson (1914) who induced pressure waves into long elastic metal bars and studied the stress pulses propagating along the rods over time.

Following this work the equipment used to study dynamic processes in materials using elastic stress-waves in long rods became known as Hopkinson pressure bars. Davis (1948) sandwiched a sample between two Hopkinson bars in series which allowed the dynamic stress-strain behaviour of the sample to be recorded, with later developments allowing testing in torsion and tension.

To assess the bond between bitumen and aggregate the most appropriate mode of testing was determined to be in tension. Yokoyama (2003) successfully used the tension SHPB to determine the tensile strength and energy absorption of cyanoacrylate adhesive butt joints. Tekalur et al. (2009) used the SHPB to determine the tensile and compressive strength of Marshall sized asphalt specimens and compared the results to traditional quasi-static testing and showed that using the high strain rate SHPB the compressive strength was increased by 5 times, and the tensile strength by 1.5 times.

A schematic of a typical tension SHPB is shown in Figure 6-18, with the University of Liverpool tension SHPB shown in Figure 6-19.

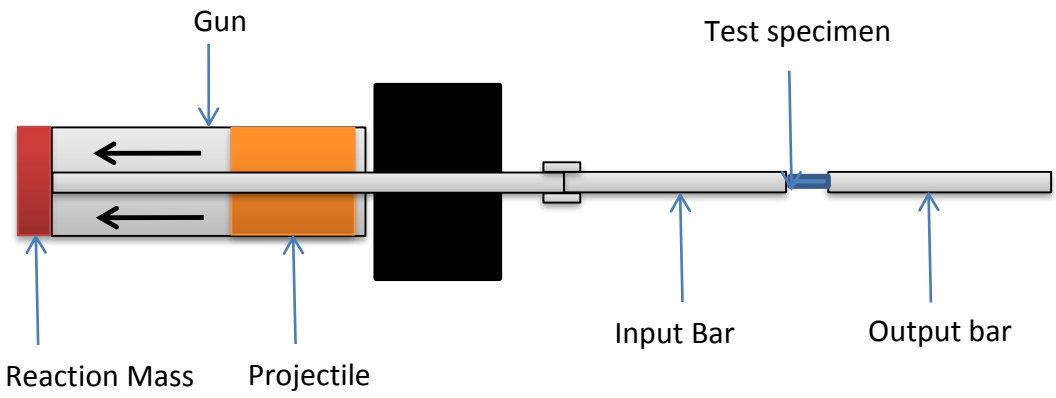

Figure 6-18 : Schematic of tension SHPB

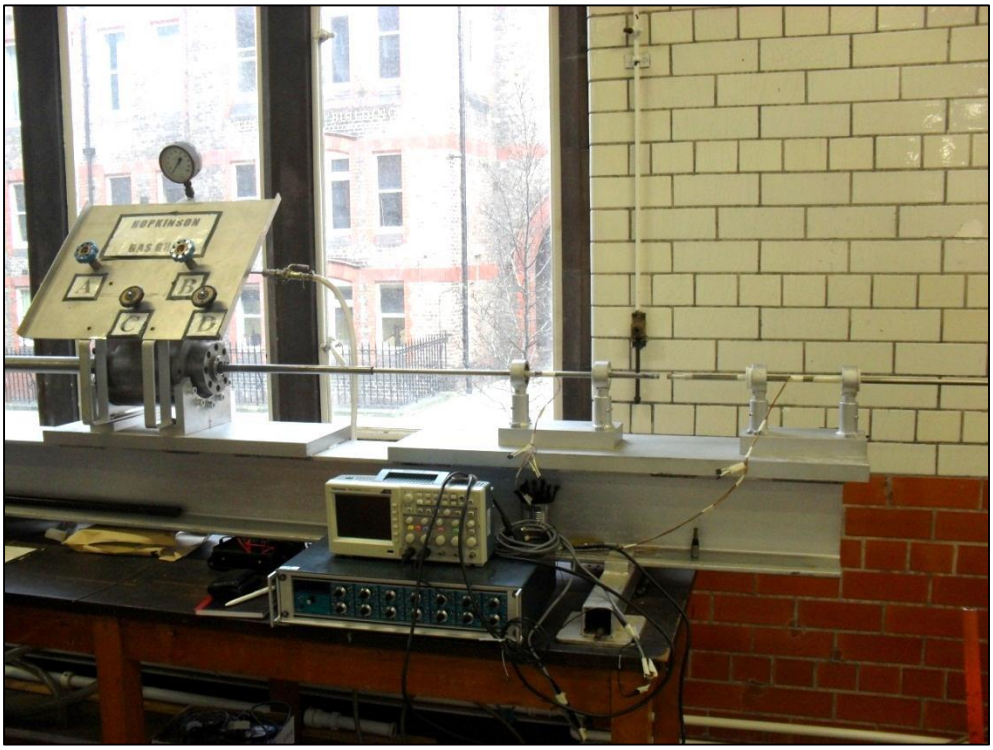

Figure 6-19 : University of Liverpool tension SHPB

The test specimen is held between the input and output bars with strain gauges attached to each of the bars. A projectile mass is fired from a pressurised chamber towards the far end of the bar where it impacts the reactive mass causing a tensile stress wave to be created in the input bar. This travels along the input bar where the energy is partly absorbed by the specimen, partly reflected back along the input bar, and the remainder travelling into the output bar. The strain gauges attached to the bars record the strain waves passing through the input and output bars. One dimensional wave analysis is performed on the strain signals allowing the determination of the full stress-strain behaviour of the specimen.

Stainless steel specimen holders were manufactured to fit the existing University of Liverpool SHPB and the aggregate/binder stubs glued into the holders using epoxy resin. The adhesive was allowed to cure for 24 hours whilst the specimens were conditioned at a further 20°C for a minimum of 4 hours prior to testing. The

specimens were then fixed into the SHPB, as shown schematically in Figure 6-20, and tested immediately.

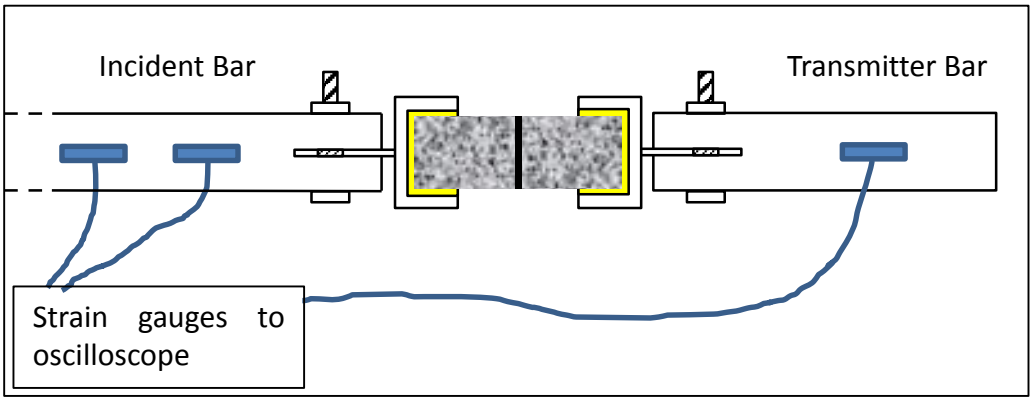

Figure 6-20 : Schematic of aggregate/binder specimen mounted in the SHPB

Following the test it was found that although the binder/aggregate bond failed adhesively, the retaining lug on the specimen holder also fractured as seen in Figure 6-21. The test was repeated three times with the same outcome. Additional specimen holders were manufactured using hardened steel, but during SHPB testing the same problem occurred.

To resolve the problem would require completely new Hopkinson bars with alternative specimen mounting points to be designed and manufactured, along with more robust specimen holders. This was not possible to achieve during this research, but should be considered by future researchers.

Figure 6-21 : Failed specimen holder after SHPB test

6.10 Pull Off Tests

As an alternative method a pull off test using a more traditional electromechanical universal testing machine fitted with a 5kN load cell was employed as shown in Figure 6-22. The specimen holders produced for the SHPB were found to be compatible with the testing machine and therefore the specimen manufacturing procedure already detailed could also be used with this device.

Figure 6-22 : Electromechanical universal test machine

As discussed, a high strain rate should be used to produce an adhesive failure and therefore a crosshead speed of 100mm/min was used. Specimens were again conditioned at 20°C for a minimum of 4 hours before being immediately tested in tension. Load and vertical displacement were recorded on a connected PC as shown in Figure 6-23. The evolution of each test was also optically recorded via an attached digital video camera as shown in Figure 6-24. For each of the binder-aggregate combinations produced three replicate tests were performed.

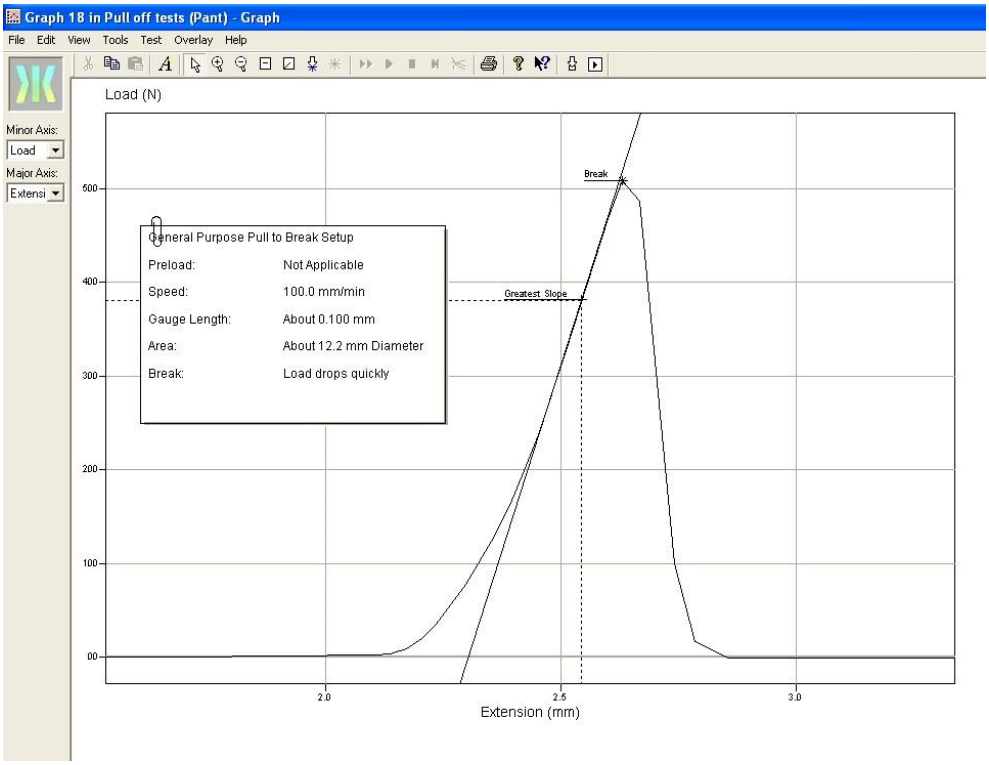

Figure 6-23 : Typical load-displacement curve produced during pull off test

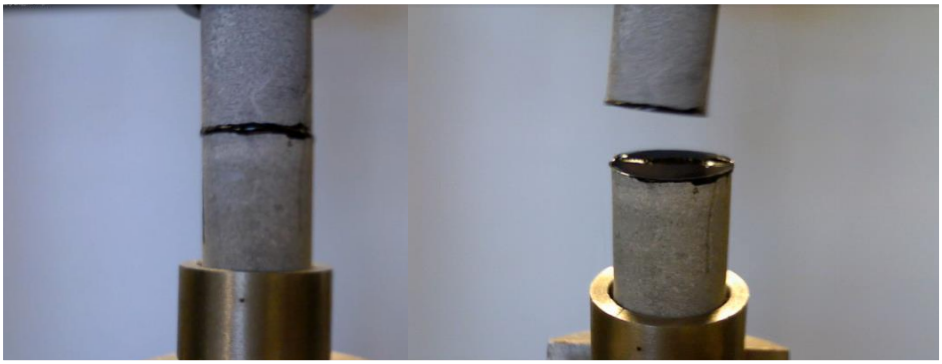

Figure 6-24 : Video capture of pull off testing

Following each test the failed specimen faces were photographed, as shown in Figure 6-25, with the mode of failure assessed as either adhesive, cohesive, or mixed mode as detailed in Table 6-6.

Binder	Limestone stub	Gritstone stub
50/70 Venezuelan	Adhesive	Adhesive
50/70 Venezuelan + 2.5% SBS Polymer	Adhesive	Adhesive
50/70 Venezuelan + 5.0% SBS Polymer	Mixed adhesive / cohesive	Cohesive
50/70 Venezuelan + 7.5% SBS Polymer	Mixed adhesive / cohesive	Cohesive
50/70 Russian	Adhesive	Adhesive
50/70 Russian + 5.0% SBS Polymer	Adhesive	Adhesive
50/70 Middle Eastern	Adhesive	Adhesive
50/70 Middle Eastern +5.0% SBS Polymer	Adhesive	Adhesive

Table 6-6 : Summary of specimen bond failure type

Figure 6-25 : Visual analysis of typical specimen post-test

As anticipated, by using a relatively high strain rate the failure was completely adhesive for all the penetration grade binders. However, the more highly polymer modified Venezuelan binders did produce mixed mode and cohesive failures. Whilst, from practical experience, it may be anticipated that a PmB may lead to a cohesive failure this is not the result predicted by the theoretical work of adhesion. It was therefore clear that additional energy dissipation processes must be occurring within the binder film leading to the change from adhesive to cohesive failure.

In contrast to the aborted SHPB tests no damage occurred to the specimen holders indicating that the holders were structurally sound and that during the very high strain rate SHPB tests the tensile strength of the binder exceeded the tensile strength of the stainless steel lugs.

The peak load at failure was used to calculate the stress at maximum load and the average results for each aggregate-binder combination shown in Figure 6-26.

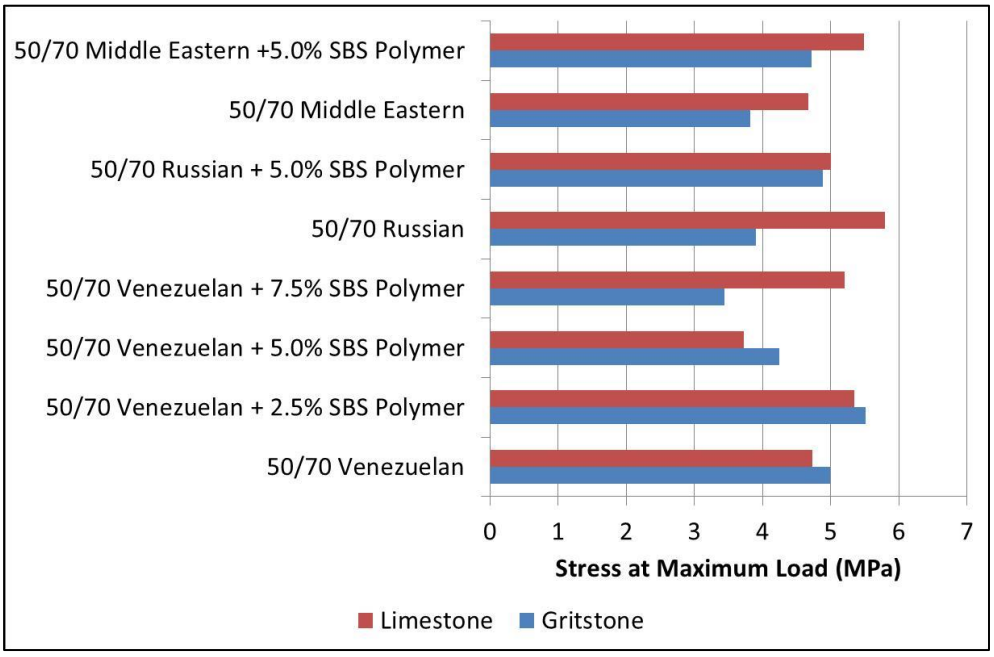

Figure 6-26 : Pull off test average stresses at maximum load

The area under the load-displacement curve was used to calculate $\Delta W_{practical}$ per m^2 as shown in Figure 6-27.

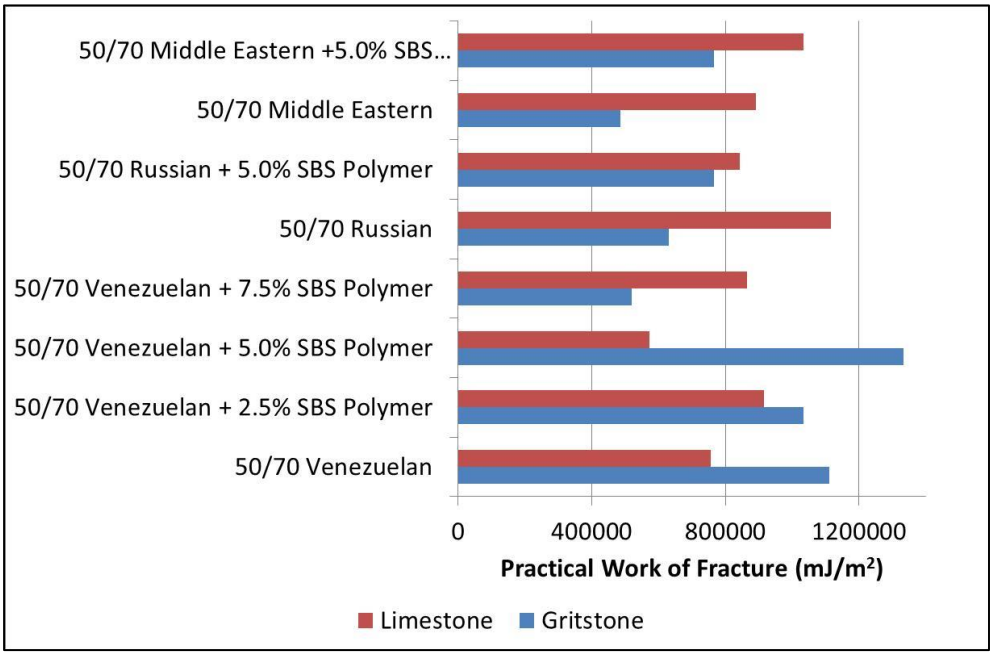

Figure 6-27 : Pull off test average practical work of fracture

Surprisingly the results indicated very little difference between either the aggregate type or binder composition. The strong correlation between binder rheology and asphalt modulus has long been recognised and numerous models to predict asphalt behaviour from binder properties have been proposed (Hirsch 1962, Witczak and Fonseca 1996, Francken and Vanelstraete 1995, Vanelstraete, Francken and Reynaert 1996, Christensen, Pellien and Bonaquist 2003). Whilst aggregate packing, binder content and void content influence the modulus of a particular mix design, in its simplest terms the asphalt modulus is a multiple of the binder modulus. It was, therefore, rational to assume that the measured fracture energy in a bulk asphalt fracture test would be related to the fracture energy between the idealised binder-aggregate specimens tested in this study. The results in SCB tests in Chapter 4 demonstrate that the modified binders produce significantly higher asphalt fracture energies than the unmodified asphalts. However, this trend was not repeated in the binder-aggregate pull off tests and there were no obvious trends between the $\Delta W_{practical}$ and the composition of the aggregate-binder stub despite the very significant differences in binder properties and aggregate types. Canestrari et al.

(2014) used the PATTI test to determine the pull off test strength of three PmBs containing 1.8, 2.8 and 3.8% SBS on basalt and limestone aggregates, and also found no clear trends between the level of polymer modification and the bond strength. These results suggest that the improved fracture resistance of asphalt containing PmBs in the field and as measured in Chapter 4 is not closely related to the high strain rate failure of the aggregate-binder bond.

6.10.1 Comparison of theoretical and practical work of adhesion

The ratio between $\Delta W_{practical}$ and $\Delta W_{adhesive}$ was calculated as shown in Table 6-7.

Binder	Ratio of practical work of fracture to theoretical work of adhesion (rounded to 2 significant figures)	
	Limestone	Gritstone
50/70 Venezuelan	6200	12000
50/70 Venezuelan + 2.5% SBS Polymer	8500	13000
50/70 Venezuelan + 5.0% SBS Polymer	5100	16000
50/70 Venezuelan + 7.5% SBS Polymer	7700	63008
50/70 Russian	11000	7400
50/70 Russian + 5.0% SBS Polymer	8200	9800
50/70 Middle Eastern	8200	5600
50/70 Middle Eastern +5.0% SBS Polymer	11000	11000

Table 6-7 : Ratio of practical work of fracture to theoretical work of adhesion

If the practical adhesive bond was only due to the thermodynamic $\Delta W_{adhesive}$ then $\Delta W_{practical}$ would equal $\Delta W_{adhesive}$. However, these results indicate that $\Delta W_{practical}$ is approximately 10,000 times $\Delta W_{adhesive}$. Kringos, Scarpas and de Bondt (2008) measured the bond strength between aggregate and mastic using a direct tensile test

and also found that $\Delta W_{practical}$ was approximately 10,000 times $\Delta W_{adhesive}$ determined from surface energy measurements. As the total energy in the system must be conserved during the debonding process $\Delta W_{practical}$ must, therefore, include additional factors to accommodate losses.

This finding is not unique to asphalt but is in fact well known in the field of adhesives. Pressure Sensitive Adhesives (PSAs) are similar to bitumen in that they are viscoelastic thermorheologically simple materials that are usually used at ambient temperatures. Kowalski, Czech and Byczynski (2013) measured $\Delta W_{practical}$ and theoretical $\Delta W_{adhesive}$ of a PSA tape against a range of substrates and found the $\Delta W_{practical}$ was between 5000 and 12000 times $\Delta W_{adhesive}$.

The first efforts to quantify this effect were made in the 1970's. Gent and Kinloch (1971) studied the bond between a crosslinked styrene-butadiene rubber and a poly(ethylene terephthalate) substrate. At very low strain rates $\Delta W_{practical}$ was found to approach $\Delta W_{adhesive}$. Whilst still higher than $\Delta W_{adhesive}$ this value was referred to as the intrinsic or threshold value of adhesion $\Delta W_{threshold}$, with the difference between $\Delta W_{adhesive}$ and $\Delta W_{threshold}$ attributed to additional contributions from mechanical interlock and chemical bonding. At higher strain rates $\Delta W_{practical}$ was orders of magnitude higher than $\Delta W_{adhesive}$ and $\Delta W_{threshold}$, and the difference attributed to energy dissipation due to material deformations.

Gent and Schultz (1972) performed peel experiments between lightly crosslinked rubbers and a poly(ethylene terephthalate) substrate in the presence of a range of alcohol and alcohol/water mixtures. They found that $\Delta W_{practical}$ was significantly higher than $\Delta W_{adhesive}$ but that the two were linked by a simple numerical factor. However, that factor was found to be strongly dependent on the temperature and peel rate.

Penn and Defex (2002) found that for a simple elastic brittle adhesive an exponential relationship existed between $\Delta W_{adhesive}$ and $\Delta W_{practical}$. However, for more complex viscoelastic adhesives significant plastic deformation occurs within the

adhesive layers, and the effects depend on temperature, strain rate, and the micromechanical properties of the substrate (Kim and Kim 1998, Xu, Hui and Kramer 1992, Shull et al. 1998, Masson and Lacasse 2000, Penn and Defex 2002, Seshadri et al. 2007).

Whilst individual studies have proposed models relating $\Delta W_{adhesive}$ and $\Delta W_{practical}$, they are typically empirical multiplicative dependencies of the form

$$\boldsymbol{\Delta W_{practical} = \Delta W_{threshold}(1 + f(T, \dot{a})\zeta)} \qquad \textbf{Equation 6-13}$$

where T is temperature, ȧ is the crack speed, ζ is a multiplicative factor and

$$\boldsymbol{\Delta W_{threshold} = f(\Delta W_{adhesive}, \Delta W_{mechanical\ interlock}, \Delta W_{chemical\ bonding})} \qquad \textbf{Equation 6-14}$$

As a result of these complex relationships it is not straightforward to relate $\Delta W_{adhesive}$ to the results from practical experiments for time and temperature dependent viscoelastic materials, and Figure 6-28 demonstrates the typical relationships between the parameters.

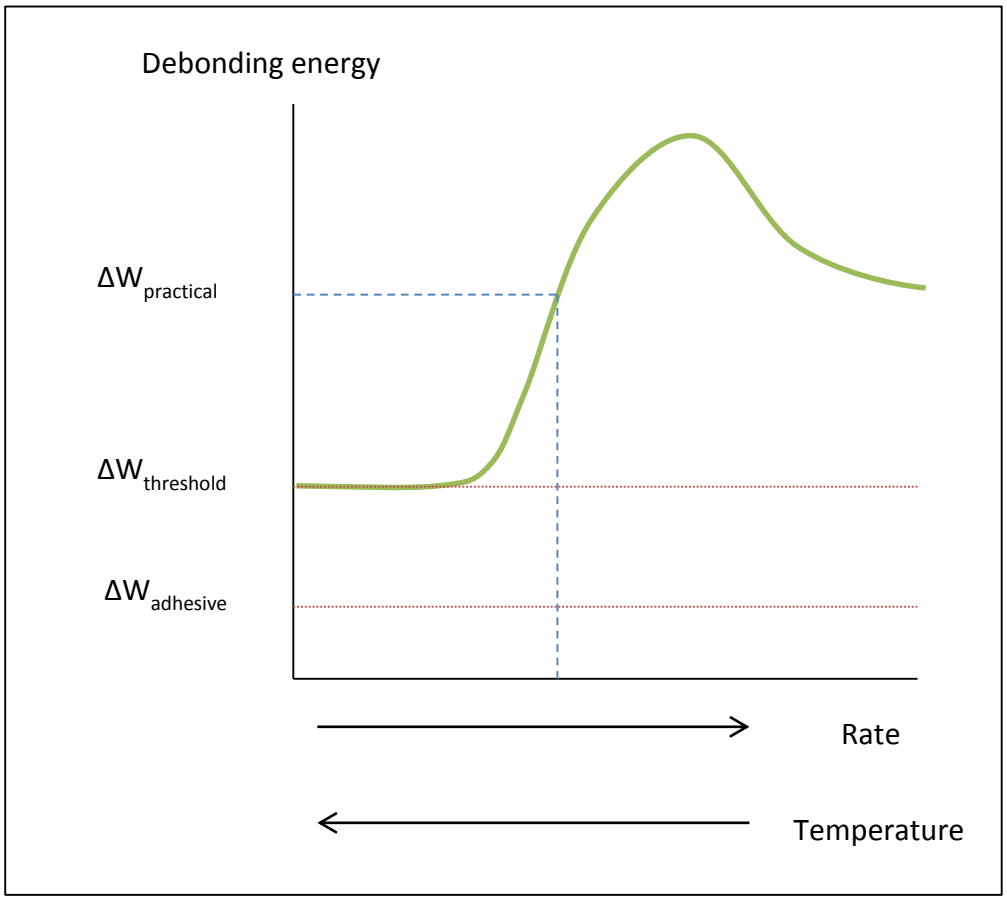

Figure 6-28 : Schematic of practical, threshold, and thermodynamic adhesive bond energy for a viscoelastic material (adapted from Dillard 2010)

At ambient temperatures and moderate strain rates the measured $\Delta W_{practical}$ will lie at some point along the curve. Whilst this result may be practically useful, without a priori knowledge of the shape of the curve it cannot be related to either $\Delta W_{threshold}$ or $\Delta W_{adhesive}$. Therefore, the target of experimental tests should be to test at the extreme left or right of the curve where the time and temperature dependence is minimised.

Measurements of bitumen-aggregate bond energy using very low displacement rates at ambient temperatures are not practical as the bitumen undergoes significant plastic flow. Al-Qadi, Fini and Dessouky (2006) studied the low temperature adhesion between crack sealants and limestone and quartzite aggregates and found limited

evidence of an exponential relationship between $\Delta W_{adhesive}$ and $\Delta W_{practical}$. Also, whilst the fracture toughness of both unmodified binders and PmBs has been measured at low temperatures (Chailleux et al. 2012, Bueno, Hugener and Partl 2013) the difficulty in obtaining reproducible results has limited this approach.

At higher than ambient temperatures bitumen becomes a viscous liquid rendering adhesive bond energy measurements meaningless. Therefore, the only remaining alternative is to employ high strain rates. However, the results of this research suggests that at ambient temperatures even at these high strain rates $\Delta W_{practical}$ does not relate in a simple manner to $\Delta W_{adhesive}$, although higher test strain rates, such as those attainable using the SHPB, may provide a closer correlation.

6.11 Concluding Remarks

In this chapter, a laboratory procedure was successfully developed enabling the practical work of fracture at relatively high strain rates to be determined between bitumen and aggregate. Surprisingly, the results showed remarkably little variation between the different binder and aggregate types. The Split Hopkinson Pressure Bar was also identified as a device capable of measuring stress-strain characteristics of adhesive bonds at very high strain rates and its use for determining bitumen-aggregate bond strength should be considered by future researchers.

The theoretical work of fracture was calculated from surface energy measurements and found to be four orders of magnitude smaller than the practical work of fracture. No clear trends were observed between the practical work of fracture, the theoretical work of fracture or the binder composition. Whilst surface energy measurements have proven useful in determining asphalt water sensitivity the realistic fracture performance of asphalt under dry conditions cannot be accurately predicted using either surface energy techniques or high strain rate binder-aggregate adhesive fracture measurements.

7 CONTINUUM DAMAGE MECHANICS ANALYSIS OF BITUMEN AND ASPHALT FATIGUE††

Repeated cyclic loading of a material produces localised and progressive structural damage resulting in a weakening of its load bearing capacity, and ultimately structural failure. Asphaltic pavements are damaged through a combination of repeated traffic loading and unloading, and induced thermal stresses resulting from changes in climatic conditions which over a period of years leads to fatigue failure of the pavement structure.

In this chapter laboratory fatigue studies of polymer modified bitumens and asphalts were carried out using classical testing geometries and small specimen sizes. The fatigue data was analysed using traditional methods and accelerated procedures employing viscoelastic continuum damage theory, and the relative merits of the approaches discussed.

7.1 Continuum Damage Mechanics Fatigue

The classical approach to characterising fatigue damage and crack propagation in terms of the Paris Law was previously discussed in Chapter 4. However, this traditional approach to assessing damage growth requires many specimens to be analysed over a range of applied stresses and strains to develop fatigue life predictions. Fatigue testing may be undertaken on full asphalt mixtures, fine

†† This chapter includes results originally published in Lancaster I.M., and H. Al-Khalid, (2015) "Viscoelastic and Damage Characterization of Polymer Modified Bitumen from Different Origins" 3rd Meeting and Technical Conference of the Middle East Society of Asphalt Technologists, American University of Sharjah, United Arab Emirates pp. 54 -63 (doi: 10.1201/b18538-5), reproduced by permission.

aggregate mixtures, mastics or binders, but in all cases for tests employing low stresses and strains each specimen may take many days or even weeks to fail.

When work is applied to an elastic body at constant temperature there is an increase in the strain energy stored within the body. If, however, the work produces damage in the body a proportion of the strain energy is consumed, and the damage may be characterised as a function of internal state variables. Schapery (1990) developed a generalised work potential theory of damage growth in elastic materials employing internal state variables.

As discussed in Chapter 4, Schapery (1984) showed how correspondence principles may be used to replace stresses and strains with pseudostresses and pseudostrains to reduce a time dependent viscoelastic problem to a linearly elastic one. In this approach the pseudostrain, γ^R, was shown to be

$$\boldsymbol{\gamma^R = \frac{1}{E_R}\int_0^t D(t-\tau)\frac{\partial \gamma}{\partial \tau}d\tau} \qquad \textbf{Equation 7-1}$$

where E^R is a reference modulus (usually taken as unity), D(t) is the linear viscoelastic relaxation modulus, t is time, and τ is the time variable of integration.

Schapery developed the constitutive equations for the time dependent damage growth in terms of a pseudostrain energy density function, W^R, and internal state variables representing damage, S_m. Kim, Lee and Lee (1995) introduced pseudo-stiffness, C, to characterise damage and in the simplest interpretation the pseudostiffness is a function of a single internal state variable, S, and the equations are

$$\boldsymbol{\sigma = \frac{\partial W^R}{\partial \gamma^R} = IC(S)\varepsilon^R} \qquad \textbf{Equation 7-2}$$

Where I is a normalising initial value used to eliminate sample to sample variability equal to $|E^*|_{N=1}/|E^*|_{LVE}$, $|E^*|_{N=1}$ is the dynamic modulus at the first cycle

and $|E^*|_{LVE}$ is the linear viscoelastic dynamic modulus of the undamaged material and

$$\frac{dS}{dt} = \left(-\frac{\partial W^R}{\partial S}\right)^{\alpha} \quad \textbf{Equation 7-3}$$

Where α is a material constant related to the rate of damage growth.

It should be noted that the units for S are $[Nm^{-2}]^{\alpha/(\alpha+1)}[s]^{1/(\alpha+1)}$ and therefore direct physical interpretation of S is not readily possible. If the material's fracture energy and the fracture stress are constant then α = 1 + 1/m, where m is the maximum slope of the log of the relaxation modulus versus log time. This form of α is suggested as most suitable for strain controlled tests whilst for a stress controlled test α = 1/m is used.

In the special case of cyclic testing with constant frequency and E_R=1 Equation 7-1 reduces to

$$\gamma_N^R = |E^*|_{LVE}\gamma_N^0 \quad \textbf{Equation 7-4}$$

Where, γ^0_N is the peak strain in the N^{th} cycle.

By combining Equations 7-2 and 7-4 the pseudostiffness C at the N^{th} cycle can be shown to be

$$C = \frac{\sigma_0^N}{I|E^*|_{LVE}\gamma_0^N} = \frac{|E^*|_N}{I|E^*|_{LVE}} = \frac{|E^*|_N}{I|E^*|_{LVE}} = \frac{|E^*|_N}{|E^*|_{N=1}} \quad \textbf{Equation 7-5}$$

Where $|E^*|_N$ is the dynamic modulus at the N^{th} cycle

Equations 7-2 may be integrated and combined with Equation 7-3 as

$$\frac{dS}{dt} = \left(-\frac{I}{2}\frac{\partial C(S)\gamma^{R^2}}{\partial S}\right)^{\alpha} \quad \textbf{Equation 7-6}$$

Lee (1996) showed how by application of the chain rule $\frac{dC}{dS} = \frac{dC}{dt}\frac{dt}{dS}$ a discrete determination of S may be derived as follows

$$\frac{dS}{dt} = \left(-\frac{I}{2}\frac{dC}{dt}\frac{dt}{dS}\gamma^{R^2}\right)^{\alpha} \quad \textbf{Equation 7-7}$$

$$\frac{dS}{dt} = \left(-\frac{I}{2}\frac{dC}{dt}\gamma^{R^2}\right)^{\alpha}\left(\frac{dS}{dt}\right)^{-\alpha} \quad \textbf{Equation 7-8}$$

$$\left(\frac{dS}{dt}\right)^{1+\alpha} = \left(-\frac{I}{2}\frac{dC}{dt}\gamma^{R^2}\right)^{\alpha} \quad \textbf{Equation 7-9}$$

$$\frac{dS}{dt} = \left(-\frac{I}{2}\frac{dC}{dt}\gamma^{R^2}\right)^{\frac{\alpha}{1+\alpha}} \quad \textbf{Equation 7-10}$$

Further use of the chain rules $\frac{dC}{dt} = \frac{dC}{dN}\frac{dN}{dt}$ and $\frac{dS}{dt} = \frac{dS}{dN}\frac{dN}{dt}$ leads to

$$\frac{dN}{dt}\frac{dS}{dN} = \left(-\frac{I}{2}\frac{dC}{dN}\frac{dN}{dt}\gamma^{R^2}\right)^{\frac{\alpha}{1+\alpha}} \quad \textbf{Equation 7-11}$$

Recalling that for a cyclic test at a frequency f

$$\frac{dN}{dt} = f \quad \textbf{Equation 7-12}$$

Therefore

$$f\frac{dS}{dN} = \left(-\frac{I}{2}\frac{dC}{dN}f\gamma^{R^2}\right)^{\frac{\alpha}{1+\alpha}} \quad \textbf{Equation 7-13}$$

At the peak of each cycle the damage parameter S may be evaluated in discrete form as

$$\left(\frac{f}{\Delta N}\right)(S_{N+\Delta N} - S_N) = \left(-\frac{I}{2}\frac{f}{\Delta N}\gamma^{R^2}(C_{N+\Delta N} - C_N)\right)^{\frac{\alpha}{1+\alpha}} \quad \textbf{Equation 7-14}$$

Which can be rearranged to

$$S_{N+\Delta N} - S_N = \left(\frac{f}{\Delta N}\right)^{-1}\left(-\frac{I}{2}\frac{f}{\Delta N}\gamma^{R^2}(C_{N+\Delta N} - C_N)\right)^{\frac{\alpha}{1+\alpha}} \quad \textbf{Equation 7-15}$$

$$S_{N+\Delta N} - S_N = \left(\frac{f}{\Delta N}\right)^{\frac{-1}{1+\alpha}}\left(-\frac{I}{2}\gamma^{R^2}(C_{N+\Delta N} - C_N)\right)^{\frac{\alpha}{1+\alpha}} \quad \textbf{Equation 7-16}$$

$$S_{N+\Delta N} - S_N = \left(\frac{\Delta N}{\mathrm{f}}\right)^{\frac{1}{1+\alpha}}\left(-\frac{I}{2}\gamma^{R^2}(C_{N+\Delta N} - C_N)\right)^{\frac{\alpha}{1+\alpha}} \quad \textbf{Equation 7-17}$$

Equation 7-17 may then be used to generate characteristic C versus S curves for the material under test.

The theory does not itself provide a suggested form for the C-S curve and researchers have selected best-fit models based on their own data. Kutay, Gibson and Youtcheff (2008) suggested using the exponential Equation 7-18 which has the advantage of ensuring that C always remains greater than zero

$$C = exp(C_a S^{C_b}) \quad \textbf{Equation 7-18}$$

$$\frac{\partial C}{\partial S} = C_a C_b S^{C_b - 1} exp(C_a S^{C_b}) \quad \textbf{Equation 7-19}$$

Where C_a and C_b are regression coefficients.

Lee and Kim (1998) suggested using a power law of the form

$$C = 1 - C_1 S^{C_2} \quad \textbf{Equation 7-20}$$

$$\frac{\partial C}{\partial S} = -C_1 C_2 S^{C_2 - 1} \quad \textbf{Equation 7-21}$$

Where C_1 and C_2 are regression coefficients.

As a consequence of the use of pseudovariables the C-S curve produces a unique damage characteristic fingerprint of the material which is independent of the loading rate. Therefore, damage produced with high stresses and strains produces the same

C-S curve as damage produced with low stresses and strains, thus and, therefore, negates the need to undertake low strain testing.

A visual comparison of C-S curves from different materials provides some insight into the relative damage characteristics, with steeper curves indicating a more rapid deterioration in modulus as damage accumulates and hence a poorer fatigue lifetime. However, a more quantitative interpretation of the C-S curve may also be undertaken to calculate the number of cycles to failure for any loading condition. Fatigue test results are often described by a phenomenological regression model of the form

$$N_{failure} = A\gamma_0^{-B} \qquad \textbf{Equation 7-22}$$

An equation of a similar form may be derived via VECD theory by starting with equation 7-6 and recalling that dt=dN/f

$$dS = \left(-\frac{I}{2}\frac{\partial C\gamma^{R^2}}{\partial S}\right)^{\alpha}\frac{dN}{f} \qquad \textbf{Equation 7-23}$$

Inserting Equation 7-21

$$dS = \left(\frac{I}{2}C_1C_2S^{C_2-1}\gamma^{R^2}\right)^{\alpha}\frac{dN}{f} \qquad \textbf{Equation 7-24}$$

Rearranging this to

$$dS(S^{C_2-1})^{\alpha} = \left(\frac{I}{2}C_1C_2\gamma^{R^2}\right)^{\alpha}\frac{dN}{f} \qquad \textbf{Equation 7-25}$$

Integrating between the initial cycle and failure

$$\int_{S_{N=1}}^{S_{failure}}(S^{C_2-1})^{\alpha}\,dS = \int_1^{N_{failure}}\left(\frac{I}{2}C_1C_2\gamma^{R^2}\right)^{\alpha}\frac{dN}{f} \qquad \textbf{Equation 7-26}$$

$$\frac{S_{failure}^{1+(1-C_2)\alpha}}{1+(1-C_2)\alpha} - \frac{S_{N=1}^{1+(1-C_2)\alpha}}{1+(1-C_2)\alpha} = \left(\frac{I}{2}C_1C_2\gamma^{R^2}\right)^{\alpha}\frac{N_{failure}-1}{f} \qquad \textbf{Equation 7-27}$$

Assuming that $S_{failure}>>S_{N=1}$ and $N_{failure}>>1$ and using $k=1+(1-C_2)\alpha$ this can be simplified to

$$\frac{S_{failure}^{k}}{k} \cong \left(\frac{I}{2}C_1C_2\gamma^{R^2}\right)^{\alpha}\frac{N_{failure}}{f} \qquad \textbf{Equation 7-28}$$

Rearranging to find $N_{failure}$

$$N_{failure} \cong \frac{fS_{failure}^{k}}{k\left(\frac{I}{2}C_1C_2\gamma^{R^2}\right)^{\alpha}} \qquad \textbf{Equation 7-29}$$

Recalling Equation 7-4

$$N_{failure} = \frac{fS_{failure}^{k}}{k\left(\frac{I}{2}C_1C_2|E^*|_{LVE}^2\gamma_0^2\right)^{\alpha}} = \frac{fS_{failure}^{k}}{k\left(\frac{I}{2}C_1C_2|E^*|_{LVE}^2\right)^{\alpha}}\gamma_0^{-2\alpha} \qquad \textbf{Equation 7-30}$$

As can be seen Equation 7-30 is of the same form as Equation 7-22 with

$A = \frac{fS_{failure}^{k}}{k\left(\frac{I}{2}C_1C_2|E^*|_{LVE}^2\right)^{\alpha}}$ and B=2α.

Therefore, Equation 7-30 may then be used to calculate the number of cycles to failure for any test conditions

7.2 Binder Fatigue Analysis

Within an asphalt mixture the elastic modulus of the aggregate component is significantly higher than that of the bituminous binder and, therefore, the vast majority of the fatigue strain will occur within the binder. As already recognised, asphalt is a highly heterogeneous material, but as an indicator of asphalt fatigue performance a number of studies of the fatigue properties of the binder have been undertaken.

Pell (1962) performed some of the earliest work on binder fatigue using a specially constructed apparatus at the University of Nottingham. However, for many

subsequent years, due primarily to a lack of an accepted methodology, most research focussed on the bulk fatigue properties of asphalt mixtures.

Interest in binder fatigue was renewed by the 1990's with a range of approaches being employed. Potschka and Schmid (1993) used the Fraass apparatus to determine binder fatigue at low temperatures whereas Anderson et al. (1994) employed a 4-point bending technique directly to binder samples. More recently Delaporte et al. (2008) developed an annular shear rheometer to fatigue binder and mastic, and Chailleux et al (2009) employed a tension-compression fatigue test using diablo shaped binder specimens. However, the vast majority of binder fatigue tests in the last two decades have been undertaken using the DSR.

7.2.1 Binder DSR Time Sweep Fatigue

The SHRP Performance Grade system made extensive use of the DSR for binder specification testing. For the first time it introduced a maximum modulus value for binders after Pressure Ageing Vessel conditioning of $G^* \times \sin(\delta) < 5MPa$ which was linked to binder fatigue performance (Anderson and Kennedy 1993, Bahia and Anderson 1995). However, this parameter was found in practice to be an unreliable predictor of the pavement's fatigue cracking performance (Deacon et al. 1997).

Subsequent to the SHRP implementation the DSR was used to directly determine binder fatigue properties by applying a cyclic sinusoidal strain loading (Bahia et al. 2001, Soenen, de la Roche and Redelius 2003) with the approach referred to as the Time Sweep (TS) test. In its most usually encountered form the test utilises the 8mm parallel plate geometry at 10Hz loading frequency at fixed strain levels with test temperatures between 10 and 20°C. The evolution of the binder's complex modulus and phase angle are recorded throughout the test, and the test terminated when the binder physically fails or the modulus reduced to a predetermined level often taken as 50% of the original modulus. Whilst the test may be performed on unaged binders the test is more commonly used with binders that have been subjected to RTFOT ageing as this simulates the state of the binder found within the pavement layer.

The binders from Chapter 2, after RTFOT, were analysed using the TS approach at a test temperature of 20°C. Initially a frequency sweep was performed from 0.1 to 30Hz to characterise the linear viscoelastic properties of the binder at a strain level of 0.1%, followed by 60 seconds of monitoring the binder's complex modulus at 0.1% strain and 10Hz to ensure the binder was in a steady state prior to fatigue testing. Three strain levels were applied for each binder type for the fatigue test, and at each strain level duplicate tests were performed. At higher polymer modification levels the applied strain was increased to enable to test to be completed within a practicable timescale.

Figures 7-1, 7-2, 7-3 and 7-4 show the typical responses of complex modulus and phase angle during the TS tests where the repeatability between the two tests at each strain level can be seen to be very good.

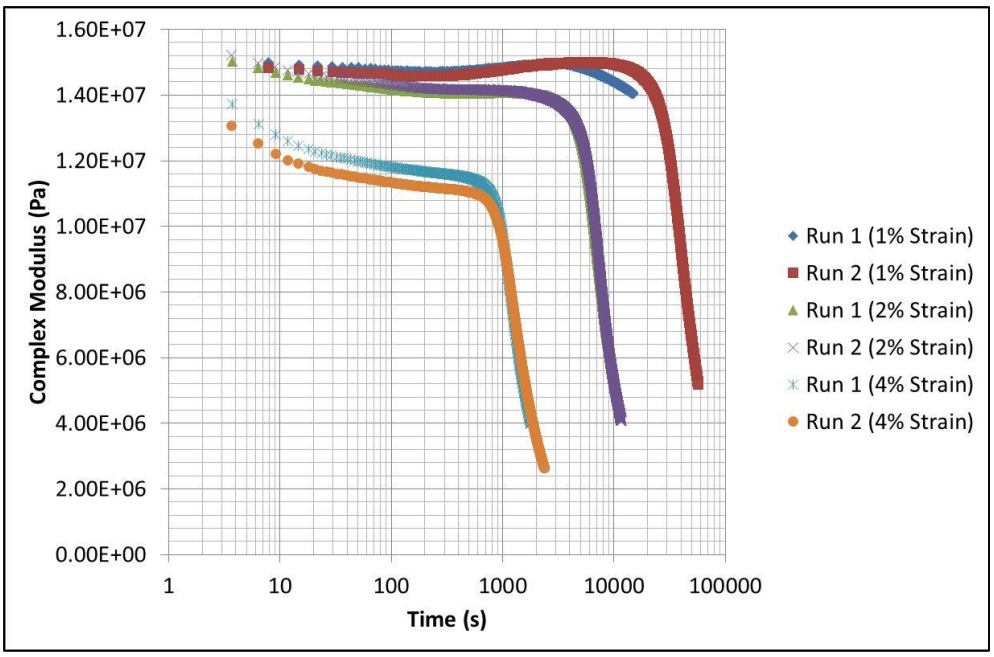

Figure 7-1 : Complex modulus versus time for 50/70V (RTFOT) at 20°C, 10Hz

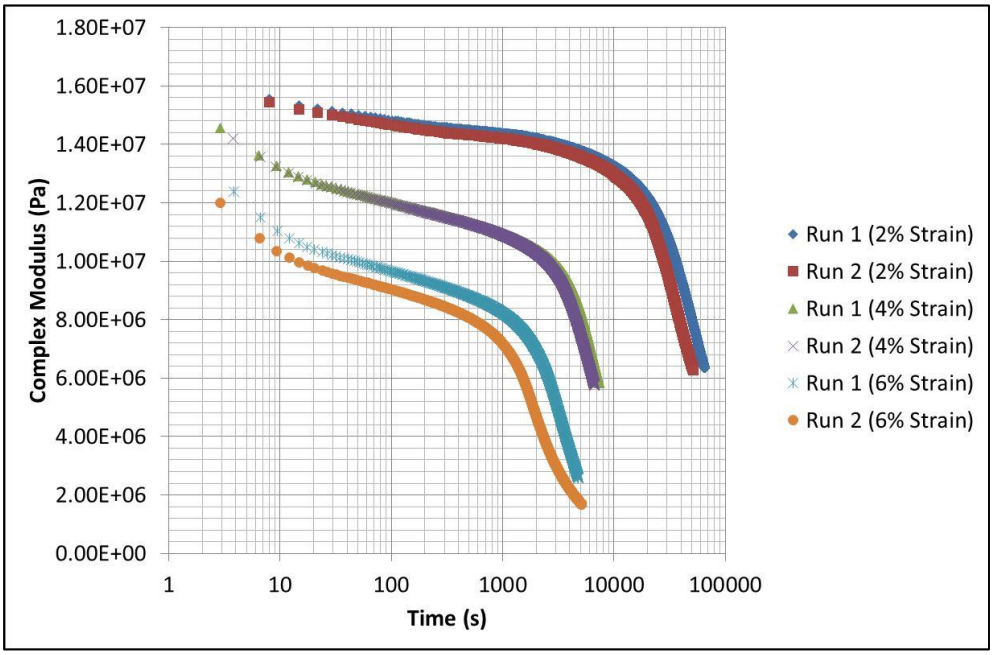

Figure 7-2 : Complex modulus versus time for 50/70V + 5% 1101 (RTFOT) at 20°C, 10Hz

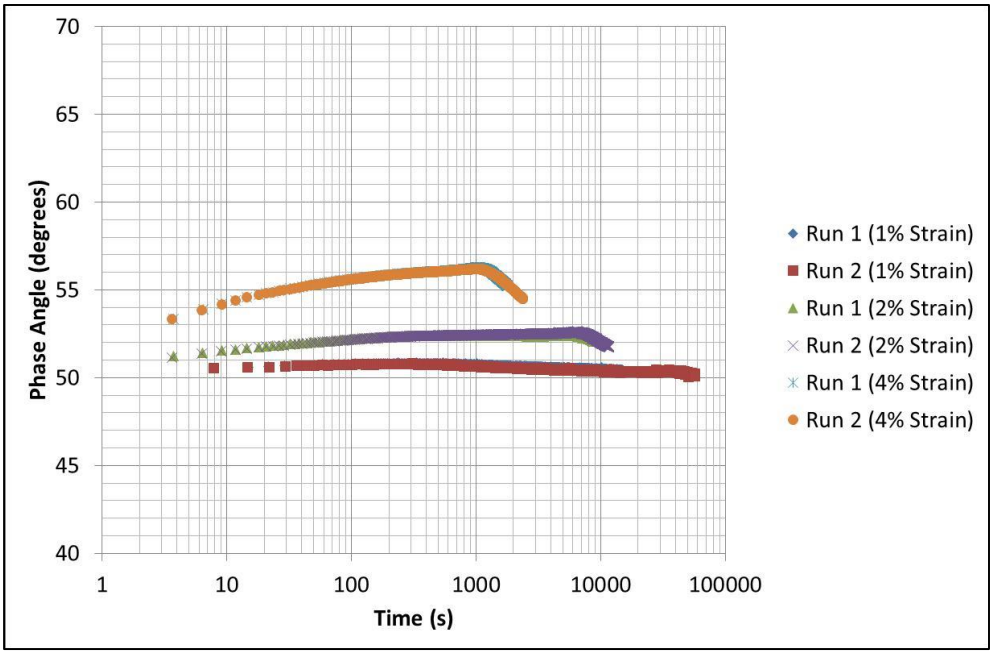

Figure 7-3 : Phase angle versus time for 50/70V (RTFOT) at 20°C, 10Hz

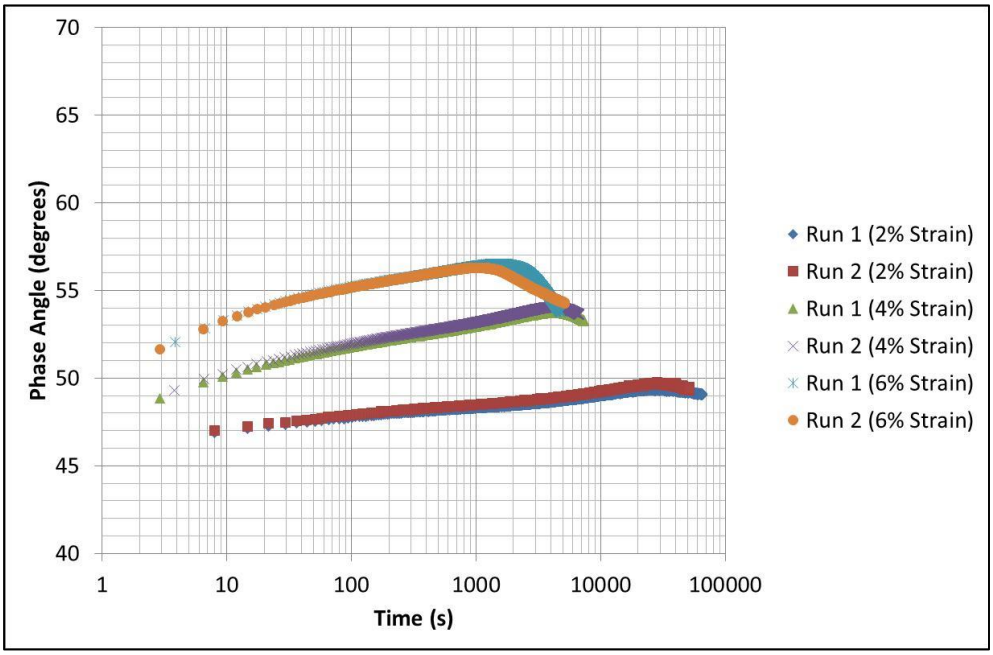

Figure 7-4 : Phase angle versus time for 50/70V + 5% 1101 (RTFOT) at 20°C, 10Hz

To more easily visualise the test data a Wöhler diagram of cycles to failure against applied strain was constructed as shown in Figure 7-5. A power law best fit line was used to determine the applied strain level corresponding to 1,000,000 cycles to failure. These results are summarised in Table 7-1

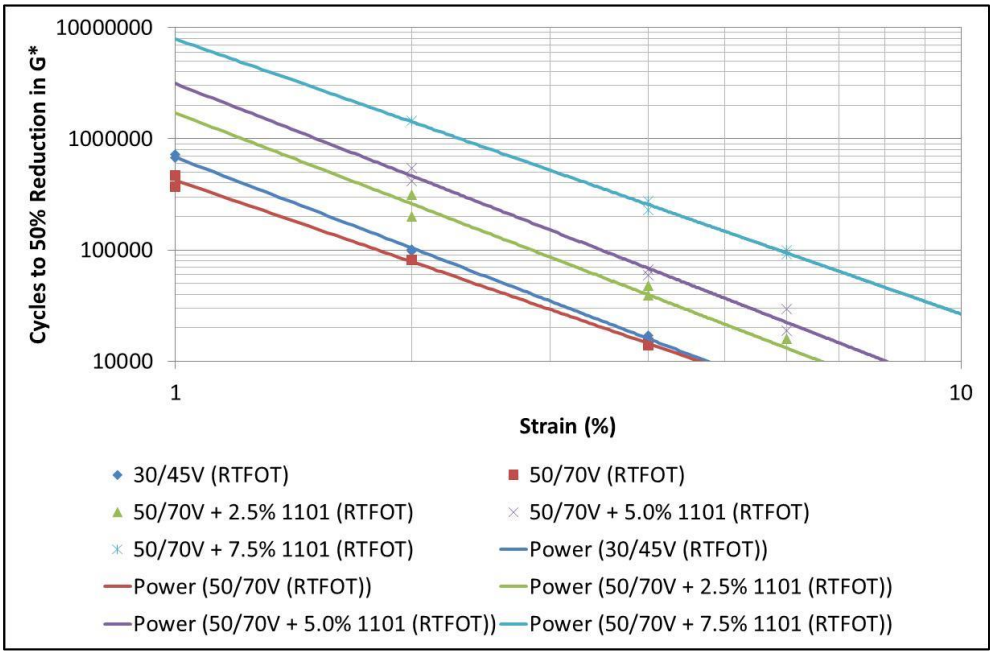

Figure 7-5 : "Wöhler curves" for Venezuelan based binders from TS tests

	Time Sweep Test, Strain for $1x10^6$ cycles to failure
30/45V	0.868 %
50/70V	0.703 %
50/70V + 2.5% 1101	1.217 %
50/70V + 5.0% 1101	1.512 %
50/70V + 7.5% 1101	2.304 %
50/70ME	1.177 %
50/70ME + 5.0% 1101	2.305 %
50/70R	1.137 %
50/70R + 5.0% 1101	3.774 %

Table 7-1 : Predicted strain level in TS test for 1,000,000 cycles to failure

As can be seen the polymer modified binders produced a significant improvement in fatigue resistance. The Venezuelan binders had a poorer fatigue resistance than either the Russian or the Middle Eastern binders.

7.2.1.1 Binder Viscoelastic Continuum Damage Analysis

Whilst the TS test is intuitively simple to perform, the time to failure at lower strain levels can be very long, particularly with modified binders, with some tests taking far in excess of 24 hours to complete. To reduce the time required VECD theory has been successfully applied to analyse fatigue testing of both asphalt (Kim, Lee and Little 1997) and binders (Wen and Bahia 2009).

To accurately determine m, a relaxation test should be performed on the binder. However, even if the applied stress is low there is potential to produce damage within the binder during the test. Johnson (2010) suggested an alternative simpler, but less rigorous, method for the determination of m. He demonstrated than the magnitude of the slope of the log-log plot of storage modulus versus frequency is approximately equal to m determined from the relaxation test. Hintz et al. (2011) compared the value of m determined by the two methods for 8 binders and found that the maximum difference between the values of m determined by the two methods was 2.24%, and was statistically insignificant. Therefore, in this study m was determined from the low strain frequency sweep testing for each binder, with the average values reported in Table 7-2

	m	α	1/(1+ α)	α/(1+ α)
30/45V (RTFOT)	0.657	1.522	0.396	0.604
50/70V (RTFOT)	0.715	1.398	0.417	0.583
50/70V + 2.5% 1101 (RTFOT)	0.615	1.627	0.381	0.619
50/70V + 5.0% 1101 (RTFOT)	0.628	1.593	0.386	0.614
50/70V + 7.5% 1101 (RTFOT)	0.543	1.842	0.352	0.648
50/70ME (RTFOT)	0.590	1.696	0.371	0.629
50/70ME + 5.0% 1101 (RTFOT)	0.515	1.942	0.340	0.660
50/70R (RTFOT)	0.560	1.786	0.359	0.641
50/70R + 5.0% 1101 (RTFOT)	0.442	2.262	0.307	0.693

Table 7-2 : Relaxation parameter m and α determined from frequency sweep data

Increasing polymer modification produced a drop in m which is intuitively correct as the binder becomes more elastic and recovers more rapidly. It was also apparent that the Venezuelan binders had a higher value of m than the equivalent Russian and Middle Eastern binders.

Equation 7-17 was then used to calculate the characteristic C-S curves for each binder from the TS data, with a typical curve shown in Figure 7-6. As can be seen the results from each of the strain levels collapse to form a unique curve for the binder. To allow the C-S curves to be directly compared with the results from the later Linear Amplitude Sweep method the calculation was performed using strain in percent and complex modulus in megapascals.

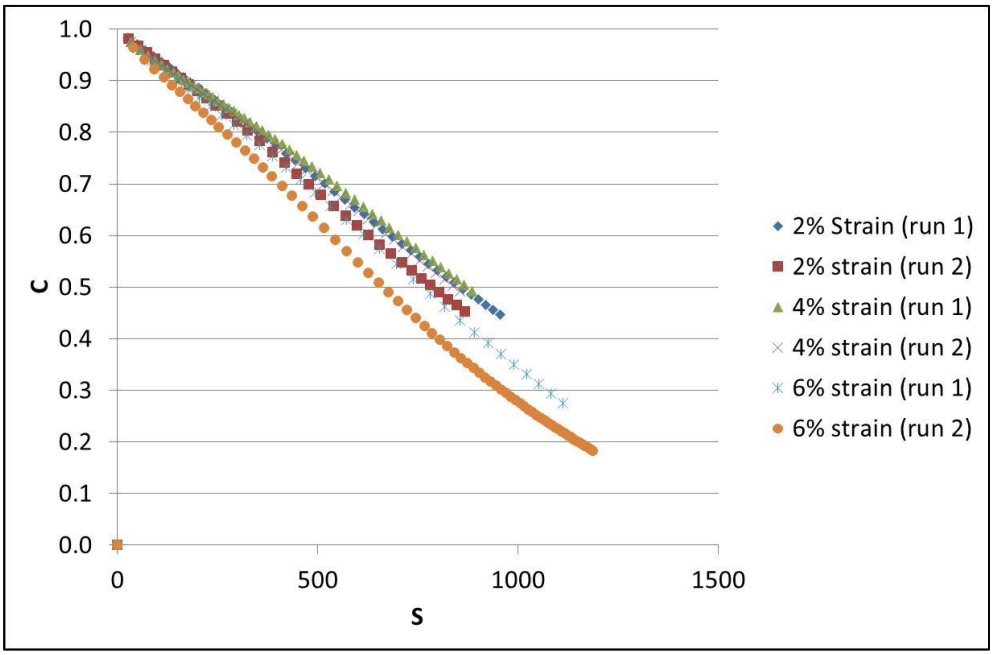

Figure 7-6 : 50/70 Venezuelan +5% SBS RTFOT C-S Collapse

It can therefore be seen that only the high strain level fatigue tests are required to produce the binder's C-S curve, saving significant testing time over TS testing alone.

7.2.2 Linear Amplitude Sweep Test

By only using the higher strain TS results the full C-S curve may be generated in less than a working day. However, Johnson and Bahia (2010) developed an accelerated procedure known as the Linear Amplitude Sweep Test (LAST) which employed VECD theory to produce a C-S curve in less than 30 minutes. The test is performed using the standard 8mm parallel plate DSR geometry with the first step being to determine m from low strain frequency sweep tests as discussed earlier. The binder damaging portion of the test is then undertaken which in the initial development of the test was 20 load steps, each of 100 cycles, starting at 1% strain and increasing in 1% steps to 20% strain at a frequency of 10Hz. A later modification of the test by Hintz et al. (2011) increased the maximum applied strain to 30%.

The VECD analysis of the damage is similar to that in section 7.1 but now the dissipated energy is taken to be

$$\boldsymbol{W = \pi I_D \gamma_0^2 |G^*| sin\delta} \qquad \textbf{Equation 7-31}$$

This then leads to the damage parameter S(t) being calculated as

$$\boldsymbol{S(t) \cong \sum_{i=1}^{N} \left[\pi I_D \gamma_0^2 (|G^*| sin\delta_{i-1} - |G^*| sin\delta_i)\right]^{\frac{\alpha}{1+\alpha}} (t_i - t_{i-1})^{\frac{1}{1+\alpha}}} \qquad \textbf{Equation 7-32}$$

The C-S curve is modelled using Equation 7-20 and the number of cycles to failure determined as

$$\boldsymbol{N_{failure} = \frac{f S_{failure}^k}{k(\pi C_1 C_2 |G^*|^2)^\alpha} \gamma_0^{-2\alpha}} \qquad \textbf{Equation 7-33}$$

The initial work was carried out on a research grade DSR but it was found that not all DSRs typically in use were capable of correctly performing the test. During the 1% step change in requested strain some DSRs were unable to respond quickly enough producing errors in the measured response. Hintz et al. (2013) modified the original method to more smoothly increase the strain in 0.1% increments up to 30% which resolved this problem.

Bahia et al. (2013) proposed a further modification to the analysis suggesting that the criteria for failure should be at the value of C relating to peak stress rather than a fixed value of C as this was found to produce an improved correlation to field fatigue data, with the method published as AASHTO TP 101-14 (AASHTO 2014)

All the binders previously assessed using TS were also assessed using the LAS method with a typical stress sweep shown in Figure 7-7.

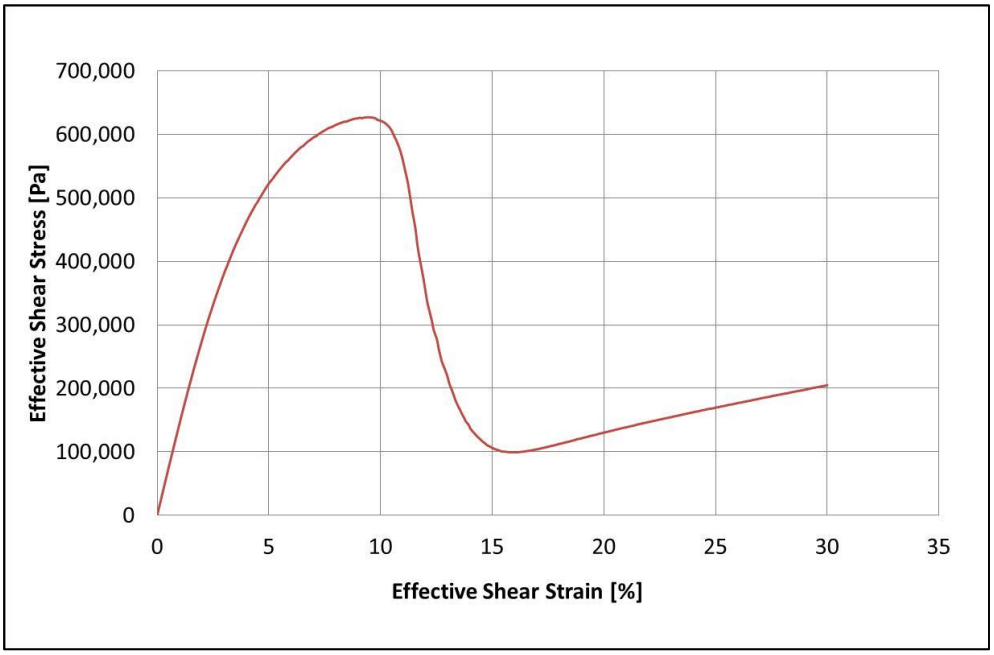

Figure 7-7 : LAS stress sweep for 50/70V (RTFOT) at 20°C

The data was analysed using both a 50% drop in G* sin(delta) and the damage at maximum peak stress criteria. The predicted strain required to produce 1,000,000 cycles to failure was calculated and compared to the results from the TS tests and the TS high strain data with VECD applied as shown in Figure 7-8.

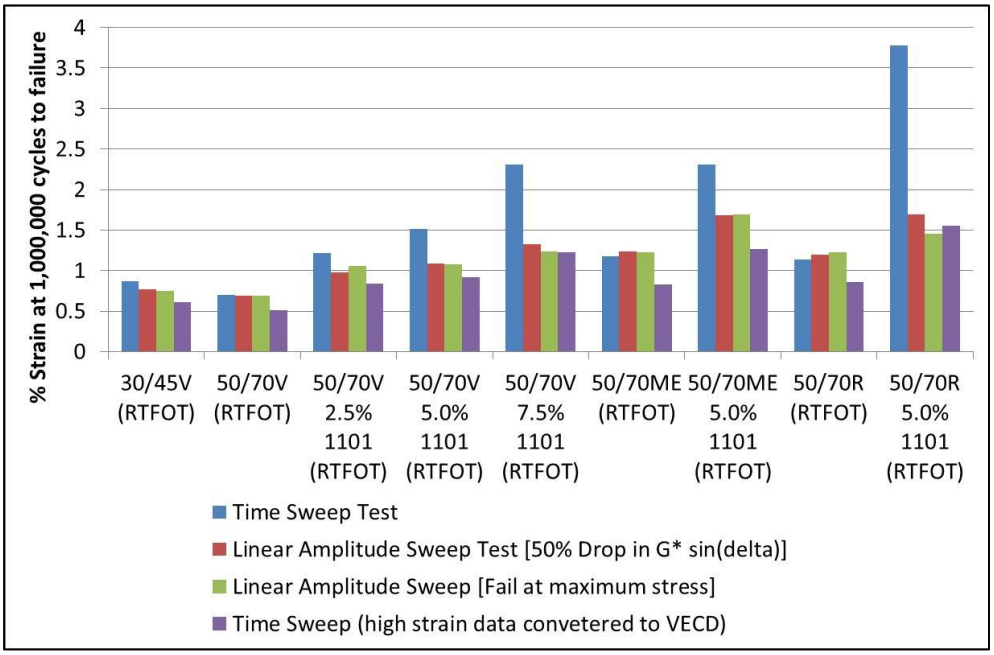

Figure 7-8 : Predicted strain level required to produce 1,000,000 cycles to failure

As can be seen the methods employing VECD did not produce a one-to-one predictive relationship between the measured fatigue life from TS tests and the predicted fatigue life from VECD calculations. However, it does allow an initial screening and ranking of the binder's fatigue performance to be accomplished.

The difference is a consequence of the VECD calculations which assume that all deviations from linear viscoelastic behaviour are damaging, whereas in reality a proportion of the binder response is actually non-linear recoverable behaviour. Underwood (2016) attempted to isolate the non-linear viscoelastic properties of binders and mastics and include it within the VECD model and found an improvement in the collapse of the C-S curves although comparisons of fatigue life predictions with and without the inclusion of non-linear effects were not presented and the testing was limited to one binder. It is, however, clear than any future model should incorporate these effects to accurately predict fatigue behaviour when useing VECD based models.

The results from this research shows that with increasing binder polymer content the difference between the TS and VECD prediction increases implying that increased polymer content also increases the amount of non-linear recoverable response. In this research as the polymer modified binders were manufactured with known composition this difference was clearly identifiable. However, in typical industrial situations the polymer content of commercially available binders is rarely disclosed so care must be taken when using LAST as a pavement design input.

7.3 Asphalt Fatigue Analysis

Full scale asphalt fatigue analysis may be undertaken under controlled conditions using specially constructed pavements and dedicated equipment such as the Accelerated Load Testing Facility on the Laboratoire Central des Ponts et Chaussées (LCPC) in Nantes, France, shown in Figure 7-9. However, due to the large amounts of materials and considerable time and expense necessary to run such facilities it is only appropriate for highly specialised applications.

Figure 7-9 : Fatigue carousel at LCPC Nantes (LCPC 2007)

More typically laboratory scale fatigue experiments are carried out although even then the quantities of materials involved can be substantial. A wide range of laboratory techniques have been developed with the most commonly encountered summarised below.

7.3.1.1 Two point bending test on trapezoidal specimens (EN 12697-24 Annex A)

In this method trapezoidal shaped specimens are utilized, most usually cut from laboratory prepared roller compacted slabs. The base of the specimen is fixed in place whereas the top is oscillated by a constant amplitude sinusoidal displacement as shown schematically in Figure 7-10.

Figure 7-10 : Schematic of two-point bending trapezoidal test

The reference test conditions are 25Hz at 10°C, although other temperatures and frequencies may be used if the equipment design permits it, with complex modulus and phase angle monitored through each test. Eighteen specimen tested over a range of strain levels are required to produce a complete fatigue determination.

This method is particularly popular in France where it is specified as part of the national design procedure for asphalt mixtures. However, the difficulty in manufacturing the trapezoidal shaped specimens combined with the dedicated equipment necessary to perform the test has restricted its acceptance more widely. In the UK fatigue properties have not been included in specifications but fatigue has been included as an option in the design for Enrobé à Module Élevé materials as this mixture was originally developed in France. However, in practice it is rarely used as mixtures with a binder richness modulus of greater than 3.6 are exempt from fatigue analysis.

7.3.1.2 Four-point bending test on prismatic shaped specimens (EN 12697-24 Annex D)

In the four point bending method long prismatic beams are analysed, and this method is probably the most commonly encountered asphalt fatigue method worldwide. Again laboratory roller compacted slabs are initially prepared, but specimen preparation is far simpler than for trapezoidal specimens due to its simpler prismatic geometry. The specimen is clamped in four positions with a load applied to the centre two clamps producing a strain within the beam measured by LVDTs on the specimens.

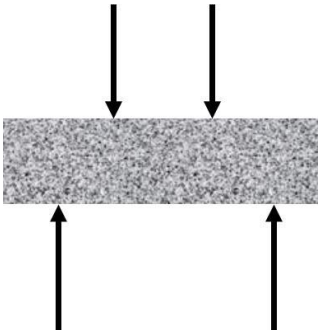

Figure 7-11 : Schematic of four point bending test

Most four point bending frames are computer operated with feedback loop control systems allowing the test to be run in either controlled stress or controlled strain modes with complex modulus and phase angle recorded. The test frequency may also be easily altered with a minimum range of 0.1 to 60Hz specified for the equipment, thus allowing a wide frequency characterisation of the material to be easily accomplished.

7.3.1.3 Indirect tensile test on cylindrical shaped specimens (EN 12697-24 Annex E)

This test employs relatively small cores so has the advantage that specimens can be prepared either using standard laboratory compaction devices, or cored directly from site. Vertical haversine loads are repeatedly applied diametrically as shown in

Figure 7-12 generating a horizontal strain within the specimen, ultimately leading to its fracture failure.

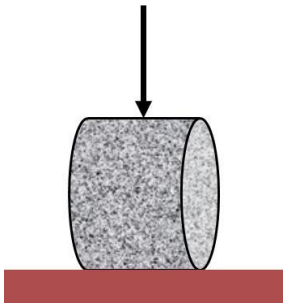

Figure 7-12 : Schematic of Indirect tensile test on cylindrical shaped specimens

The test is commonly referred to as the Indirect Tensile Fatigue Test (ITFT) which was a development draft specification (BS DD ABF:1995) but the ITFT method is not strictly according to the EN standard as this also requires a horizontal extensometer fixed to the specimen to measure strain.

The test is usually performed at 20°C in the UK where it remains a popular test, or at lower temperatures in the Scandinavian countries where it is also in common use. Its popularity is a consequence of comparatively simple specimen preparation combined with the relatively low cost equipment necessary to perform the test. However, as the test is in reality a fracture test rather than a true fatigue test and can only be performed in controlled stress mode, its application in fundamental research is limited.

7.3.1.4 Direct tension cyclic fatigue of cylindrical specimens

Following the introduction of the Superpave asphalt design process in the early 1990's it was recognized that it did not include a final measurement of the asphalt modulus. In 1996 the Federal Highway Administration provided funding into the development of a new test to address this problem which led to the development of the Simple Performance Tester (Witczak et al. 2002, Bonaquist, Christensen and Stump 2003, Bonaquist 2008).

This method uses cylindrical specimens 100mm in diameter by 150mm high cored from larger gyratory prepared cores. The end of the specimens must be accurately sawn parallel to one another and platens adhered to the top and bottom. To measure the specimen deformation LVDT's are mounted directly onto the specimen, as shown schematically in Figure 7-13. A sinusoidal load is applied to the specimen to determine its dynamic modulus and phase angle at frequencies from 0.1Hz up to 25Hz. Static and repeated load creep tests may also be performed to determine flow characteristics as an indicator of rutting potential.

More recently the device has also been used in cyclic fatigue mode to determine asphalt fatigue and the method standardised as AASHTO TP 107 (2014).

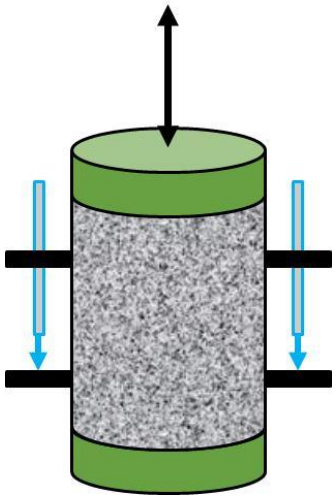

Figure 7-13 : Schematic of direct tension cyclic testing of cylindrical specimens

The complex LVDT arrangement and comparatively difficult specimen preparation has so far limited the introduction of this device outside of the USA. Furthermore, the large specimen sizes usually precludes the use of site cores and not all gyratory compactors are able to manufacture tall enough specimens in the laboratory.

7.3.2 DSR Small Specimen Fatigue

The use of a DSR to characterise the linear viscoelastic properties of small asphalt specimens was demonstrated in Chapter 3. The logical extension of this testing was to employ higher strain levels on the DSR to damage the specimens and hence produce fatigue failure.

Low strain oscillatory tests demonstrated that at 20°C 1Hz the asphalts had G* typically in the range 1×10^8 to 1×10^9 Pa. The torque produced by the air bearing in a DSR is relatively small compared to the forces available in traditional laboratory asphalt fatigue tests but it was found that when using 12.2mm diameter specimens the maximum torque available on the DSR produced strains of over 0.2% even for the highest modulus materials, and therefore in the damaging zone.

To produce the small specimens for fatigue testing asphalt slabs 305x305x70mm were prepared to the mix-design detailed in section 3.2. These were sawn into 50mm thick sections and small cores extracted as shown in Figure 7-14. Smaller Marshall or gyratory cores could have been used, but the slabs were also required for the later trapezoidal testing and by taking the small cores from slab slices a direct comparison of results from the two methods was possible.

Figure 7-14 : Asphalt slab sections after small specimen coring

Prior to each fatigue test a low strain frequency sweep was carried out at a strain of 0.001% from 0.1 to 100Hz to characterise the linear viscoelastic properties. The specimen was then further conditioned for 5 minutes at 1Hz, 0.001% to determine the undamaged properties of the specimen.

Fatigue testing was carried out in controlled strain mode on the DSR at 20°C at a frequency of 1Hz and a strain of 0.2%, with the test terminated when the complex modulus had reduced to less than 1 x 10^7 Pa. For each asphalt mixture six specimens were analysed with the typical evolutions for complex modulus and phase angle shown in Figure 7-15 and Figure 7-16.

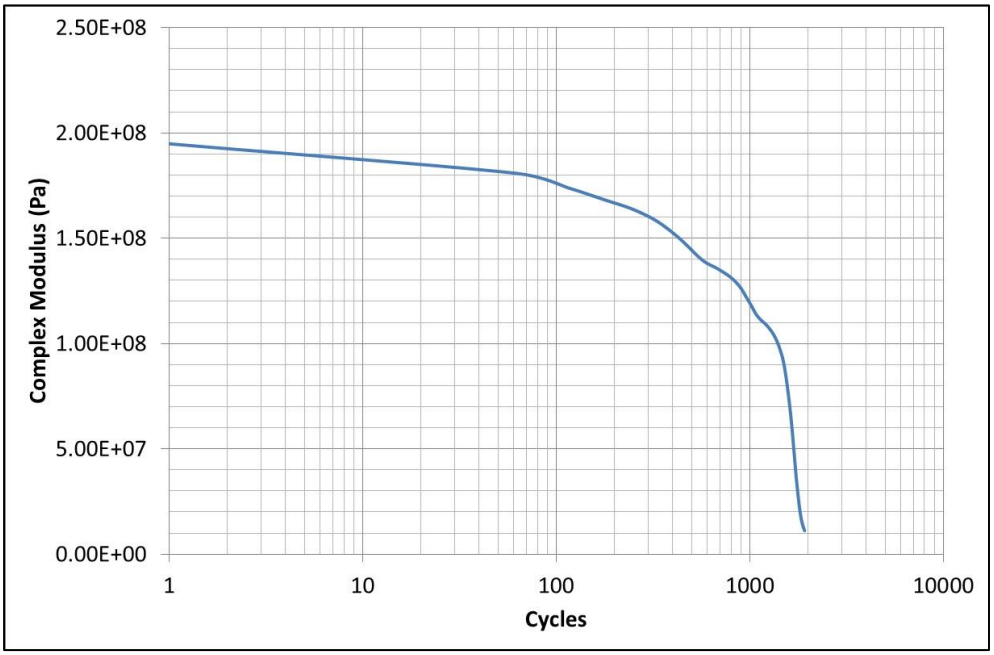

Figure 7-15 : Evolution of complex modulus in small specimen fatigue for asphalt AV0

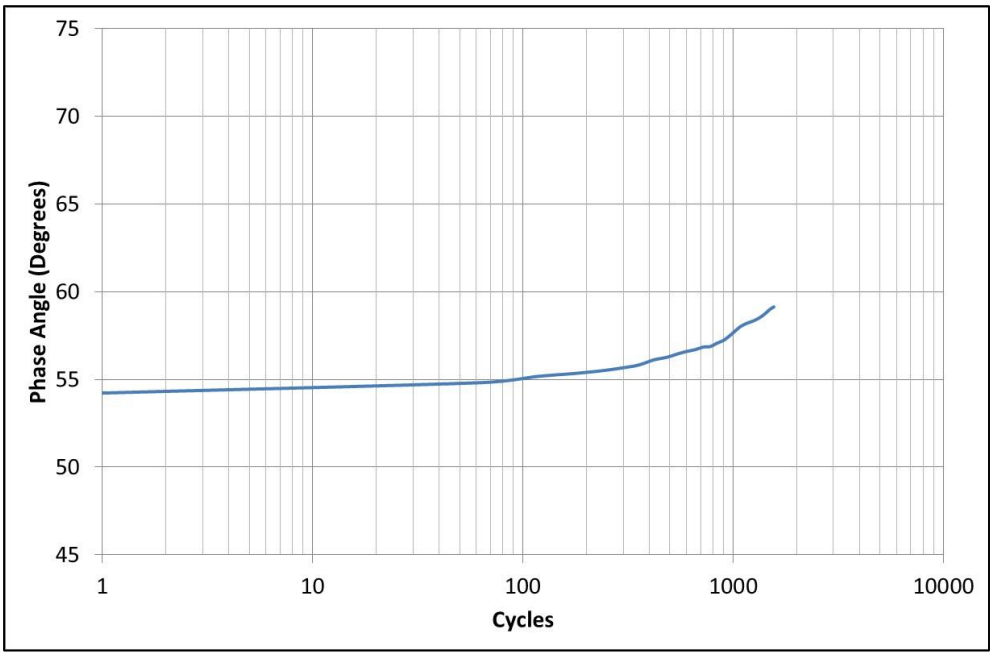

Figure 7-16 : Evolution of phase angle in small specimen fatigue for asphalt AV0

Figure 7-17 shows the six fatigue curves for asphalt AVH, and as can be seen all the tests follow the expected evolution pattern with a reasonable degree of correlation between each test when plotted on a logarithmic scale.

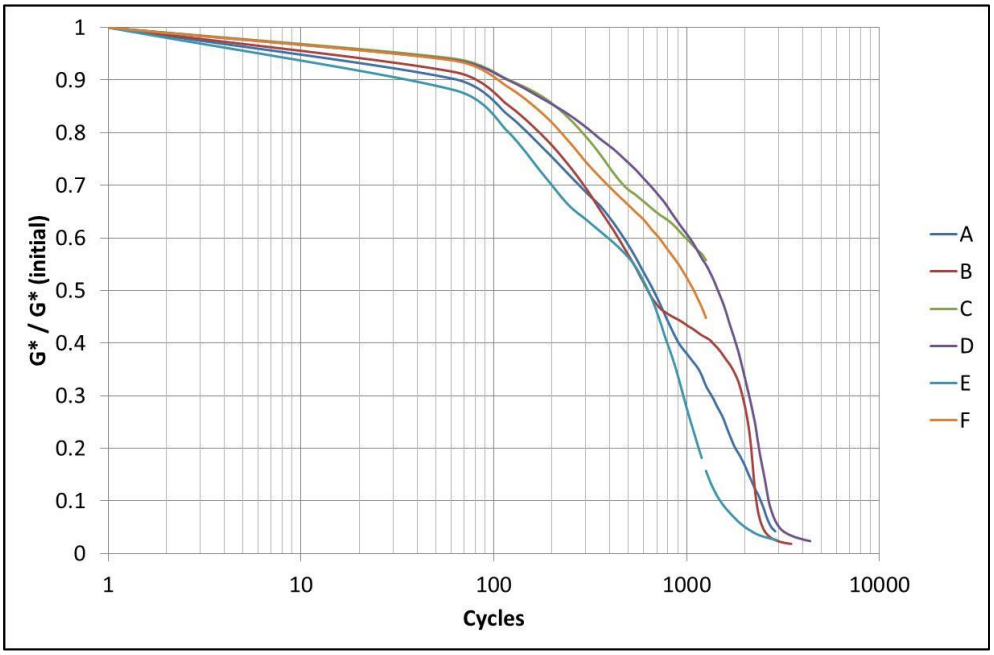

Figure 7-17 : Small specimen fatigue results for asphalt AVH

However, if the point of specimen failure is taken as a 50% drop in initial modulus and the number of cycles to failure plotted on a linear scale the range of results can be seen to be rather high as seen in Figure 7-18.

Unexpectedly, the binder composition was also seen to have little effect on the number of cycles to failure, with the unmodified asphalts outperforming the asphalts produced with PmBs.

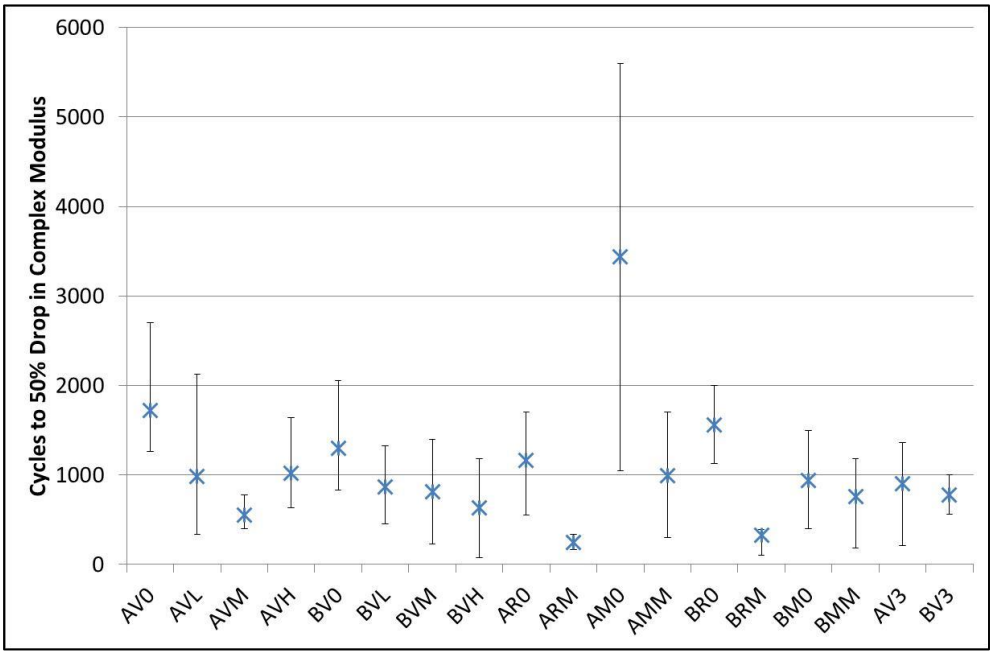

Figure 7-18 : Mean, minimum and maximum cycles to failure for small asphalt specimen fatigue tests

During the coring of the small specimens some cores fractured during extraction from the slab slice. Whilst these broken specimens were discarded it can be surmised that a degree of microcracking occurred during the coring process for all the specimens, and that these microcracks led to multiple crack initiation sites which in turn resulted in the large spread of fatigue life results. Whilst this microcracking is likely to be common to all fatigue testing where specimens are cored or sawn, for small specimens the effect is exaggerated due to the large nominal maximum aggregate size relative to the specimen size.

The results of these tests therefore imply that whilst traditional fatigue testing of small specimens is possible using the DSR it has limited direct potential as a predictor of engineering behaviour using a tradition cycles to failure approach.

7.3.2.1 Application of VECD Theory to Small Specimens

The majority of VECD asphalt analysis has been performed in the uniaxial push-pull geometry (Kutay, Gibson and Youtcheff 2008, Xie and Shen 2015) although it has

also been successfully applied to other geometries such as the 4-point bending method (Mello, Kaloush and Farias 2010, Haddadi et al. 2015)

Whilst in this research the spread of data from small specimen fatigue testing was found to be high during the traditional fatigue tests a VECD analysis of the results was still possible. The relaxation parameter, m, was first determined from the specimen's linear viscoelastic properties with the mean results for each asphalt mixture shown in Figure 7-19.

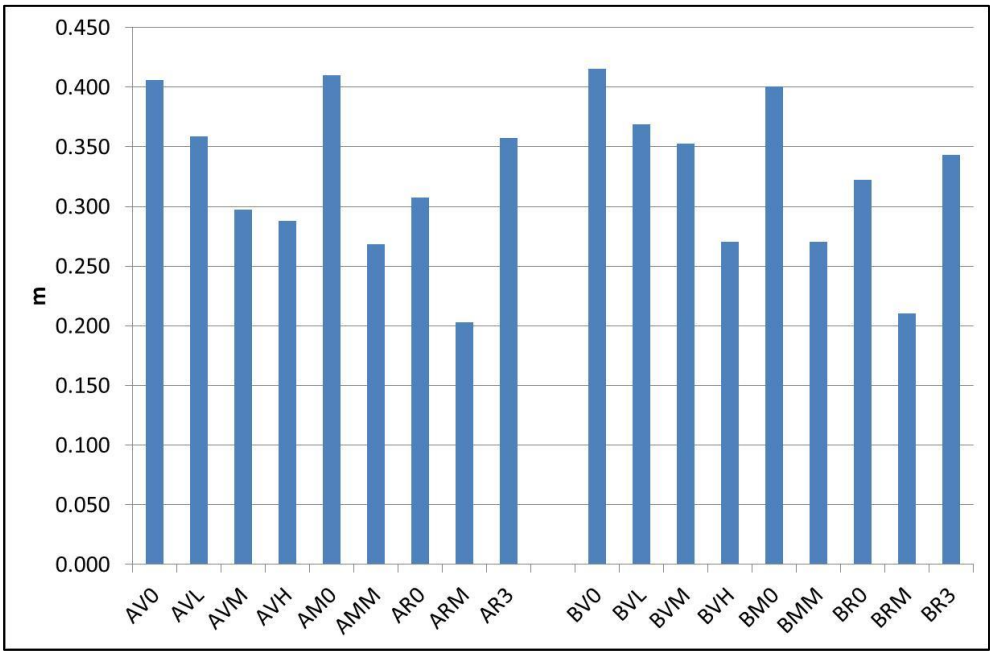

Figure 7-19 : Relaxation parameter m determine from small specimen tests

These results show that m decreases with increasing polymer modification, with broadly similar values for the two asphalt mixtures. It was also noteworthy that the 30/45 based asphalts had m-values similar to the other unmodified asphalts even though they were closer in stiffness to the polymer modified asphalts.

The C-S curves for each asphalt mixture were then calculated using Equation 7-17, with the results for asphalt AVH shown in Figure 7-20. The units used in the calculation were engineering strain and modulus in kilopascals to enable a direct comparison to be made with the work of Kutay, Gibson and Youtcheff (2008) with

the same units used in all subsequent analysis of alternative asphalt geometries. For each set of six small specimen tests a best fit C-S line of Equation 7-20, was determined. The solver function in Excel was used to determine the best fit coefficients for C_1 and C_2 by reducing the absolute mean error between the best fit C-S curve and the measured data to a minimum as shown in Figure 7-20.

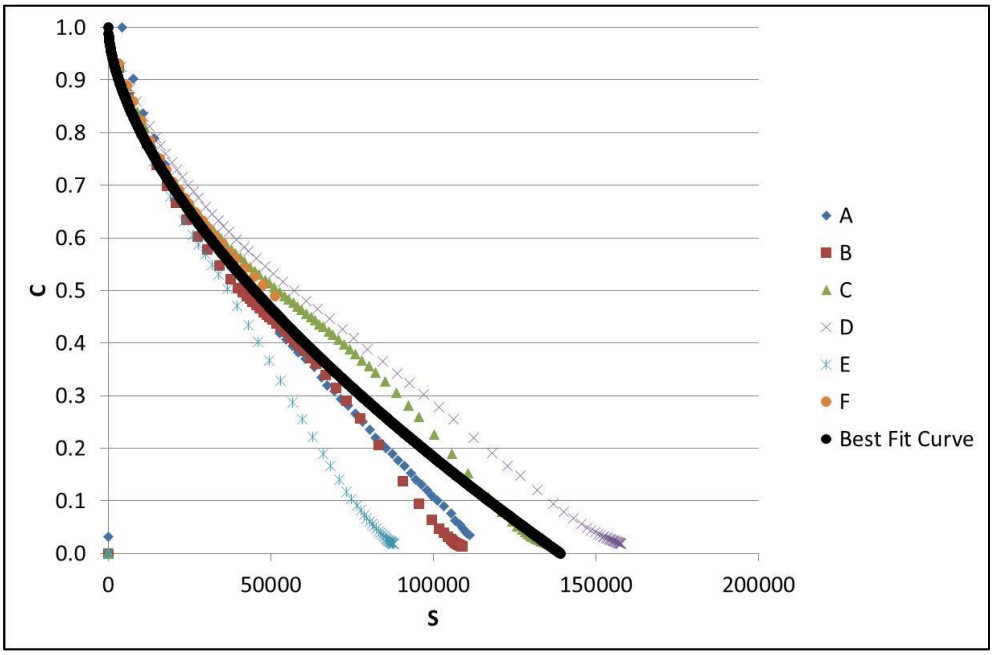

Figure 7-20 : C-S curves for asphalt AVH

As can be seen the high degree of scatter in the traditional test data is also reflected in the C-S curves, particularly at higher damage levels where significant crack propagation within the specimen has already taken place. However, up to C = 0.5, which is the traditional value taken for fatigue failure, the curve overlap is more reasonable, implying broadly equivalent asphalt damage performance. By restricting the data used in the calculation of C-S best fit curves to a minimum of C=0.5 the specimen to specimen scatter was reduced, and also allowed a direct comparison to traditional fatigue testing using the 50% reduction in modulus as the failure criteria.

To estimate the error in the C-S curves to a fixed value of C Equation 7-20 may be rearranged to allow a least squares linear regression of the C-S curves to be performed as follows

$$C_1 S^{C_2} = 1 - C \qquad \textbf{Equation 7-34}$$

$$logC_1 + C_2 logS = \log(1 - C) \qquad \textbf{Equation 7-35}$$

$$logS = \frac{\log(1-C)}{\log C_2} - \frac{logC_1}{logC_2} \qquad \textbf{Equation 7-36}$$

Therefore, a least squares linear regression plot of log S versus of log (1-C) will have a slope of 1/log C2 and intercept $-\log C_1/\log C_2$. The best fit values of C_1 and C_2 were determined for each asphalt mixture along with the standard error which allowed the 95% maximum and minimum confidence level curves to also be determined as shown in Figure 7-21 below.

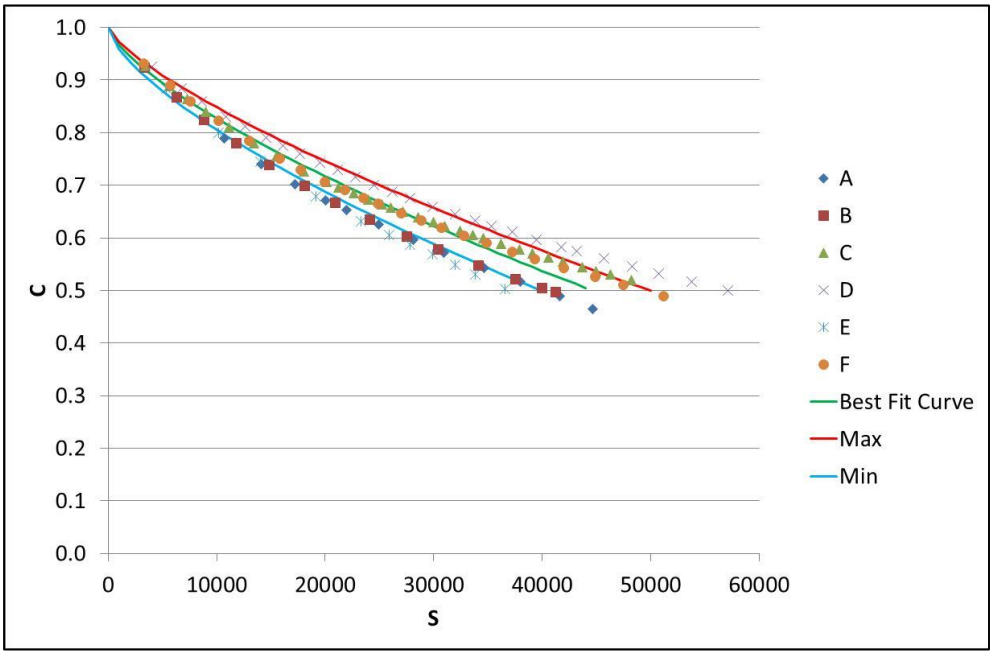

Figure 7-21 : C-S curves with best fit and 95% confidence intervals for asphalt for asphalt AVH using data points with C>=0.5

The best fit lines were then used to calculate the strain level necessary to produce 1,000,000 cycles to failure using Equation 7-30 as shown in Figure 7-22 and Figure 7-23, with the error bars representing the 95% confidence levels.

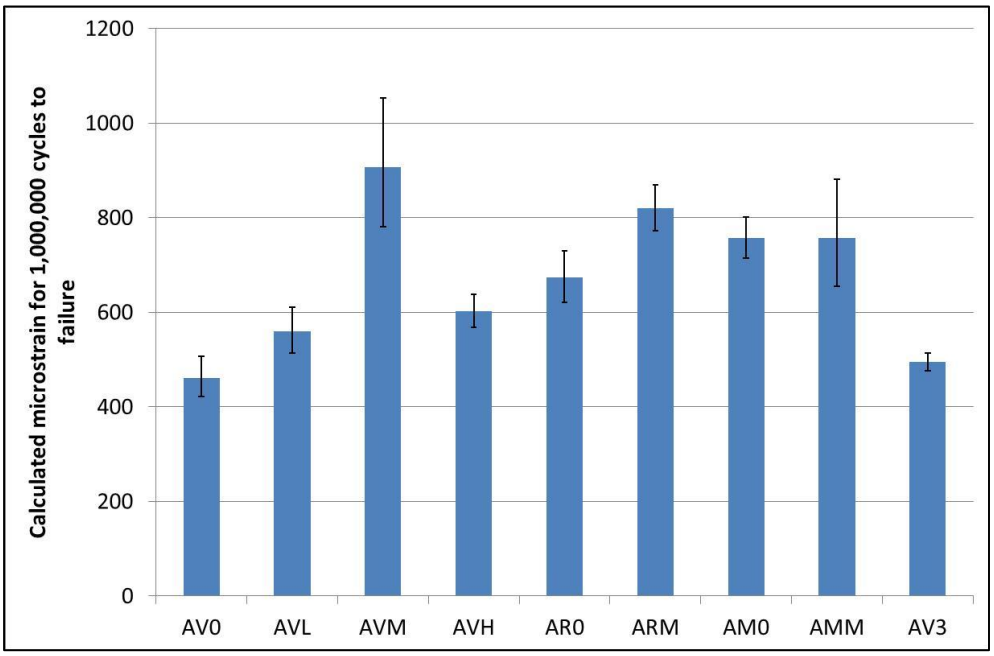

Figure 7-22 : Calculated microstrain for 1,000,000 cycles to failure for limestone based small specimens

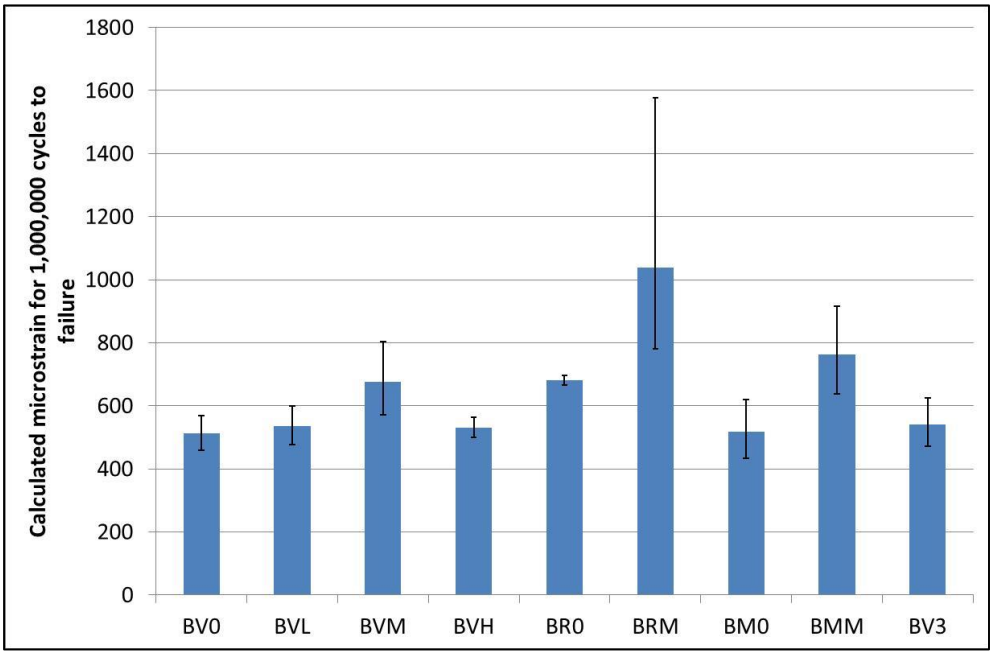

Figure 7-23 : Calculated microstrain for 1,000,000 cycles to failure for gritstone based small specimens

In contrast to the results in Figure 7-18 clear differences were seen between the unmodified and polymer modified asphalts with increase microstrain required to produce the same number of cycles to failure in the polymer modified materials. However, the magnitude of the predicted error in the necessary microstrain was seen to be variable and in some cases relatively high, implying that this approach should be best considered as a screening tool rather than a quantitative pavement design tool. Analysis of additional test specimens could be considered to improve the confidence in the result, but the extra material and testing time would negate many of the advantages of the small specimen approach.

7.3.3 2 point bending trapezoidal

To support the results of the small specimen testing results from an established asphalt fatigue method were also required, with the 2 point bending trapezoidal method selected.

To prepare the specimens for fatigue testing a cutting tool was developed to allow the trapezoidal specimens to be cut from the large slabs on the Clipper saw with details of the procedure included as Appendix B.

The trapezoidal specimens were tested on the apparatus shown in Figure 7-24. All specimens were conditioned and tested at 20°C at a test frequency of 25Hz. For each asphalt mixture four specimens were tested with two each at 120 and 160 microstrain. Each pair of tests was halted when the modulus reduced to 10% of its original value.

Figure 7-24 : Trapezoidal 2-Point Bending Apparatus

The measured strain, phase angle and modulus were periodically recorded on a local PC throughout the test as shown in Figure 7-25 and Figure 7-26 for asphalt AVM.

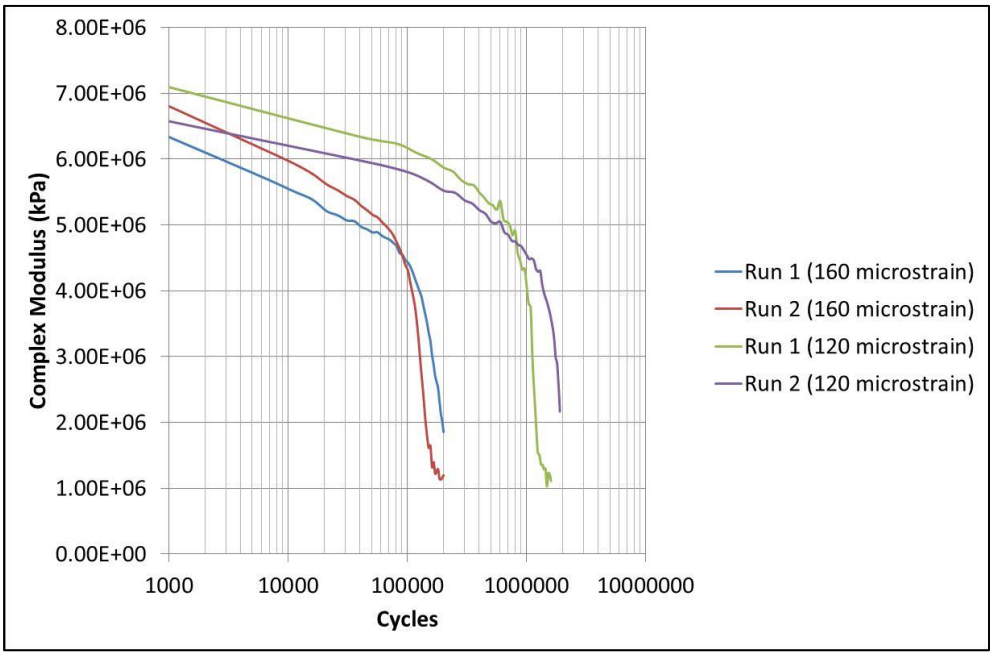

Figure 7-25 : Evolution of complex modulus for asphalt AVM in 2PB fatigue

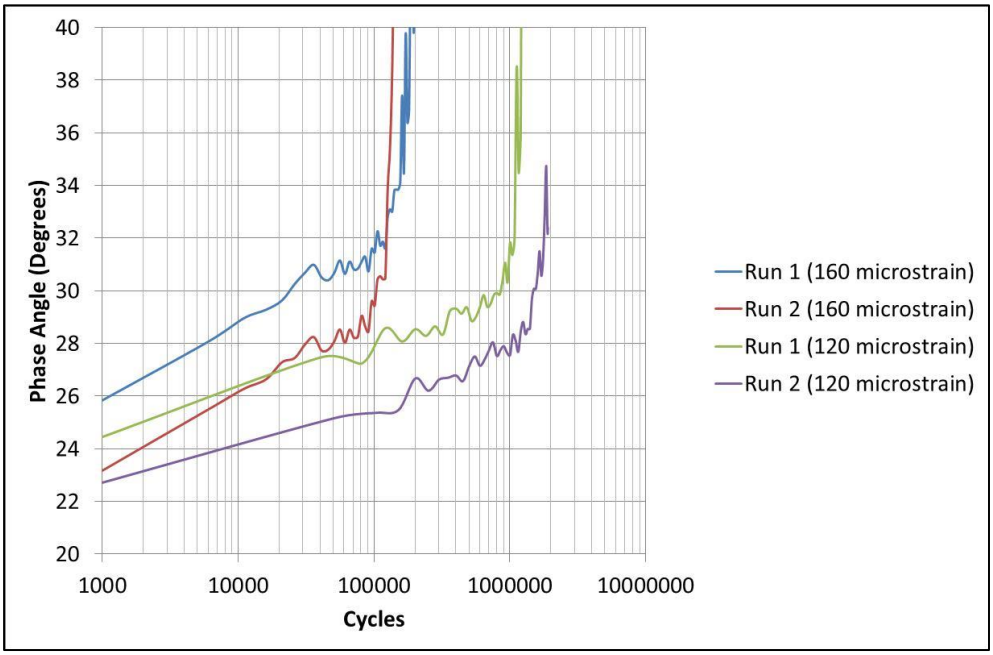

Figure 7-26 : Evolution of phase angle for asphalt AVM in 2PB fatigue

A reasonable degree of repeatability was observed in these tests, although for some asphalts the repeatability between specimens at the same strain level was far poorer such as in asphalt AV0 as shown in Figure 7-27.

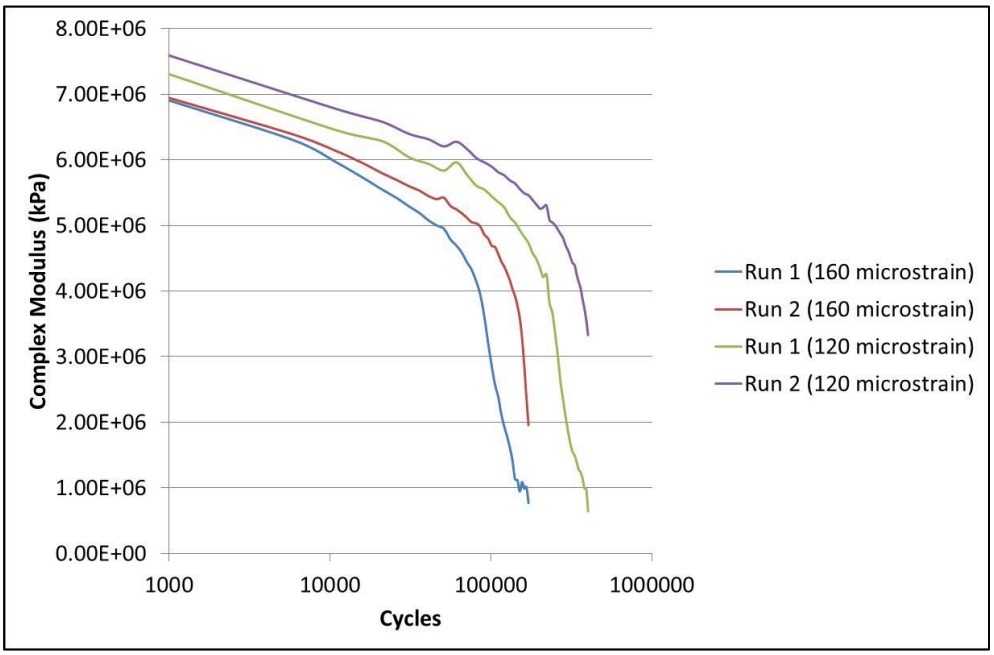

Figure 7-27 : Evolution of complex modulus for asphalt AV0 in 2PB fatigue

To produce a S-N curve according to EN 12697-24 eighteen specimens should be tested. However, even though in this study only four specimens were tested at two strain levels an estimate of S-N performance was still possible as shown in Figure 7-28 for asphalt AV0 with a best-fit regression power law applied to each asphalt.

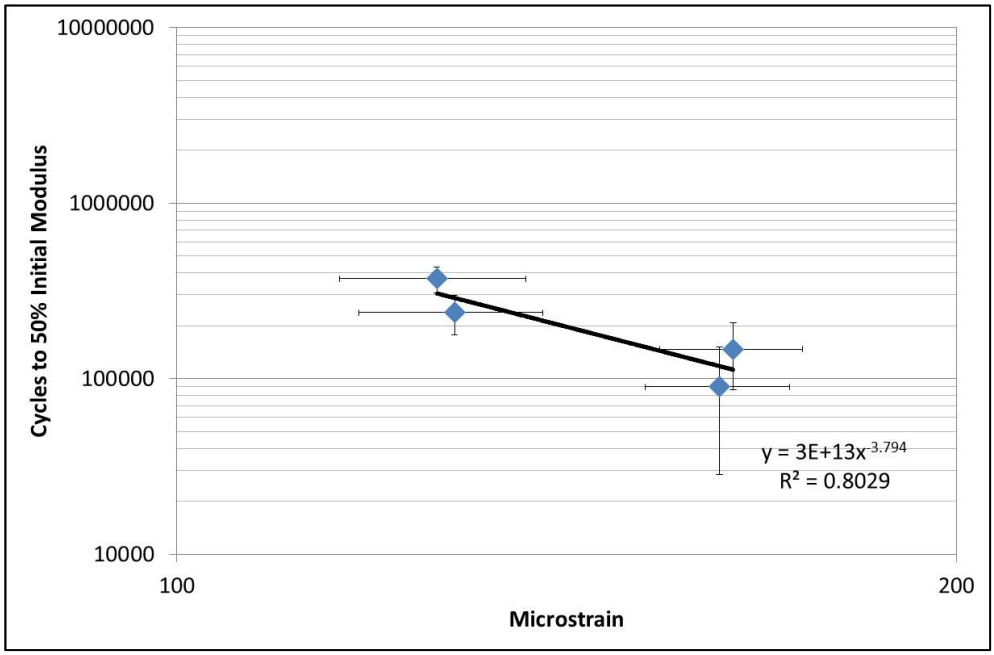

Figure 7-28 : S-N diagrams for 2 point trapezoidal bending

As only four data points were used to construct the S-N diagrams the accuracy of the predicted fatigue lines could be questioned, but with the exception of asphalt BM0 all the fatigue lines followed the expected pattern with the polymer modified asphalts demonstrating a greater number of cycles to failure.

Using the same approach as previously the trapezoidal fatigue data was converted into C-S curves with the m-value determined earlier in the small specimen testing used in the calculation. As can be seen in the examples Figure 7-29 and Figure 7-30 a good overlap is again observed. This was particularly interesting for asphalt AV0 which in Figure 7-27 displayed an apparently poor repeatability between individual specimens, but in Figure 7-30 the data converges implying the internal damage evolution is equivalent for all specimens.

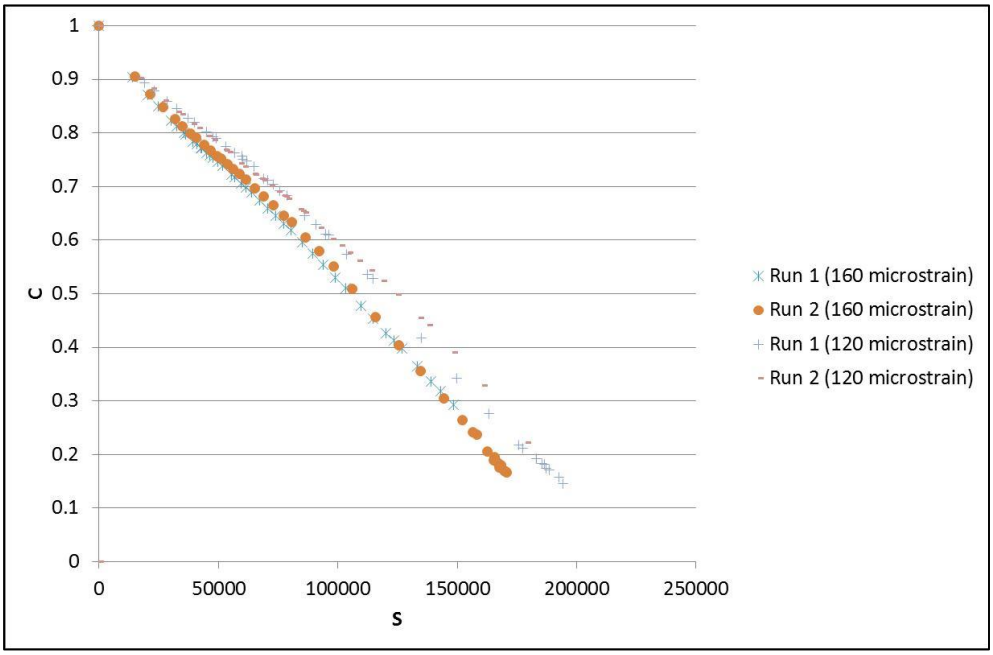

Figure 7-29 : C-S curves for asphalt AVM

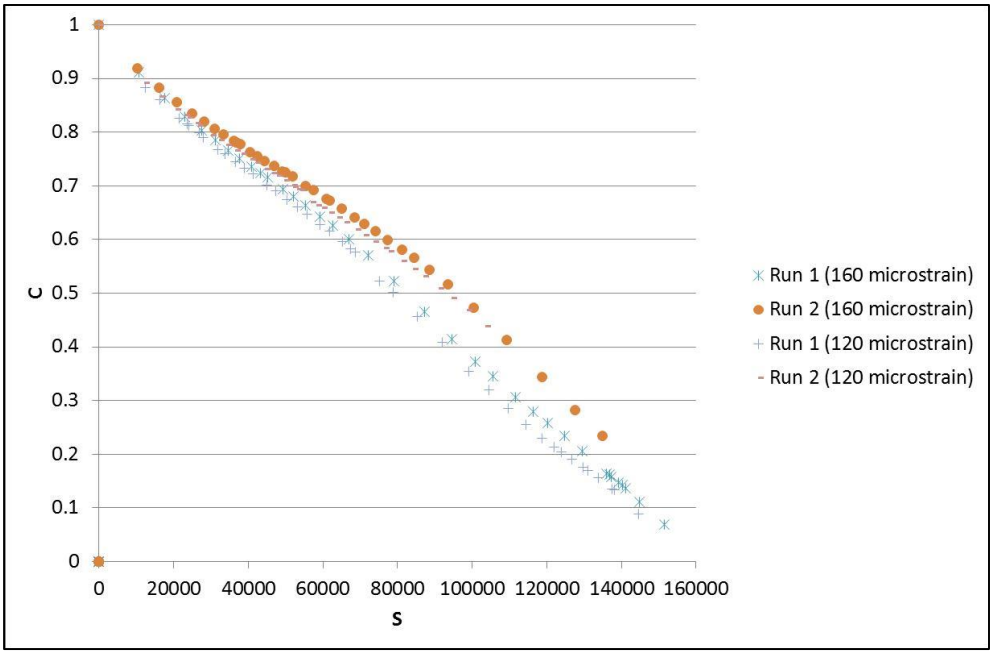

Figure 7-30 : C-S curves for asphalt AV0

The same methodology used in section 7.3.2.1 was then used to calculate the best fit C-S curves. Figure 7-31 shows the best fit curve for asphalt AVO along with the 95% confidence intervals for the best fit curves.

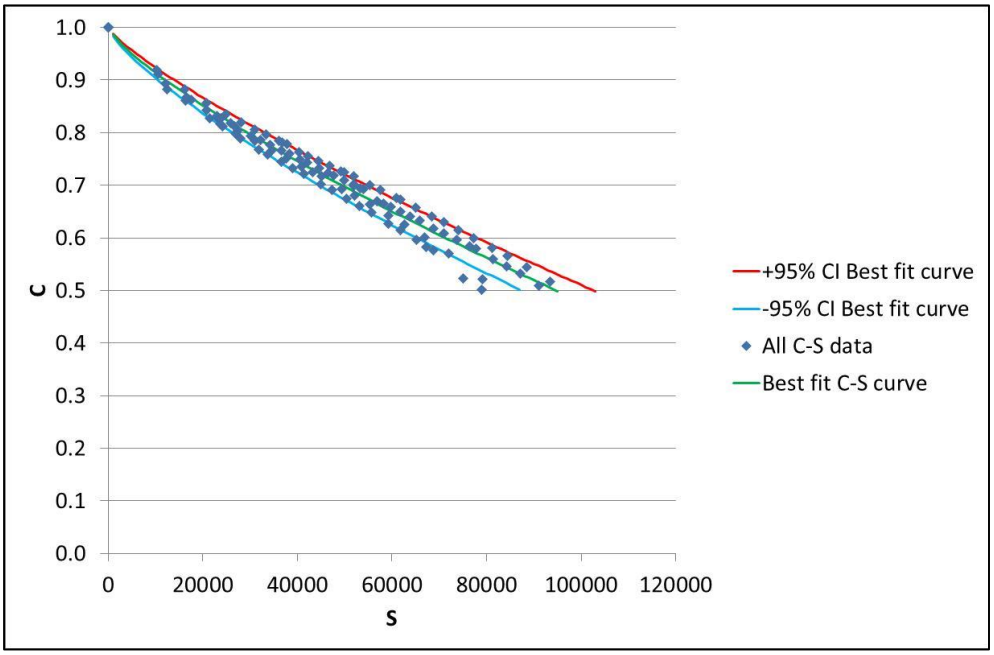

Figure 7-31 : C-S data with best fit and 95% confidence intervals for asphalt AV0

BS EN 12697-24 states the 95% repeatability for the determination of 1,000,000 cycles to failure is 4.2 microstrain. This is for a complete test with 18 specimens so the error using only 4 specimens as in this research will actually be higher. Figure 7-32 demonstrates the correlation between the strain for 1,000,000 cycles to failure using VECD calculation and the traditional Wöhler diagram with the estimated error in each value included as error bars. The degree of correlation was remarkably high confirming that an accelerated test regime analysed via VECD provided a good estimation of the performance of a traditional test at low strain levels.

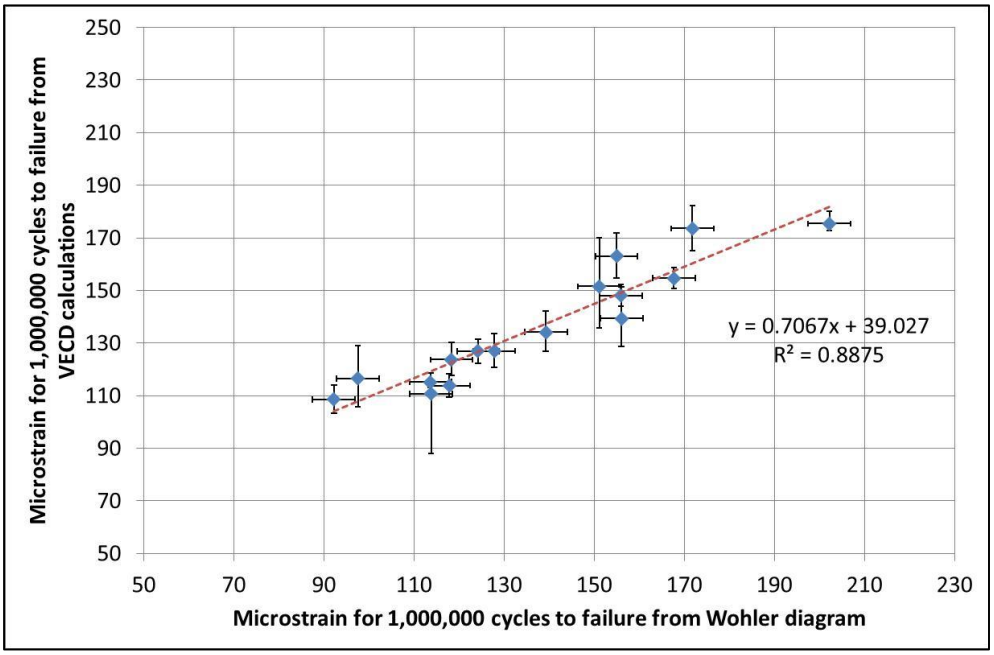

Figure 7-32 : Correlation between 1,000,000 cycles to failure from VECD calculations and traditional Wöhler diagrams

7.3.4 Correlation between Small Specimen and Trapezoidal Fatigue

As observed earlier the spread of data from the small specimen fatigue tests was higher than desirable even when transformed into C-S space. However, to assess the potential applications of small specimen tests the mean complex modulus and phase angles were compared to the results from the trapezoidal tests in Figure 7-33 and Figure 7-34.

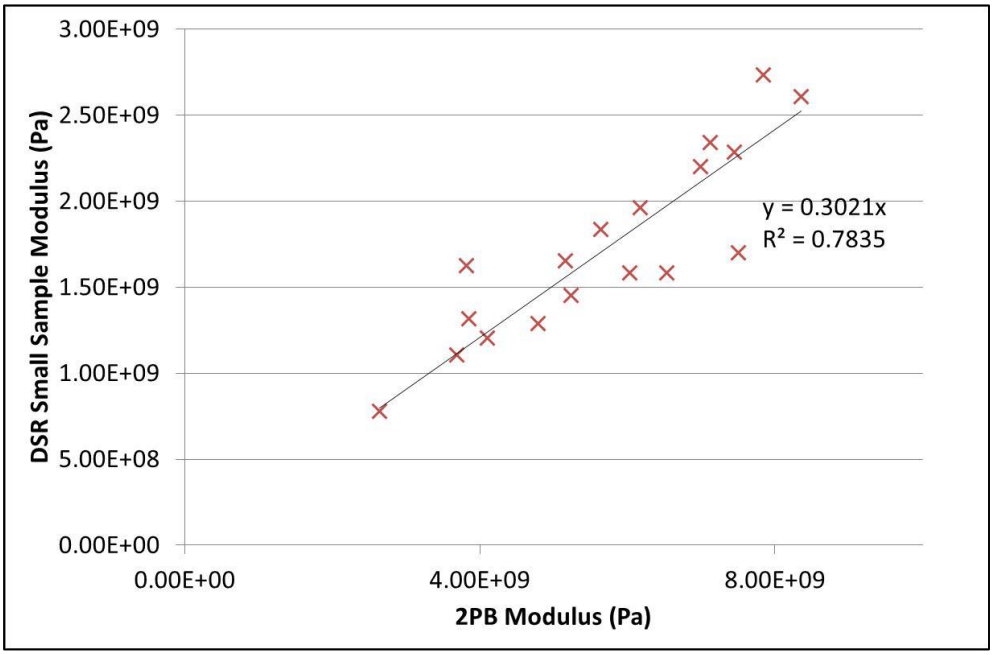

Figure 7-33 : Correlation between small specimen and trapezoidal modulus at 25Hz

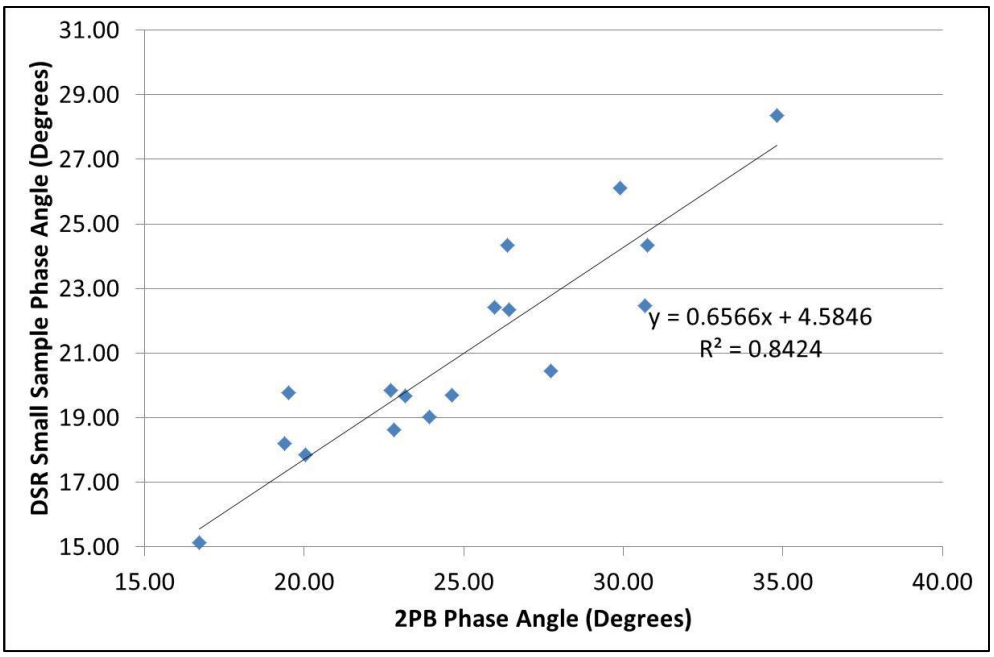

Figure 7-34 : Correlation between small specimen and trapezoidal phase angle at 25Hz

A good degree of correlation was observed in both cases, confirming the results from Chapter 3 that DSR testing of small specimen linear viscoelastic produces valid results in good agreement with more traditional full sized specimens. Furthermore,

the trapezoidal test was performed at a higher frequency than was possible with the uniaxial testing demonstrating that small specimen testing is effective across a wide range of frequencies.

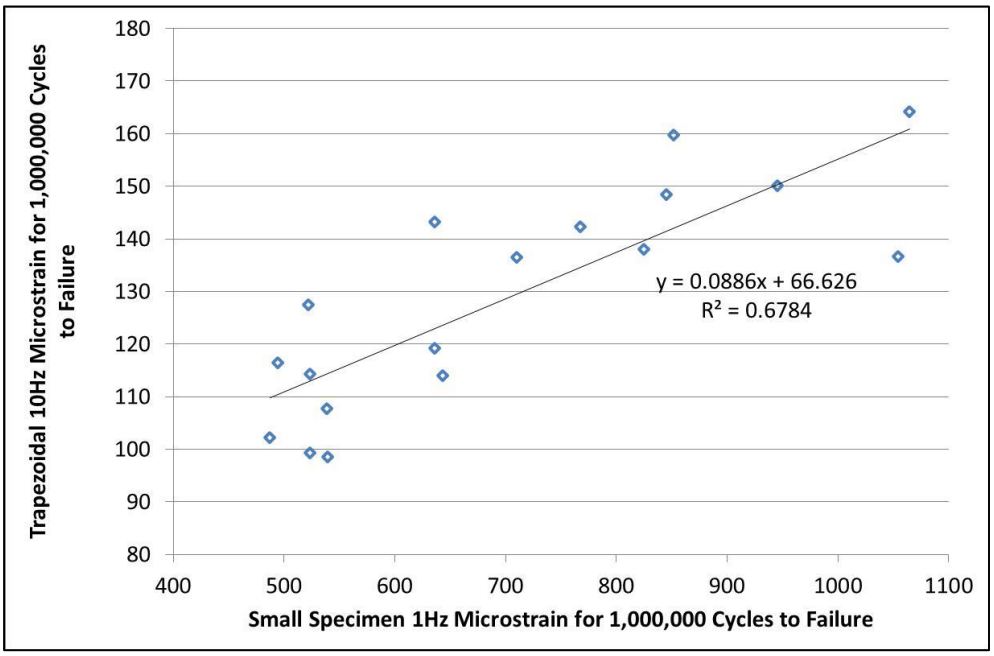

Figure 7-35 : Correlation between strain at 1,000,000 cycles to failure from small specimen VECD calculations and trapezoidal Wöhler diagrams

The correlation between the strain at 1,000,000 cycles to failure calculated using VECD for small specimens and the estimated value for trapezoidal specimens from Wöhler diagrams is shown in Figure 7-35 and demonstrates a remarkably good degree of correlation.

Whilst the correlation would not be sufficient to allow engineering judgements to be made using the small specimen approach it could be useful as a screening tool prior to full fatigue analysis for pavement design compliance purposes. This would only require a relatively small quantity of asphalt such as a Marshall or gyratory specimen to be prepared for each asphalt mixture type, from which ample small specimen cores could be drilled to allow a rapid VECD analysis to be undertaken in one to two days. This compares to even a short investigatory trapezoidal assessment

which would require a full sized asphalt slab to be prepared and take a minimum of a week to test.

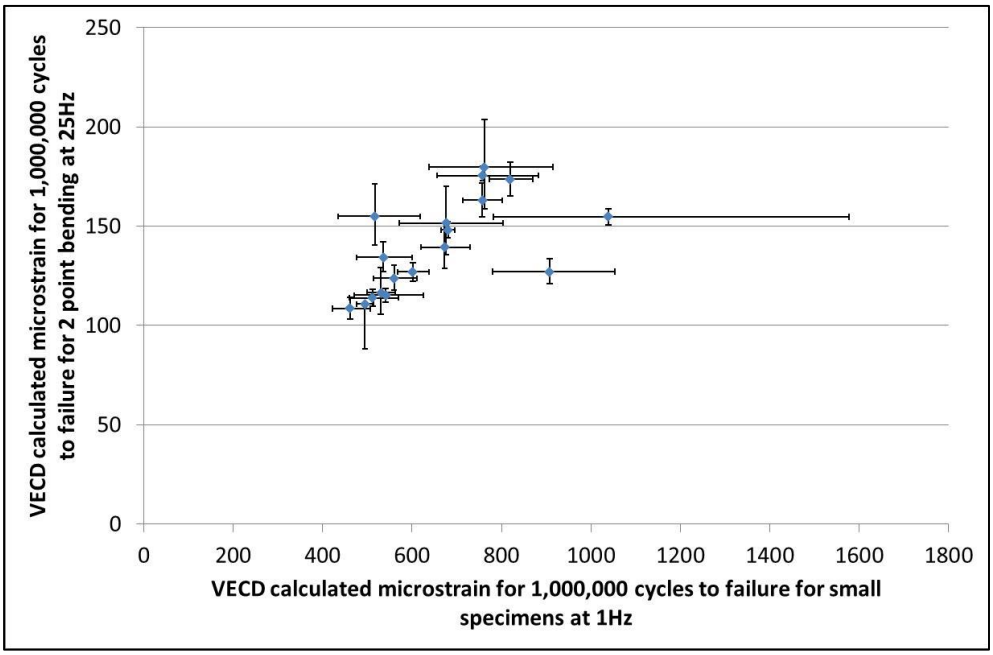

Figure 7-36 : Correlation between VECD calculated strain at 1,000,000 cycles to failure from small specimens and trapezoidal tests

The VECD calculated strain at 1,000,000 cycles to failure for both small specimens and trapezoidal tests are shown in Figure 7-36 with the calculated 95% confidence limits included as error bars. Although two outlier points were seen there was still a surprisingly good correlation between the two strain levels, again suggesting that a VECD small specimen approach could be a valuable mixture fatigue life assessment tool.

7.3.5 SCB Crack Growth and Fatigue

In Chapter 4 cyclic SCB testing of notched specimens was undertaken with the results analysed in terms of their crack growth rates. Figure 7-37 shows the results from these tests summarised as a classical Wöhler or S-N diagram.

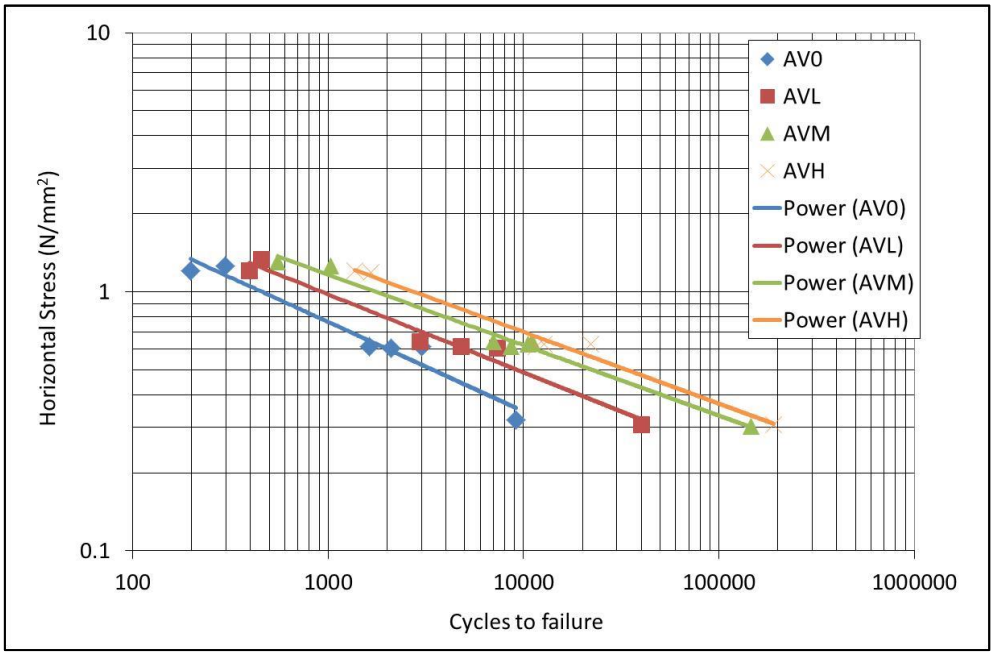

Figure 7-37 : S-N diagram for limestone based dynamic SCB testing

A best fit power curve was applied and from this regression line the stress necessary to achieve 100,000 cycles to failure was calculated and reported in Table 7-3. This demonstrates the significant increase in stress necessary to produce the same level of damage with increasing polymer modification.

	AV0	AVL	AVM	AVH
Initial horizontal stress for 100,000 cycles (Nmm^{-2})	0.156	0.245	0.333	0.368
R^2	0.956	0.975	0.986	0.983

Table 7-3 : Horizontal stresses for 100,000 cycles to failure

7.3.5.1 VECD Fatigue Life

Whilst cyclic SCB testing is relatively straightforward in terms of sample preparation it still requires many hours or days to complete the testing, especially at low stresses when constructing a traditional Wöhler diagram.

Equation 7-17 was again used to determine the characteristic C-S damage curves for each asphalt, and a good collapse of the test results observed as shown in Figure 7-38.

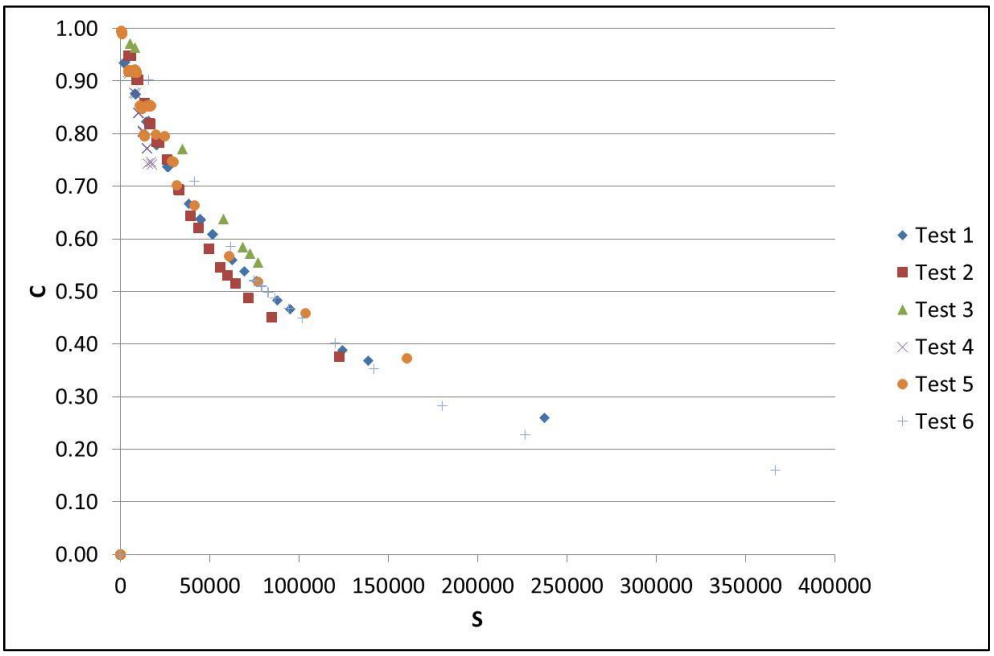

Figure 7-38 : C-S curves for asphalt AVH

7.3.5.2 Fatigue Life Predictions using VECD Model Data

As discussed earlier one of the major practical inconveniences with traditional fatigue testing is the very long test duration with lower applied loads. Therefore, the C-S curves were determined using only the higher stress tests with 1kN and 2kN peak to peak loadings and the same Equation 7-20 as previously used for the trapezoidal testing was employed to model the C-S curves. A best fit C-S curve was determined and the C_1 and C_2 regression coefficients found for each asphalt mixture.

Underwood, Kim and Guddati (2006) showed how, once the characteristic C-S curve for a material is known, it may be used to model further laboratory tests carried out under alternative test conditions by iteratively solving Equation 7-37

$$S_{N+\Delta N} = S_N + \left(\frac{\Delta N}{f}\right)\left(-\frac{I\gamma^{R^2}}{2}\frac{\partial C}{\partial S}\right)^{\alpha} \qquad \textbf{Equation 7-37}$$

To demonstrate this an additional cyclic SCB test was performed on asphalt AVH at the lower 0.5kN peak to peak load level. The specimen's initial modulus was 6502 MPa and was tested to failure as normal. The values of C_1 and C_2 which had been previously determined using the higher loading levels were used to solve Equation 7-37 and hence predict the specimen's modulus throughout the test as shown in Figure 7-39.

Whilst each specimen is undamaged with S = 0 at N = 0, due to the iterative method employed a small value for S at N = 1 was necessary for the simulation to progress with S = 100 found to produce satisfactory results.

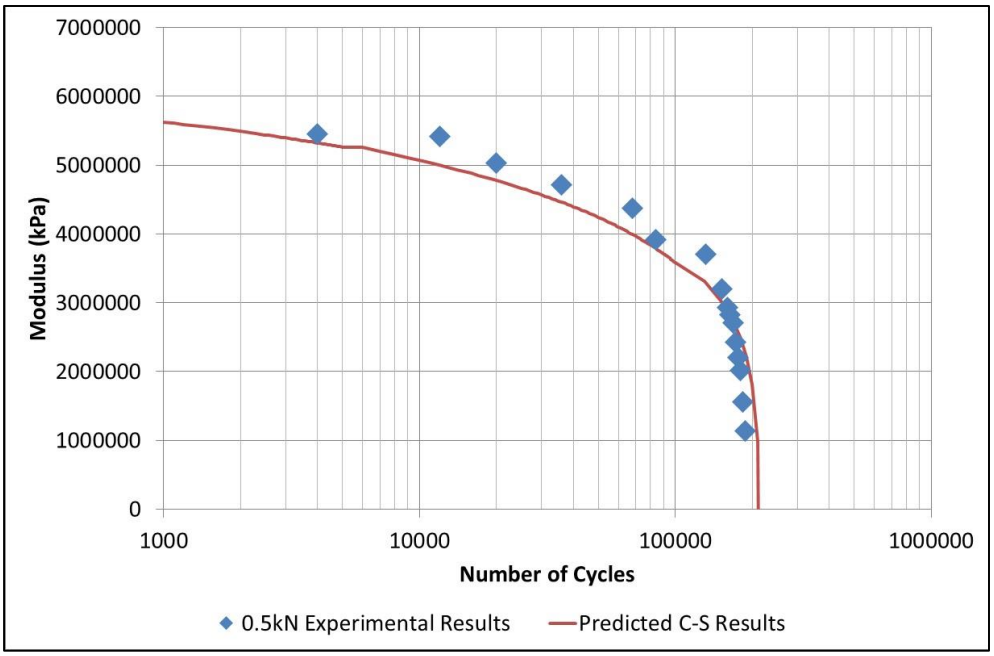

Figure 7-39 : Predicted and measured asphalt AVH SCB modulus evolution with 0.5 kN peak to peak loading

As can be seen the VECD model shows a good agreement with the experimental data further demonstrating the predictive capabilities of the theory.

7.4 Concluding Remarks

This chapter has demonstrated the application of VECD theory to reduce both test duration and the material requirements for fatigue testing of binders and asphalts.

VECD theory was applied to Time Sweep binder fatigue tests and to results from the Linear Amplitude Sweep Test. In both cases predictions were made of the strain levels necessary for 1,000,000 cycles to failure, with the results ranking in line with traditional Wöhler analysis. However, the VECD technique was found to underestimate the strain level compared to the traditional analysis, with the difference increasing with higher levels of polymer modification. This was attributed to the VECD analysis including non-linear recoverable strain as damage, and therefore implying that in practical situations PmBs withstand higher levels of strain before permanent damage occurs.

Fatigue analysis of small specimens was undertaken with no clear correlation between the number of cycles to failure and the asphalt composition. However, a VECD analysis of the data revealed that practically useful fatigue performance data could be generated, and that the expected behaviour of improved fatigue performance with increasing polymer content in the binder demonstrated. Furthermore, the small specimen fatigue data was compared to results from full scale trapezoidal two-point bending fatigue tests with a good degree of correlation. Whilst some scatter in the correlation and data was found, it was suggested that the small specimen fatigue tests could be a valuable screening tool during the initial mixture design stage and that it could be performed with considerably less material and in a shorter time period than a traditional test technique.

A VECD analysis of the SCB notched cyclic test performed in chapter 4 demonstrated that unique C-S damage curves could also be generated in this testing mode. Furthermore, the C-S curves were used to successfully predict the behaviour

of low applied stress tests using the C-S curves produced from higher stress tests, saving significant experimental time.

8 CONCLUSIONS AND RECOMMENDATIONS

8.1 Conclusions

This research has clearly identified approaches for both binders and asphalt which allow the improved cracking and fatigue performance of asphalt to be characterised.

A standard laboratory Dynamic Shear Rheometer (DSR) was successfully employed to determine the linear viscoelastic properties of small 12- 14mm diameter specimens of full asphalt mixtures. The correlation of the small specimen results to those from full sized specimens, in both uniaxial and trapezoidal geometries, demonstrated the remarkable potential of this approach to generate valuable engineering information. Due to the already wide availability of DSRs in bitumen and asphalt laboratories this technique allows the viscoelastic properties of asphalt to be determined at a considerably reduced cost. Furthermore, as multiple small specimen cores can be obtained from a single laboratory produced gyratory or Marshall sized specimen, the quantity of material necessary to perform an investigation is dramatically reduced.

Viscoelastic Continuum Damage (VECD) theory was successfully applied to the fatigue analysis of binders and asphalts. Significant improvements in the fatigue lifetimes of materials containing polymer modified bitumen (PmBs) were demonstrated using both a traditional Time Sweep (TS) number of cycles to failure approach and the VECD approach.

VECD was applied to asphalt fatigue tests of trapezoidal and notched Semi-Circular Bend (SCB) geometries. In both these geometries VECD analysis allowed the prediction of low stress and strain fatigue performance from high stress and strain tests which could be completed in only a few hours, therefore significantly reducing the required total fatigue test duration which would usually be many days, weeks, or even months.

Small specimens were also tested in fatigue mode, but the number of cycles to failure were found to be a poor predictor of fatigue performance in full sized specimens. This was believed to be a consequence of the increased density of microcracks and crack initiation points in the small specimens compared to traditionally sized specimens. However, when the small specimen fatigue tests were analysed using VECD, the results were found to produce a good level of correlation to fatigue results of traditional full sized trapezoidal specimens. Therefore, this technique could provide a useful screening tool for asphalt fatigue performance during the mix design stage as it requires far lower quantities of material, utilises a relatively low cost piece of equipment and is able to be completed in a few days. As a consequence, the improved performance of the asphalts manufactured with PmBs was demonstrated with reduced time, equipment and material costs than traditional techniques.

However, during binder fatigue testing, it was found that whilst the ranking of the fatigue performance was the same using VECD and TS approaches the absolute values did not agree, with the difference increasing with polymer content of the PmB. This is a consequence of non-linear recoverable strain being included as damage within the VECD analysis, and also implies that PmBs are able to tolerate higher strain levels before incurring permanent damage.

Binder testing demonstrated the significant differences in binder rheology between crude sources, with polymer modification shown to reduce the short term ageing of the binder. Crude source was also shown to have a significant impact on polymer-binder compatibility and the internal microstructure of the modified binder. A quantitative technique to determine the storage stability of the PmB was developed using attenuated Fourier Transform Infra-Red spectroscopy which used less material and could be performed more rapidly than traditional empirical techniques.

Monotonic SCB tests demonstrated that, at 20°C, asphalt displays a predominantly plastic rather than elastic fracture response. Therefore, the use of a linearly elastic model is unable to fully characterise the asphalt's fracture behaviour. The critical strain energy release rate (J_{IC}) was shown to provide an improved explanation of the fracture performance of asphalt containing PmB, with equi-stiffness unmodified asphalts displaying very low J_{IC} due to brittle failure.

Crack propagation in cyclic SCB testing was characterised using a Paris Law and a generalised J-integral model. Surprisingly it was found that the model coefficients did not clearly relate to the asphalt's binder properties. However, the models were successfully used to predict crack propagation rates in a model pavement structure where the J-integral model predicted a longer service life than the Paris Law model in all but one of the assessments. This was further evidence that to accurately depict asphalt performance a simple linearly elastic model is insufficient to capture the full material properties.

The eXtended Finite Element Method (XFEM) was successfully used to model the monotonic crack propagation in the notched SCB test. It was concluded that XFEM presents a highly efficient approach for the modelling of cracks in viscoelastic materials such as asphalt as the crack is free to propagate in any direction. Therefore, the XFEM approach has the potential to model multiple and more complex mode mixed mode cracks which will more accurately depict real pavement structure performance.

A technique was developed to allow high-strain rate measurements of the binder to aggregate practical work of adhesion to be determined. The theoretical work of adhesion was also determined via surface energy measurements and surprisingly no correlations were found between the theoretical or practical work of adhesion and the measured fatigue and fracture properties of asphalt. This implies that the dry fracture and fatigue failure mechanism of asphalt is not related to the surface energy properties of either the binder or aggregate, but it must instead be a bulk binder

property. Furthermore, the lack of differentiation between the practical work of adhesion from substantially different binders in this study also implies that high strain rate testing is not the most appropriate test regime.

8.2 Recommendations for Further Work

The PmBs used in this research were all laboratory produced and shown to be unstable. The majority of commercially available PmBs are storage stable and extending the test regime to include these, or laboratory produced storage stable PmBs, could offer further insights as a homogenous PmB may lead to a change in fracture and fatigue performance. The inclusion of alternative polymer structures and chemistries could also be considered.

The crack propagation analysis of cyclic SCB tests was found to include a high degree of scatter in the results. Improved techniques to monitor and record the crack tip position are clearly necessary to fully capture the fracture properties of the asphalt before accurate modelling can be realised.

The XFEM model of asphalt cracking could be extended to include the effects of temperature or micromechanical models of the aggregate-mastic behaviour. Whilst computationally intensive, extension to modelling of cyclic loading would also be of great interest and offer further insights into asphalt crack propagation and fatigue performance.

Further aggregate-binder adhesion tests could be considered at alternative strain rates and temperatures. Whilst lower strain rate testing would include the energy expended in binder ductile flow in the measured bond energy, this may prove a more effective indicator of asphalt's practical fracture and fatigue performance.

The results of this research demonstrate that the small specimen test technique can be used to determine the linear viscoelastic properties of asphalt and provide rapid screening of asphalt fatigue by employing VECD theory. However, as this research only evaluated two mixtures and nine binders, it is recommended that

additional materials are assessed to determine the full scope for the technique. Whist the correlation to large scale specimen linear viscoelastic properties in this research was remarkable it is unknown at this stage if this also applies to mixtures with larger nominal maximum aggregate sizes relative to the small specimen diameter, or to higher void content mixtures where edge effects could be more significant. To further improve the precision of linear viscoelastic determinations larger diameter specimens could be analysed on the DSR. However, this would limit the technique to non-damaging strain levels due to the torque limitations of the DSR.

9 PUBLICATIONS

9.1 Journal papers

Lancaster I. M., and H. Al-Khalid, (2012) “Attenuated total reflection Fourier transform infrared spectroscopy of polymer modified bitumen” Journal of the Institute of Asphalt Technology, Issue 53, pp. 10-15

Lancaster I. M., H. Al-Khalid, and I. Kougioumtzoglou, (2013) “Extended FEM modelling of crack propagation using the semi-circular bending test” Construction and Building Materials, Volume 48, pp. 270 – 277 (doi:10.1016/j.conbuildmat.2013.06.046)

Lancaster I. M., and H. Al-Khalid, (2014) “Crack propagation in the cyclic semi-circular bending test” Proceedings of the ICE - Construction Materials, Volume 167, Issue 4, pp. 191 –200 (doi:10.1680/coma.13.00025)

9.2 Conference papers

Lancaster I. M., and H. Al-Khalid, (2011) “Crack growth analysis of polymer modified asphalt using linear and non linear fracture mechanics” In: Nikolaides A.F. eds. Proceedings of the 5th Int. Conf. on Bituminous Mixtures & Pavements. International Conference on Bituminous Mixtures & Pavements, Hyatt Regency. Thessaloniki: Aristotle University of Thessaloniki, pp. 612-623

Lancaster I. M., and H. Al-Khalid, (2013) “Inter-conversion between oscillatory and quasi-static loading to evaluate asphalt behavior in the Dynamic Shear Rheometer” Proceedings of the 2nd Meeting and Technical Conference of the Middle East Society of Asphalt Technologists, American University of Sharjah, United Arab Emirates, Paper no. 30

Lancaster I. M., and H. Al-Khalid, (2013) “Viscoelastic characterisation of asphalt using small specimen sizes” Proceedings of the 5th European Asphalt Technology Association Conference, Braunschweig, Germany, Paper no. 36

Lancaster I. M., and H. Al-Khalid, (2015) “Viscoelastic and Damage Characterization of Polymer Modified Bitumen from Different Origins” 3rd Meeting and Technical Conference of the Middle East Society of Asphalt Technologists, American University of Sharjah, United Arab Emirates pp. 54 -63 (doi: 10.1201/b18538-5)

Lancaster I. M., and H. Al-Khalid, (2015) “Viscoelastic Continuum Damage Analysis of Polymer Modified Asphalt in the Cyclic Semi-circular Bending Test” In: Nikolaides A.F. eds. Proceedings of the 6th Int. Conf. on Bituminous Mixtures & Pavements. International Conference on Bituminous Mixtures & Pavements, Hyatt Regency. Thessaloniki: Aristotle University of Thessaloniki pp. 21-26

9.3 Book contributions

Lancaster I. M., and H. Al-Khalid, (2012) “A rapid quantitative determination of polymer modified bitumen storage stability by FTIR” In: Tyrer M., Blacker A. and Bensted J. eds. Young Researchers' Forum in Construction Materials Society of Chemical Industry pp. 101 – 104

10 REFERENCES

AASHTO TP 101, (2014) “Estimating damage tolerance of asphalt binders using the linear amplitude sweep” American Association of State Highway and Transportation Officials Standards for Tests

AASHTO TP 107, (2014) “Determining the damage characteristic curve of asphalt mixtures from direct tension cyclic fatigue” American Association of State Highway and Transportation Officials Standards for Tests

Abdo A. M. A., S. J. Jung, and S. I. Baek, (2013) “Verification of testing parameters of semi-circle notched beam fatigue test” Asian Journal of Civil Engineering, Volume 14, Issue 5, pp. 643-654

Adamson R. M., L. H. Shapiro, and J. P. Dempsey, (1997) “Core-based SCB fracture of aligned first-year sea ice” Journal of Cold Regions Engineering. Volume 11, Issue 1, pp. 30-44

Al-Haddad, A. H. A. A., and H. Al-Khalid, (2015). “Development of a new aggregate-binder adhesion test method” In: Nikolaides A.F. eds. Proceedings of the 6th Int. Conf. on Bituminous Mixtures & Pavements. International Conference on Bituminous Mixtures & Pavements, Hyatt Regency. Thessaloniki: Aristotle University of Thessaloniki, pp. 385-394

Al-Qadi I. L., E. H. Fini, and S. H. Dessouky, (2006) “Adhesion of hot-poured crack sealants to aggregates” Proceedings 85th Annual Meeting of the Transportation Research Board, Transportation Research Board, Washington, D.C.

Anderson D. A., R. Dongre, D. W. Christensen, and E. L. Dukatz, (1992), “Effects of minus no. 200-sized aggregate on fracture behavior of dense-graded hot-mix asphalt” In Effects of Aggregates and Mineral Fillers on Asphalt Mixture

Performance. Proceedings of a Symposium, Held 10th December 1991, San Diego (ASTM Special Technical Publication STP 1147)

Anderson D. A., and T. W. Kennedy, (1993) "Development of SHRP binder specification" Journal of the Association of Asphalt Paving Technologists, Volume 62, pp. 481-507

Anderson, D. A., D. W. Christensen, H. U. Bahia, R. Dongre, M. G. Sharma, C. E. Antle, and J. Button, (1994) "Binder characterization and evaluation", Volume 3, Physical Characterization Strategic Highway Research Program. Washington, DC, Report No. SHRP-A-369

Anderson T. L., (2005) "Fracture mechanics fundamentals and applications" 3rd ed. Boca Raton, FL: CRC Press. pp. 345-348

Aragao F., and Y-R. Kim, (2011) "Characterization of fracture properties of asphalt mixtures based on cohesive zone modeling and digital image correlation technique" Proceedings 91st TRB Annual Meeting, Transportation Research Board, Washington, D.C.

Artamendi I., and H. Khalid, (2006) "A comparison between beam and semi-circular bending fracture tests for asphalt" International Journal of Road Materials and Pavement Design, Volume 7, Special Ed, pp. 163-180

Asphalt Industry Alliance, (2015) "Annual local authority road maintenance (ALARM) survey", HMPR Limited

ASTM D1560-92, (1992) "Standard test methods for resistance to deformation and cohesion of bituminous mixtures by means of Hveem apparatus" American Society for Testing and Materials, Philadelphia

ASTM E1290, (2008) “Standard test method for crack-tip opening displacement (CTOD) fracture toughness measurement” American Society for Testing and Materials, Philadelphia

Bahia H. U., and D. A. Anderson, (1995) “Strategic highway research program binder rheological parameters: background and comparison with conventional properties” Transportation Research Record: Journal of the Transportation Research Board, Volume 1488, pp. 32-39

Bahia H. U., H. Zhai, M. Zeng, Y. Hu, and P. Turner, (2001) "Development of binder specification parameters based on characterization of damage behavior", Journal of Association of Asphalt Paving Technologists, Volume 70, pp. 442-470

Bahia H., H. A. Tabatabaee, T. Mandal, and A. Faheem, (2013) “Field evaluation of Wisconsin modified binder selection guidelines – phase II” University of Wisconsin Madison, Wisconsin Highway Research Program

Belytschko T., and T. Black, (1999) “Elastic crack growth in finite elements with minimal remeshing” International Journal for Numerical Methods in Engineering, Volume 45, Issue 5, pp. 610-620

di Benedetto H., F. Olard, C. Saureat, and B. Delaporte, (2004) “Linear viscoelastic behaviour of bituminous materials: from binders to mixes” Road Materials and Pavement Design, Volume 5(sup 1), pp. 163-202

Bhasin A., E. Masad, D. Little, and R. Lytton, (2006) “Limits on adhesive bond energy for improved resistance of hot-mix asphalt to moisture damage” Transportation Research Record: Journal of the Transportation Research Board, Volume 1970, pp. 3-13

Bhasin A., and D. N. Little, (2007) “Characterization of aggregate surface energy using the universal sorption device” Journal of Materials in Civil Engineering, Volume 19, Issue 8, pp. 634-641

Bhasin A., J. Howson, E. Masad, D. Little, and R. Lytton, (2007) “Effect of modification processes on bond energy of asphalt binders” Transportation Research Record: Journal of the Transportation Research Board, Volume 2001, pp. 29-37

Bonaquist R.F., D.W. Christensen, and W. Stump, (2003) “NCHRP Report 513: Simple performance tester of Superpave mix design: first-article development and evaluation” Transport Research Board, National Research Council, Washington, D.C.

Bonaquist R. F., (2008) “NCHRP Report 614: Refining the simple performance tester for use in routine practice” Transport Research Board, National Research Council, Washington, D.C.

Branco, V. C., E. Masad, A. Bhasin, D. N. Little, (2008) “Fatigue analysis of asphalt mixtures independent of mode of loading” Transportation Research Record: Journal of the Transportation Research Board, Volume 2057, pp. 149–156

BS 594987, (2007) “Asphalt for roads and other paved areas – Specification for transport, laying and compaction and type testing protocols”, British Standards Institution

Bueno M., M. Hugener, and M. N. Partl, (2013) “Fracture toughness testing aspects for assessing low temperature behaviour of bituminous binders” In Multi-Scale Modeling and Characterization of Infrastructure Materials. Springer Netherlands. Volume 8 of the series RILEM Bookseries, pp. 1-12

Canestrari F., G. Ferrotti, F. Cardone, and A. Stimilli, (2014) “Innovative testing protocol for evaluation of binder-reclaimed aggregate bond strength” Transportation Research Record: Journal of the Transportation Research Board, Volume 2444, pp. 63-70

Celauro C., M. Di Paulo, D. Lo Presti, F. Marino and A. Pirrotta, (2009) “Modelling of the viscoelastic behaviour of paving grade bitumen using fractional derivatives” Meccanica dei Materiali e delle Strutture, Volume 1, Issue 2, pp. 38-51

Chailleux E., D. Bodin, C. De La Roche, M. Leguern, and N. Vignard,. (2009) “Fatigue behaviour of bitumen in tension-compression loading mode: Rheological analysis and comparison with mix fatigue” In Loizos A., Partl M., Scarpas T. and Al-Qadi I. eds. Advanced testing and characterization of bituminous materials, CRC Press, pp. 773-784

Chailleux E., E. Scholten, M. Hugener, T. Gallet, I. M. Lancaster, S Buchler, A. Jones, V. Mouillet, T. Lorino, and T. Blomberg, (2012) “Round robin test of the fracture toughness test for the low temperature properties of bituminous binders” In 5th Eurasphalt & Eurobitume Congress Istanbul, Turkey (Paper P5EE-366)

Chang S-H, C-I. Lee and S. Jeon, (2002) “Measurement of rock fracture toughness under modes I and II and mixed-mode conditions by using disc-type specimens” Engineering Geology, Volume 66, Issues 1-2, pp. 79-97

Cheng D., D. N. Little, R. L. Lytton, and J. C. Holste, (2002) “Use of surface free energy of asphalt-aggregate systems to predict moisture damage potential” Journal of the Association of Asphalt Paving Technologists, Volume 71, pp. 59-88

Cherepanov G. P., (1967) “The propagation of cracks in a continuous medium” Journal of Applied Mathematics and Mechanics, Volume 31, Issue 3, pp. 503-512

Christensen D. W., T. Pellien, and R. F. Bonaquist, (2003) “Hirsch model for estimating the modulus of asphalt concrete” Journal of Association of Asphalt Paving Technologists, Volume 72, pp. 97-121

Cho D., T. S. Lee, S. Y. Lee, and H. U. Bahia, (2009), "Comparison of linear visco-elastic complex modulus and yield shear stress in DSR moisture damage test" Journal of Testing and Evaluation, Volume 37, no. 6, pp. 573-581

Clec'h P., C. Sauzeat, and H. Di Benedetto, (2010) "Linear viscoelastic behaviour and anisotropy of bituminous mixture compacted with a french wheel compactor" asphalt paving material characterization and modelling: Proceedings of the GeoShanghai International Conference, Geotechnical Special Publication No. 203, pp. 103-115

Collop A. C., A. J. Sewell, and N. H. Thom, (2004) "Laboratory assessment of the crack propagation in high stiffness asphaltic materials" Proceedings of the Institute of Mechanical Engineers, Part L : Journal of Materials Design and Applications, Volume 218, Issue 1, pp. 55-66

Cui, S., B. R. Blackman, A. J. Kinloch, and A. C. Taylor, (2014) "Durability of asphalt mixtures: Effect of aggregate type and adhesion promoters". International Journal of Adhesion and Adhesives, Volume 54, pp. 100-111

Daniel J. S., W. Bisirri, and Y. R. Kim, (2004) "Fatigue evaluation of asphalt mixtures using dissipated energy and viscoelastic continuum damage approaches" Journal of Association of Asphalt Paving Technologists, Volume 73, pp. 557-583

Dannenberg H., (1961) "Measurement of adhesion by a blister method" Journal of Applied Polymer Science, Volume 5, Issue 14, pp. 125-134

Davies R. M., (1948) "A simple modification of the Hopkinson pressure bar" In Proceedings of the 7th International Congress on Applied Mechanics, Volume 1

Deacon J. A., J. T. Harvey, A. Tayebali, and C. L. Monismith. (1997) "Influence of binder loss modulus on the fatigue performance of asphalt concrete pavements."

Journal of the Association of Asphalt Paving Technologists, Volume 66, pp. 633-668

Delaporte B., J. Van Rompu, H. Di Benedetto, P. Chaverot, and G. Gauthier, (2008) "New procedure to evaluate fatigue of bituminous mastics using an annular shear rheometer prototype" In Proceedings of the 6th RILEM international conference on cracking in pavement, pp. 457-467

Delorme J.L., C. de la Roche, and L. Wendling, (2007) "LCPC Bituminous Mixtures Design Guide" Laboratoire central des ponts et chaussées, Paris, France.

Di Benedetto H., C. Sauzeat, K. Bilodeau, M. Buannic, S. Mangiafico, Q. Nguyen, S. Pouget, N. Tapsoba, and J. Van Rompu, (2011) "General overview of the time-temperature superposition principle validity for materials containing bituminous binder" International Journal of Roads and Airports, Volume 1, Issue 1

Di Paola M., A. Pirrotta, and A. Valenza, (2011) "Visco-elastic behaviour through fractional calculus: An easier method for best fitting experimental results" Mechanics of Materials, Volume 43: pp. 799-806

Dillard D., (2010) "Advances in structural adhesive bonding" Woodhead Publishing, Cambridge, UK

Elseifi M. A., L. Mohammad, H. Ying and S. Cooper III, (2012) "Modeling and evaluation of the cracking resistance of asphalt mixtures using the semi-circular bending test at intermediate temperatures" Road Materials and Pavement Design, Volume 13 Sup 1, pp. 124-139

Elster C., J. Honerkamp, and J. Weese, (1991) "Using regularization methods for the determination of relaxation and retardation spectra of polymeric liquids" Rheologica Acta, Volume 30, pp. 161-174

EN ISO 4624, (2003) “Paints and varnishes - Pull-off test for adhesion” British Standards Institution

EN 12591, (2009) “Bitumen and bituminous binders – Specifications for paving grade bitumens” British Standards Institution

EN 12697-6, (2012) “Bituminous mixtures — Test methods for hot mix asphalt —Part 6: Determination of bulk density of bituminous specimens” British Standards Institution

EN 12697-8, (2003) “Bituminous mixtures — Test methods for hot mix asphalt —Part 8: Determination of void characteristics of bituminous specimens” British Standards Institution

EN 12697-24, (2004) “Bituminous mixtures — Test methods for hot mix asphalt — Part 24: Resistance to fatigue” British Standards Institution

EN 12697-26, (2004) “Bituminous mixtures — Test methods for hot mix asphalt — Part 26: Stiffness” British Standards Institution

EN 12697-44, (2010) “Bituminous mixtures — Test methods for hot mix asphalt — Part 44: Crack propagation by semi-circular bending test” British Standards Institution

EN 13043, (2002) “Aggregates for bituminous mixtures and surface treatments for roads, airfields and other trafficked areas” British Standards Institution

EN 13302, (2010) “Bitumen and bituminous binders - Determination of dynamic viscosity of bituminous binder using a rotating spindle apparatus” British Standards Institution

EN 13399, (2010) “Bitumen and bituminous binders – Determination of storage stability of modified bitumen” British Standards Institution

EN 14023, (2010) “Bitumen and bituminous binders - framework specification for polymer modified bitumens” British Standards Institution

Fowkes F. M., (1964) “Attractive forces at interfaces” Industrial and Engineering Chemistry, Volume 56, Issue 12, pp. 40-52

Francken L., and A. Vanelstraete, (1995) “Relation between mix stiffness and binder complex modulus. The rheology of bituminous binders” Eurobitume Rheology Workshop, Brussels

Gent A. N., and A. J. Kinloch, (1971) “Adhesion of viscoelastic materials to rigid substrates III. Energy criterion for failure” Journal of Polymer Science: Part A-2, Volume 9, pp. 659-669

Gent A. N., and J. Schultz, (1972) “Effect of wetting liquids on the strength of adhesion of viscoelastic materials” The Journal of Adhesion, Volume 3, Issue 4, pp. 281-294

Gershkoff D., (1995) “Polymer Modified Bitumens – performance in empirical and rheological tests” First European Workshop on the Rheology of Bituminous Binders, Paper 34

Good R. J., (1992) “Contact angle, wetting, and adhesion: a critical review” Journal of adhesion science and technology, Volume 6, Issue 12, pp. 1269-1302

Grenfell J., N. Ahmad, Y. Liu, A. Apeagyei, D. Large, and G. Airey, (2014) “Assessing moisture susceptibility through intrinsic adhesion, bitumen stripping and mechanical damage” Road Materials and Pavement Design, Volume 15, Issue 1, pp. 131-152

Griffith A. A., (1921) “The phenomena of rupture and flow in solids” Philosophical Transactions of the Royal Society of London. Series A, Containing Papers of a Mathematical or Physical Character, pp. 163-198

Grönniger, J. and M. Wistuba, (2013) “New approach of addressing adhesion in bitumen-aggregate systems”. Proceedings of the 5th International Conference of the European Asphalt Technology Association, 3-5 June 2013, Braunschweig, Germany

Haddadi F., M. Ameri, M. H. Mirabimoghadam, and H. R. A. Hosseini, (2015) “Validation of a simplified method in viscoelastic continuum damage (VECD) model developed for flexural mode of loading” Construction and Building Materials, Volume 95, pp. 892-897

Hajj E. Y., P. E. Sebaaly, T. Sathanathan, and S. Shivakolunthar, (2012). “Impact of antistrip additives on pavement performance using mechanistic-empirical pavement design guide” Journal of Materials in Civil Engineering, Volume 25, Issue 3, pp. 308-317

Haryanto I., and O. Takahashi, (2008) “Ductile fracture assessment of Indonesian wearing course mixtures using critical J integral and crack tip opening angle” International Journal of Pavement Engineering, Volume 9, Issue 3, pp. 165-176

Hassan M. M. and H. Khalid, (2010) “Fracture characteristics of asphalt mixtures containing incinerator bottom ash aggregate” Transportation Research Record: Journal of the Transportation Research Board, Volume 2180, pp. 1-8

Heukelom W. (1973), “An improved method of characterizing asphaltic bitumens with the aid of their mechanical properties” Journal of Association of Asphalt Paving Technologists, Volume 42, pp. 62-98

Hefer A. W., A. Bhasin, and D. N. Little, (2006) “Bitumen surface energy characterization using a contact angle approach” Journal of Materials in Civil Engineering, Volume 18, Issue 6, pp. 759–767

Highways Agency (2006), “Design Manual for Roads and Bridges Vol 7 Pavement Design and Maintenance Part 3 HD26/06” The Stationery Office, London, UK

Hintz C., R. Velasquez, C. Johnson, and H. Bahia, (2011) “Modification and validation of linear amplitude sweep test for binder fatigue specification” Transportation Research Record: Journal of the Transportation Research Board, Volume 2207, pp. 99-106

Hintz C., and H. Bahia, (2013) “Simplification of the Linear Amplitude Sweep (LAS) test and specification parameter” Transportation Research Record: Journal of the Transportation Research Board, Volume 2370, pp. 10-16

Hirsch T. J., (1962) “Modulus of elasticity of concrete affected by elastic moduli of cement paste matrix and aggregate” Proceedings of the American Concrete Institute, Volume 59, Issue 3, pp. 427-452

Hofman R., B. Oosterbaan, S. M. J. G. Erkens, and J. van der Kooij, (2003) “Semi-circular bending test to assess the resistance against crack growth” In Proceedings of the Sixth RILEM Symposium on Performance Testing and Evaluation of Bituminous Materials, Zurich, Switzerland, pp. 257–263

Hopkinson B., (1914) "A method of measuring the pressure produced in the detonation of high explosives or by the impact of bullets." Philosophical Transactions of the Royal Society of London. Series A, Containing Papers of a Mathematical or Physical Character, pp. 437-456

Horgnies M., E. Darque-Ceretti, H. Fezai, and E. Felder, (2011) “Influence of the interfacial composition on the adhesion between aggregates and bitumen: Investigations by EDX, XPS and peel tests” International Journal of Adhesion and Adhesives, Volume 31, Issue 4, pp. 238-247

Howson J., E. Masad, A. Bhasin, D. Little, and R. Lytton, (2011) “Comprehensive analysis of surface free energy of asphalts and aggregates and the effects of changes in pH” Construction and Building Materials, Volume 25, Issue 5, pp. 2554-2564

Howson J., E. Masad, D. Little, and E. Kassem, (2012) ” Relationship between bond energy and total work of fracture for asphalt binder-aggregate systems” Road Materials and Pavement Design, Volume 13, pp. 281-303

Huang B., X. Shu, and G. Zuo, (2013) “Using notched semi circular bending fatigue test to characterize fracture resistance of asphalt mixtures” Engineering Fracture Mechanics, Volume 109, pp. 78-88

Huang C., E. Masad, A. H. Muliana, and H. Bahia, (2007) "Analysis of nonlinear viscoelastic properties of asphalt mixtures" Proceedings of the 15th U.S. National Congress of Theoretical and Applied Mechanics, American Society of Civil Engineers, Boulder, CO, United States, pp. 64-72

Huang L., C. Keming, and M. Zeng, (2009) “Evaluation of semi-circular bending test for determining tensile strength and stiffness modulus of asphalt mixtures” Journal of Testing and Evaluation, Volume 37, Issue 2, pp. 1-7

Inglis C. E., (1913) “Stresses in a plate due to the presence of cracks and sharp corners” Transactions of the Institute of Naval Architects, Volume 55, pp. 219-241

Irwin G. R., (1957) “Analysis of stresses and strains near the end of the crack traversing a plate” Journal of Applied mechanics, Volume 24, pp. 361–364

Isacsson U., and X. Lu, (1999) “Characterization of bitumens modified with SEBS, EVA and EBA polymers” Journal of Materials Science, Volume 34, Issue 15, pp. 3737-3745

Jakarni F., (2012) “Adhesion of asphalt mixtures” PhD Thesis, University of Nottingham

Johnson C. M., (2010) “Estimating asphalt binder fatigue resistance using an accelerated test method” PhD Thesis, University of Wisconsin, Madison

Johnson C. M., and H. U. Bahia, (2010) “Evaluation of an accelerated procedure for fatigue characterization of asphalt binders” Submitted for publication in Road Materials and Pavement Design

Kanitpong K., and H. Bahia, (2003) “Role of adhesion and thin film tackiness of asphalt binders in moisture damage of HMA” Journal of the Association of Asphalt Paving Technologists, Volume 72, pp. 502-528

Kanitpong, K., and H. Bahia, (2005) “Relating adhesion and cohesion of asphalts to the effect of moisture on laboratory performance of asphalt mixtures” Transportation Research Record: Journal of the Transportation Research Board, Volume 1901, pp. 33-43

Kennedy T. W., G. A. Huber, E. T. Harrigan, R. J. Corninsky, C. S. Hughes, H. Von Quintus, and J. S. Moulthrop, (1994) “Superior Performing Asphalt Pavements (Superpave): The product of the SHRP asphalt research program” Publication SHRP-A-410, Strategic Highway Research Program, National Research Council, Washington DC

Kim K. S., and J. Kim, (1988) “Elasto-plastic analysis of the peel test for thin film adhesion” Journal of Engineering Materials and Technology, Volume 110, Issue 3, pp. 266-273

Kim Y-R., Y. C. Lee, and H. J. Lee, (1995) “Correspondence principle for characterization of asphalt concrete” Journal of Materials in Civil Engineering, Volume 7, Issue 1, pp. 59-68

Kim Y-R, H. J. Lee, and D. N. Little, (1997) “Fatigue characterization of asphalt concrete using viscoelasticity and continuum damage theory” Journal of the Association of Asphalt Paving Technologists, Volume 66, pp. 520-569

Kim Y-R, D. Little, and R. Lytton, (2002) “Use of dynamic mechanical analysis (DMA) to evaluate the fatigue and healing potential of asphalt binders in sand asphalt

mixtures", Journal of the Association of Asphalt Paving Technologists, Volume 71, pp. 176-199

Kim Y-R, H. Lee, and D. Little, (2006) "A simple testing method to evaluate fatigue fracture and damage performance of asphalt mixtures" Journal of the Association of Asphalt Paving Technologists, Volume 75, pp. 755-785

Koeller R. C., (1984) "Applications of fractional calculus to the theory of viscoelasticity" Journal of Applied Mechanics, Volume 51, Issue 2, pp. 299-307

Kok B. V., and M. Yilmaz, (2009) "The effects of using lime and styrene–butadiene–styrene on moisture sensitivity resistance of hot mix asphalt" Construction and Building Materials, Volume 23, Issue 5, pp. 1999-2006

Kowalski A., Z. Czech, and Ł Byczyński, (2013) "How does the surface free energy influence the tack of acrylic pressure-sensitive adhesives (PSAs)?" Journal of Coatings Technology and Research, Volume 10, Issue 6, pp. 879-885

Kraus G., (1982) "Modification of asphalt by block polymers of butadiene and styrene" Rubber Chemistry and Technology, Volume 55, pp. 1389–1402

Kringos N., A. Scarpas and A. de Bondt, (2008) "Determination of moisture susceptibility of mastic-stone bond strength and comparison to thermodynamical properties" Journal of Association of Asphalt Paving Technologists, Volume 77, pp. 435-478

Kuai H. D., H. J. Lee, G. Zi, and S. Mun, (2009) "Application of generalized J-Integral to crack propagation modelling of asphalt concrete under repeated loading" Transportation Research Record: Journal of the Transportation Research Board, Volume 2127, pp. 72-81

Kuai H. D., H. J. Lee, J. H. Lee, and S. Mun, (2010) "Fatigue crack propagation model of asphalt concrete based on viscoelastic fracture mechanics" Transportation

Research Record: Journal of the Transportation Research Board, Volume 2181, pp. 11-18

Kutay M.E., N. Gibson, and J. Youtcheff (2008). “Conventional and Viscoelastic Continuum Damage (VECD) based fatigue analysis of polymer modified asphalt pavements” Journal of the Association of Asphalt Paving Technologists, Volume 77, pp. 395-434

Kwok D. Y., T. Gietzelt, K. Grundke, H. J. Jacobasch, and A. W. Neumann, (1997) “Contact angle measurements and contact angle interpretation. 1. Contact angle measurements by axisymmetric drop shape analysis and a goniometer sessile drop technique” Langmuir, Volume 13, Issue 10, pp. 2880-2894

Kwok D. Y., A. Leung, C. N. C. Lam, A. Li, R. Wu, and A. W. Neumann, (1998) “Low-rate dynamic contact angles on poly (methyl methacrylate) and the determination of solid surface tensions” Journal of Colloid and Interface Science, Volume 206, Issue 1, pp. 44-51

Laboratoire Central des Ponts et Chaussées, (2007) “Accelerated load testing facility : the fatigue carousel” Available from http://media.lcpc.fr/ext/pdf/gdsequipements/manege_200709-en.pdf [accessed 3 December 2015]

Landrock A. H., and S. Ebnesajjad, (2008) “Adhesives technology handbook” 2nd edition, William Andrew Publishing, USA

Lee H. J., (1996) ‘‘Uniaxial constitutive modeling of asphalt concrete using viscoelasticity and continuum damage theory.’’ PhD thesis, North Carolina State Univ., Raleigh, N.C.

Lee H. J., and Y. R. Kim, (1998) “Viscoelastic continuum damage model of asphalt concrete with healing” Journal of Engineering Mechanics, Volume 124, Issue 11, pp. 1224-1232

Lesueur D., (2009) “The colloidal structure of bitumen: Consequences on the rheology and on the mechanisms of bitumen modification” Advances in colloid and interface science, Volume 145, Issue 1, pp. 42-82

Lim I. L., I. W. Johnson, and S. K. Choi, (1993) “Stress intensity factors for semi-circular specimens under three-point bending” Engineering Fracture Mechanics, Volume 44, Issue 3, pp. 363–382

Linde S., and Johansson U., (1992) “Thermo-oxidative degradation of polymer modified bitumen” Polymer Modified Asphalt Binders, American Society for Testing and Materials, Philadelphia

Little D. N., A. Bhasin, and A. W. Hefer, (2006) “Using surface energy measurements to select materials for asphalt pavement” NCHRP Project 9-37, Transportation Research Board

Lu X., U. Isacsson, and J. Ekblad, (1999) “Phase separation of SBS polymer modified bitumens” Journal of Materials in Civil Engineering, Volume 11, pp. 51-57

Lyne Å. L., P. Redelius, M. Collin, and B. Birgisson, (2013). Characterization of stripping properties of stone material in asphalt. Materials and structures, Volume 46, Issue 1-2, pp. 47-61

Lytton R. L., (2005) “Adhesive fracture in asphalt concrete mixtures” in “Asphalt Technology Handbook” ed: J. Youtcheff

Malkin A. and A. Isayev, (2012) “Rheology: concepts, methods, and applications” 2nd edition, ChemTec Publishing

Marek C.R. and M. Herrin, (1968) “Tensile behavior and failure characteristics of asphalt cements in thin films” Journal of Association of Asphalt Paving Technologists, Volume 37, pp. 386-421

Masad E., C. Huang, G. Airey, and A. Muliana, (2008a) "Nonlinear viscoelastic analysis of unaged and aged asphalt binders" Construction and Building Materials, Volume 22, Issue 11, pp. 2170-2179

Masad E., V. T. F. Castelo Branco, D. N. Little, and R. Lytton, (2008b) "A unified method for the analysis of controlled-strain and controlled-stress fatigue testing", International Journal of Pavement Engineering, Volume 9, Issue 4, pp. 233-246

Masad E., J. Howson, A. Bhasin, S. Caro, and D. Little, (2010) "Relationship between ideal and practical work of fracture: Background and experimental results," Journal of the Association of Asphalt Paving Technologists, Volume 79, pp. 81 - 118

Masson J-F., and M. A. Lacasse, (2000) "A review of adhesion mechanisms at the crack sealant/asphalt concrete interface" Proceedings of the 3rd International Symposium on Durability of Building and Construction Sealants. RILEM, Paris

Masson J-F., L. Pelletier, and P. Collins, (2001) “Rapid FTIR method for quantification of styrene-butadiene type copolymers in bitumen” Journal of Applied Polymer Science, Volume 79, Issue 6, pp. 1034 – 1041

McBain J. W., and D. G. Hopkins, (1925) “On adhesives and adhesive action” The Journal of Physical Chemistry, Volume 29, Issue 2, pp. 188-204

Mehta P., and A. Ranka, (2015) “Zycotherm nanotechnology for asphalt road paving” 3rd Meeting and Technical Conference of the Middle East Society of Asphalt Technologists, American University of Sharjah, United Arab Emirates pp. 64-76

Melenk J. M. and I. Babuska, (1996) “The partition of unity finite element method: basic theory and applications” Computer Methods in Applied Mechanics and Engineering, Volume 139, pp. 289- 314

Mello L. G., K. E. Kaloush, and M. M. Farias, (2010) “Damage theory applied to flexural fatigue tests on conventional and asphalt rubber hot mixes” Road Materials and Pavement Design, Volume 11, Issue 3, pp. 681-700

Merusi F., A. Caruso, L. Chiapponi, and F. Giuliani, (2013) “Mechanical analysis of failure processes at bitumen/aggregate interface“ Proceedings of the 92nd TRB Annual Meeting, Transportation Research Board, Washington, D.C

Moës N., J. Dolbow and T. Belytschko, (1999) “ A finite element method for crack growth without remeshing”, International Journal for Numerical Methods in Engineering, Volume 46, Issue 1, pp 131-150

Mohammad L. N., Z. Wu, and M. A. Mull, (2004) “Characterization of fracture and fatigue resistance on recycled polymer-modified asphalt pavements” In Proceeding of the Fifth RILEM International Conference on Cracking in Pavements, Limoges, France, pp. 375-382

Molenaar A. A. A., A. Scarpas, X. Liu, and S. M. J. G. Erkens, (2002) "Semi-circular bending test; simple but useful?" Journal of Association of Asphalt Paving Technologists, Volume 71, pp. 794- 815

Molenaar A. A. A., (2007) “Prediction of Fatigue Cracking in Asphalt Pavements: Do We Follow the Right Approach?” Transportation Research Record: Journal of the Transportation Research Board, Volume 2001, pp. 155-162

Moraes R., R. Velasquez, and H. Bahia, (2011) “Measuring the effect of moisture on asphalt-aggregate bond with the bitumen bond strength test”. Transportation Research Record: Journal of the Transportation Research Board, Volume 2209, pp. 70-81

Mull, M. A., A. Othman, and L. Mohammad, (2006) “Fatigue crack growth analysis of HMA employing the semi-circular notched bend specimen.” Proceedings 85th TRB Annual Meeting, Transportation Research Board, Washington, D.C.

Nguyen M. T., H. J. Lee, and J. Baek, (2013) “Fatigue analysis of asphalt concrete under indirect tensile mode of loading using crack images” Journal of Testing and Evaluation, Volume 41, Issue 1, pp. 1-17

Nocedal J., and S. J. Wright, (2006) “Numerical optimization” 2nd edition, Springer

Nutting P. G. (1921) “A new general law deformation”. Journal of the Franklin Institute, Volume 191, pp. 678-685

Oeser M., S. Freitag, B. Moller, F. Wellner, and S. Werkmeister, (2006) “3D constitutive model for asphalt on the basis of fractional creep functions” Proceedings of the ISAP conference, Quebec, Canada, Volume 1, pp. 755-764

Oeser M., T. Pellinen, T. Scarpas, and C. Kasbergen, (2008) “Studies on creep and recovery of rheological bodies based upon conventional and fractional formulations and their application on asphalt mixture” International Journal of Pavement Engineering, Volume 9, Issue 5, pp. 374-386

Paris P. C., and F. Erdogan, (1963) “A critical analysis of crack propagation laws” Journal of Fluids Engineering, Volume 85, Issue 3, pp. 528-34

PD 6691, (2007) “Guidance on the use of BS EN 13108 Bituminous mixtures – Material specifications”, British Standards Institution

Pell P. S., (1962) “Fatigue characteristics of bitumen and bituminous mixes” In International Conference on the Structural Design of Asphalt Pavements, Ann Arbor, University of Michigan, pp. 43-58

Penn L.S., and E. Defex, (2002) “Relation between work of adhesion and work of fracture for simple interfaces” Journal of Materials Science, Volume 37, Issue 3, pp. 505-513

Pfeiffer J. P., and P. M. Van Doormaal, (1936) “The rheological properties of asphaltic bitumens” Journal of the Institute of Petroleum Technologists, Volume 22, pp. 414-440

Potschka V., and Schmidt H., (1993) “Fatigue life of polymer modified bitumen” In: Proceedings of 5th Eurobitume Congress, Stockholm, pp. 103-105

Redelius P., and H. Soenen, (2015) “Relation between bitumen chemistry and performance” Fuel, Volume 140, pp. 34-43

Rice J. R., (1968) “A path independent integral and the approximate analysis of strain concentration by notches and cracks” Journal of Applied Mechanics, Volume 35, pp. 379-386

Rullkotter J., and A. Nissenbaum, (1988), “Dead sea asphalt in Egyptian mummies: molecular evidence” Naturwissenschaften, Volume 75, Issue 12, pp. 618-621

Schapery R. A., (1984) “Correspondence principles and a generalised J integral for large deformation and fracture analysis of visco-elastic media” International Journal of Fracture, Volume 25, pp. 195-223

Schapery R. A., (1990) “A theory of mechanical behavior of elastic media with growing damage and other changes in structure” Journal of the Mechanics and Physics of Solids, Volume 38, Issue 2, pp. 215-253

Scott-Blair G. W., and J. E. Gaffyn, (1949) “An application of the theory of quasi-properties to the treatment of anomalous strain-stress relations” The Philosophical Magazine, Volume 30, Issue 1, pp. 80-94

Seshadri M., S. Saigal, A. Jagota, and S. J. Bennison, (2007) “Scaling of fracture energy in tensile debonding of viscoelastic films” Journal of Applied Physics, Volume 101, Issue 9, pp. 093504-093508

Sewell A. J., A. C. Collop, N. H. Thom, and S. F. Brown, (2000) “Assessing crack growth in high modulus base materials” in Proceedings of the 2nd Eurasphalt and Eurobitume Congress, Barcelona, Spain, pp. 819–826

Shell International Oil Products (1998) BISAR Bitumen Structures Analysis in Roads Version 3.0. Amsterdam

Shih C. F., (1981) “Relationship between the J-Integral and the crack opening displacement for stationary and extending cracks” Journal of the Mechanics and Physics of Solids, Volume 29, pp. 305-326

Shull K. R., D. Ahn, W. L. Chen, C. M. Flanigan, and A. J. Crosby, (1998) “Axisymmetric adhesion tests of soft materials” Macromolecular Chemistry and Physics, Volume 199, Issue 4, pp. 489-511

Soenen H., C. de la Roche, and P. Redelius, (2003) “Fatigue behaviour of bituminous materials: from binders to mixes” Road Materials and Pavement Design, Volume 4, Issue 1, pp. 7-24

Soenen H., X. Lu, and P. Redelius, (2008) “The morphology of bitumen-SBS blends by UV microscopy” Road Materials and Pavement Design, Volume 9, Issue 1, pp. 97-110

Sousa J. M. B., and C. L. Monismith, (1987) “Dynamic response of paving materials” Transportation Research Record: Journal of the Transportation Research Board, Volume 1136, pp. 57-68

Sun D., L. Zhang, and X. Zhang, (2011) “Quantification of SBS content in SBS polymer modified asphalt by FTIR” Advanced Materials Research, Volume 287, pp. 953-960

Tarrar A. R., and V. P. Wagh, (1992) “The effect of the physical and chemical characteristics of the aggregate on bonding” Publication SHRP-A/UIR-91-507,

Strategic Highway Research Program, National Research Council, Washington, D.C.

Tekalur S. A., A. Shukla, M. Sadd, and K. W. Lee, (2009) “Mechanical characterization of a bituminous mix under quasi-static and high-strain rate loading” Construction and Building Materials, Volume 23, Issue 5, pp. 1795-1802

Tsai B., and C. L. Monismith (2005) “Influence of asphalt binder properties on the fatigue performance of asphalt concrete pavements” Journal of the Association of Asphalt Paving Technologists, Volume 74, pp. 773–790

Tschoegl N. W., (1989) “The phenomenological theory of linear viscoelastic behavior”, Springer-Verlag, Berlin

Underwood B. S., A. H. Heidari, M. Guddati, and Y. R. Kim, (2005) “Experimental investigation of anisotropy in asphalt concrete” Transportation Research Record: Journal of the Transportation Research Board, Volume 1929, pp. 238-247

Underwood B. S., Y. R. Kim, and M. Guddati, (2006) "Characterization and performance prediction of ALF mixtures using a viscoelastoplastic continuum damage model", Journal of Association of Asphalt Paving Technologists, Volume 75, pp. 577-636

Underwood, B. S., (2016) “A continuum damage model for asphalt cement and asphalt mastic fatigue” International Journal of Fatigue, Volume 82, pp. 387-401

Valkering C. P., D. J. L. Lancon, E. Dehilster, and D. A. Stoker, (1990). “Rutting resistance of asphalt mixes containing non-conventional and polymer modified binders” Journal of the Association of Asphalt Paving Technologists, Volume 59, pp. 590-609

Van Oss C. J., M. K. Chaudhury, and R. J. Good, (1988) “Interfacial Lifshitz–van der Waals and polar interactions in macroscopic systems” Chemical Reviews, Volume 88, Issue 6, pp. 927-941

Vananroye A., P. Leen, P, Van Puyvelde, and C. Clasen, (2011) “TTS in LAOS: validation of time-temperature superposition under large amplitude oscillatory shear” Rheologica acta, Volume 50, Issue 9, pp.795-807Vanelstraete A., L. Francken, and R. Reynaert, (1996) “Influence of binder properties on the performance of asphalt mixes” First Eurasphalt and Eurobitume Congress, Strasburg

Venables J. D., (1984) “Adhesion and durability of metal-polymer bonds” Journal of Materials Science, Volume 19, Issue 8, pp. 2431-2453

Wagnoner M.P., W. G. Buttlar, and G. H. Paulino, (2005) "Disk-shaped compact tension test for asphalt concrete fracture" Experimental Mechanics, Volume 45, pp. 270-277

Walubita L. F., A. N. Faruk, A. E. Alvarez, R. Izzo, B. Haggerty, and T. Scullion, (2013) “Laboratory hot-mix asphalt cracking testing : evaluation of three repeated loading crack tests” Transportation Research Record: Journal of the Transportation Research Board, Volume 2373, pp. 81-88

Wei J., and Y. Zhang, (2012) “Application of sessile drop method to determine surface free energy of asphalt and aggregate” Journal of Testing and Evaluation, Volume 40, Issue 5, pp. 807-813

Wells A. A., (1961) “Unstable crack propagation in metals - cleavage and fast fracture” Cranfield Crack Propagation Symposium, Volume 1, Paper 84

Wen H., and H. Bahia, (2009) “Characterizing fatigue of asphalt binders with viscoelastic continuum damage mechanics” Transportation Research Record: Journal of the Transportation Research Board, Volume 2126, pp. 55-62

Wiechert E., (1893) “Gesetze der elastischen Nachwirkung für constante Temperatur”, Annalen Der Physik, Volume 286, Issue 10, pp 335-348

Williams M. L., R. F. Landel, and J. D. Ferry, (1955) “The temperature dependence of relaxation mechanisms in amorphous polymers and other glass-forming liquids” Journal of the American Chemical Society, Volume 77, Issue 14, pp. 3701-3707

Williams M. L., (1969). “The continuum interpretation for fracture and adhesion” Journal of Applied Polymer Science, Volume 13, Issue 1, pp. 29-40

Witczak M., and O. Fonseca., (1996) ”Revised predictive model for dynamic (complex) modulus of asphalt mixtures” Transportation Research Record: Journal of the Transportation Research Board, Volume 1540, pp. 15-23

Witczak M., R. Bonaquist, H. Von Quintus, and K. Kaloush, (2000) “Specimen geometry and aggregate size effects in uniaxial compression and constant height shear tests” Journal of Association of Asphalt Paving Technologists, Volume 69, pp. 733 – 793

Witczak, M., K. Kaloush, T. Pellinen, M. El-Basyouny, and H. Von Quintus, (2002) “NCHRP Report 465: Simple performance test for superpave mix design” Transport Research Board, National Research Council, Washington, D.C.

Xie Z., and J. Shen, (2015) “Fatigue performance of rubberized stone matrix asphalt by a simplified viscoelastic continuum damage model” Journal of Materials in Civil Engineering

Xu D. B., C. Y. Hui, and E. J. Kramer, (1992) “Interface fracture and viscoelastic deformation in finite size specimens” Journal of Applied Physics, Volume 72, Issue 8, pp. 3305-3316

Yildirim Y., M. Solaimanian, and T. W. Kennedy, (2000) “Mixing and Compaction Temperatures for Hot Mix Asphalt” University of Texas, Center for Transportation Research, Research Report #1250-5

Yokoyama T., (2003) “Experimental determination of impact tensile properties of adhesive butt joints with the split Hopkinson bar” The Journal of Strain Analysis for Engineering Design, Volume 38, Issue 3, pp. 233-245

Yut I., and A. Zofka, (2011) ”Attenuated total reflection Fourier transform infrared spectroscopy of oxidized polymer-Modified Bitumens“ Applied Spectroscopy, Volume 65, pp. 765-770

Zhang F., J. Yu, and J. Han, (2011) “Effects of thermal oxidative ageing on dynamic viscosity, TG/DTG, DTA and FTIR of SBS- and SBS/sulfur-modified asphalts” Construction and Building Materials, Volume 25, Issue 1, pp. 129-137

Zhang Y., R. Luo, and R. Lytton, (2012) “Anisotropic viscoelastic properties of undamaged asphalt mixtures” Journal of Transportation Engineering, Volume 138, Issue 1, pp. 75–89

Zollinger C., (2005) “Application of surface energy measurements to evaluate moisture susceptibility of asphalt and aggregates” PhD thesis, Texas A&M University

Appendix A : Crack growth rate figures

The complete set of crack growth rate figures from Chapter 4 are shown below.

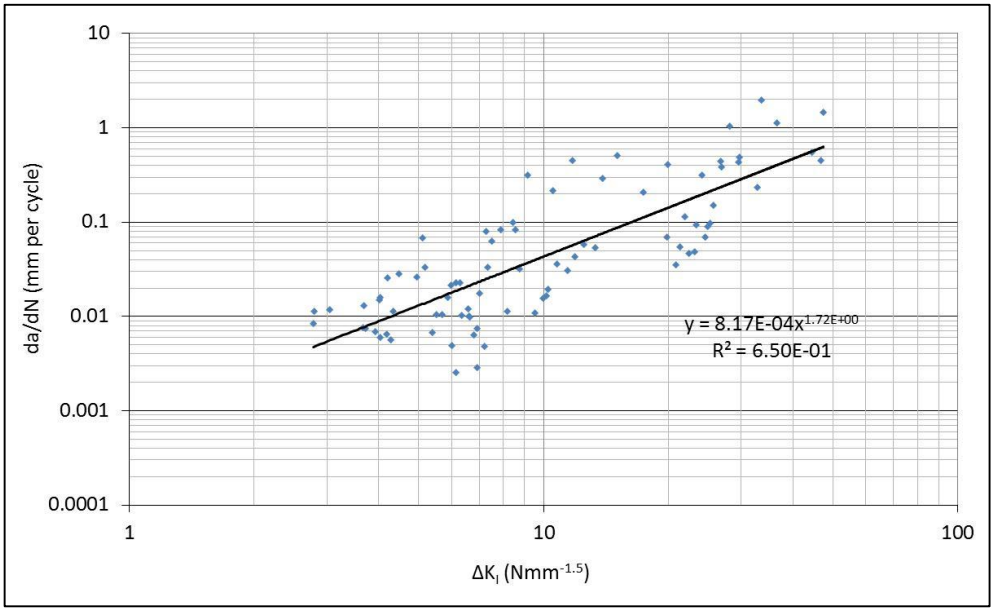

Figure A-1 : Crack growth rate versus ΔK_1 for AV0

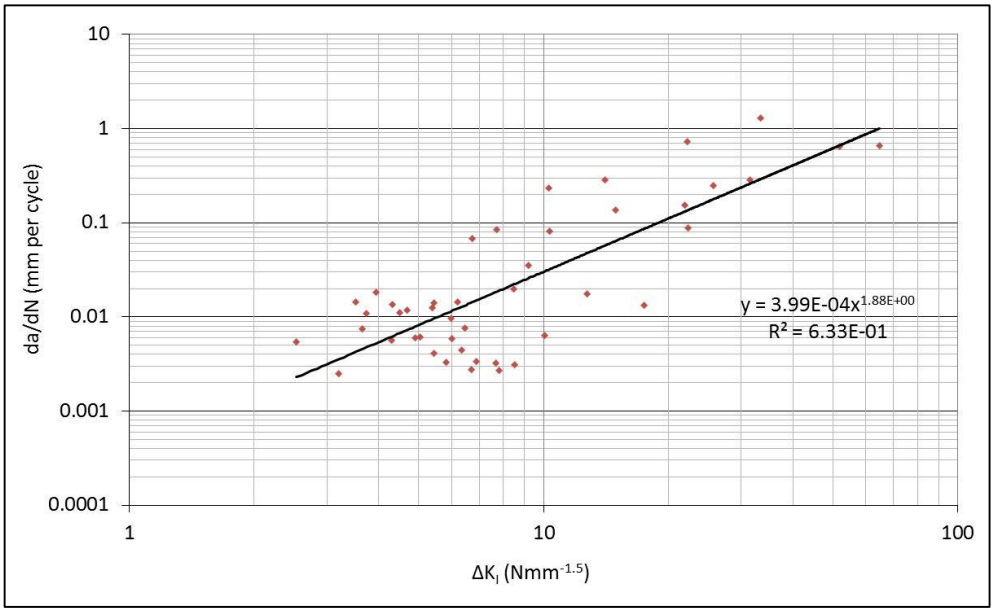

Figure A-2 : Crack growth rate versus ΔK_1 for AVL

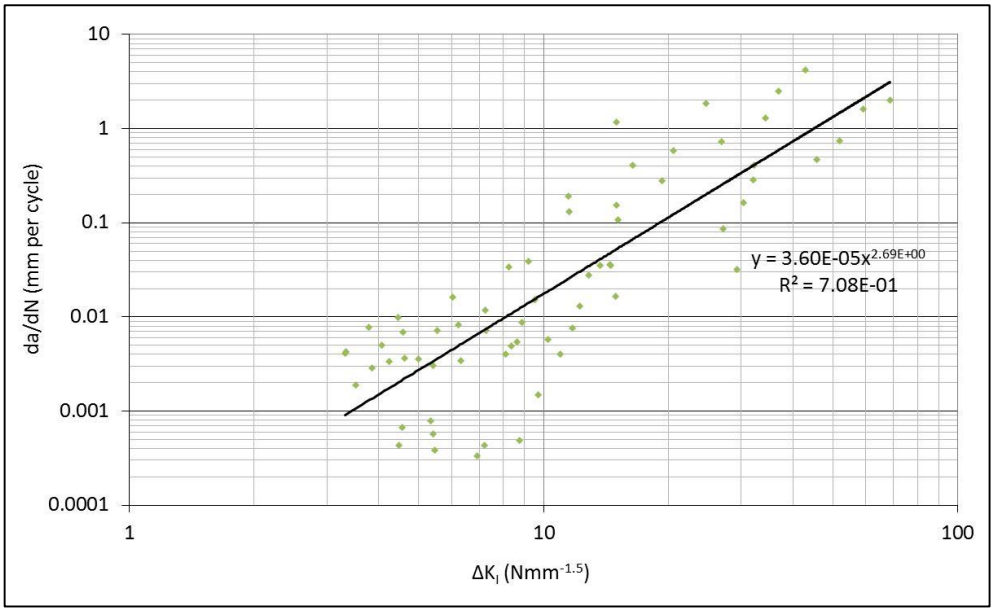

Figure A-3 : Crack growth rate versus ΔK_1 for AVM

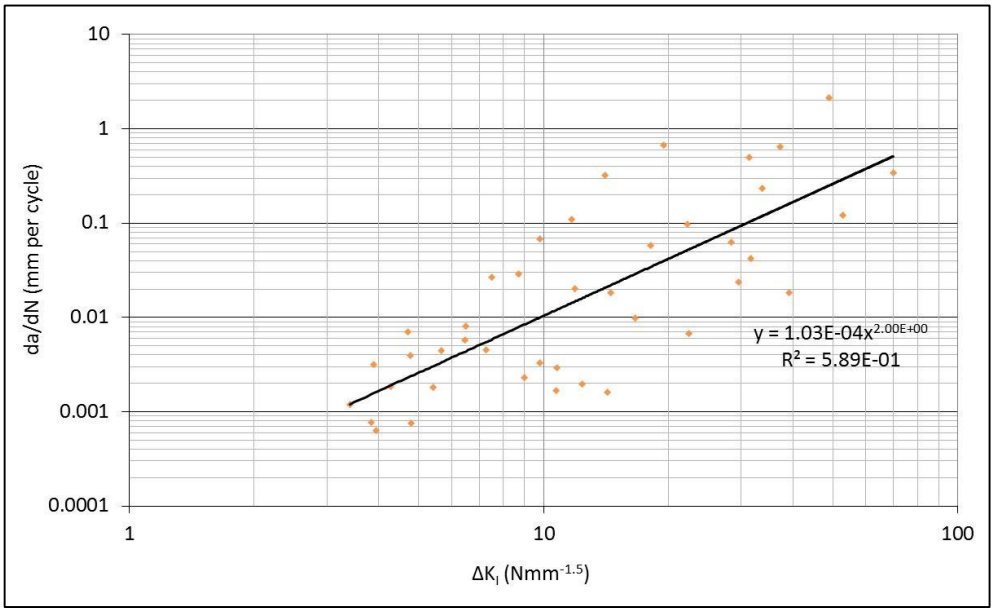

Figure A-4 : Crack growth rate versus ΔK_1 for AVH

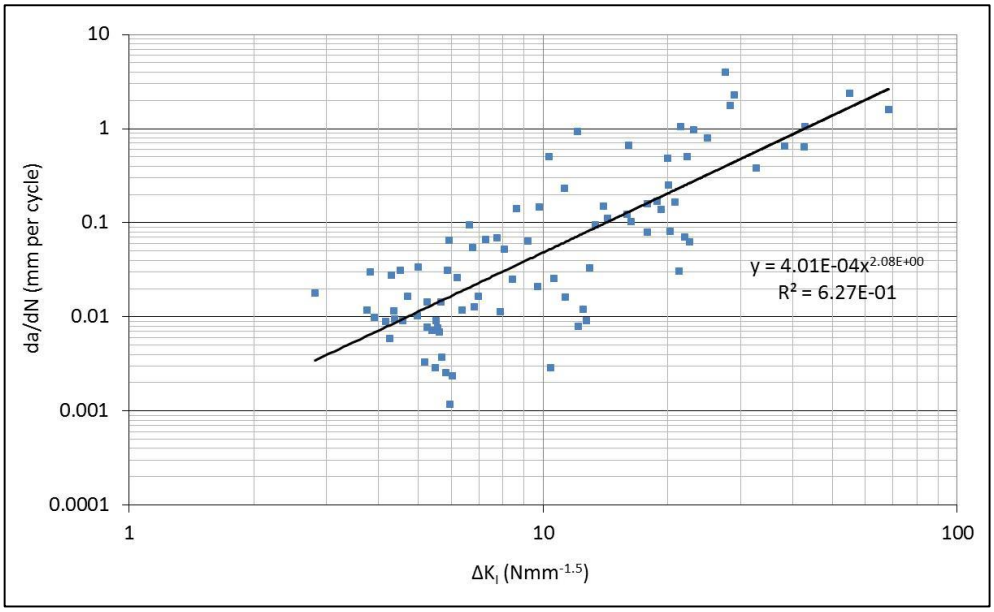

Figure A-5 : Crack growth rate versus ΔK_1 for BV0

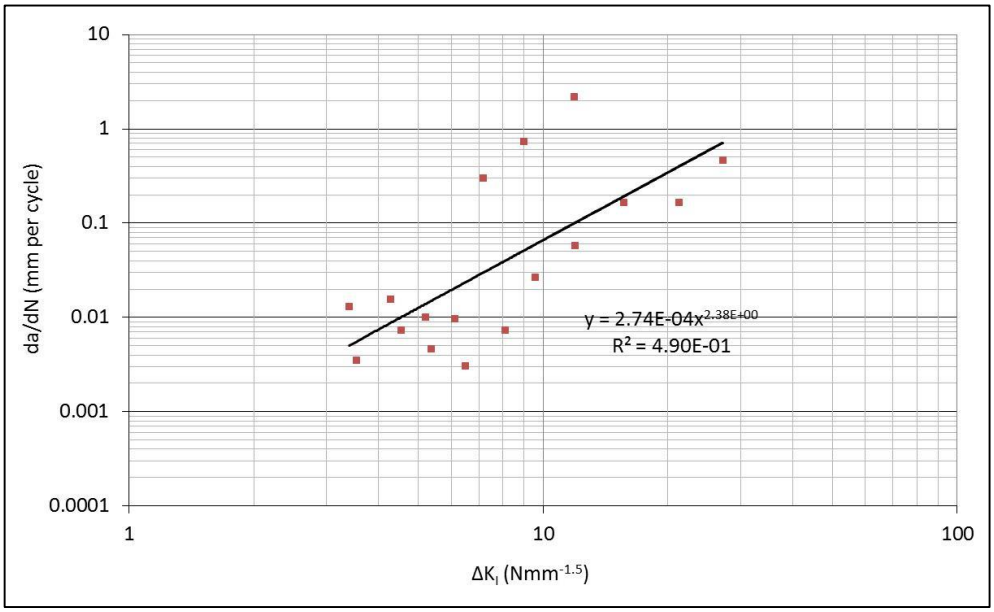

Figure A-6 : Crack growth rate versus ΔK_1 for BVL

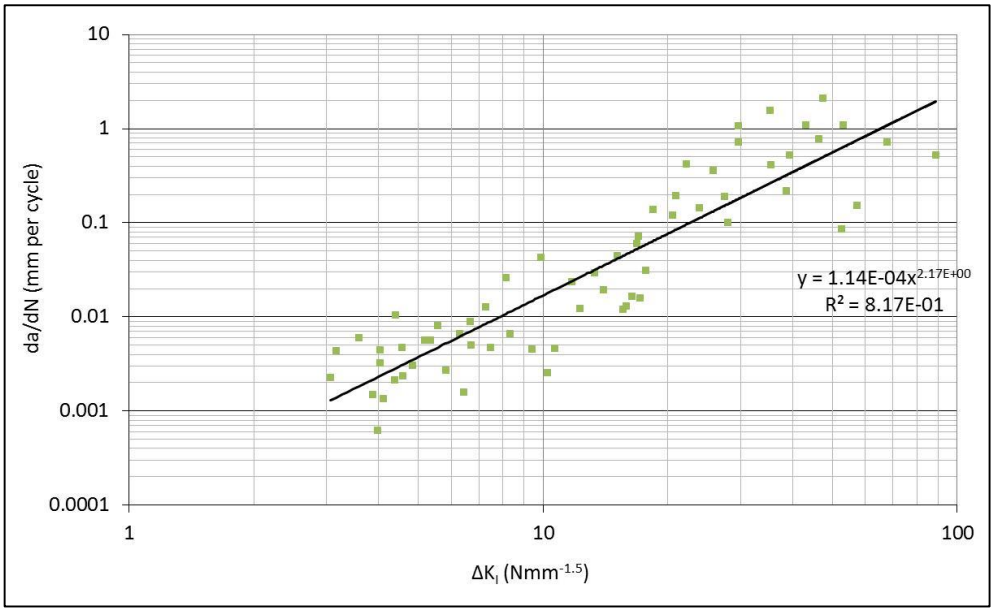

Figure A-7 : Crack growth rate versus ΔK_1 for BVM

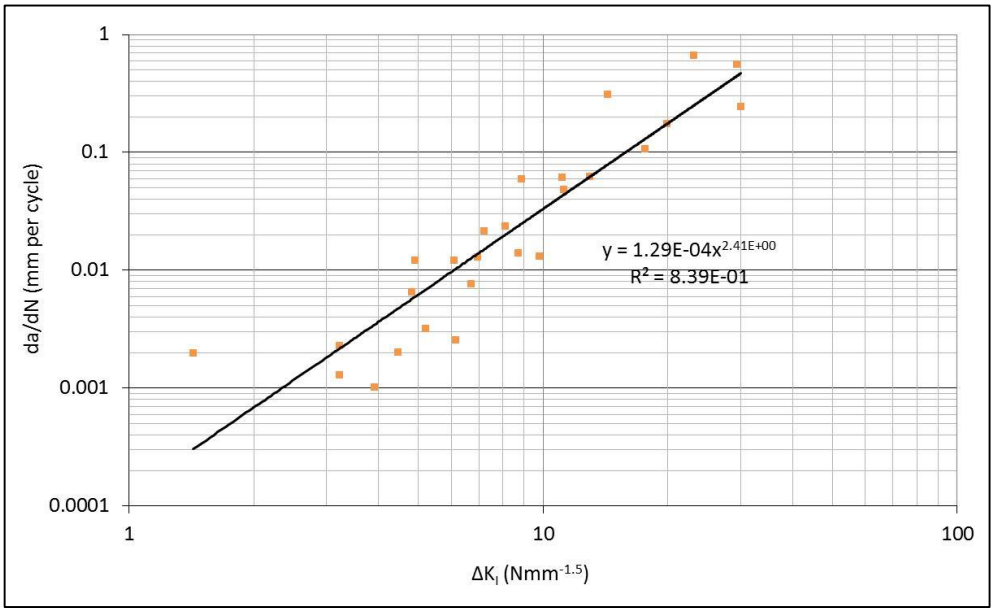

Figure A-8 : Crack growth rate versus ΔK_1 for BVH

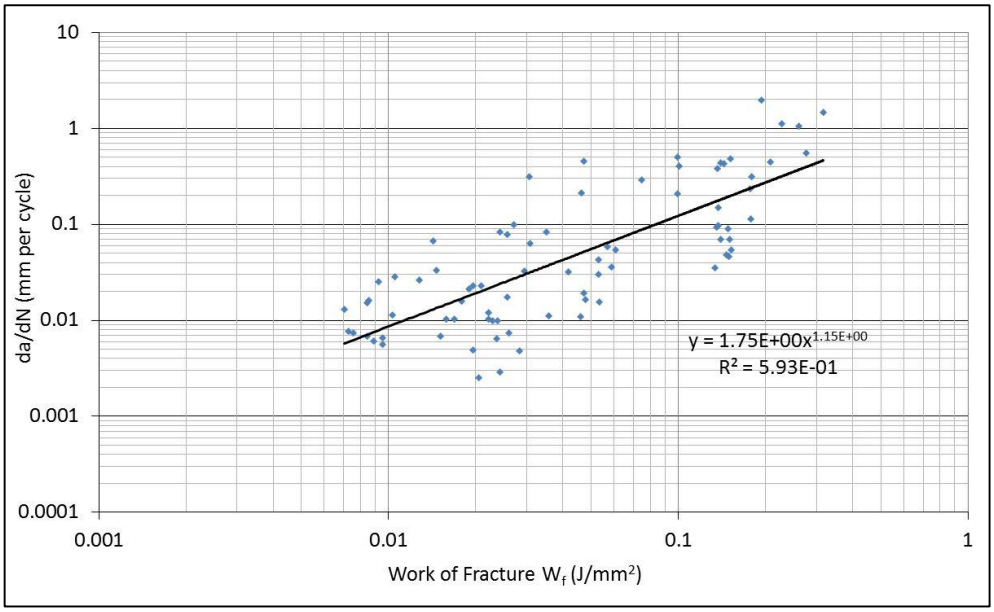

Figure A-9 : Crack growth rate versus W_f for AV0

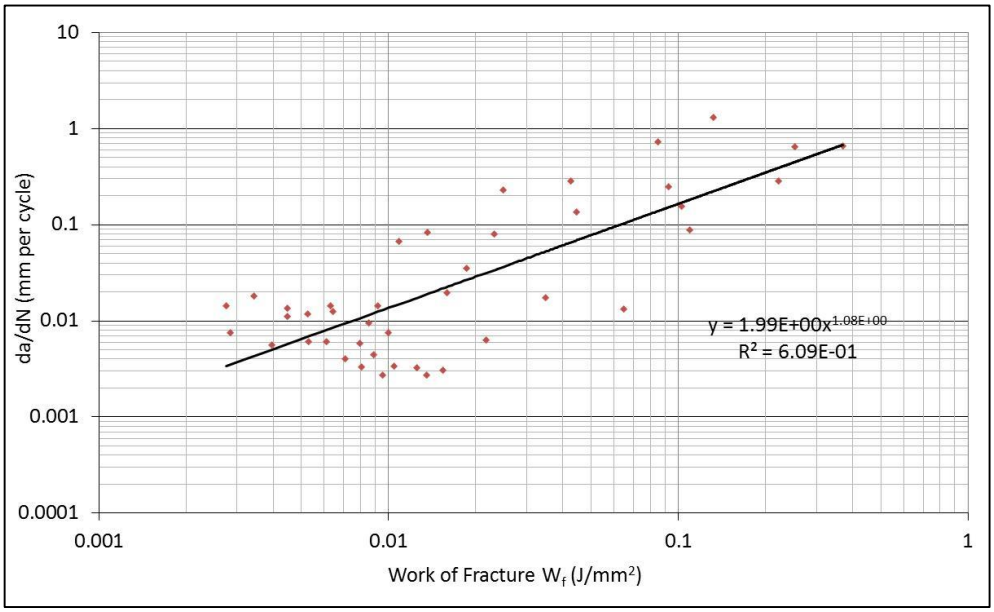

Figure A-10 : Crack growth rate versus W_f for AVL

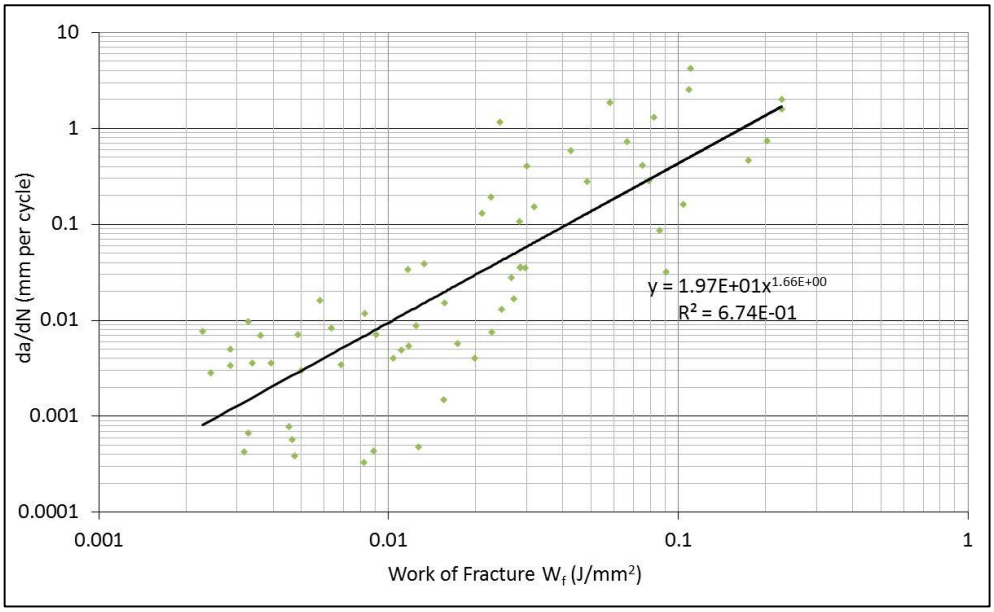

Figure A-11 : Crack growth rate versus W_f for AVM

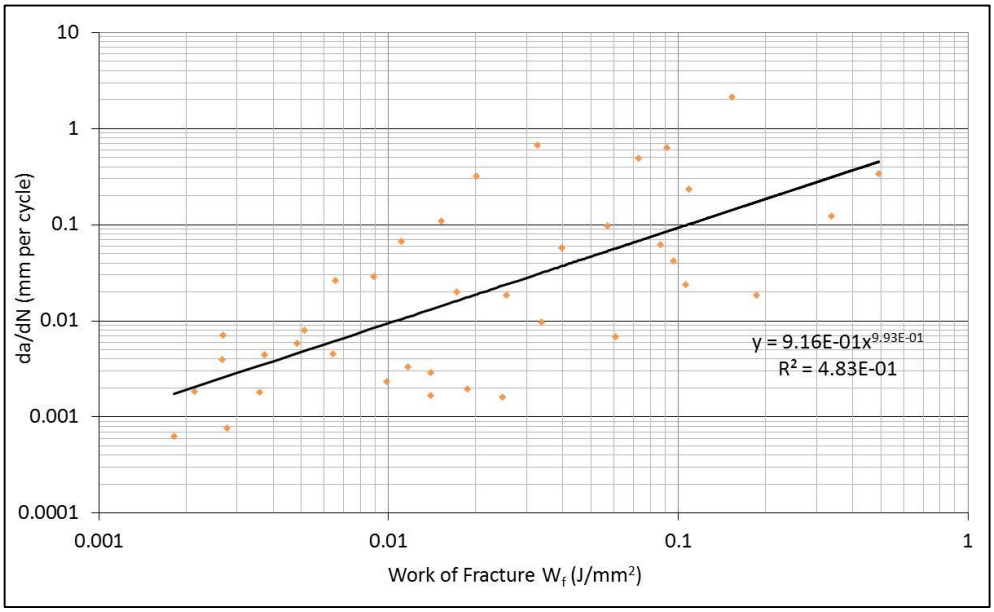

Figure A-12 : Crack growth rate versus W_f for AVH

Figure A-13 : Crack growth rate versus W_f for BV0

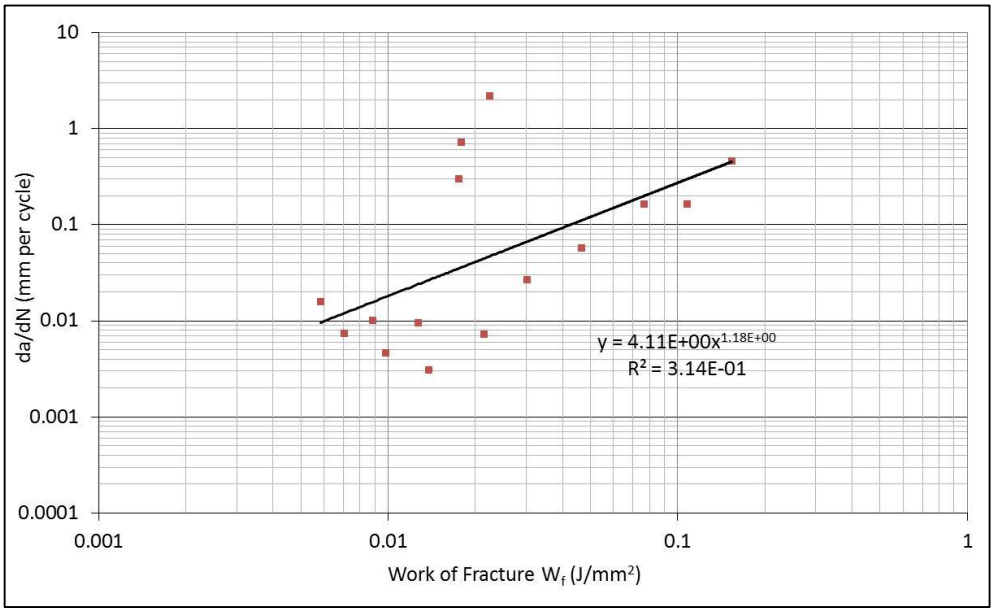

Figure A-14 : Crack growth rate versus W_f for BVL

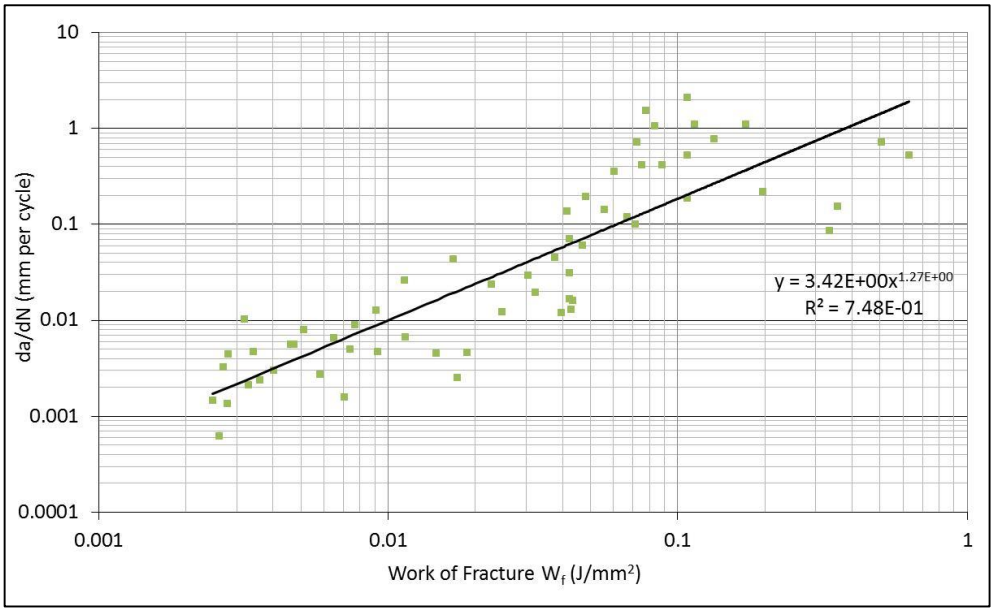

Figure A-15 : Crack growth rate versus W_f for BVM

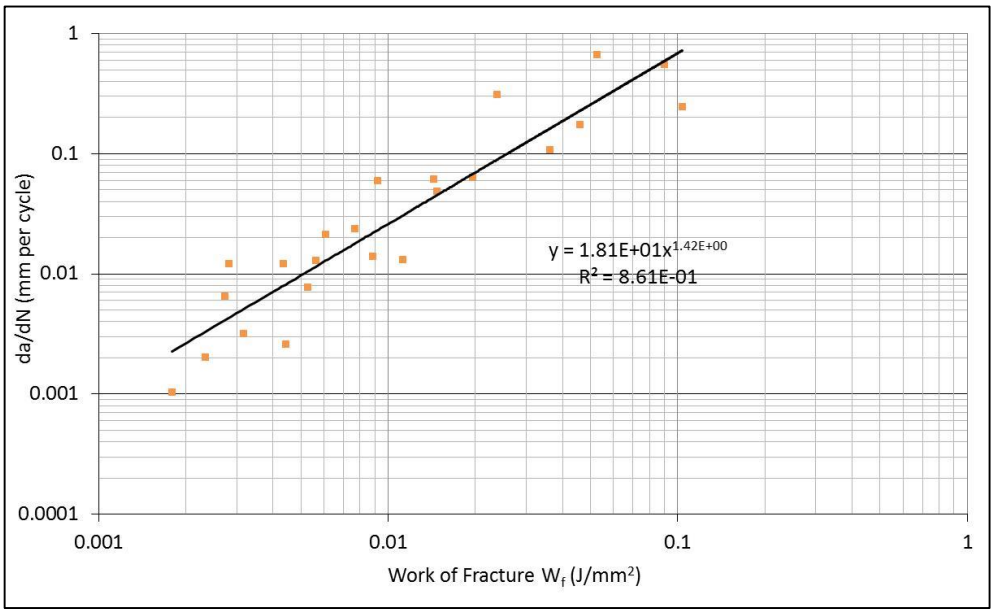

Figure A-16 : Crack growth rate versus W_f for BVH

Appendix B : Preparation of trapezoidal specimens for 2 point bending tests

The specimens required for modulus and fatigue testing on the 2-point bending apparatus according to BS EN 12697-24 (Bituminous mixtures – Test methods for hot mix asphalt Part 24:Resistance to fatigue) must be prepared to the dimensions in Table B-1 below, where D is the nominal maximum aggregate size.

Dimensions of the specimens	D <= 14mm	14 < D <=20mm	20 < D <= 40mm
B	56 ± 1 mm	70 ± 1 mm	70 ± 1 mm
b	25 ± 1 mm	25 ± 1 mm	25 ± 1 mm
e	25 ± 1 mm	25 ± 1 mm	50 ± 1 mm
h	250 ± 1 mm	250 ± 1 mm	250 ± 1mm

Table B-1 : Dimension of the trapezoidal specimens to BS EN 12697-24

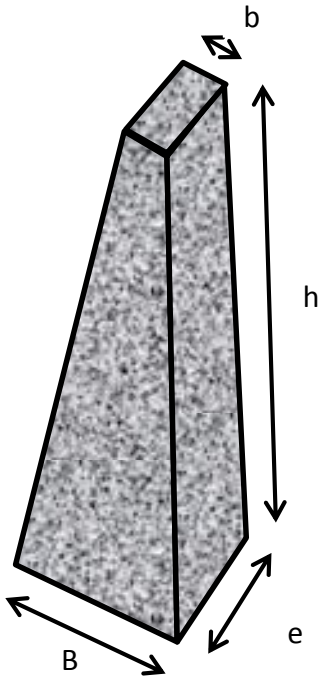

Figure A-1 : Trapezoidal specimen geometry

Specimens with D ≤ 14mm were manufactured from standard lab prepared asphalt samples 305mm x 305mm x 70mm using a clipper saw and bespoke jig. Safety boots, safety glasses, ear plugs/defenders, and lab coat/overalls must be worn during the cutting operation. The procedure for cutting the specimens is detailed below.

Tools Required : Cutting jig, clipper saw, 6 and 8mm hex key, mole grips, paint scraper.

Fix the base plate to the Clipper saw table.	
Ensure the blade is aligned and square to the edge of the base plate.	

Position the slab and cut 25mm slices (or as required). Take care not to use excessive force as this will damage the blade and the asphalt. Ensure adequate water is present in the saw reservoir to cool the blade during cutting. Label each slice after cutting.	
Insert dowel pin in the far left position, and trim the top of the slice.	
Move the dowel pin to the second position. Rotate the slice and trim the other end. This should produce a specimen with a length of 250mm.	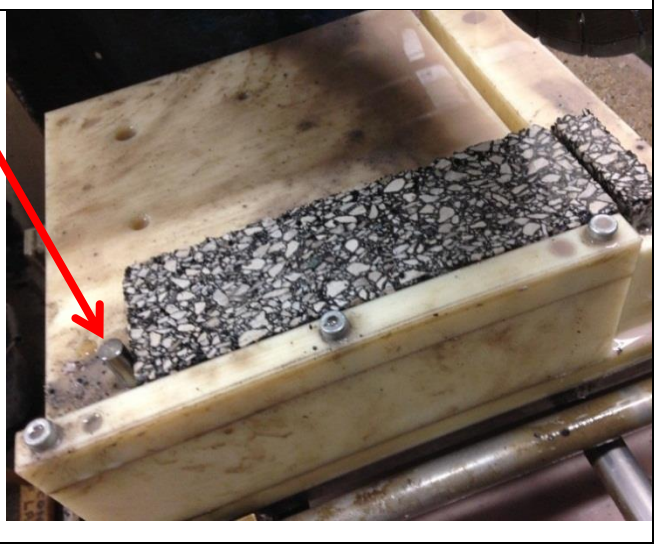

Remove the large table block from the base plate. Clamp the slice in the trapezoidal cutting jig and locate jig onto the base plate with the dowels. Trim one edge of the trapezoidal specimen.	
Lift the jig assembly from the base plate but do not remove the specimen from its clamp. Unscrew the supporting block from the base plate. Swap the positions of the jig/block to cut the second side of the trapezoidal specimen. Remove the completed specimen from the clamp.	
Example trapezoidal specimens showing the pieces cut from each slice.	

Once dried each specimen must be measured for height and width to ensure compliance with the specification.	
Finally the specimens must be adhered to the top and bottom platens using 2 part epoxy glue.